Integrating Autonomous Load Controllers in Power Systems

Douglass, Philip James

Publication date:
2014

Document Version
Publisher's PDF, also known as Version of record

Technical University of Denmark

Philip James Douglass

Integrating Autonomous Load Controllers in Power Systems

Thesis submitted for the degree of
Doctor of Philosophy, June 2014

DTU Electrical Engineering
Department of Electrical Engineering

Integrating Autonomous Load Controllers in Power Systems

Philip James Douglass

Advised by
Professor Jacob Østergaard, Center for Electric Power and Energy, DTU Elektro
and
Preben Nyeng, Ph.D., Energinet.dk

June 2014
(version 1.0)

Abstract

Electric energy systems stand on the brink of radical change as the urgent need to reduce greenhouse gas emissions pushes more efficient utilization of energy resources and the adoption of renewable energy sources. New renewable sources such as wind and solar have a large potential, but they are characterized by variable generation that is only partly predictable. Managing loads is already used in limited circumstances to improve security and efficiency of the power system. In power systems with a large penetration of variable generation, load management has large role to play in adapting consumption to the fluctuating production. The large number and geographic dispersion of loads make coordinating their behavior challenging. New telecommunication technology has reduced the cost of linking devices, promising a future "Internet of Things" where loads are fully networked. Strict real-time constraints and reliability constraints in power systems are motivating research into new control architectures suitable for such a large and complex system.

The focus of this thesis is on an intermediate stage of evolution between today's largely passive loads and a future "Internet of Things". Specifically, this intermediate stage is autonomous devices with sensors, actuators, and software to control local processes but without digital communications interfaces. The architectures explored in this thesis are newly emergent, so the focus is on feasibility and system modeling.

Earlier research has proposed using autonomous load controllers to provide primary frequency reserves. This previous research has mainly focused on the effect of autonomous loads at a high level of abstraction, in large-scale power systems. High-level analysis ignores a significant difference between conventional frequency reserves and frequency-sensitive loads, namely the effects of reduced load diversity on the frequency response. To address this shortfall, time-domain models of the frequency-sensitive loads were constructed that include the variation of frequency response resulting from changes in load diversity.

Experiments and analysis have revealed potential drawbacks of high penetrations of autonomous frequency-sensitive loads: time constraints on the underlying processes which reduce the frequency response, and violations of voltage constraints in the distribution systems arising from synchronized loads. Addressing these drawbacks, two mitigation strategies are proposed, each of which add valuable services in addition to preventing the above mentioned problems.

The first strategy to address time constraints is to operate a synchronous power system at off-nominal frequencies in discrete domains, thus limiting unintended state changes of frequency-sensitive loads. The effect of operating in discrete frequency domains is to dispatch frequency-sensitive loads. Large synchronous machines can only change their frequency setpoint slowly, greatly limiting the

rate of change of dispatch symbols. However, energy sources interfaced with power electronics can change their frequency setpoint very rapidly, creating a stream of symbols that can be decoded with conventional telecommunication protocols.

The second strategy is to merge a voltage-sensitive control loop into the frequency-sensitive controller to directly avoid violations of voltage constraints. This voltage-sensitive controller can also operate alone, without the frequency-sensitive controller, to provide voltage regulation service and increase load diversity in any distribution network where lower voltage level corresponds to higher load.

The frequency-sensitive load controller has been designed, implemented, and tested in real-life settings. Its performance demonstrated a large potential resource, in some cases greater than the average power consumption. The accuracy of load models was validated by comparison with field data. A voltage-sensitive controller was designed, implemented in an embedded system, and tested in laboratory settings. The voltage-sensitive controller was also implemented in a software simulation environment and tested in representative distribution systems. The problems anticipated by large-scale deployment of frequency-sensitive loads were simulated, and mitigation strategies were applied. To support the feasibility of the proposed frequency dispatch system, analysis of existing power systems was conducted using existing technical norms, specifications, and data collected from operating power systems.

The results shows that frequency-sensitive and voltage-sensitive autonomous load are viable alternatives to conventional frequency and voltage control devices. When used in combination, they complement each other. In systems where the operator has centrally dispatchable resources to regulate frequency, these resources can be used to dispatch otherwise autonomous frequency-sensitive loads. Moreover, where centrally dispatchable frequency regulation resources can rapidly change operating points, such as in a micro-grid, the energy sources can be used as transmitters for a ultra-low-bandwidth uni-directional power line communication system.

Dansk Resumé

"Integration af autonome belastnings kontroller i elektrisk energi systemer"

Elektriske energisystemer undergår radikale forandringer, fordi et presserende behov for at nedsætte drivhusgasudledningen forudsætter en mere effektiv udnyttelse af energiressourcerne og en overgang til mere vedvarende energi. Nye vedvarende energikilder som vind og sol har et stort potentiale, men er karakteriseret ved en fluktuerende produktion, som kun delvist er forudsigelig. Styring af forbrug er allerede brugt i begrænset omfang for at forbedre leveringssikkerhed og effektiviteten af energisystemet. I energisystemer med en høj andel fluktuerende vedvarende energikilder kan intelligent styring af forbruget spille en stor rolle i balanceringen af systemet. Det store antal og den geografiske spredning af forbruget gør koordinering af forbrugets respons en udfordring. Nye kommunikationsteknologier har reduceret omkostningerne til at forbinde apparater og lover et "Internet of Things" ("Tingenes internet") i fremtiden, hvor apparater er fuldt forbundet til en globalt datanetværk. Strenge realtids- og pålidelighedskrav til elsystemet har motiveret forskning i nye styrings arkitekturer velegnet til sådan et stort og komplekst system.

Denne afhandling har fokus på et mellemstadie i evolutionen fra dagens passive belastninger mod et "Internet of Things". Mere præcist udgøres dette mellemstadie af autonome apparater med sensorer, aktautorer, og software til at kontrollere lokale processer, men uden et digital kommunikationsinterface. De arkitekturer der er undersøgt i denne afhandling er ret nye, så fokus ligger på gennemførlighed og system modelleringer.

Tidligere forskning har foreslået brug af frekvensfølsome autonome belastninger til at levere primær frekvensreserve. Denne forudgående forskning har fokuseret på effekten af autonome belastninger på et højt abstraktionsniveau i store energisystemer. Analyser på dette høj niveau analyser ignorerer en væsentlig forskel mellem konventionel frekvensereserve og frekvensfølsom belastning, nemlig effekten af reduceret belastningsmangfoldighed på frekvensresponsen. For at adressere denne mangel udførte man tidsdomænemodeller af frekvensfølsomme belastninger for at tage højde for den variation i frekvens responsen, som stammer fra variationen i belastningerne.

Eksperimenter og analyser har afsløret potentielle ulemper ved høj andel af frekvensfølsom belastning: tidsafhængigheder i processer, som begrænser frekvensresponsen og overskridelse af spændingskrav i elforsyningsnettet. For at håndtere disse ulemper er to strategier fremlagt, som hver for sig tilføjer vær-

difulde tjenester udover at de forhindrer de før-nævnte problemer.

Den første strategi for at håndtere tidsafhængigheder er at drive et synkront netområde på ikke-nominelle frekvenser i diskrete domæner. Det begrænser uønsket skift af tilstand i de frekvensfølsomme belastninger og fungerer som direkte kontrol af den pågældende belastning. Store synkrone maskiner kan kun langsomt ændre frekvensens setpunkt, hvilket begrænser takten, hvorved kontrol kommandoer kan blive sendt. Derimod har energikilder, der er forbundet igennem effektelektronik, mulighed for at ændre frekvenssetpunkt meget hurtigt og kan skabe en strøm af kommandoer som kan tolkes med eksisterende kommunikations protokoller.

Den anden strategi er at forene en spændingsfølsom styring med en frekvensfølsom styring, og på den måde direkte undgå uønskede spændinger. Denne spændingsfølsomme styring kan også blive brugt alene, uden den frekvensfølsomme del, for at stabilisere spænding og og reducere behovet for netforstærkninger alle steder hvor lavere spænding falder sammen med højere forbrug.

En frekvensfølsom styring er udviklet, implementeret, og testet under realistiske forhold. Resultatene viste en stor potentiel ressource, i nogen tilfælde større end gennemsnittet af effektforbruget. Nøjagtigheden af belastningsmodeller var verificeret ved hjælp af måledata. En spændingsfølsom styring var udviklet, implementeret og testet under laboratorie forhold, og dens opførsel var simuleret i repræsentative energisystemer. Problemerne forårsaget af udbredt anvendelse af frekvensfølsomme belastninger var simuleret, og afværgelsesstrategier anvendt. For at underbygge gennemførligheden af det fremlagte frekvensebaserede belastningskontrolsystem er analyser af eksisterende energisystemer blevet gennemført med henvisninger til tekniske standarder, specifikationer og endeligt data indsamlet fra systemer i drift.

Resultatene viser, at frekvens- og spændingsfølsomme autonome belastninger er leveringsdygtige alternativer til konventionel frekvens- og spændingsregulerende teknikker. Når de bruges sammen, komplementerer de hinanden. I systemer, hvor operatøren har mulighed for at regulere frekvensen centralt, kan de direkte kontrollere de ellers autonome frekvensfølsomme apparater. Derudover, i systemer, hvor frekvens reguleringsressourcer tillader hurtigt skift af frekvenssetpunkt, for eksempel micro-grids, kan energikilder blive brugt som sender i et lavhastigheds-envejs- kommunikationssystem.

Contents

List of Figures

Glossary

AGC automatic generation control.

ARMA autoregressive moving average.

DAC digital to analog converter.

DER distributed energy resources.

DG distributed generation.

DLC direct load control.

DSO distribution system operator.

DTU the Technical University of Denmark.

ENTSO-E European Network of Transmission System Operators for Electricity.

EV electric vehicle.

EVE "Expected Voltage Estimator".

FS-DER frequency-sensitive distributed energy resources.

FSL frequency-sensitive load.

HV high voltage (130 kV and higher).

IP Internet Protocol.

LED light emitting diode.

LV low voltage (400 V and lower).

MIPS million instructions per second.

MV middle voltage (50 kV to 1 kV).

OLTC on-load tap changing.

p.u. per unit.

PFC power frequency communication.

PLC power line communication.

PNNL Pacific Northwest National Laboratory.

PV photo-voltaics.

RES renewable energy source.

RMS root mean squared.

ROCOF rate of change of frequency.

TCL thermostat controlled load.

TEC thermal equivalent circuit.

TOU time-of-use.

TSO transmission system operator.

VG variable generation.

VLC visible light communication.

VS-DER voltage-sensitive distributed energy resources.

VSI voltage source inverter.

VSL voltage-sensitive load.

Acknowledgements

I have great gratitude to my advisers for all their guidance and encouragement. Professor Jacob Østergaard used his incredible breadth and depth of insight into power system to identify tractable research problems where I could direct my efforts. Preben Nyeng used his perspective from the Danish Transmission System Operator to ensure my research was relevant to the problems faced by system operators today. Preben also gave invaluable practical advice from the perspective of a recently finished PhD student.

Rodrigo Garia-Valle was my teacher in "Fundamentals of Electric Power Systems", the first course I took to enter into the power systems domain. My work to a great extent follows in his footsteps, both with the frequency-sensitive and voltage-sensitive load controllers. I'm grateful he was available to answer my basic questions, as well as to debate and develop our research ideas.

Kia Hueßen also served as an informal adviser and teacher. His willingness to listen to my wild ideas for disruptive changes to power system operations, and consider the feasibility and consequences of these changes resulted in important research results during this project. He also pushed me to refine and improve the presentation of my ideas, a skill I will certainly use in my future career.

The experimental work in this project depended on Christian Brandt Rassumssen's hardware design, and his drive to ensure that the hardware he produced worked and was deployed as intended. Mikael Togeby and his colleagues at EA Energianalyse were also central to the success of the experimental work on Bornholm.

I am also indebted to the researchers and engineers at the Pacific Northwest National Laboratory for hosting my external stay. Dave Chassin gave me a home away from home, and enlightened me about the details of load modeling, and well as the big picture of energy systems. Jason Fuller, Andy Fisher, and Matt Hauer began immediately implementing my suggestions for improvements to GridLAB-D, as if I had my own development team.

The M.Sc. students I advised, Jakob Zimmermann, Dennis Lykke Nielsen, and Octavian C. Tudora, also contributed to my project by implementing and demonstrating load control algorithms that I didn't have time to pursue myself.

Shi You was always ready to share his knowledge and experience with me, which was especially important in the beginning of my project. Fabrizio Sossan, and Peder Bacher helped de-mystify the process of making statistical models of thermal processes. Zhao Xu gave valuable advise about fruitful lines of research to build upon his earlier work with frequency-sensitive loads.

The anonymous reviewers of my papers have also contributed valuable feedback to improve my work; thanks whoever you are!

And away from school, my family deserves acknowledgment for not just

tolerating my desire to be a student again, but also supporting my pursuit of another degree. Esther, my little girl, challenged me to explain the world from a child's perspective. Thanks goes to my sister, Margaret, for proof-reading, bringing the quality of my English up to publishable standards. My wife Rui, the woman behind this work, thanks for all your support. And last, but not least, thanks to my parents.

List of Publications

The following publications were produced during the course of this Ph.D. project. Publications [A-F] can be found in appendices with the corresponding name. Publications [g-i] are papers whose content is not central to this thesis, or whose content is fully contained elsewhere in the thesis.

[A] P. J. Douglass, R. Garcia-Valle, P. Nyeng, J. Østergaard, and M. Togeby, "Demand as Frequency Controlled Reserve: Implementation and practical demonstration," in *Innovative smart grid technologies (ISGT europe), 2nd IEEE PES International Conference and Exhibition on*, Oct. 2011.

[B1] ——, "Smart Demand for Frequency Regulation: Experimental results," *Smart Grid, IEEE Transactions on*, vol. 4, no. 3, pp. 1713–1720, Sept. 2013.

[B2] P. J. Douglass, "Demand of Frequency Controlled Reserve: Water Treatment, Relay-Controlled Loads, Micro-grid," Technical University of Denmark, Tech. Rep., Mar. 2013.

[C] P. J. Douglass, R. Garcia-Valle, O. C. Tudora, and J. Østergaard, "Voltage Sensitive Load Controllers for Voltage Regulation and Increased Load Factor in Distribution Systems," *Smart Grid, IEEE Trans. on*, vol. 5, no. 5, pp.2394–2401, Sept. 2014.

[D] P. J. Douglass, R. Garcia-Valle, F. Sossan, J. Østergaard, and P. Nyeng, "Design and Evaluation of Autonomous Hybrid Frequency-Voltage Sensitive Load Controller," in *Innovative smart grid technologies (ISGT europe), 4th IEEE PES International Conference and Exhibition on*, Oct. 2013.

[E] P. J. Douglass and S. You, "Direct Load Control by AC frequency Modulation," in *6th European Conference on PV-Hybrids and Mini-Grids*, 2012.

[F] P. J. Douglass, K. Heussen, S. You, O. Gehrke and J. Østergaard, "System Frequency as Information Carrier in AC Power Systems," *Power Delivery, IEEE Trans. on*, vol. 30, no. 2, pp. 773–782, April 2015.

[g] P. J. Douglass, S. You, and K. Heussen, "Broadcast Communication by System Frequency Modulation," in *Smart Grid Communications (SmartGridComm), 2012 IEEE Third International Conference on*, 2012, pp. 199–204.

[h] P. J. Douglass, R. Garcia-Valle, and O. C. Tudora, "Autonomous Voltage Load Controller," PCT Patent Application 13184885.5, September 18, 2013.

[i] S. You, H. W. Bindner, J. Hu, and P. J. Douglass, "An Overview of Trends in Distribution Network Planning: A Movement Towards Smart Planning," *IEEE PES Transmission & Distribution Conference & Exposition*, 2014.

Chapter 1

Introduction

1.1 The Impact of Human Energy Use

The proposed "Anthropocene" epoch is differentiated from previous time periods by the large scale impact of human activities on earth systems. Already the loss of biodiversity has accelerated to rate that exceeds 4 of the 5 previous mass extinction events [1], and more than half of all bio-available nitrogen comes from anthropogenic sources [2]. Emissions of electromagnetic radiation from electric lighting and telecommunications systems can be detected by extrasolar observers.

Anthropogenic emissions of carbon dioxide into the atmosphere trap heat on the earth's surface and are diffusing into the oceans, increasing their acidity. The combustion of fossil fuels account for approximately 65% of the total anthropogenic carbon emissions [3], which makes transitioning to a carbon-neutral energy system an urgent priority made difficult by the large scale of human exosomatic energy demand[1]. The human exosomatic energy demand exceeds limits on the available supply of the mature carbon-neutral renewable energy sources: biomass and hydropower [4, 5]. New primary renewable energy sources (RESs) such as solar and wind power are feasible, but they differ from existing power sources in being non-dispatchable; the availability of primary energy varies on all time scales (seconds to hours) as a function of weather conditions. These variations are only partly predictable.

Wind and Solar energy resources can be harnessed to directly provide mechanical power (wind) and thermal power (solar), but to provide a complete palette of energy services, wind and solar energy must first be converted to electrical energy. Electric energy is a versatile energy carrier because it can be converted into any energy service, and the conversion technologies are among the most efficient known (i.e. LEDs for lighting, motors for mechanical power, heat pumps for thermal energy). However, electricity can not be easily stored; it must be consumed as it is produced.

[1] Endosomatic energy consumption, required for homeostasis, is a tiny fraction of exosomatic energy usage, so there is scope for reducing primary energy demand without compromising human well-being.

1.2 Evolution of Electric Power Systems

A broad coalition of Danish politicians has agreed upon long term targets to completely phase out fossil-fuel energy sources by 2050 [6]. The strategy for achieving this goal calls for decreasing primary energy demand and increasing production from RES. Within the roadmap agreed to as part of this plan, the use of electric energy will increase in both relative and absolute terms. The dominant RES resource in Denmark is wind power, located onshore and offshore. In 2012 wind turbines produced 30% of the electric energy consumed in Denmark, compared to 14% in 2006 [7]. In the 16 months prior to the time of writing, photo-voltaics (PV) production capacity in Denmark has increased by an order of magnitude, from 50 MW to 500 MW [8]. In the future, the installed capacity of RES in the power system will continue to grow. This development creates challenges for the system planners and operators.

Until now, fluctuations in power output from variable generation (VG), both predicted and unpredicted, have been balanced by dispatching thermal power plants in Denmark and by exchanging power with Denmark's neighbors. The dispatch of generation is coordinated among the various actors through trade on the Nordpool spot market. This has resulted in a cost effective deployment of VG, but it is likely that these integration strategies are insufficient for continued VG growth.

Thermal power plants are presently being de-commissioned without being replaced by new capacity. In the long term, a limited amount of thermal capacity, burning biofuels, is expected remain part of the power system, but the economics of maintaining large amounts of thermal production capacity at low utilization rates is questionable. Increasing the capacity to trade power between Scandinavia and continental Europe will help smooth the variations in VG production, but large scale weather patterns will cause VG production to be positively correlated of across the region. Electric energy storage may one day help balance the fluctuating output of VG, but cost effective solutions, adapted to countries lacking mountains for pumped-hydro storage, remain elusive [9].

In general, VG have a lower capacity factor than dispatchable power plants. In Denmark, wind turbines, onshore and offshore together, produce on average 28% of their rated capacity [7, 10], but occasionally they produce almost at capacity, and occasionally they produce almost nothing. Not only must power and energy balancing resources be available to compensate for that fluctuation, but the capacity to transmit and distribute electricity, regardless of the source, must also be available. With a continuation of the present network planning paradigm, transmission and distribution assets could also see lower levels of utilization, and they will be correspondingly higher costs per unit of delivered energy.

1.3 Autonomous Control of Demand

A characteristic of historical and contemporary power system planning and operating methods is to take demand as exogenous; inelastic over operational time scales. The opportunity cost of not serving loads is assumed to be large, so energy production and distribution infrastructure is dimensioned to meet all demand at all times. The opportunity cost of not serving demand is high, be-

cause power system operators cannot differentiate between high-value critical loads and low-value marginal loads. Their tools for curtailing demand are very course-grained, with load shedding occurring at the substation level, effecting thousands of customers at a time.

Providing differentiated levels of power-system service to different load classes is an attractive method in increasing the efficiency of the power system as a whole. Where demand management has already been deployed [11], it has either relied on time-of-use (TOU) tariffs or uni-directional communication signals. The TOU tariffs can motivate load shifting on a fixed schedule, but to handle fluctuating VG, time-varying load control is needed. Time-varying real-time load control signals are dispatched from central controllers to loads using radio communications, power line communication, and packet data networks (i.e. Internet Protocol (IP)).

In contrast, real-time control of generators does not exclusively rely on telecommunications infrastructure to coordinate their actions. Instead, generators make local measurements of the electric power system's properties (voltage and AC frequency) and autonomously react to these measurements in parallel. This thesis concerns methods for controlling autonomous loads in parallel to provide ancillary services, comparable to the services provided by generators.

Being robust and simple, local control loops for autonomous loads have technical advantages and economic advantages over load control systems relying on telecommunications infrastructure. However, significant work remains to be done before these autonomous load controllers are ready for operational deployment. There has previously been little field experience with these devices in operation. Questions about how to accurately predict the response of the loads and how to ensure that they respect distribution system capacity constraints have not been adequately addressed.

1.4 Contributions of this Thesis

This thesis contributes to the field of demand management with design and analysis of autonomous load controllers that are differentiated from prior work by considering the challenges associated with deployment in low voltage (400 V and lower) (LV) power distribution systems. Earlier work in this area (see Sec. 2.5) has proposed algorithms for providing frequency regulation service from flexible loads, and the performance of these algorithms has been analyzed with simulations of large power systems and lab-scale tests. Earlier work has also proposed algorithms for providing voltage regulation service from flexible loads and simulated their performance (see Sec. 2.5.2). Finally, power line communication (PLC) using specialized transmission equipment is a mature technology at high frequencies (3-148.5 kHz [12]). This thesis builds on this state-of-the-art in the following ways:

1.4.1 Experimentally Derived Frequency-Sensitive Load Models

In Chapter 3, results from a field test of autonomous loads providing frequency regulation services are presented. The frequency-sensitive loads (FSLs) were bottle cooling refrigerators, resistive space heaters, motors (including pumps)

in a water treatment plant, and miscellaneous small loads. These results demonstrate that these devices are able to provide a linear frequency response over two different frequency ranges. From the data, estimates of the size of the resource, the speed of its activation, and duration of the response are found. A statistical model of the refrigerator response is found, and its performance evaluated.

Author's Contributions

This experiment was done in collaboration with industrial partners and the local utility on the island of Bornholm. The author's role in this project was first, to write software for the experimental devices, then to analyze the experimental data, and finally to disseminate the results.

1.4.2 Autonomous Voltage-Sensitive Loads for Voltage Regulation and Increased Load Factor

In Chapter 4, the design of an autonomous load controller to provide voltage regulation service in distribution feeders is presented. The controllable resource is identical to the devices providing frequency regulation (Chapter 3), only the software of the controller is modified. Measurements of root mean squared (RMS) voltage replace frequency measurements as input to the control algorithm. In contrast to the previously proposed algorithms for voltage regulation (described Sec. 2.5.2), the algorithm normalizes voltage measurements to account for the strength of the network and the impact of the load itself on voltage measurements. In addition to reducing voltage fluctuations, this algorithm also shifts power consumption away from high-load time periods, increasing the load factor of distribution systems.

Author's Contributions

This work builds on the earlier work of R. Garcia-Valle that addressed the role of under-voltage load shedding to speed recovery from transient voltage dips [13]. The author created a significantly different load control algorithm to address voltage regulation at longer time scales. The author then created a simulation model of the controller, analyzed the performance, and disseminated the results. Under R. Garcia-Valle's and the author's supervision, a master's student, O. C. Tudora, implemented the proposed controller, conducted a laboratory experiment, and analyzed data for his M.Sc. thesis [14]. In the patent application filed in connection with this work [h], 50% of the credit for the invention was given to the author and 25% to each of the other two collaborators.

1.4.3 Hybrid Voltage-Frequency Sensitive Controller Algorithm

Chapter 5 describes how the algorithms for providing frequency regulation (Chapter 3) and voltage regulation (Chapter 4) can be combined into a single algorithm that balances the two services. Simulations are conducted showing that this hybrid controller can provide frequency regulation service, and is effective at mitigating overloads in distribution systems, created by the frequency regulation service.

Author's Contributions

The author contributed all the substance of this section, with notable assistance in the description of the thermal load model from F. Sossan.

1.4.4 Dispatch of Autonomous Distributed Energy Resources - Power Frequency Communication

A novel PLC system is presented in Chapter 6. This work blurs the distinction between a purely reactive autonomous load and a directly controlled dispatchable resource. Using the same controllable resource as Chapter 3, two methods are described for system operators to control them. Both methods create a communication system using energy sources are transmitters.

The first method (see Sec. 6.1) utilizes dispatchable frequency regulation resources to operate a system in discrete off-nominal frequency setpoints. The operator exploits the direct relation between system frequency and frequency-sensitive load (FSL) state to dispatch loads.

The second method (see Sec. 6.2) differs from the first only in the speed of changes to system frequency setpoints. Rapidly changing frequency setpoints create a general purpose unidirectional communications channel. This type of system was dubbed "power frequency communication" in [15].

Author's Contributions

The author created this concept and synthesized information from standards, existing literature, and experimental data. Co-authors encouraged the feasibility of the concepts and gave helpful advise on the presentation of the analysis results.

Chapter 2

Background and Review of State-of-the-Art

This section will review existing literature and practice relevant to the sections that follow. First, in Sec. 2.1, existing methods of frequency regulation are examined. Frequency regulation maintains the balance between power production and load across an entire synchronous power system at short time scales (from milliseconds to minutes). Second, in Sec. 2.2, voltage regulation in distribution systems is discussed. Voltage levels at all points in distribution systems must be maintained within given intervals under a wide range of operating conditions. Distributed energy resources (DER) can cause voltage levels to fluctuate, but autonomous control techniques can help mitigate this problem. Then, in Sec. 2.3, small isolated power systems are discussed. The fundamental principles of electrical engineering are independent of system scale, but in practice, the design constraints of small power system are rather different from continent-scale systems. The techniques for control of autonomous DER presented in later chapters are especially relevant for addressing these constraints. Next, in Sec. 2.4, a brief introduction to demand-side management, including the modeling of thermal loads, is given. Finally, in Sec. 2.5, previous work in the area of autonomous control of loads is presented.

2.1 Frequency Regulation

Power system operators seek to maintain the frequency of alternating current to be within 1% of nominal values during normal operation. The standard used in Europe [16] requires the frequency of large power systems to be between 47-52 Hz[1] at all times. The frequency regulation resources must have enough power to be able to cope with the largest conceivable fault in the system, i.e. the tripping of the largest power plant in an area. Compared to the power rating, the amount of *energy* dispatched for frequency regulation is relatively small, because deviations in the positive and negative direction cancel each other out within an hour or less.

System planners specify 3 types of reserves, each acting at different time

[1]This range is derived by allowing deviations of +4 % and -6 % from the nominal 50 Hz.

scales, to limit the extent of disturbances, and to restore the system to a secure operating state. The temporal relation of frequency containment (primary), frequency restoration (secondary), and reserve replacement (tertiary) reserves is shown in Fig. 2.1. Primary frequency control, also called the frequency containment process [17], is active at the shortest time scale, and has a function of limiting the extent of frequency deviations during disturbances. It is implemented using a speed droop governor (see Sec. 2.1.2), where each participating generator in parallel locally measures system frequency and reacts autonomously. Providing primary frequency control is costly with thermal generators because it requires them to run at sub-optimal operating points, resulting in an efficiency loss of 10 - 20 % [18]. These losses could increase as new thermal generators (i.e. combined-cycle) are optimized to gain higher efficiency at the expense of less flexibility [19]. The cost of providing regulating power in a system heavily dependent on carbon-neutral energy sources (wind and nuclear) is higher than today's fossil-fueled power system [20].

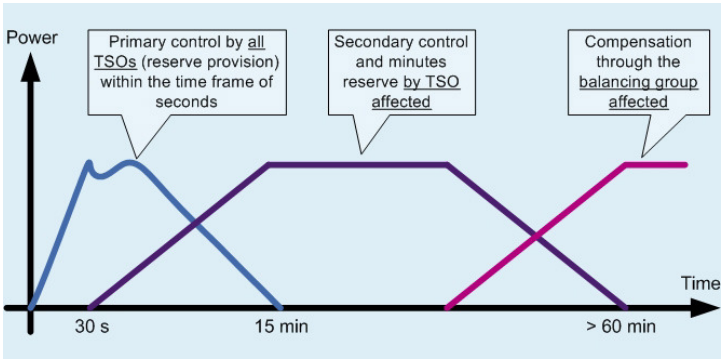

Figure 2.1: Frequency containment (primary), frequency restoration (secondary), and reserve replacement (tertiary) reserves shown in chronological sequence. Figure reprinted from [21]. Note the time axis is schematic, being neither linear, nor logarithmic.

The frequency containment process results in unscheduled transfers of power between areas and a steady-state frequency offset. Secondary frequency control restores scheduled inter-area power flows and corrects the frequency offset. Secondary frequency control, called the frequency restoration process in [17], can not be done by autonomous generators operating in parallel. Either a single generator in the system has the responsibility to perform secondary frequency regulation, or more commonly in large systems, a central dispatcher coordinates the contribution of several generators with automatic generation control (AGC) [22].

Tertiary reserves, also known as the reserve replacement process [17], are called online to relieve primary and secondary reserves. They need time to warm up and synchronize, therefore, from the time the activation signal is given, they have up to a half-hour to deliver output. Primary and Secondary reserves must sustain their response until tertiary reserves can relieve them.

Considering the scale of contemporary synchronous areas, Denmark is a very

small country[2]. Nevertheless, Denmark is split between two synchronous areas: Jutland is synchronous with continental Europe, while the islands East of the Great Belt are synchronous with the Nordic region. Without the shared resources of these larger power systems, Denmark would be unable to integrate large-scale power injection from fluctuating power sources. The larger continental European system has more inertia, and a significantly more stable frequency, than the Nordic region.

In the Nordic region, the frequency range 49.9 - 50.1 Hz is considered the secure operating range. Presently, in the Nordic power system frequency quality is in long term decline [23, 24], putting the integrity of the system at risk, and increasing the probability of lost load. During the circa 16 hours per month when the Nordic system frequency is outside the secure operating range, the system reserves are not adequate to protect the system if a large disturbance were to occur.

2.1.1 Frequency Disturbances

Frequency disturbances result from an imbalance between energy delivery from generators and energy extraction by loads. In a single-machine system, the rate of change of frequency (ROCOF) can be derived from the swing equation [22]:

$$ROCOF = \Delta\dot{f} = \frac{f_{\mathrm{o}}}{2H}(\Delta P_{\mathrm{g}} - \Delta P_{\mathrm{l}}) \tag{2.1}$$

where Δf [Hz] is the deviation to system frequency (relative to nominal frequency), f_{o} [Hz] is the nominal frequency and H [s] is the system inertia, ΔP_{g} [p.u.] is the electrical power delivered by the generators, and ΔP_{l} [p.u.] is the power withdrawn by loads. The kinetic energy stored in the rotating masses of synchronous machines, is the only inherent energy storage buffer available to buffer power imbalances. The magnitude of energy stored, which is proportional to H, is typically enough to supply full load for 4-5 seconds [25]. Therefore, frequency regulation resources must react very quickly to disturbances. According to Nordic operation rules, 50% of the total balancing power from emergency reserves must be delivered within 5 s of a disturbance [26][3].

The response of the system to transient imbalances is determined by the magnitude of the power imbalance, the system's inertia and time constants on ramping up (or down) the primary and secondary frequency controlled reserves. During large imbalances, under-frequency load shedding [28–30], or other special protection schemes [31] are triggered and modify the system response. Adaptive underfrequency loads shedding schemes such as [32] have been proposed to optimize the timing and quantity of load shed, but are not in widespread use.

A common assumption for power system analysis is that the system frequency is uniform across an entire synchronous area. In a multi-machine sys-

[2]For comparison, the state of Texas, more than 10 times the area of Denmark, operates the smallest synchronous area in North America.

[3]In the Nordic region, primary frequency reserves are allocated is two categories: normal operating reserves, and emergency reserves. The timing requirements for the speed of response from normal operating reserves, active in the frequency range 49.9 - 50.1 Hz, are more lenient than the requirements for emergency reserves. Normal reserves have 180 s to deliver their full response. In contrast, the continental European equivalent of normal operating reserves are expected to begin their response within 2 s [27], which contributes to the significantly better frequency quality compared to the Nordic region.

tem, a large disturbance will cause the frequencies observed at various busses to be incoherent at very short time scales (from 10s of cycles to seconds) [33, 34], a phenomena a simple lumped generator model can not describe. Therefore care must be taken when analyzing the frequency observed in power distribution systems because it will have a wider distribution than the system average frequency [35]. In [36] the time taken for disturbances to propagate in a synchronous area was used to derive a limit to the geographic area can be safely served by frequency-sensitive load.

The analysis in Sec 3.2 does not explicitly assume that frequency is coherent in the synchronous area. The time-domain analysis in Sec. 3.3 does rest on the assumption of a coherent frequency across the synchronous area. Considering the time-scale of the frequency data (1-minute averages), this assumption does not compromise the accuracy of the analysis.

2.1.2 Speed Droop Governors

In the event of a disturbance, primary frequency regulation acts to stabilize the frequency on short time scales (milliseconds to minutes) by reestablishing the balance between generation and load. Primary frequency regulation is done by a $(P - f)$ droop response which makes generator power inversely proportional to system frequency, shown in Fig. 2.2. The droop response results in a steady state frequency deviation, the magnitude of which indicates the amount of load on the droop controlled generators.

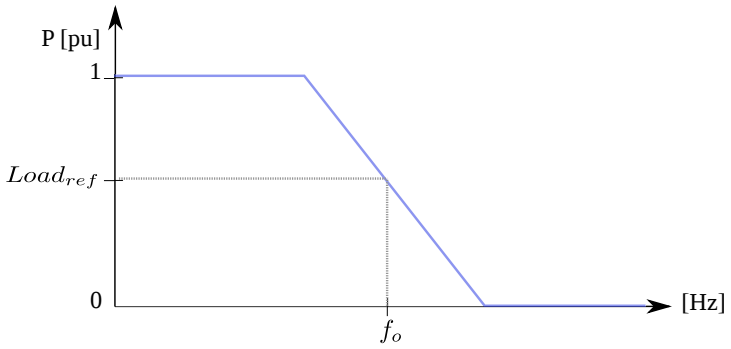

Figure 2.2: Droop Controller. Power output is shown as a function of system frequency. The scheduled power ($Load_{ref}$) is produced at the nominal frequency (f_o). The y-axis shows the power output of the generator capacity allocated to frequency regulation, which in practice, may be a fraction of the total capacity.

Large synchronous generators are characterized by relatively slow response times to operating point changes. When a change of output power is requested of a thermal power plant, time delays are introduced by the combustion of fuel, transfer of heat to steam, and the inertia of the turbine mass. The spinning mass of the rotor contributes inertia to the system (H in eq. (2.1)), limiting the ROCOF during imbalances. Motors also contribute to system inertia, but relative to the rated power they contribute less than half the inertia of generators [37].

At times of high VG production, central generators are taken off-line, and

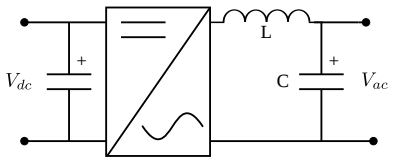

Figure 2.3: Inverter with LC output filter functions to convert DC primary energy into AC [F].

they are not available to provide frequency regulation services. VG, such as wind power plants, can provide frequency regulation services [38], but at the cost of spilled energy[4]. When a thermal generator is part-loaded, the fuel not burned (relative to full load production) can be saved for later. Wind power plants producing less than their potential do not have the same option of storing fuel for later; the unused wind energy is spilled.

The control hierarchy for wind power plants is comparable to conventional energy sources because they offer an interface to a centralized plant controller. Distributed generation (DG) can also provide frequency regulation services, but the practice of "fit and forget" means that these resources are not part of a centralized control system. The behavior of the DG is specified at the time of manufacturing, and the control rules are difficult to change after the devices are deployed. This can create a problem when uncertainty about the future causes a behavior considered desirable in one system configuration, to become a liability when the system development takes an unexpected turn.

For example, in Germany, PV was required to curtail power injection when the system frequency rose above 50.2 Hz. As PV capacity exploded, this security protocol turned into a threat to the system because all PV units were designed to instantaneously and simultaneously cut all power production during overfrequency events [39]. Revised grid codes now require a gradual ramp-down of production at high frequency, just like droop controlled generators [40].

Flexible loads providing frequency regulation services can avoid spilling VG, but they must be deployed in a manner that avoids large step changes in load. The algorithms and parameters of autonomous loads must be carefully chosen before they are deployed, because they can be difficult to change in field. These topics studied in Chapter 3.

2.1.3 Empty Networks

Since the dawn of the electric age at the end of the 19th century, rotating machines have been in use, and they continue to supply most power today. PV and variable speed wind turbines are fundamentally different from rotating machines because they use power electronics to interface to the AC power system. Semiconductors are used to create solid-state switches to regulate the flow of current through circuits; real-time software controls the state of the switches. An archetypical DC-to-AC inverter is shown in Fig. 2.3

Voltage source inverters (VSIs) are not constrained by the swing equation (2.1), and their response to changes in load is a function of sampling times and

[4] An exception to this generalization is short-term inertial response, which can be provided without spilled energy.

switching times, on the order of microseconds. Inverters can be programmed to supply virtual inertia by adjusting power output based on ROCOF, but their ability to deliver power above their rated maximum is limited by the short thermal time constants of semiconductor components. Networks dominated by power electrics interfaced energy sources don't have frequency variations. If all motors are also interfaced by power electronics (as in variable speed drives), then the network does not have any physical inertia, creating an "empty network" [41].

This lack of inertia gives power sources the ability to rapidly modify system frequency, a degree of freedom that is applied to power line communication in Chapter 6.

2.2 Voltage Regulation

Utilities are required to deliver voltage to their customers within specified limits [16,42]. Loads are designed to operate within those limits, and may malfunction if voltage levels deviate from those specifications, even if the duration of such an excursion is only a few milliseconds. Voltage quality is a broad topic [43], covering phenomena from high frequency transients and harmonic distortion, to voltage swells and sags occurring over minutes. The focus of the work in Chapter 4 is on power quality at relatively long time scales, specifically overvoltage and undervoltage conditions. In [16] overvoltage is defined as occurring when the 10-minute moving average of RMS voltage exceeds 10% of the nominal value, undervoltage occurs when the 10-minute average voltage is 10% below nominal.

RMS voltage is regulated at all levels of the system (transmission, sub-transmission, and distribution), with wider tolerances for variation accepted farther down the hierarchy.

Voltage will drop as power is transmitted through the distribution lines from source to load. The voltage drop ΔU[V] is caused by both active and reactive power:

$$\Delta U = IRcos(\Theta) + IXsin(\Theta) \tag{2.2}$$

where Θ is the power angle, I[A] is the current and $R[\Omega]$, $X[j\Omega]$ are the resistance and reactance of the transmission line. In high voltage (130 kV and higher) (HV) transmission systems, line reactance is greater than resistance, and AC power flows are commonly used approximated using DC power flow analysis, which ignores the effect of line resistance entirely.

Transmission systems generally regulate voltage using central generators, capacitors, and inductors to dispatch reactive power. In extreme contingencies, under-voltage load shedding can be applied [44,45], but like conventional under-frequency load shedding, it operates at course granularity, and is used only as a last resort.

In the low voltage (400 V and lower) portions of the network, the lines are predominantly resistive, so the active power component dominates voltage drop in these line segments.

2.2.1 Feeder Voltage Regulation

Typically, at the interface between transmission systems and distribution systems, voltage regulation devices smooth variations in transmission system volt-

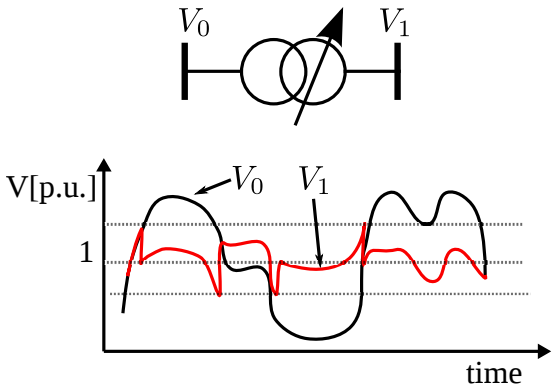

Figure 2.4: Schematic depiction of OLTC (top). The voltage at the input and output terminals (below) shows that the OLTC reduces the range of voltage variation at the output.

age, and hold the voltage on the transformer's secondary circuit within fixed bounds. This is done with on-load tap changing (OLTC) transformers that mechanically switch the positions of taps to alter the winding turn ratio, the effect of which is shown in Fig. 2.4. The OLTC will control the position of the tap based on local measurements of voltage levels, creating a local autonomous feedback loop. Voltage regulators can perform line drop compensation, regulating voltage at a nominal supply point instead of the output terminals. When performing line drop compensation, transformer tap position is a function of supply voltage, and the current flow, where higher currents lead to higher output terminal voltage.

At middle voltage (50 kV to 1 kV) (MV) to LV secondary substations, OLTC are being introduced to address voltage constraints in LV distribution feeders with PV [46, 47], but this is a high-cost intervention [48].

Distributed Generation and Voltage Regulation

For the first century of power system design and operation, power distribution was assumed to be in one direction: from central bulk generators, through the bulk power transmission system, and down the hierarchy through distribution systems to loads. Distribution system planning and operation has matured in a era when only loads were located in distribution systems, and planners have made due with very sparse instrumentation of power flows. Typically, only the cumulative energy consumption of customers was measured, at quarterly or annual intervals. Load estimates for planning time scales extrapolate power consumption from these energy measurements using heuristic methods such as Velander's formula [49]. Using these estimates of peak loads, voltage profiles are then analyzed to ensure all busses have voltages within specified bounds. Methods like Velander's formula are expedient, but leave large margins of error, which in turn lead to conservative dimensioning practices.

The spread of DG makes such rough-and-ready estimates untenable because as the range of operating conditions increases, the estimation errors also increase. Distribution system operators need to account for reverse power flows

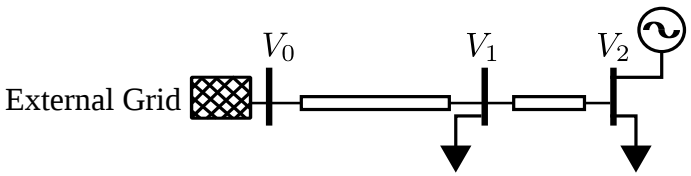

Figure 2.5: Simple feeder with 3 busses, and DG located at the end of the line.

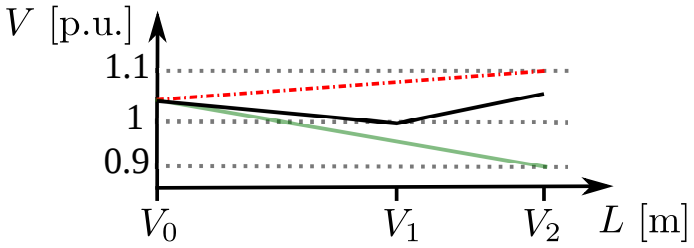

Figure 2.6: Voltage profiles of simple feeder. Voltage is fixed at 1.05 p.u. at the external grid connection. The light green solid line represents a typical voltage profile of a feeder without DG. The dashed red line shows the voltage profile of a feeder with DG production, and little load. The solid black line shows a complex voltage profile where the DG feeds part, but not all, of the load at bus 1.

from busses that produce more energy than they consume. Busses that produce power in a distribution system effect voltage profiles and protection systems [50–52]. In some networks, limits on current and thermal overload may limit the feasible DG penetration [53]. Both thermal constraints and voltage constraints place limits on the total system load (and DG production). The dependency of RMS voltage on the feeder load allows autonomous DER to infer feeder load by measuring RMS voltage. For illustration, a simple feeder is shown in Fig. 2.5, and the expected voltage profile on this feeder in 3 scenarios is shown in Fig. 2.6.

DG in the form of PV has seen explosive growth, not only in Denmark as described in the introduction, but all across Europe. Distribution system operators (DSOs) have not had time to adapt their networks to this rapid change, and the result is widespread overvoltages [47]. New DG in the form of household-scale wind turbines and micro-combined-heat-and-power (μCHP) are on the horizon, and may further stress LV networks.

The control of DG to regulate voltage is well studied [54–58] and has matured to the extent that these techniques are now written into grid codes [40, 58]. Methods to control DG for voltage regulation fall into 3 general strategies:

- **Constant cos φ**: DG output has a fixed ratio of active to reactive power. At unity power factor, the DG maximizes it's power output without considering voltage constraints in the LV network. A power factor less than unity mitigates the voltage rise, while leading to more line losses.

- **cos φ(P)**: The power factor is reduced as production increases. This method compensates for the voltage rise caused by injecting DG power.

- **Q(U)**: Reactive power absorption proportional to line voltage. This strategy lowers power factor only when line voltage rise occurs.

In the cos φ(P) and Q(U) methods, reactive power output is a piecewise linear function of the inputs (power and voltage, respectively). The stability of systems with multiple Q(U) controlled generators was investigated in [59] in simulations backed by laboratory validation. They found that high gain values can cause significant voltage oscillations.

In [60], they show that the distributed autonomous provision of reactive power from DG with Q(U) control achieves similar performance to an optimal centralized scheme. In [55] and [54], they propose curtailing active power production when voltage rises above the DG's ability to absorb reactive power.

Load can also be controlled to stabilize voltage in a feeder. This is attractive because the DG energy can be fully utilized by loads without increasing line losses or spilling primary energy. This is the subject of Chapter 4.

2.3 Microgrids

In the taxonomy of power systems, there is no rigorous definition of a "small island" microgrid; Ireland, home to more than 6 million people, can be called a "small island" power system. In this work, a "small island" microgrid is considered to be much smaller than Ireland, or even Bornholm[5], on the order of peak loads less than 1 MW. This type of power system is found on in isolated locations, such as very small islands[6], and in rural regions of developing countries. The vast majority of these systems are supplied by generators burning liquid fuel (i.e. diesel). Diesel motors are a mature technology, but have a number of drawbacks: fuel cost, maintenance cost, and emissions[7]. In the past 10 years, world market prices for liquid fuels have tripled, in nominal terms. Delivering fuel from supply hubs to remote locations greatly adds to its cost.

Meanwhile, the cost of RES alternatives to diesel generators have fallen. According to [61], nominal PV system prices have fallen by two-thirds in the past 6 years. Without subsidies, the levelized cost of energy from RES is now competitive with diesel generators [62]. In the future, microgrids may increase in importance as a method to increase reliability in large power systems with DG. Today, anti-islanding features are required in DG, forcing them to trip offline if the grid to which they're connected collapses [63][8]. This is a mechanism to ensure the safety of workers servicing the distribution system. But if these safety concerns can be addressed, allowing DG to continue to run when the bulk power system collapses can reduce the frequency and duration of service interruptions of customers in the vicinity of DG. Operating a distribution system as an intentional island with DG was demonstrated in Denmark with the "Cell Project" [64, 65].

[5] Bornholm, Denmark is home to around 50,000 people.

[6] Such as Christiansø, Denmark, population around 100.

[7] Emissions from burning diesel include noise, particles, volatile organic compounds (VOC), and CO_2.

[8] DG are also required to ride-through short-term faults in the system. Careful choice of timing requirements is needed to balance the conflicting goals of stability in the presence of short-term faults, and the need to avoid islanded operation.

Besides relatively high costs of energy, microgrids are challenging environments because the capacity margins[9] are smaller, and reliability is generally lower. System frequency is especially volatile in microgrids supplied by rotating machines because of the low level of inertia, and frequency constraints can be a limiting factor to integrating fluctuating VG [66]. At the other extreme, migrogrids supplied by VG can be considered "empty networks", described in Sec. 2.1.3, without any frequency disturbances. Microgrids are interesting test cases for applying new technology because there is a wide diversity of systems, and more degrees of freedom when planning interventions: system-wide changes in the generation fleet, distribution lines, and loads can be considered feasible.

In [67] a comprehensive review of microgrid control is given. The resistive nature of microgrid conductors requires control paradigms fundamentally different from those adapted to large-scale systems with inductive (or capacitive) HV lines [68–70]. Analysis of HV transmission lines often neglects line resistance, so system frequency is assumed to depend only on the active power balance, and voltage depends on the flows of reactive power. In microgrids, the decoupling of frequency regulation and voltage regulation is not appropriate because voltage depends on active power flows, and (on very short time scales) system frequency is influenced by reactive power flows. These analytical insights can be applied to all distribution systems, interconnected systems and microgrids alike. The load control system described in Chapter 5 shows the advantages of coupling frequency regulation controllers and voltage regulation controllers in demand-side resources, and the results are not restricted to islanded microgrids.

The power line communication system described in Chapter 6 is especially relevant to microgrids, since microgrids are already operated at off-nominal frequencies, and their low inertia allows relatively rapid communication speeds [F].

2.4 Demand-Side Management

One of the most effective methods of increasing end-use energy efficiency is to provide energy consumers with direct feedback on their patterns of power usage [71]. Investments in improving energy efficiency often have high returns, but in themselves they do not improve the flexibility to adapt in real-time to fluctuating VG output.

For real-time services, demand-side resources are used to increase the security of operations (by responding to rare, but serious contingencies), and increase the economic efficiency of normal operations (by deferring demand from expensive peak load periods). A recent review of the opportunities and challenges of providing real-time ancillary services from flexible demand-side resources is found in [72]. A key difference between ancillary services supplied from dispatchable central generators and ancillary services from demand-side resources is that the primary purpose of demand-side resources is to provide an energy services to users. The flexibility to vary the timing of power consumption is limited by the tolerance of energy users to degradations in their energy service. When the need to provide ancillary services conflicts with the need to provide end-use energy services, priority is given to ancillary services only in emergency

[9] Capacity Margin: ratio of installed capacity to peak load

situations where the integrity of system is in question. Otherwise, during normal operation, providing high quality end-use energy services is the first priority.

Industrial loads are attractive for providing ancillary services because relatively few industrial load have relatively large demand. Controlling large loads eases the administrative burden of recruiting, managing, and compensating participants, and allows rigorous (and expensive) monitoring and verification protocols. But industrial loads are often custom-made, each one requiring specialized knowledge to be adapted to provide ancillary services. Like other centralized ancillary service providers, there is risk that their services can become stranded if line outages isolate the ancillary providers from the areas where their services are needed. In the future, the loads providing ancillary services may become smaller and greater in number. When serially produced appliances are designed to provide ancillary services, the engineering costs are amortized over many devices. For the smallest, mass-produced loads, the cost-benefit tradeoff will favor load control strategies with minimal hardware costs. Small loads are attractive providers of ancillary services because they are geographically distributed throughout the power system, located close to the (uncontrolled) load, and DG.

Two broad categories of load control are recognized: direct load control, and indirect load control (i.e. control by price) [73]. Chapter 6 of thesis is focused on direct load control.

2.4.1 Direct Load Control

Existing systems for real-time demand response are mainly direct load control (DLC) schemes, where the utility controls a remote ON/OFF switch from their operations control room. Participants in these load management schemes are typically compensated with a fixed incentive, regardless of whether their resources were activated during a specific event or not. Often, there is no direct feedback to the users when their load is curtailed; the users should not notice any inconvenience, so there is no reason to draw attention to the demand response events. In the residential sector, DLC is typically targeted towards high-power flexible appliances, such as residential air conditioners or hot water heaters.

The DLC scheme fits into the existing structure of utility operations, shown in Fig. 2.7, where all assets respond to control signals with a very high level of reliability. In this architecture, a utility controlling levels 1 and 2, sends signals to demand-side resources located at level 3 of Fig. 2.7. This control signal is a setpoint whose value must incorporate knowledge of the appliance to be controlled. Level 4 would represent a local controller, such as a thermostat, controlling the final energy using process. Load aggregators can create virtual power plants to mimic the services of traditional power plants using a fleet of smaller assets spread over a large area to deliver ancillary services. A figure similar to 2.7, but more generic, can be found in books on computer-controlled automation such as [74] and [75].

This classic control structure has been applied to demand response in [77]; Fig. 2.8 shows the co-existence of local real-time control loops and a slower supervisory control loop. The topic of this thesis is algorithms and analysis of local control loops, the “behaviors” in the “controller” of Fig. 2.8.

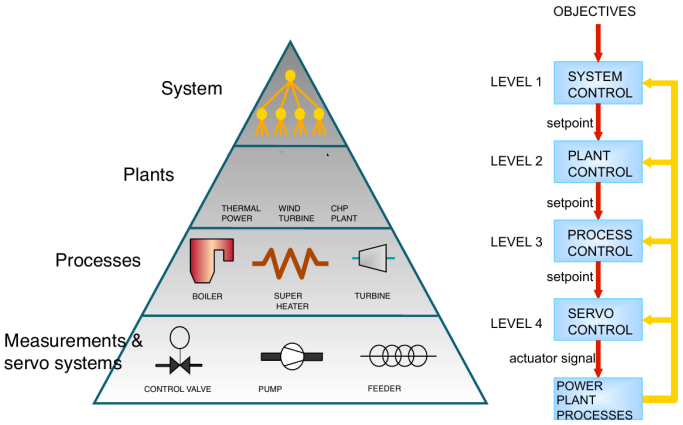

Figure 2.7: Typical hierarchical control of industrial system. The figure illustrates control of a thermal power plant (left-hand side), but the principles (right-hand side) can be applied more broadly to energy management systems including demand-side resources. Figure reprinted from [76].

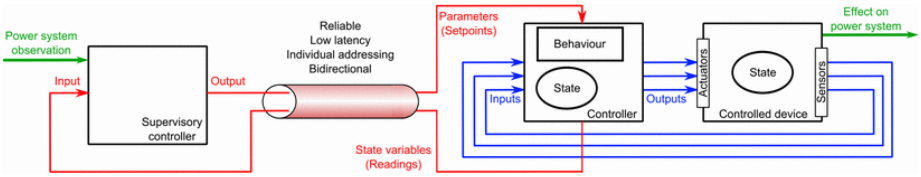

Figure 2.8: Architecture of a DER control system with central supervisory controller, and local real-time control loops. Figure reprinted from [77].

2.4.2 Communication Systems for Demand Management

Central power plants can easily justify the expense of a high-speed, highly-reliable dedicated communications media connected to system operators. Historically, high voltage substations were the next to be remotely monitored; often telecommunication companies provided fiber optic media to utilities in exchange for use of transmission line right-of-way. However, for controlling small loads, it is infeasible to create a communications channel only for providing power system services[10]. Instead of dedicated point-to-point communications media, DLC to small loads relies on broadcast communication using radio signals [78], or PLC [79].

Today, Internet backbone traffic is dominated by video entertainment and traffic originating from desktop PCs, but machine-to-machine traffic is growing at a rate 24% p.a. [80]. This communication between machines is the beginning of the "Internet of Things" (IOT) [81], a future scenario when all appliances (energy producing and using alike) are connected to a global data network. The IOT will allow sophisticated optimization of energy consumption, but a number of fundamental issues will need to be addressed in this scenario, namely:

[10]In some cases, loads may have communications resources to enable other valuable functionality, in which case power system services can piggy-back on these existing resources.

real-time constraints, and fault-tolerance. The extreme case of real-time constraints in the power system are protection systems which must break a circuit within a few milliseconds of a fault [82]. Frequency regulation also demands very rapid response (see 2.1.1). In keeping with the strict requirements for power system availability (N-1), operation must be resilient to any single fault in the system, including communication outages. These two factors motivate the use of autonomous load control algorithms, even in devices that have digital communications interfaces.

2.4.3 Thermal Load Modeling

One of the central problems with demand-side management is predicting and verifying the response to a given command. High fidelity measurements of each load would greatly increases the cost of the system. In a sparsely instrumented system, predicting responses is done by utilizing simulations models. Thermostat controlled loads (TCLs) are given special attention because they are a large [83], and flexible load class. The internal state of a TCL, and therefore its flexibility to provide ancillary services, evolves as a non-linear function of energy fluxes, which makes them challenging to model. The modeling problem is compounded when considering an aggregate population of heterogeneous devices.

For simple thermal models, thermal equivalent circuit (TEC) is a method of modeling thermodynamic processes using circuit diagrams familiar to electrical engineers. These models are well suited to serve as "grey-box" models for fitting measurements of single entities [84] by leveraging *a priori* knowledge about a system, but low order models can not describe the state of a population of devices. Simulations in Chapters 4 and 5 use TEC models of a domestic hot water heater, with a unique instance for each of more than 1000 loads in the simulated network.

The problem of modeling populations of TCLs in power systems was first addressed in the context of modeling the load during cold load pickup[11]. In [85], conventional electric load models are extended with a single parameter, the "harmonic constant", derived from the ON and OFF times of the load. This parameter then determines the fraction of load that will be active after a service interruption of a given duration. More recently, data-driven approaches to modeling a homogenous population of TCL using Markov chains are described in [86,87]. These models seek to represent a discrete distribution of temperature states of loads by observing (or more commonly, simulating) the probability of devices changing from one state to another.

The approach for load modeling used in Sec. 3.3 uses a more generic autoregressive moving average (ARMA) model as suggested by [88], a method which does not make use of *a priori* knowledge of the loads. This model has the form [89]:

$$x_t = \phi_1 x_{t-1} + ... + \phi_p x_{t-p} + w_t + \theta_1 w_{t-1} + ... + \theta_q w_{t-q} \tag{2.3}$$

where the estimate for the output at timestep x_t is a function of the previous p values of x_t, with weighting factors ϕ_i, and the previous q observations of an error process w_t, with weighting factors θ_i.

[11] Cold load pickup describes the situation when power is restored after a blackout, and a high load is initially observed as thermal loads recover their temperature to acceptable levels.

In [90] the problem of synchronization of hysteresis controlled TCLs is shown by statistical analysis. When TCLs curtail power demand in response to a system event, a rebound where power consumption spikes above the steady-state level occurs afterward to recover the desired temperature state. The paper addresses the problem of synchronization by proposing a stochastic load control algorithm where the probability of switching state is a function of system frequency. Compared to the demand response from thermostat offsets [91, 92], stochastic load control does a much better job of maintaining population diversity, and avoiding rebound peaks in consumption. But on its own it can not guarantee[12] compliance with temperature constraints. An aggregated model of this stochastic load control algorithm is described in [93]. In [94] an alternative method of avoiding large rebounds is proposed where loads remember their pre-curtailment state, and revert to that state to re-establish load diversity after an event.

The work in this thesis applies the more simple thermostat offset technique [91, 92], and addresses the issue of rebound load peaks by applying a voltage-sensitive controller in Chapter 5.

2.5 Autonomous Load Control

Sec. 2.4 showed how demand-side resources are currently utilized to provide ancillary services. Compared to classic central generators, the rated power of demand-side resources is 3-6 orders of magnitude smaller[13], and their number correspondingly larger. Methods for controlling demand-side resources must account for this fundamental difference in scale.

Autonomous control of supply-side power system assets is well established and was described in Sec. 2.1.2 (droop control for frequency regulation), and 2.2.1 (OLTC transformers for voltage regulation). These examples each illustrate different niches for autonomous control. Frequency regulation from central generators relies on the dynamic response of autonomous droop controlled plants to satisfy the strict timing constraints on providing frequency response. Voltage regulation from OLTC is geographically spread towards the edge of the network, with a relatively large number of units each regulating a small section of the network.

Today, systems are found that augment both of these autonomous control loops to optimize efficiency of the system. AGC coordinates the power setpoints of a fleet of generators to improve frequency quality, and remote control of OLTC is used to optimize losses and end-use efficiency[14] [95]. These practices show that autonomous control loops are not made obsolete in the presence of remote control.

The following sections describe previous research into autonomous load controllers for providing frequency and voltage regulation services.

[12] The probability of exceeding temperature constraints can be derived. Alternatively, the algorithm can be combined with hysteresis thermostat control, so that the stochastic behavior occurs in the deadband, but the TCL is forced to change state when a temperature constraint is reached.

[13] A thermal generation unit can easily exceed 100 MW rated power, while the loads under consideration are as small as 100 W.

[14] This practice goes by the name Conservation Voltage Reduction, or Volt-VAR Optimization.

2.5.1 Frequency Regulation

In 1979 a patent was issued for the "Frequency Adaptive Power-Energy Rescheduler" (FAPER) [96], a device that controls loads based on system frequency as an input signal. In 2001 the concept was extended in a controller that used fuzzy logic to switch loads for regulating system frequency [97]. This controller was implemented in a low-cost microcontroller and tested in microgrids with VG with favorable results.

In 2003 a low-cost proof-of-concept FSL controller was described in [98]. In 2007, a large scale[15] field trial of FSLs in the form of clothes dryers was conducted by researchers at the US Department of Energy's Pacific Northwest National Laboratory (PNNL) [99]. In PNNL's experiment, the resistive heating element of a clothes dryer was turned off during underfrequency events, while the fan and tumbler remained on.

In connection with [99], a design method for setting parameters of FSL was reported in [100]. The method analyzed a time series of historical frequency data, and then simulated the response of FSL with different sensitivity settings. The scope of this method was limited to looking at discrete devices (ON/OFF) providing up-regulation spinning reserve[16]. A similar method using historical data and simulations for choosing controller parameters is described in [101].

In [91] an algorithm for controlling TCLs as FSL was described. In the algorithm, the thermostat setpoint is varied as a linear function of system frequency. Models of the frequency dynamics of the UK power system were combined with first-order TEC models of refrigerators to simulate the behavior of the complete system. The effect of the FSL on system frequency was characterized, as well as the effect of the system frequency on refrigerator internal temperatures. When a system with fluctuating wind energy was simulated, the FSL had superior performance compared to conventional droop controlled generators because the fridges were able to react faster than generators. This frequency response was provided without unacceptable temperature fluctuations inside the fridges. An interesting detail in [91] was the proposal to recover deferred energy consumption by operating the system above nominal frequency after an underfrequency event. The purpose of this procedure is to quickly restore the state of the fridges to steady-state equilibrium.

In [102,103] the authors also propose intentionally varying system frequency to effect the state of FSL. They suggest using variations of system frequency to communicate real-time energy prices. Their simulations of FSL in the Indian power system with varying frequency setpoints show frequency-sensitive TCL has significant value in reducing the need for conventional regulating power. This proposal of intentionally operating a system at off-nominal frequencies to effect the state of FSL is a concept expanded to include discrete domains in Chapter 6.

In [104,105], frequency sensitive water heaters are simulated with wind power systems to demonstrate the effectiveness of utilizing demand-side resources for continuous regulation during normal operation. The unique aspect of the algorithm proposed in this work is to consider demand-side constraints from the

[15] 50 residential test subjects participated.

[16] Up-regulation services is provided by curtailing load. These appliances are interfaced to the power system by a relay which is normally closed, and which is opened briefly during underfrequency events

perspective of satisfying a given energy demand within a given time frame (i.e. recharging a hot water tank overnight). The duty cycle required to fulfill the energy demand then determines the frequency thresholds for turning the heaters ON and OFF.

In [106] constraints on loads are formulated exclusively as timing constraints (i.e. minimum OFF time, maximum OFF time, minimum ON time). Further, the algorithm for load control described in [106] accounts for the magnitude and duration of frequency excursions, and the simulation study includes a heterogeneous population of refrigerators, space heaters, and water heaters. Their results confirm that a smooth droop response can be created with a population of bimodal (ON/OFF) FSL.

In [107] the design of FSL is extended to divide a population of devices into N groups, where each group samples frequency once during a time interval T. This scheme tries to reconcile the need to provide a quick and strong response to frequency transients, with the stability concerns that arise from high-gain frequency-sensitive controllers [36]. For example, during a brief underfrequency transient, only one of the N groups may be curtailed, leaving the other groups in their steady-state conditions. A longer underfrequency event will curtail more load groups until finally, the FSL is fully curtailed.

In [92] FSL algorithms are described for both TCL, and relay controlled loads. The TCLs respond to frequency with a thermostat offset (like [91]), and the relay controlled loads have frequency thresholds and timing constrains (like [106]). The Nordic power system and the island of Bornholm are simulated with FSL. The simulations showed FSL improved frequency quality as measured by the nadir after a large fault and the frequency distribution during operation with high VG production.

A more abstract approach to modeling FSL was used in [108]. In this work, transmission systems are modeled with a given fraction of load being continuously modulated to provide frequency regulation. Scenarios with all frequency regulation services provided by loads showed fast and stable responses. More realistic simulations accounting for the speed of propagation of disturbances [34] and load timing constraints were examined in [109]. The results showed that the most critical parameter in designing the FSL was the speed of response: delays of more than 500 ms could cause instability in the system. Similar investigations on the UK power system in [110] found that delays over 1 s greatly reduced the contribution of FSL to frequency containment during contingencies, but delays up to 200 ms had no effect (relative to a no delay scenario).

The effect of FSL on large power system frequency dynamics was simplified in [25] with the concept of "effective inertia". Effective Inertia is created by FSL that react to ROCOF, rather than to the level of frequency. By reacting quickly to high ROCOF values, the effect on system frequency is comparable to physical inertia. Effective inertia is comparable to the virtual inertia delivered by inverters, but different in that inverters can act within one AC cycle, and the inertia provided by FSL has longer delays (i.e. 500 ms). The effective inertia model is only applicable during transient disturbances; at steady-state FSL stabilize frequency, an outcome which physical inertia can never achieve.

In [111], they compared system dynamics of the UK power system considering bottom-up load models of differing granularity. FSL in the form of thermal loads were lumped into TEC models with 10^2, 10^3, and 10^4 temperature states. The regulating power of the total FSL population was held constant, and the

study found that the model with the smallest granularity (10^2) did not accurately represent the dynamic behavior of the population, while the model with the finest granularity (10^4) did not substantially differ from the moderately detailed model (10^3), indicating that the optimal balance between accuracy and complexity is achieved with 1000 discrete units scaled to represent the power of the total population.

Finally, in addition to the simulation and experimental studies previously mentioned, in [112] an analytical model of frequency stability with FSL was analyzed. This model further formulated the conditions for optimizing the frequency response by accounting for the cost ("disutility") of response on the customers' side.

This ongoing research has attracted the attention of the European Network of Transmission System Operators for Electricity (ENTSO-E), whose proposed "Demand Connection Codes" [113] open up the possibility of requiring a frequency response in new TCLs. Justification for this mandate in [114] is based on cost-benefit analysis that shows attractive returns for investing in this technology. There is still large uncertainty in the assumed capital costs of the devices[17], and the monetary value of the frequency regulation service[18]. But notwithstanding that uncertainty, even the most pessimistic assumptions of the cost-benefit analysis found FSL in domestic TCL appliances to have a strong business case. Similar cost-benefit analysis in [92] found the cost of deploying FSL to be under half the cost of existing frequency regulation resources. Consideration of the economic effects of FSL refrigerators on generator dispatch in [20] found the value to be greatly increased in low-carbon future scenarios.

If such a mandate becomes law, device manufacturers will be required to submit device models to the transmission system operators (TSOs), though the format of such a model was not elaborated upon.

2.5.2 Voltage Regulation

Voltage quality has many aspects (see Sec. 2.2), and methods to improve voltage quality with controllable loads reflect that diversity. Autonomous load controllers have been proposed to reduce harmonic distortion in [115], and to speed up recovery from voltage sags [13]. These devices operate at short time scales, the first on the order of microseconds, the second on the order of milliseconds. The time scale of milliseconds is comparable to the response time of FSL, and some of the use-cases for the voltage-sensitive load (VSL) are also similar to FSL: large faults in the transmission system trigger disturbances in both frequency and voltage on short time scales over large areas, and curtailing demand can facilitate recovery from such faults.

Operating at longer times scales (minutes), several VSL schemes have been described to allow loads to mitigate overvoltages and undervoltages. A voltage droop response, where power consumption is modulated linearly as a function of measured RMS voltage was proposed for electric vehicle (EV) charging in [116]. The accompanying simulations show that voltage deviations are greatly reduced with a sufficiently large population of EVs. The simulations also show a clear correlation between the charging rate and location on the feeder; those nodes

[17] Estimated range between 2 € and 29 €.
[18] 6-22 k€/ MW / year.

farthest from the energy sources experience the lowest voltage, and therefore are controlled to charge the slowest. This location dependency breaks with the long-standing practice of providing equivalent service to all customers, and brings up questions of fairness. Related work in [117] describes a prioritization of loads to provide voltage response over a wide range of voltage values.

In [118] they partially address the fairness issue by proposing customized droop constants for each load based on its location in the network. The central objective of [118] is to compare voltage droop controlled EVs to a centrally controlled optimization scheme. The VSL had marginally worse performance compared to the optimal changing scheme, but it was a large improvement over the base case of uncontrolled loads.

Work in [68,69] shows how VSL can work together with power sources interfaced with voltage source inverters (VSIs) to optimally utilize fluctuating energy sources. They propose two load control algorithms: a voltage droop for loads able to continuously modulate their power consumption, and an algorithm with fixed voltage thresholds for load cutoff and reconnection suitable for discrete ON/OFF loads.

Electric springs [119] are a demand-side technology to adjust the power factor of loads to stabilize voltage, comparable to the Q(U) method of controlling of DG interfaced with power electronics (see Sec. 2.2.1). Followup work in [120] modified the original controller to automatically adapt the magnitude of the voltage reference to the local conditions observed at different locations in a feeder. The electric spring assumes that loads can operate on a wide range of input voltages and powers, a behavior only feasible with the use of power electronics.

2.6 Summary

This chapter has given a short review of power system ancillary services, and demand-side management. It has presented the background and context in which the original research results in the following chapters can be understood. In summary, non-dispatchable VG will call for new services from demand-side resources. These services will make use of flexible loads, especially TCLs. Today, autonomous local control is found in central generators, distribution system assets, and DG. Autonomous local control of loads has potential to provide ancillary services with very low implementation costs. The following chapters will demonstrate that potential, and address the limits to their adoption.

Chapter 3

Frequency-Sensitive Autonomous DER

Today, frequency regulation in power systems, described in Sec. 2.1, is mainly[1] done by central generators. Central generators are being removed from power systems to make space for RES. But even though the energy production of central generators is superfluous at times, their ancillary services, including frequency regulation, are still required[2]. This motivates the search for alternative frequency regulation resources that are compatible with power systems with high portions of VG.

After a frequency disturbance, the power balance can either be restored by modulating generation, or equivalently, modulating load in the opposite direction. In essence, the goal of the frequency-sensitive load (FSL) control algorithm described in this section is to mirror the generator droop response (see Sec. 2.1.2) from a population of loads. This is shown graphically in Fig. 3.1.

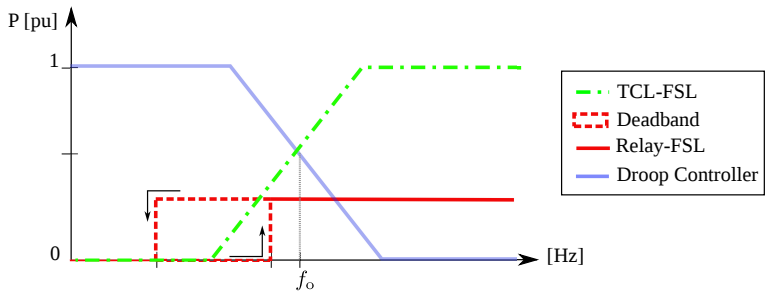

Figure 3.1: Power output (from droop controller) and consumption (of FSL) as a function of system frequency. The droop controlled generator response is the inverse of the relay-controlled FSL, and TCL-FSL response.

[1] In Denmark, large electric boilers in district heating plants have recently begun offering frequency regulation service.

[2] In Denmark, negative power prices on spot markets are partly caused by the need to maintain minimum load levels on those thermal generators that "must-run" to provide ancillary services.

3.1 Experiment Description

The project "Demand as Frequency-controlled Reserve", funded by the Danish government's Energy Technology Development and Demonstration Program (EUDP), aimed to demonstrate FSL providing frequency reserves on the island of Bornholm [121]. The project logo, with logos of all the project partners is shown in Fig. 3.2. The local DSO, Østkraft, helped with recruiting participants, Danfoss and Vestfrost supplied the energy using appliances, and Ea Energianalyse collaborated with the Technical University of Denmark (DTU) in processing and presenting the experimental data.

Figure 3.2: "Smartbox- Experiment with the electric power system of the future". Demand as Frequency-controlled Reserve project logo with DTU and partners. A sticker with this image was placed on the cover of each experimental Smartbox.

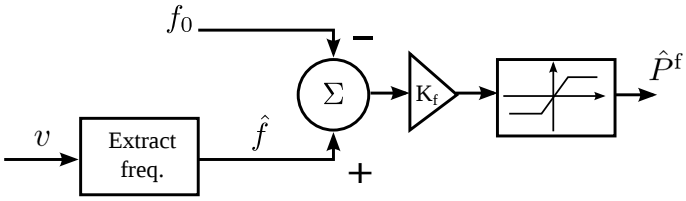

Figure 3.3: Block diagram of FSL controller. The constant f_o is the nominal frequency, K_f is the controller gain, v is the mains voltage which is sampled and processed to estimate the system frequency $\hat{f}$. The range of the output $\hat{P}^f$ is limited.

The details of the experimental setup, and initial proof-of-concept results, are described in [A], see Appendix A.

Aggregate power consumption of TCLs is controlled to be proportional to the system frequency, as depicted in the block diagram in Fig. 3.3. TCLs can map the control signal, $\hat{P}^f$ in Fig. 3.3, directly (linearly) to thermostat offsets. While each TCL is an ON/OFF discrete device, the diversity of the internal

temperature states of the devices creates a smooth frequency response in aggregate[3]. For other experimental devices controlled by a relay, a smooth response could not be provided. Instead, the relay-controlled devices were programmed to all turn OFF at a given frequency threshold, and turn ON again at a higher threshold, creating a simple hysteresis, shown in Fig. 3.1 and Fig. 3.4.

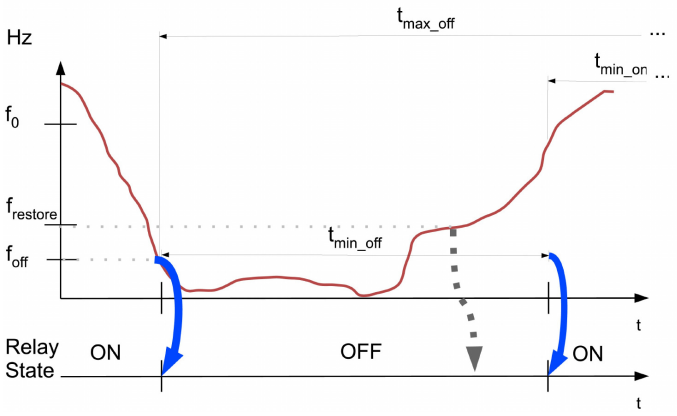

Figure 3.4: Timing constraints of relay-controlled frequency controlled loads. The action of the controller is shown with solid blue arrows, and the dashed gray arrow shows the action that would be taken in the absence of timing constraints. In the scenario shown, the frequency first drops under f_{off}, and then rises above f_{restore} before the minimum OFF time constraint is fulfilled.

Fig. 3.4 shows that the state of the relay is a function of both frequency constraints, and timing constraints. The role of timing constraints is to respect the needs of the end-use energy service; the need to maintain a given level of energy service takes precedence over the frequency response. The implications of timing constraints for the system behavior are discussed in Sec. 3.4.

The control box implementing this algorithm, called the "Smartbox", shown in detail in Fig. 3.5, was produced by DTU using off-the-shelf components. The Smartboxes were connected to the thermostats of refrigerators and heaters through a serial cable, shown in Fig. 3.6. The refrigerator itself was a bottle cooler designed for commercial use. Compared to a residential refrigerator, this model of had a larger compressor, and higher thermal losses[4]. The analysis in [20] found that relatively poorly insulated TCL appliances with a duty cycle closer to 50% provided better frequency regulation service. This suggests that FSL controllers in commercial refrigerators, like the ones used in this experiment, will be more valuable per appliance, than FSL controllers in residential refrigerators.

[3]This holds for a sufficiently large population of devices. The experimental results included data from 30 devices, which was not a large enough population to see a smooth response in timeseries graphs.

[4]Sources of thermal losses not present in residential fridges were the glass door, and the frequent opening of the door.

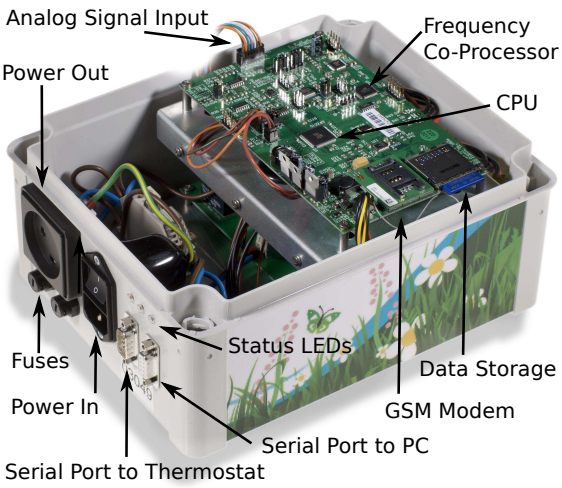

Figure 3.5: Close up of the with cover removed. Analog board (not shown) located under the digital board contains voltage divider and current measurement coil. These measurement circuits feed signals into the analog signal input.

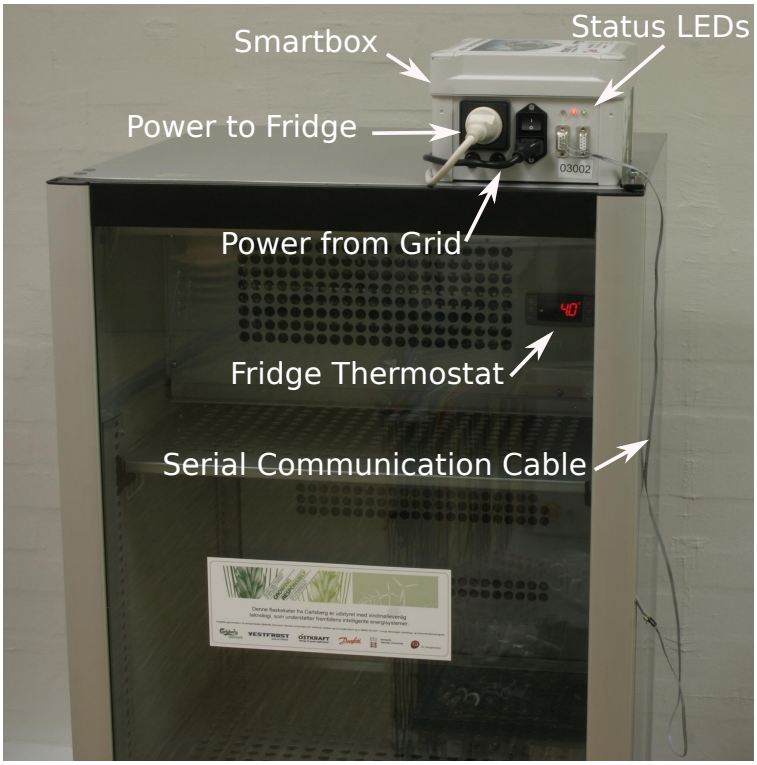

Figure 3.6: Smartbox and refrigerator with programmable thermostat. Note: In the field deployment, unlike the lab setup pictured, the serial communication cable was connected to the thermostat through the rear of the fridge without compromising the door seal.

3.2 Results of Experiment

Figs. 3.7 and 3.8 illustrate the effect of the frequency response on the refrigerator duty cycle and internal air temperature respectively.

The behavior of the TCL-FSLs providing frequency regulation services are described in detail in [B1], see Appendix B.1. The behavior of the industrial and relay-controlled loads is described in [B2], Appendix B.2.

The different loads tested (refrigerators, heaters, and relay-controlled loads) were each suitable for different services. Refrigerator load has diurnal variation, but little seasonal variation, and the size of their thermal energy storage buffer allowed load shifting for around 6 minutes. This time scale is sufficient for secondary frequency reserves to respond. Space heater load was highly seasonal, but offered very large scope for load shifting (45 minutes), large enough to allow the start-up of tertiary reserves. The TCLs were able to provide up- and down-regulation services; the relay-controlled loads were only suitable for up-regulation service. Considering that up-regulation is much more valuable than down-regulation, this is not a serious limitation in relay-controlled loads.

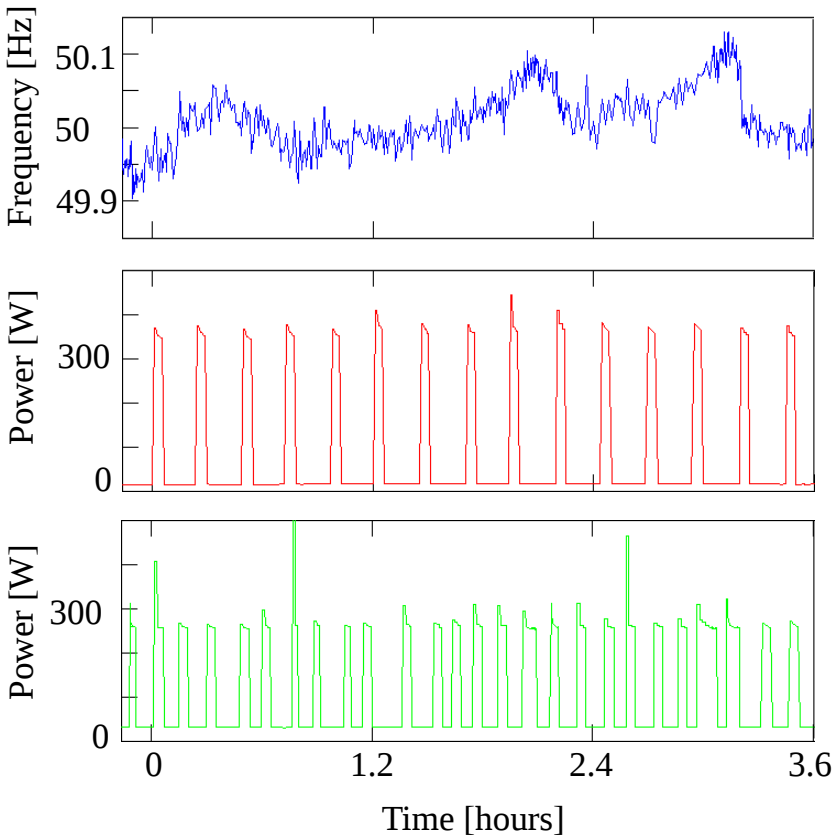

Figure 3.7: Timeseries of frequency and power of one standard refrigerator and one FSL over 3.6 hours. The two refrigerators differ only in the rated power of their compressors and their contents. System frequency (top) has extended periods above and below nominal values. The standard refrigerator (middle) has a regular duty cycle. The duty cycle of the FSL (bottom) is irregular because it is influenced by the system frequency. In the FSL some of the startup transients are captured in the data set.

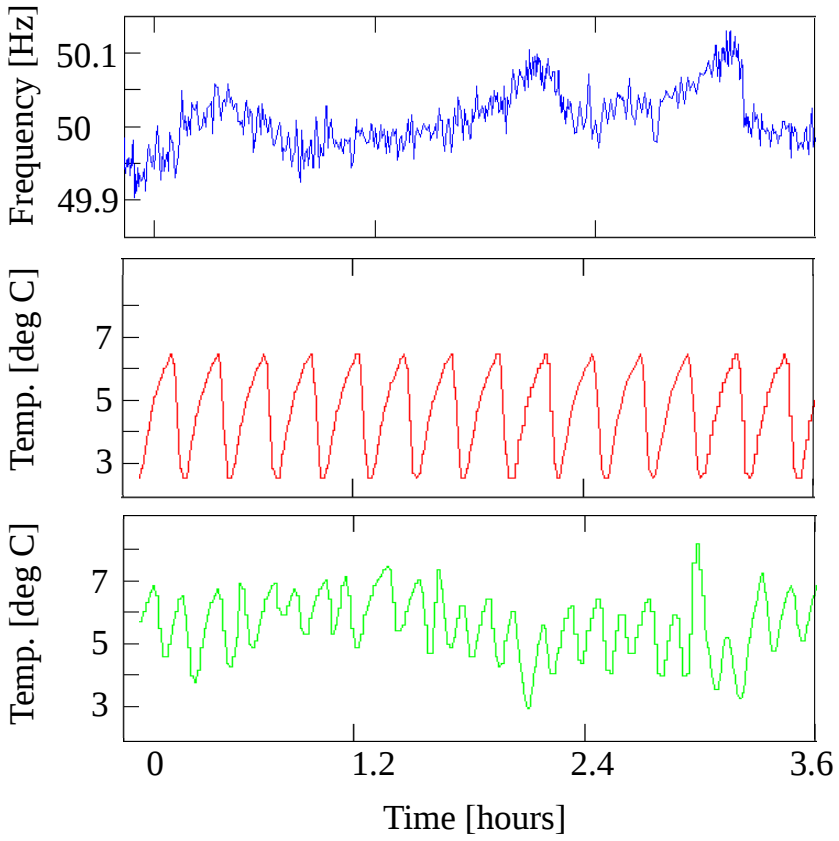

Figure 3.8: Timeseries of frequency and internal air temperature of one standard refrigerator and one FSL over the same 3.6 hour time period as shown in Fig. 3.7. Top: system frequency, Middle: temperature in standard refrigerator, Bottom: temperature in FSL.

3.3 Load Model

An autoregressive moving average (ARMA) model is used to estimate values of the aggregate refrigerator load as a function of system frequency. This form of model was chosen because it can be relatively easily imported into existing power system frequency analysis tools, such as [122]. To create a viable model, the raw data must be first pre-processed, and then a best-fit of parameter values is found. This modeling approach is justified by an earlier report [88] that fit ARMA models to aggregate FSL data derived from simulations.

3.3.1 Data Pre-Processing

The raw timeseries data collected from each refrigerator was subject to discontinuities, as Smartboxes were occasionally turned off. Data was sampled at 60 s intervals for the entire experimental period, and at 2 s intervals during underfrequency events and overfrequency events. If a discontinuity in a Smartbox data persisted for 10 minutes, the device was considered inactive until new data was received, otherwise, a zero-order hold was assumed for the time between samples. An aggregate timeseries of system frequency, power consumption, compressor state, and the number of active units was constructed over the entire experimental period of 105 days. The number of active units was used to normalize the timeseries by deriving the average power consumption per fridge, and the percentage of active compressors (duty cycle). When the aggregate timeseries was constructed, the timestep between samples was not constant because of the variable sampling interval mentioned earlier, and because the device sample times were not synchronized.

This aggregate timeseries with variable timestep, was then downsampled to a constant 60 s time step. All samples within the 60 s timestep were averaged together. With this one minute timeseries, the longest continuous interval with at least 15 active devices was found. Within this 10 day interval, the first day was used to train the model fitting function, and the following 9 days were used to validate the goodness of the model fit.

3.3.2 Model Fitting

The built-in functions of Matlab's System Identification toolbox were used to fit ARMA models to the training data. System frequency was the control input, and the duty cycle of the population of refrigerators was the output. Aggregate power consumption was also examined as an output for model fitting. Fitting a model to average power consumption data was less accurate than fitting duty cycle because the average power consumption was subject to considerably more noise than the duty cycle data. For example, power consumption data shows a spike around 4-times greater than rated power in the moment when the compressor turns ON, as the motor accelerates [14] (a few such spikes are visible in Fig. 3.7). Even the high-resolution 2 s sample time was too long to capture this spike reliably, and as a result the data during this transition shows considerable variance.

Table 3.1: ARMA Parameter Values

Index i	ϕ_i	θ_i
1	-1.856	1.727
2	1.321	-0.820
3	-0.427	-1.403
4	-0.061	0.149
5	0.119	0.180
6	-0.064	0.172
7	0	-0.304
8	-0.040	0.056
9	-0.026	0.292
10	0.040	-0.049

3.3.3 Load Model Evaluation and Discussion

In terms of the ARMA system model of eq. (2.3) introduced in Sec. 2.4.3, the best-fit of the training data has the parameters shown in table 3.1. When comparing the ARMA model output with the validation data set, shown for a representative time slice in Fig. 3.9, the normalized root mean squared error was 16 % indicating a poor agreement between the model output and the validation data set.

For the purposes of studying the effect of FSL on load flows in power distribution systems, it is the variance of the power consumption, rather than the timing that is of primary importance. In this respect, the model also falls short, as shown in Fig. 3.10. The model variance of FSL duty cycle was 9×10^{-3}, while the measured data had a variance of 26×10^{-3}. It may be that the ARMA model successfully represents the behavior of a large population of devices, but the experimental data can not be extrapolated to defend or reject this hypothesis. Despite these shortcomings, the ARMA model closely fits the experimental data when looking at the frequency response, shown in Fig. 3.11.

Finally, in Fig. 3.12 the step response of the ARMA model is shown. There is no comparable experimental data in this case, but some attributes of the model can be revealed by exposing it to step-change input. First it should be noted that the model uses one-minute time steps, so this scenario does not represent a sharp drop in frequency, the ROCOF is only 1.7 mHz/s. The response of the ARMA model to the fall (rise) in frequency shows that the duty cycle nadir (maximum) occurs after 3 minutes and is more than 40 % below (above) the average duty cycle. In the field data, the average duty cycle of the refrigerators was 33 %, so when using this model care must be taken to limit the duty cycle to be greater or equal to zero, otherwise the loads will show a negative duty cycle. After each step change, the ARMA model shows a rebound in duty which peaks 18-19 minutes after the step change. In both step changes, the rebound does not reach (nor exceed) the duty cycle before the step change.

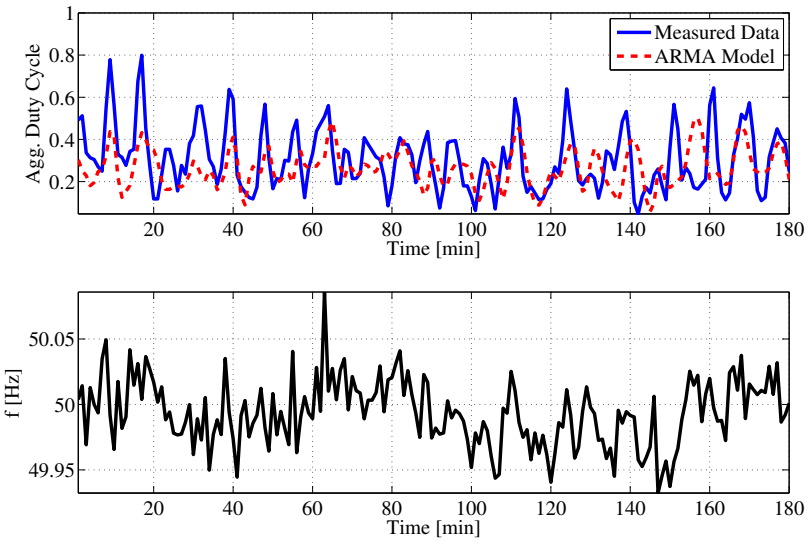

Figure 3.9: Timeseries of ARMA FSL model and measured data for a representative 3-hour period. The duty cycle of the refrigerators is shown at the top, the system frequency is shown below.

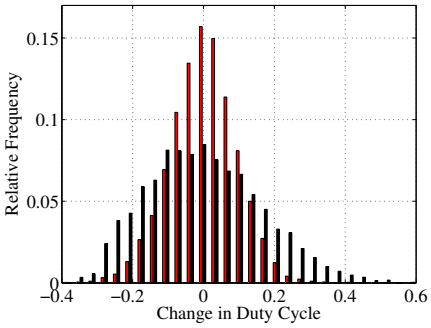

Figure 3.10: Relative frequency of duty cycle of ARMA (salmon colored) and measured data (black) over the 9 day validation data set. The duty cycle is plotted relative to the steady-state duty cycle. The ARMA model has more narrow, and more symmetric duty cycle changes than the measured data.

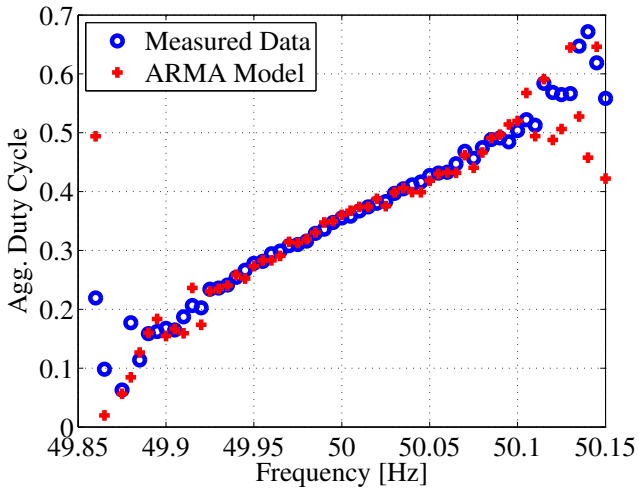

Figure 3.11: Refrigerator duty cycle vs. system frequency for ARMA model and measured data. They show good agreement in the active region 49.9 - 50.1 Hz. Outside this region, the controller is saturated and the data is sparse, leading to wider variance.

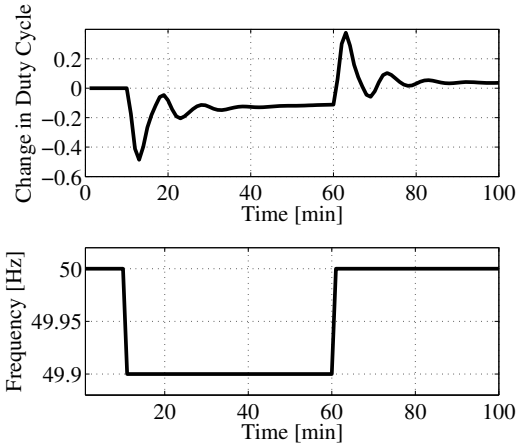

Figure 3.12: Timeseries of step response of ARMA FSL model for a 100 minute time period. In this scenario, the frequency drops by 100 mHz in minute 10, and then is restored to the nominal value in minute 60. The deviation in duty cycle relative to steady state is shown at the top, the system frequency is shown below.

3.4 Time Constraints

When demonstrating relay controlled loads for frequency regulation, the initial results were not a success [B1]. Timing constraints were chosen conservatively in the absence of detailed knowledge of the loads under control. The timing constraints dominated the response, so the relation between system frequency and average power consumption was the inverse of the intended, shown in Fig. 3.13. In this trial, relay devices were configured to turn OFF at frequencies below $f_{\text{off}} = 49.90$ Hz, and ON at $f_{\text{restore}} = 49.95$ Hz. The minimum OFF time was set to be $t_{\text{min\_off}} = 30$ s, maximum OFF time $t_{\text{max\_off}} = 180$ s, and the maximum reconnect time set to 6 minutes, $t_{\text{min\_on}} = 320$ s.

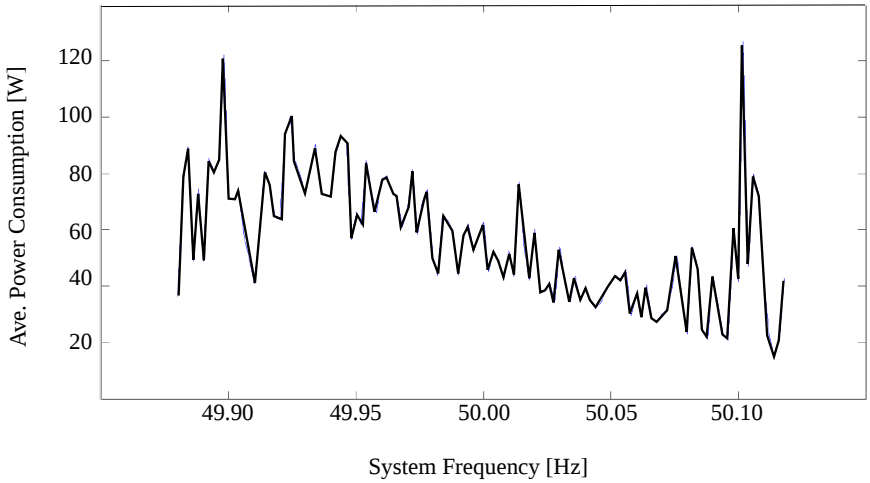

Figure 3.13: Frequency response of poorly configured relay FSL. Note: The density of samples at frequency extremes (< 49.92 Hz, > 50.08 Hz) is low, resulting in a larger variance.

A simple hypothesis might suppose that the timing constraints would cause power to be uncorrelated with system frequency. Instead, the response is negatively correlated with system frequency because of the spike in power consumption when the devices transition from the OFF to ON state. The dominating time constraint in the typical timeseries shown in Fig. 3.14 is the maximum OFF time $t_{\text{max\_off}}$. When $t_{\text{max\_off}}$ expires, the controller restores power to the load, causing the previously mentioned spike of inrush/upstart power consumption. This restoration of load occurs especially at low frequencies, and this explains the poor results of this trial.

Simulations of microgrids show a large problem associated with timing constraints in FSL when a low number of FSL comprise a large portion of total load, see Appendix E. The work in [109] showed timing constraints[5] for emergency up-regulation were not a problem at short time scales, but [93] showed that for continuous regulation the effect can be significant.

[5]They investigated the effect of "inhibit restore" in air conditioning loads. This function prevents the compressor from quickly restarting after being turned OFF. Refrigerators are subject to the same constraints.

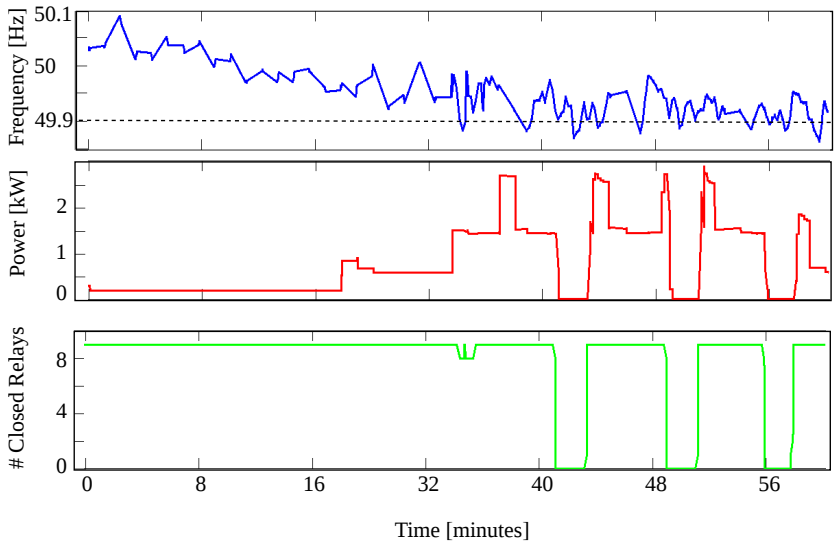

Figure 3.14: Typical timeseries of 8 poorly configured frequency-sensitive loads over one hour. System frequency (top) declines in the time period, and around minute 40, it falls under the f_{off} threshold (49.9 Hz). The state of the FSL relays (bottom) shows they all turn OFF at this point, and aggregate power (middle) falls to zero. After $t_{\text{max\_off}}$ the relays turn the loads ON again, resulting in a spike of power consumption, even though the system frequency is still critically low. The relays open again after $t_{\text{min\_on}}$ expires, and the cycle repeats.

This problem can be handled by a better choice of configuration parameters, specifically, more relaxed time constraints, or lower f_{off} so that devices turned OFF less often, for shorter times. In [100] and [101], they approach the parameter selection problem empirically, by gathering historical frequency data from the target power system, and simulating the response of FSL with different configuration parameters.

In most cases, choosing FSL configuration parameters will be the only way to avoiding the predominance of timing constrains, but in some cases, for example micro-grids, the system frequency itself can be changed to make it compatible with a given FSL configuration. This is to say that, instead of taking the distribution of system frequency as an exogenous parameter, the system operator can configure other (conventional) frequency regulation resources to produce a desired system frequency distribution. Shaping system frequency to be compatible with FSL is an alternative method for dealing with timing constraints, and is discussed further in Chapter 6.

3.5 Reduced Load Diversity

Besides accounting for timing constraints in FSL, a second problem with operating systems with FSL is creation of new demand peaks as FSLs are synchronized. Synchronizing demand is an intended consequence of operating FSL; they should consume more power when system frequency is high. But if FSL is widely deployed, some distribution lines may become overloaded if high resid-

ual demand occurs together with FSL peaks. FSL peaks obviously occur during down-regulation[6] , but new peaks may also result from up-regulation. When power consumption is curtailed for up-regulation, it is later recovered in the so-called "rebound effect".

In the experiment described in [B1], the frequency response of the electric space heaters depended on the ambient temperature. In a subset houses on moderately cold days[7] it was observed that the electric heaters were able to provide a frequency response that ranged from 90% of full rated power to complete curtailment, see Fig. 3.15.

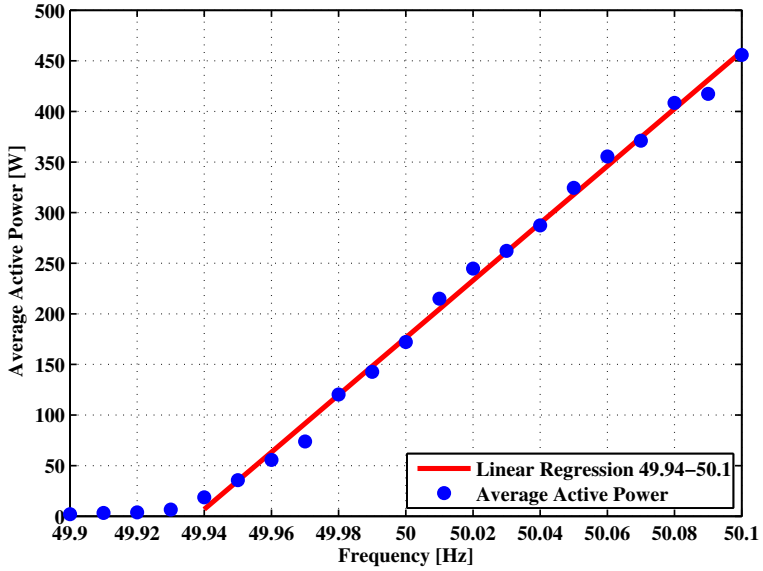

Figure 3.15: Frequency response of 2 space heaters measured over 11 days in March 2012 during the field test described in [B1]. The rated power of the heaters is 500 W. The ambient temperature conditions during this time were highly favorable for providing frequency regulation from these devices.

Reduced load diversity is not only a problem of FSL. In [124] they show that in general, demand-side management will reduce load diversity MV and LV distribution systems. In their simulations of generic distribution systems, reduced load diversity threatened to overload transformers, and violate voltage constraints.

Simulations of a realistic distribution system, with 100 % penetration of FSL are presented in [D], see Appendix D. They show that the presence of FSL increases the peak load from 4 MW to 7 MW. This is the motivation for developing the voltage-sensitive load (VSL) controller presented in Chapter 4, and then combining the VSL and FSL controllers in Chapter 5.

[6]The term down-regulation is understood from the generator perspective which reduces power output at high frequency. Demand-side resources increase their power consumption to provide down-regulation service.

[7]The time period was in March when the ambient temperature was on average 4.6℃ [123]

Chapter 4

Voltage-Sensitive Autonomous DER

Previous efforts directed at providing voltage regulation service from loads have proposed variants of a droop response (see Sec. 2.5.2). The droop method can stabilize feeder voltage, satisfying utility goals, but it has two key drawbacks for customers. First, the power consumption of the load depends on its location on the feeder. Customers connected to a weak node, farthest from energy sources, will see their demand curtailed more than customers on a strong node, close to an energy source. Second, the literature reviewed in Sec. 2.5.2 bases their analysis on simulation studies. Proof-of-concept laboratory experiments [14] revealed that cyclic loads could oscillate between ON and OFF states if the effect of the load itself on voltage levels was not accounted for.

These design considerations lead to a new VSL controller design, described in [C, h], see Appendix C.

A system with the VSL controller is shown in Fig. 4.1. The load controller algorithm is shown in a block diagram is Fig. 4.2. Compared to [C], Fig. 4.2 is more general because it allows for an arbitrary number of device states (S_n). The number of states is limited by the need for the device to reside in each state long enough to establish a reference long-term voltage value.

Simulations of a LV feeder with VSL show that the distribution of voltages

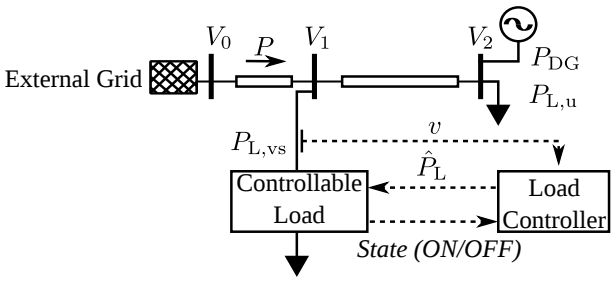

Figure 4.1: Oneline system diagram showing controllable load and DG in a radial feeder. Dashed lines represent control signal paths. The total power drawn from the grid is P. The VSL acts to regulate voltage V_1 [C].

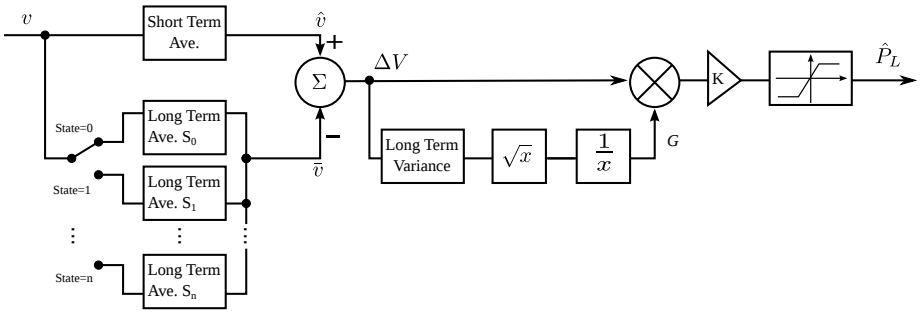

Figure 4.2: Block diagram of VSL controller. Moving averages of the voltage measurements are taken over short and long time scales. A different long-term average is found for each device state $(\mathrm{S}_1, \mathrm{S}_2, ..., \mathrm{S}_n)$. The difference between the short-term and long-term moving averages ΔV is multiplied by the gain G to give the normalized voltage deviation. The gain G is found by finding the moving standard deviation, then inverting. The output $\hat{P}_L$ results from scaling by a user-given constant K, and limiting the output to be between [-1,1].

measured on the line, shown in Fig. 4.3, are shifted with fewer extremely high voltage observations, and fewer low voltage observations [C]. Despite the widely different voltage profiles at each node, shown in Fig. 4.4, the response of the loads is normalized, as shown in Fig. 4.5.

The final case study in [C] considers the load on a MV distribution system topology typically found in North America. North American distribution systems are characterized by very simple LV networks, usually consisting of a cluster of customers less than 50 m from a small secondary transformer. In contrast, Danish distribution systems, like other Western European countries, often consist of larger LV networks, with longer lines, and larger secondary transformers. These secondary lines are at risk of experiencing bottlenecks before higher MV lines reach their limits because early-adopting customers (i.e. PV or EV) cluster locally on the same streets. The effect of the voltage controller was shown to be more significant in LV networks, making it especially valuable in the context of European power systems.

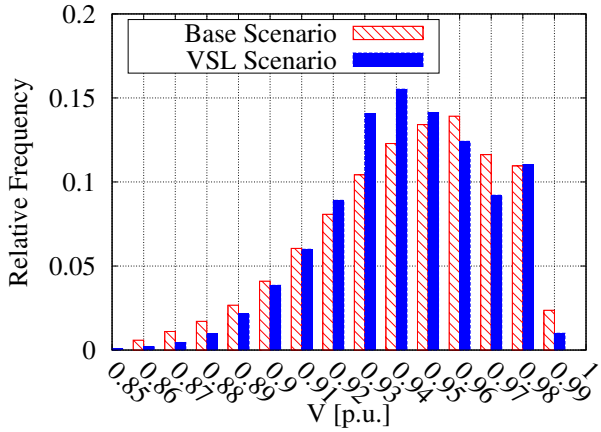

Figure 4.3: Distribution of voltage measurements in base case and VSL scenario [C].

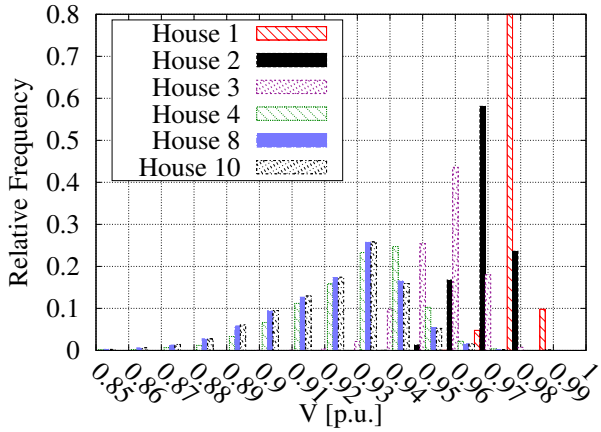

Figure 4.4: Distribution of voltage measurements at houses with VSL in the VSL scenario. House 1, located closest to the grid connection, sees the highest voltage and lowest variance [C].

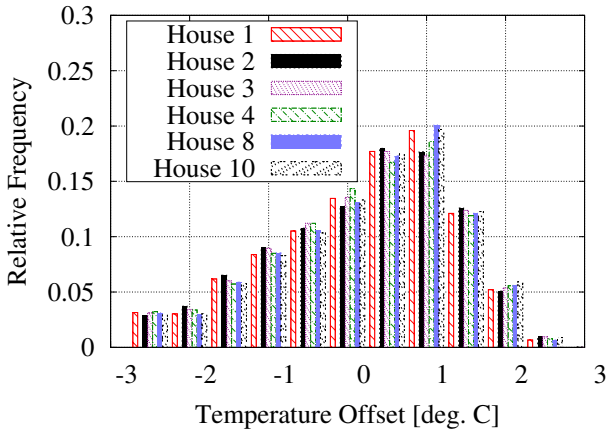

Figure 4.5: Distribution of temperature setpoint offsets. The devices show a similar distribution irrespective of their location [C].

4.1 Generalization of Expected Voltage Estimator

The load controller described in [C], requires that loads have discrete states and the load must reside in each state long enough to accumulate an estimate of the typical voltage seen in each state. In this section, a more general algorithm suitable for devices with continuously variable power consumption is presented.

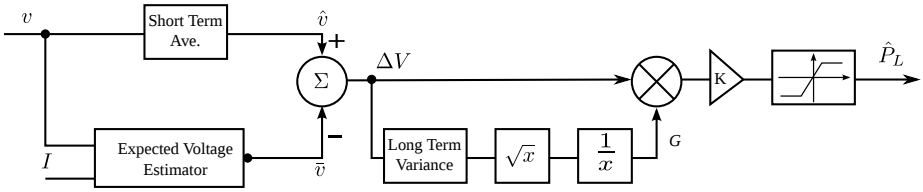

Figure 4.6: System overview of general VSL. Compared to Fig. 4.2, a new block "Expected Voltage Estimator" (EVE) replaces the long term average functions. The EVE measures voltage (v) and load current(I).

The general algorithm is similar to the algorithm for discrete devices, except the calculation of the expected voltage value $\bar{v}$ is performed in a new block, the "Expected Voltage Estimator" (EVE), shown in Fig. 4.6. Unlike the discrete voltage-sensitive load controller, the EVE needs to measure the load current $I[t]$. The expected voltage $\bar{v}[t]$ is the no-load expected voltage $\hat{v}[t]$ minus the voltage drop caused by the load current:

$$\bar{v}[t] = \hat{v}[t] - I[t]\hat{Z}[t]. \tag{4.1}$$

This voltage drop is estimated by applying Ohm's law to measurements of the load current $I[t]$, and an estimate the upstream Thevenin equivalent impedance $\hat{Z}[t]$. The state variables $\hat{v}[t]$ and $\hat{Z}[t]$ are found as follows:

$$\hat{Z}'[t] = \frac{\hat{v}[t-1] - v[t]}{I[t]} \tag{4.2}$$

$$\hat{Z}[t] = \alpha\hat{Z}[t-1] + (1-\alpha)\hat{Z}'[t] \tag{4.3}$$

The impedance is estimated in each timestep in eq. (4.2) by finding the difference between the previous estimate of no-load expected voltage $\hat{v}[t-1]$ and the actual measured voltage $v[t]$ and dividing by the measured current $I[t]$. Like all measurements in the system, there is considerable noise, so using the law of large numbers, the final impedance estimate $\hat{Z}[t]$ is the average of many such measurements. $\hat{Z}'[t]$ can only be estimated when power is being consumed by the load, i.e. $I[t] > 0$.

To estimate the no-load voltage the following formulas are applied:

$$\hat{v}'[t] = v[t] + I[t]\hat{Z}[t] \tag{4.4}$$

$$\hat{v}[t] = \alpha\hat{v}[t-1] + (1-\alpha)\hat{v}'[t] \tag{4.5}$$

Like the final estimate of $\hat{Z}[t]$, the final estimate of $\hat{v}[t]$ is a moving average. A block diagram of the EVE is shown in Fig. 4.7.

The output of the EVE, eq. (4.1), depends on the measured current $I[t]$, and the final estimates of $\hat{Z}[t]$ and $\hat{v}[t]$. Considering that $\hat{Z}[t]$ and $\hat{v}[t]$ are the average of many estimates, their value will change slowly, and in the short term variations in $\bar{v}[t]$ will primarily be caused by variations in $I[t]$.

The two estimated parameters $\hat{Z}[t]$ and $\hat{v}[t]$ depend on each other, and need to be initialized with reasonable values to ensure convergence. Ideally $\hat{v}[t]$ would be initialized during periods with no load, and then form the basis for deriving $\hat{Z}[t]$.

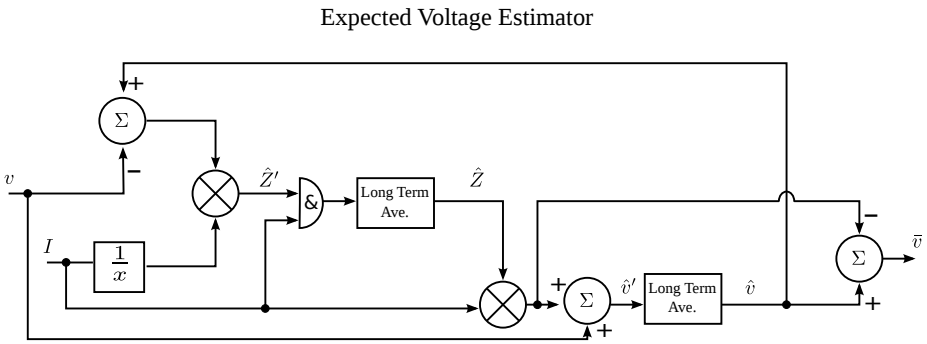

Figure 4.7: "Expected Voltage Estimator" (EVE) in detail. The "&" operator signifies that the estimate of the upstream equivalent impedance ($\hat{Z}$) is only updated when $I > 0$.

4.1.1 Status

The general VSL described in the previous section has not yet been tested rigorously, neither in the lab nor simulation. This is an area of future work (see Sec. 7.1.2).

Chapter 5

Hybrid Frequency-Voltage Sensitive DER

Section 3.5 described an issue with integrating frequency-sensitive load (FSL) into power distribution networks, namely new load peaks caused by reduced load diversity. In the past, distribution planners could be reasonably assured that the peak load of each household (or each appliance in a class) would not be synchronized to occur simultaneously. The difference between the sum of individual peak loads, and the peak aggregate load is captured with the *diversity factor*. Because FSL are synchronized to respond to the system frequency, the diversity factor is 1; in the worst case, the peak power of the population is the sum of the rated power of each device. This is not merely a theoretical possibility, a frequency response ranging from 90 % of full rated power to full curtailment was observed in field trials of FSL in the form of space heaters, see Fig. 3.15.

The voltage-sensitive load (VSL) controller described in Chapter 4 provides a solution to addressing congestion in the distribution system. Combining the VSL and FSL into a single hybrid load controller was the next logical step, shown in a block diagram in Fig. 5.1.

A study of this controller is presented in [D], Appendix D. The synthesis of the two control objectives can be seen in Fig. 5.2[1], and the resulting power consumption is shown in Fig. 5.3.

The results in [D] show that a hybrid controller can be applied to mitigate congestion in distribution systems caused by FSL. The case study uses the same network topology as in the MV test network in [C], replacing the purely VSL with the hybrid FSL and VSL. That network was typical of a North American system, which differs from European systems in the extent of the LV network. Simulation results in [C] showed that the purely VSL was most effective at spreading load in LV networks, and the same could be assumed for the hybrid controller. Since the analysis in [D] was limited to aggregate effects at the MV

[1]Fig. 5.2 is a modified version a Fig. 8 in [D]. After publication of [D] an error was discovered in the value of $\hat{P}^{\mathrm{f}}$ which was scaled to be half of the correct value. In the corrected figure, it is clear that $\hat{P}^{\mathrm{L}}$ is the arithmetic mean of $\hat{P}^{\mathrm{f}}$ and $\hat{P}^{\mathrm{V}}$. It should be emphasized that the error only affected the visualization of the simulated timeseries, not the numerical results of the simulation itself.

level, a focus on LV networks may reveal a more significant impact in reducing peak loads.

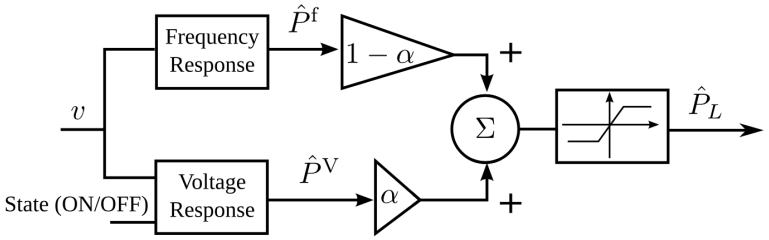

Figure 5.1: Block diagram of hybrid controller. Frequency subsystem as in Fig. 3.3, voltage subsystem as in Fig. 4.2, with a minor difference in that the value of the output of these subsystems is not limited, only the final output of the hybrid controller is limited. The relative weight of the two subsystems is determined by α [D].

The study in [D] assumed that the loads were providing continuous frequency regulation over the normal frequency operating range. The voltage response had a deadband in the normal operating range and only curtailed (increased) power consumption, relative to the purely frequency-sensitive response, when voltage deviated widely from expected values. This is one of many potential use-cases for the hybrid controller. An alternative configuration could be where the controller parameters[2] were chosen to provide continuous voltage regulation, and only deviate from the purely voltage-sensitive response when critically low (high) frequency levels are measured. The value of the weighting factor α can be varied to reflect the relative importance of voltage and frequency regulation. The optimal values of the controller parameters will depend greatly on the composition of the power system (ie. VG production profiles, fuel costs, line limits), and the predicted load flexibility.

[2]The specific parameters to be modified would be the gain constants (K_{v}, K_{f}), α, and the size of the voltage and frequency deadbands.

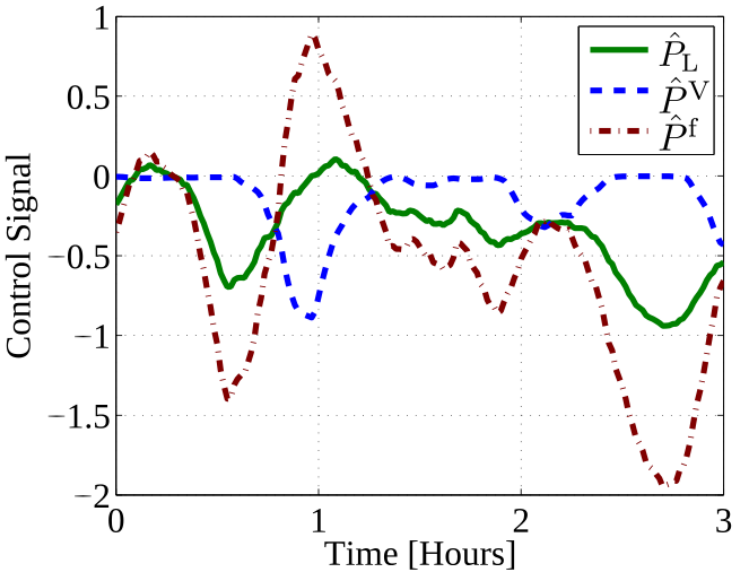

Figure 5.2: Representative time series of hybrid control $\hat{P}_{\mathrm{L}}$ signal and the voltage $\hat{P}^{\mathrm{V}}$ and frequency $\hat{P}^{\mathrm{f}}$ components.

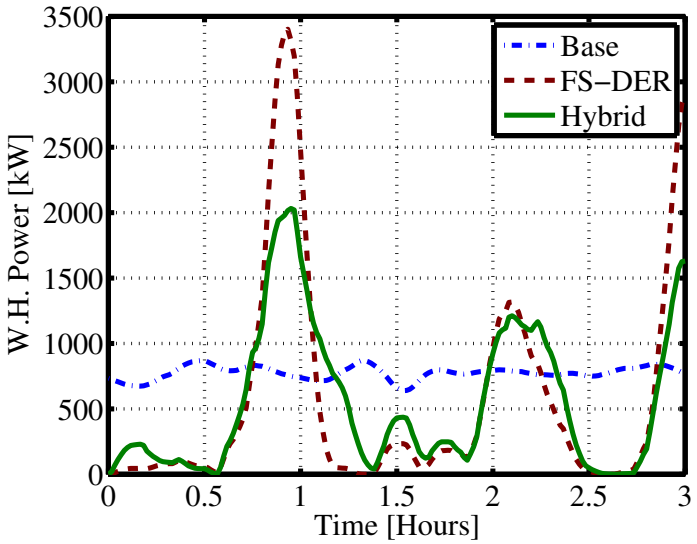

Figure 5.3: Time series of aggregate water heater power consumption for base case, FSL, and hybrid controller [D].

Chapter 6

Dispatch of Autonomous DER

The name "autonomous DER" implies a purely reactive device, beyond the reach of a system operator. However, the distinction between autonomous devices and directly controlled devices (see Sec. 2.4.1) is blurred if system operators use the assets they do control (i.e. central generators) to induce changes to the system parameter values with the goal of affecting the state of autonomous DER. To the extent that the existing dispatchable centralized control system is preserved and maintains the ability of influence system parameter values, these centralized resources can be used to communicate to otherwise autonomous DER. This communication concept can be used for frequency-sensitive distributed energy resources (FS-DER) and voltage-sensitive distributed energy resources (VS-DER). Frequency modulation is described in this chapter, voltage modulation is a matter of future research (see Sec. 7.1.6).

The communications concepts presented in [F], Appendix F, are a variant of power line communication (PLC). But where conventional PLC uses a separate transmitter device to superimpose a high-frequency component onto the voltage waveform, this communications system uses the existing energy sources to modulate the frequency of the energy-carrying waveform itself. Using the AC system frequency (50 Hz or 60 Hz) as a carrier greatly limits the speed of communications, but it allows the signal to be carried for effectively unlimited distances.

Using energy sources as communication transmitters can be compared to visible light communication (VLC) using LEDs [125]. The primary function of LEDs are to provide illumination, but the use of semi-conductors for energy conversion allows such precise and rapid modulation of energy output that they can be used to transmit information without sacrificing perceived light quality. VSI power sources are similarly able to precisely and rapidly modulate the shape of the output voltage waveform without harming energy-using devices.

The premise of these communication protocols is that international standards [16, 27] allow a degree of frequency variation in synchronous systems. Where system operators have sufficient dispatchable frequency regulation assets to satisfy these frequency variation constraints with a margin to spare, this margin can be utilized as a degree of freedom to vary system frequency setpoints.

The work in [E], Appendix E, motivates the need for exercising control over FSL when they compose of large portion of total load. Simulations of microgrids in [E] illustrate the situation when timing constraints of FSL (described in 3.4) can threaten system security. Microgrids already operate with significant deviations from nominal frequency, as shown with field data in Fig. 6.1. During the experiment where these measurements were taken, these frequency deviations caused unwanted behavior in FSL that were configured to operate in a large synchronous area. For almost one month, the test microgrid operated with an average frequency (50.12 Hz) that was outside the range of normal operation in the Nordic grid.

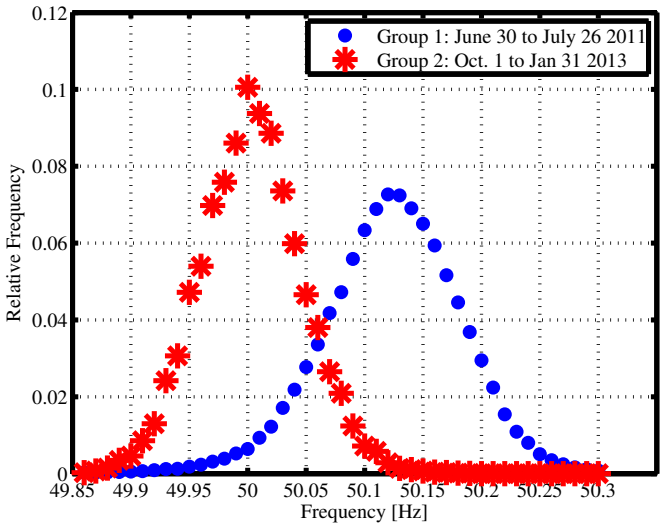

Figure 6.1: Distribution of system frequency measurements for two selected time periods in a microgrid. The two distinct regimes were caused by operating different (diesel) generators in the microgrid's fleet [B2].

Two protocols for communicating to frequency-sensitive distributed energy resources (FS-DER) are described in the following sections.

6.1 Direct Load Control by System Frequency Modulation

Looking back at Fig. 3.1, and the placement of (discrete) relay-controlled FS-DER relative to the placement dispatchable droop controlled generators (see Sec. 2.1.2), we see that the generators (and TCL-FSL) are active in the frequency range around nominal values. The discrete FS-DER is curtailed at low frequencies, after the droop response is saturated. Consider a more general deployment of discrete FS-DER with 3 states, shown in Fig. 6.2. By choosing different frequency setpoints for the droop controlled dispatchable generators, the FS-DER is forced into different states.

The key design issue in this communication system the spacing between

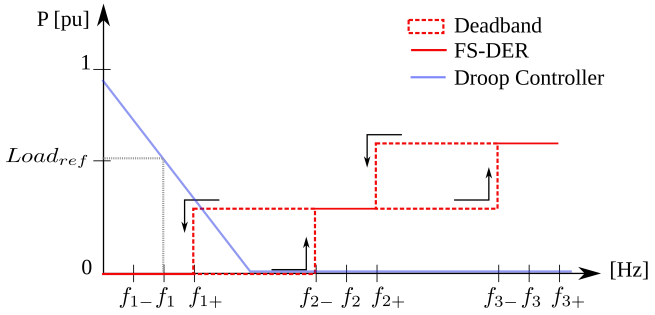

Figure 6.2: Allocation of droop controlled generator to dispatch discrete FS-DER. In the top figure, the generators' are set to a low frequency setpoint (f_1), and the FS-DER resides in state 1. In the middle figure, the generators' frequency setpoint (f_2) is chosen to dispatch FS-DER into state 2. In the bottom figure, the generators' produce at a high frequency (f_3), forcing the FS-DER into state 3.

frequency setpoints: they must be separated by enough bandwidth to ensure a low probability of uncontrolled state changes in FS-DER. The range of frequency setpoints is constrained, so the closer they are spaced, the greater the number of feasible discrete states. The spacing of frequency setpoints and the distribution of frequency measurements that results from different setpoints is shown in Fig. 6.3.

An important caveat with FS-DER operating in conventional power systems is that the FS-DER states mapped to lower frequencies must use less power than the states mapped to higher frequencies. If not, system disturbances large enough to unintentionally push the FS-DER out of the intended state will be difficult to contain because of positive feedback[1].

[1]I.e. If lower frequency causes loads to increase power consumption, the frequency will decline further.

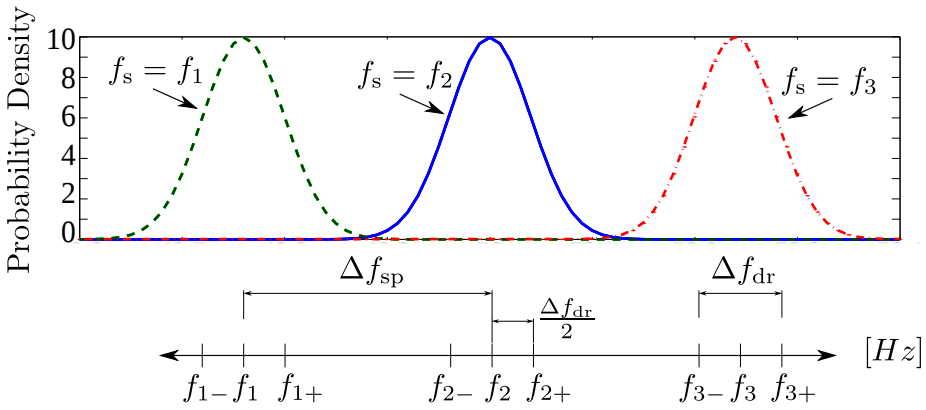

Figure 6.3: Distribution of system frequency for 3 different frequency setpoints [F]. Criteria for setting the spacing between generator frequency setpoints (Δf_{sp}), and the size of the FS-DER decision region (Δf_{dr}) are elaborated upon in [F].

6.2 Energy Sources as Power Frequency Communication transmitters

In power systems supplied by rotating machines (the vast majority, large and small), frequency regulation is a challenge because of delays in changing generator output power. The inertia of the rotating masses slows the ROCOF experienced during a power imbalance, giving the generators time to restore the power balance. As discussed in Sec. 2.1.3, an new type of power system is on the horizon, where energy is primarily supplied (and consumed) by power electronic interfaced devices. These empty networks can modulate system frequency on a potentially cycle by cycle basis, allowing FS-DER state changes many times per second.

The protocol described in Sec. 6.1 is not a general purpose communications protocol, because each frequency band is mapped to one FS-DER state, which in turn leads to a given load profile. Empty networks are not exposed to frequency disturbances, so they do not require FS-DER to consume less power at lower frequencies and vice versa. Instead, a general purpose communications channel can be created to allow a sequence of FS-DER states to be interpreted as a digital message. A timing sequence familiar to any serial communications protocol is shown in Fig. 6.4. Correctly decoding a sequence of states requires synchronization between the transmitter and receiver, and markers to delimit the beginning and end of messages. There are well established methods for handling these problems in existing data network protocols (i.e. IEEE 802.3).

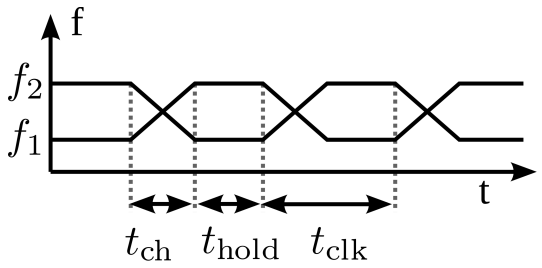

Figure 6.4: Timing diagram for PFC. The signal is sampled at the receiver at the end of t_{hold}. The signal is modulated by the transmitter during t_{ch} [F].

Chapter 7

Discussion and Conclusion

This thesis has examined the role of autonomous DER, especially demand-side resources, for providing ancillary services to power systems.

Real-time local control loops have always been part of industrial control system design (see Sec. 2.4.1). Considering the precedent of autonomous controllers found in existing power system assets, this thesis has shown that autonomous controllers in DER are also viable for providing frequency regulation (Chapter 3) and voltage regulation services (Chapter 4).

By testing autonomous frequency-sensitive load (FSL) in real-world settings, this work has observed and extrapolated drawbacks to their implementation. While the algorithms for control of autonomous DER are relatively simple, predicting their response in aggregate is difficult. Sec. 3.3 showed how an ARMA model can be applied to FSL. The model accurately represented the average frequency response, but it did not closely fit the timeseries of experimental data, and the distribution of output values was significantly different from the experimental data.

Cost estimates for autonomous load controllers in the existing literature vary significantly [20, 92, 114]. The experience of this project supports the lower end of the range of price estimates (< 5 €). The costs of autonomous load controllers can be divided into 4 categories:

- **One-time engineering costs**: Most undergraduate students in the class "Hands-on Microcontroller Programming" managed to design, implement, and test a FSL within 3-weeks, indicating negligible per-unit engineering costs for mass produced devices.
- **Data processing costs**: Many embedded systems have spare data processing capacity to execute these algorithms without upgrading CPU[1]. Sufficiently accurate instruments for measuring power system frequency and voltage magnitude are built into standard low-cost microcontrollers of the kind found in may common appliances[2]. Only a few passive components are needed to divide mains voltage down to a level compatible with digital to analog converter (DAC) input levels.

[1] The data processing resources available in experimental implementations were less than 16 MIPS and less than 8 kB memory.

[2] An 11-bit DAC has been shown sufficiently accurate to measure frequency with a precision of $\pm$ 5 mHz in laboratory experiments.

- **End-use process costs**: The cost related to energy conversion and the end-use energy service will naturally depend on the appliance being controlled. In the relay-controlled ON/OFF TCL process considered throughout this thesis, the relay will experience greater wear from the more frequent cycling. Efficiency may also be reduced if loads do not operate in their optimal duty cycle, a cost comparable to the efficiency loss in part-loaded central generators.

- **User Disutility**: In the best case, users do not notice that their appliance is delivering ancillary services to the power system. The field experiments conducted in this project support the assumption that users do not perceive a degraded energy service.

Autonomous load control has been shown to be simple to implement with inexpensive components, making them well suited to control small loads. Experiments have shown that the power available for ancillary services varies from the loads' average power up to 90 % of the rated power, depending on flexibility of the load.

With such a large scope for deployment, the project has considered the factors limiting the integration of autonomous load controllers in power systems. Analysis of the frequency regulation service provided by FSL located in LV distribution systems identified two drawbacks that were addressed: congestion of distribution lines and timing constraints in relay-controlled loads. The danger of overloading distribution bottlenecks if/when FSL became synchronized motivated the design of a voltage-sensitive load (VSL) control algorithm (Chapter 4), and the synthesis of a hybrid frequency-voltage sensitive control algorithm (Chapter 5). The need to avoid timing constraints in FS-DER motivated the use of centralized frequency regulation resources to dispatch FS-DER into known states (Chapter 6).

With respect to the near-term future for this class of demand-side management, deployment of FSL and VSL depends on creating incentives for device manufacturers and end-users. Today, the end-users (and by extension the device manufacturers) do not benefit directly from the ancillary services they can provide. And while the benefits are socialized among all power system users, the costs, though small in relation to the benefits, fall entirely on the device user. Existing markets for procuring ancillary services dispatch the lowest-cost providers in fixed time-slots[3]. This periodic re-dispatch of ancillary service providers is incompatible with "fit-and-forget" autonomous load controllers that incur most costs up-front and continue to provide ancillary services for their entire lifetime.

ENTSO-E has proposed mandating new thermostat controlled load to be FSL [113], potentially solving this problem by socializing the costs of the technology. In the public comments to this proposal, this initiative has met resistance from devices manufacturers, who would prefer soft (financial) incentives, rather than firm mandates. The proposal is also controversial among existing ancillary service providers because ENTSO-E can be considered to be "picking winners", rather than allowing the marketplace to discover the lowest-cost solution. There is clearly an interplay between the market rules and the technical capabilities of different ancillary service providers. A task remains to determine

[3]Time slots can be as short as 4-hours or as long as one year.

how to adapt market rules to enable efficient demand-side participation considering the transaction costs and verification costs associated with providing ancillary services from large numbers of small loads.

Assuming incentives are created, FSL controllers may be built-in to mass produced consumer appliances. Since it is infeasible to determine the FSL hosting capacity of each LV feeder before installing each new residential appliance, an automatic mechanism to curtail[4] FSL in congested feeders is desirable. This thesis has demonstrated that a VSL controller can mitigate the risk of congestion caused by FSL (or other demand-side management systems) in LV distribution systems. Unlike FSL, requiring a voltage response in loads is not on system operators' agenda, but a preventative approach, rather than a reactive/corrective approach, should be prioritized because highly dispersed autonomous DER are difficult to reconfigure once deployed.

The prospects for deploying power frequency communication (PFC) depend on the willingness of system operators to utilize the degree of freedom they have to intentionally vary system frequency. Operators of small synchronous areas, such a microgrids, have both the means and incentive to use this method. Changing system frequency setpoints of existing energy sources is not always easy; future energy sources supporting PFC will need to expose a user interface to control frequency setpoints. New FS-DER will need to be created to receive and decode the information embedded in the system frequency. Our research has documented that these receivers can be created using off-the-shelf components, so pilot projects can implement their own FS-DER without waiting for a mass-market of standard products to develop.

7.1 Future Work

In the course of this project, some research questions arose that limited resources did not allow pursuit of. These topics are listed below to direct future research as a follow-up to this project.

7.1.1 Demonstration of the Effect of Frequency-Sensitive Load on System Frequency

Our field tests demonstrated the effect of system frequency on FSL, but the loads were too small to have a measurable effect on the frequency of the power system they were connected to. A microgrid experiment, comparable to [97], where a small load would have a relatively large impact on the system frequency, would plug this gap. An experiment with several heterogeneous FSL would reveal the extent to which their internal states (i.e. temperature) become synchronized.

7.1.2 Simulation of Generalized Voltage-Sensitive Autonomous Load Controller

The general VSL controller described in Sec. 4.1 has not yet been implemented nor simulated. A complete study of this controller will show the performance of a distribution system with variable power VSLs. The performance can then

[4] Or, in systems with high DG production, increase.

be compared to the droop controlled electric spring in [120]. Unlike the droop controlled electric spring, the VSL controller described in Sec. 4.1 accounts for the variation in the magnitude of voltage variance, and thus it is expected to give a more uniform response .

7.1.3 Stability Evaluation of Voltage-Sensitive Autonomous Load Controller

In [59] they investigate the stability of a distribution system with DG controlled by with a Q(U) algorithm (see Sec. 2.2.1) and found that oscillations between generators appeared when both the impedance and controller gain were large. Similar oscillations were occasionally observed in simulations of VSL, though no systematic investigation of this phenomena was performed. A comprehensive analysis of VSL would map the stable region of VSL parameter values.

7.1.4 Voltage-Sensitive Load Controller System Test

Our lab test of a single voltage-controlled refrigerator [14] validated the feasibility of our controller design, but the test did not show how the load effected the load profile elsewhere on the feeder. Results showing the behavior of numerous VSLs in a larger distribution system are based on simulation studies. These system-scale simulations have yet to be validated in a laboratory setting. The experimental facilities at SYSlab, located at DTU's Risø campus, would be suitable for such an experiment.

7.1.5 Laboratory Test of Power Frequency Communication using Energy Sources as Transmitters

The analysis in Sec. 6.2 argued that VSI based energy sources could change their output frequency on a cycle-by-cycle basis. This analysis was based on generic considerations about the properties of power electronics. The next step is to demonstrate the ability of a particular VSI to change frequency setpoint, and to measure the speed of this transition. The facilities in DTU Risø's SYSlab contain VSI energy sources with variable output frequency which can be used to implement a proof-of-concept. Furthermore, a potentially difficult, and unaddressed, technical challenge would be to coordinate rapid changes to frequency setpoints in multiple VSIs operating in parallel on the same network.

7.1.6 Voltage as Information Carrier

In the same way the centralized frequency regulation resources can be harnessed to signal the system state to FS-DER, centrally controlled voltage regulation resources can be used to signal the system state to voltage-sensitive distributed energy resources (VS-DER).

Something similar was described in [126], namely using OLTC to communicate the availability of energy to DG. However in [126] the voltage response algorithm of the VS-DER was a droop method, whose drawbacks have already been discussed (see Sec. 2.5.2). The transmitter communicating to loads implementing the algorithm described in Chapter 4 would need to operate at a speed

between the time constants of the short-term average voltage and the long-term average voltage.

Voltage as an information carrier complements frequency as an information carrier (Chapter 6), because the two parameters are independent, forming orthogonal signals. While the frequency is coherent across an entire synchronous area, voltage modulation is only propagated down the system hierarchy. In that way voltage is a local signal allowing a natural sub-division of a network, while frequency is globally available.

Bibliography

[1] A. D. Barnosky, N. Matzke, S. Tomiya, G. O. U. Wogan, B. Swartz, T. B. Quental, C. Marshall, J. L. McGuire, E. L. Lindsey, K. C. Maguire, B. Mersey, and E. A. Ferrer, "Has the earth's sixth mass extinction already arrived?" *Nature*, vol. 471, no. 7336, pp. 51–57, Mar 2011. [Online]. Available: http://dx.doi.org/10.1038/nature09678

[2] J. Rockstrom, W. Steffen, K. Noone, A. Persson, F. S. Chapin, E. F. Lambin, T. M. Lenton, M. Scheffer, C. Folke, H. J. Schellnhuber, B. Nykvist, C. A. de Wit, T. Hughes, S. van der Leeuw, H. Rodhe, S. Sorlin, P. K. Snyder, R. Costanza, U. Svedin, M. Falkenmark, L. Karlberg, R. W. Corell, V. J. Fabry, J. Hansen, B. Walker, D. Liverman, K. Richardson, P. Crutzen, and J. A. Foley, "A safe operating space for humanity," *Nature*, vol. 461, no. 7263, pp. 472–475, 24 Sep. 2009. [Online]. Available: http://dx.doi.org/10.1038/461472a

[3] IPCC Core Writing Team, *Climate Change 2007: Synthesis Report. Contribution of Working Groups I, II and III to the Fourth Assessment Report of the Intergovernmental Panel on Climate Change*, R. Pachauri and A. Reisinger, Eds. IPCC, Geneva, Switzerland, 2007.

[4] M. L. Imhoff, L. Bounoua, T. Ricketts, C. Loucks, R. Harriss, and W. T. Lawrence, "Global patterns in human consumption of net primary production," *Nature*, vol. 429, pp. 870–873, 24 Jun. 2004.

[5] V. Smil, "21st century energy: Some sobering thoughts," *OECD Observer*, Dec. 2006.

[6] International Energy Agency, "Energy Policies of IEA Countries: Denmark 2011 Review," 2011.

[7] Energi Styrelsen (Danish Energy Agency), "Elforsyningsstatistik (Electricity Suppy Statistics)," Tech. Rep., Jan. 2013.

[8] Energinet.dk, "Samlet Solcellegraf (Aggregate Solar Cell Graph)," 26 Sep. 2013.

[9] Electric Power Research Institute (EPRI), "Electric Energy Storage Technology Options," Tech. Rep., 2010.

[10] Energinet.dk, "Vindmøller: Samlet kapacitet i DK (Windturbines: Aggregate Capacity in Denmark," 26 Sep. 2013.

[11] "Demand Response Programs of Public Power Utilities," American Public Power Association, Tech. Rep., Jul. 2010, accessed November 18, 2013. [Online]. Available: http://appanet.cms-plus.com/files/PDFs/PublicPowerDemandResponseprograms.pdf

[12] CENELEC, "EN 50065-1: Signalling on low-voltage electrical installations in the frequency range 3 kHz to 148,5 kHz - Part 1: General requirements, frequency bands and electromagnetic disturbances," 2011.

[13] R. Garcia-Valle, L. P. Da Silva, Z. Xu, and J. Østergaard, "Smart demand for improving short-term voltage control on distribution networks," *I E T Generation, Transmission and Distribution*, vol. 3, no. 8, pp. 724–732, 2009.

[14] O. C. Tudora, "Smart Demand for Voltage Control in Power Networks," Master's thesis, Technical University of Denmark, Nov. 2012.

[15] S. Mak and D. Reed, "TWACS, A new viable two-way automatic communication system for distribution networks. Part I: Outbound communication," *Power Apparatus and Systems, IEEE Transactions on*, vol. PAS-101, no. 8, pp. 2941 –2949, aug. 1982.

[16] CENELEC, "EN 50160: Voltage characteristics of electricity supplied by public electricity networks," 2010.

[17] ENTSO-E, "Network Code on Load-Frequency Control and Rsereves," ENTSO-E, Tech. Rep., 28 Jun. 2013.

[18] T. Bopp and G. Strbac, "Value of fault ride through capability of wind generation in the UK," Centre for Distributed Generation and Sustainable Electrical Energy, Tech. Rep., Oct. 2004.

[19] F. Starr, *Renewable electricity and the grid electronic resource : the challenge of variability.* Earthscan, 2007, ch. Flexibility of Fossile Fuel Plant in a Renewable Energy Scenario: Possible Implications for the UK, pp. 1 online resource (xxiii, 219 s.).

[20] M. Aunedi, P.-A. Kountouriotis, J. Calderon, D. Angeli, and G. Strbac, "Economic and environmental benefits of dynamic demand in providing frequency regulation," *Smart Grid, IEEE Transactions on*, vol. 4, no. 4, pp. 2036–2048, 2013.

[21] Amprion, "Procurement of control power and energy in Germany," Online, Oct. 2013, accessed October 31, 2013. [Online]. Available: http://www.amprion.net/en/control-energy

[22] P. Kundur, N. Balu, and M. Lauby, *Power system stability and control.* McGraw-Hill New York, 1994.

[23] Z. Xu, J. Ostergaard, M. Togeby, and F. Isleifsson, "Evaluating frequency quality of nordic system using pmu data," in *Power and Energy Society General Meeting - Conversion and Delivery of Electrical Energy in the 21st Century, 2008 IEEE*, 2008, pp. 1–5.

[24] E-Bridge, "Analysis & Review of Requirements for Automatic Reserves in the Nordic Synchronous System," Tech. Rep., 21 May 2011.

[25] V. Trovato, S. H. Tindemans, and G. Strbac, "Demand Response Contribution to Effective Inertia for System Security in GB 2020 Gone Green Scenario," in *Innovative smart grid technologies (ISGT europe), 4th IEEE PES International Conference and Exhibition on*, Oct. 2013.

[26] Nordel, "System operation agreement," 13 Jun. 2006, accessed April 27, 2012. [Online]. Available: https://www.entsoe.eu/

[27] ENTSO-E, "Draft Network Code for Requirements for Grid Connection applicable to all Generators," 24 Jan. 2012.

[28] L. Sigrist, I. Egido, and L. Rouco, "A method for the design of ufls schemes of small isolated power systems," *Power Systems, IEEE Transactions on*, vol. 27, no. 2, pp. 951 –958, may 2012.

[29] C. Concordia, L. Fink, and G. Poullikkas, "Load shedding on an isolated system," *Power Systems, IEEE Transactions on*, vol. 10, no. 3, pp. 1467 –1472, aug 1995.

[30] J. Jones and W. Kirkland, "Computer algorithm for selection of frequency relays for load shedding," *Computer Applications in Power, IEEE*, vol. 1, no. 1, pp. 21 –25, jan 1988.

[31] W. Freitas, W. Xu, C. Affonso, and Z. Huang, "Comparative analysis between rocof and vector surge relays for distributed generation applications," *Power Delivery, IEEE Transactions on*, vol. 20, no. 2, pp. 1315 – 1324, april 2005.

[32] U. Rudez and R. Mihalic, "Monitoring the first frequency derivative to improve adaptive underfrequency load-shedding schemes," *Power Systems, IEEE Transactions on*, vol. 26, no. 2, pp. 839–846, 2011.

[33] V. Terzija, "Adaptive underfrequency load shedding based on the magnitude of the disturbance estimation," *Power Systems, IEEE Transactions on*, vol. 21, no. 3, pp. 1260 –1266, aug. 2006.

[34] J. Thorp, C. Seyler, and A. Phadke, "Electromechanical wave propagation in large electric power systems," *Circuits and Systems I: Fundamental Theory and Applications, IEEE Transactions on*, vol. 45, no. 6, pp. 614–622, 1998.

[35] Z. Zhong, C. Xu, B. Billian, L. Zhang, S. Tsai, R. Conners, V. Centeno, A. Phadke, and Y. Liu, "Power system frequency monitoring network (fnet) implementation," *Power Systems, IEEE Transactions on*, vol. 20, no. 4, pp. 1914–1921, 2005.

[36] Y. Li, M. Olama, and J. Nutaro, "Frequency waves, grid friendly appliances and geographic limits in a smart grid," in *Innovative Technologies for an Efficient and Reliable Electricity Supply (CITRES), 2010 IEEE Conference on*, 2010, pp. 220–224.

[37] IEEE Task Force, "Standard load models for power flow and dynamic performance simulation," *Power Systems, IEEE Transactions on*, vol. 10, no. 3, pp. 1302 –1313, aug 1995.

[38] G. C. Tarnowski, P. Kjær, S. Dalsgaard, and A. Nyborg, "Regulation and frequency response service capability of modern wind power plants," in *Power and Energy Society General Meeting, 2010 IEEE*, 2010, pp. 1–8.

[39] K. Burges, P. Zolotarev, and J. Lehner, "Impact of Large-scale Distributed Generation on Network Stability During Over-Frequency Events & Development of Mitigation Measures," Sep. 2011. [Online]. Available: http://www.vde.com/en/fnn/pages/50-2-hz-study.aspx

[40] VDE, "VDE-AR-N 4105:2011-08 Power generation systems connected to the low-voltage distribution network - Technical minimum requirements for the connection to and parallel operation with low-voltage distribution networks," 1 Aug. 2010. [Online]. Available: http://www.vde.com/en/fnn/pages/n4105.aspx

[41] M. Reza, A. Dominguez, P. Schavemaker, A. Asmara, F. Viawan, and W. Kling, "Controlling the power balance in an 'empty network'," *Int. J. of Energy Technology and Policy*, vol. 5, no. 5, pp. 584 – 603, 2007.

[42] ANSI, "C84.1-2006 American National Standard for Electric Power Systems and Equipment - Voltage Ratings," 2006.

[43] M. H. Bollen, *Understanding Power Quality Problems: Voltage Sags and Interruptions*, ser. IEEE - TP 139-0. Wiley, 2000.

[44] S. Anrborg, G. Andersson, D. Hill, and I. Hiskens, "On Influence of Load Modellling for Undervoltage Load Shedding Studies," *IEEE Transaction on Power Systems*, vol. 13, no. 13, pp. 395–400, May 1998.

[45] C. Taylor, "Concepts of undervoltage load shedding for voltage stability," *Power Delivery, IEEE Transactions on*, vol. 7, no. 2, pp. 480–488, Apr. 1992.

[46] "Fitformer reg," Online, 2012, accessed Sept. 1, 2012. [Online]. Available: http://www.energy.siemens.com

[47] M. Kaspirek, D. Mezera, and J. Jiricka, "Problems of Voltage Stabilization in MV and LV Distribution Grids Due to the Operation of Renewable Energy Sources," in *CIRED 22nd International Conference on Electricity Distribution*, Jun. 2013.

[48] T. Stetz, F. Marten, and M. Braun, "Improved low voltage grid-integration of photovoltaic systems in germany," *Sustainable Energy, IEEE Transactions on*, vol. 4, no. 2, pp. 534–542, Apr. 2013.

[49] A. Seppala, "Load research and load estimation in electricity distribution," Ph.D. dissertation, Helsinki University of Technology, 29 Nov. 1996.

[50] R. Dugan, T. McDermott, and G. Ball, "Planning for distributed generation," *Industry Applications Magazine, IEEE*, vol. 7, no. 2, pp. 80–88, 2001.

[51] M. Baran, H. Hooshyar, Z. Shen, and A. Huang, "Accommodating high pv penetration on distribution feeders," *Smart Grid, IEEE Transactions on*, vol. 3, no. 2, pp. 1039 –1046, june 2012.

[52] E. Coster, J. Myrzik, B. Kruimer, and W. Kling, "Integration issues of distributed generation in distribution grids," *Proceedings of the IEEE*, vol. 99, no. 1, pp. 28 –39, jan. 2011.

[53] S. Conti, S. Raiti, G. Tina, and U. Vagliasindi, "Distributed generation in lv distribution networks: voltage and thermal constraints," in *Power Tech Conference Proceedings, 2003 IEEE Bologna*, vol. 2, june 2003, p. 6 pp. Vol.2.

[54] Q. Zhou and J. Bialek, "Generation curtailment to manage voltage constraints in distribution networks," *Generation, Transmission Distribution, IET*, vol. 1, no. 3, pp. 492 –498, may 2007.

[55] T. Sansawatt, L. Ochoa, and G. Harrison, "Smart decentralized control of dg for voltage and thermal constraint management," *Power Systems, IEEE Transactions on*, vol. 27, no. 3, pp. 1637–1645, 2012.

[56] C. Su, "Comparative analysis of voltage control strategies in distribution networks with distributed generation," in *Power Energy Society General Meeting, 2009. PES '09. IEEE*, july 2009, pp. 1 –7.

[57] E. Demirok, P. Casado Gonzalez, K. Frederiksen, D. Sera, P. Rodriguez, and R. Teodorescu, "Local reactive power control methods for overvoltage prevention of distributed solar inverters in low-voltage grids," *Photovoltaics, IEEE Journal of*, vol. 1, no. 2, pp. 174 –182, oct. 2011.

[58] P. Kotsampopoulos, N. Hatziargyriou, B. Bletterie, and G. Lauss, "Review, analysis and recommendations on recent guidelines for the provision of ancillary services by Distributed Generation," in *Annual Conference of IEEE Industrian Electronics Society (IECON)*, Nov. 2013.

[59] A. Constantin, R. Dan Lazar, and S. B. Kjar, "Voltage regulation (mv) by means of q(u); simulation and measurement on a 12 mva pv power plant," in *Integration of Renewables into the Distribution Grid, CIRED 2012 Workshop*, 2012, pp. 1–4.

[60] P. Vovos, A. Kiprakis, A. Wallace, and G. Harrison, "Centralized and distributed voltage control: Impact on distributed generation penetration," *Power Systems, IEEE Transactions on*, vol. 22, no. 1, pp. 476–483, 2007.

[61] Bundesverband Solarwirtschaft (BSW), "BSW-Solar Price Index," Bundesverband Solarwirtschaft (BSW), Tech. Rep., May 2013. [Online]. Available: http://www.solarwirtschaft.de/fileadmin/media/pdf/2013_2_BSW-Solar_fact_sheet_solar_power.pdf

[62] P. Blechinger, K. Bognar, M. Hlusiak, and C. Breyer, "Energy Supply in Mini-Grids Regarding Renewable Energies: An Optimization for Petite Martinique," in *6th European Conference of PV-Hybrids and Mini-Grids*, 2012.

[63] J. Vieira, W. Freitas, W. Xu, and A. Morelato, "Efficient coordination of rocof and frequency relays for distributed generation protection by using the application region," *Power Delivery, IEEE Transactions on*, vol. 21, no. 4, pp. 1878 –1884, oct. 2006.

[64] P. Lund, "The danish cell project - part 1: Background and general approach," in *Power Engineering Society General Meeting, 2007. IEEE*, 2007, pp. 1–6.

[65] Energinet.dk, "Cell Controller Pilot Project - 2011 Public Report," Energinet.dk, Tech. Rep., 2011.

[66] J. R. Pillai, K. Heussen, and P. A. Østergaard, "Comparative analysis of hourly and dynamic power balancing models for validating future energy scenarios," *Energy*, vol. 36, no. 5, pp. 3233 – 3243, 2011.

[67] L. A. C. Lopes, F. Katiraei, K. Mauch, M. Vandenbergh, and L. Arribas, "PV Hybrid Mini-Grids: Applicable Control Methods for Various Situations," International Energy Agency, Tech. Rep., Apr. 2012.

[68] T. Vandoorn, B. Renders, L. Degroote, B. Meersman, and L. Vandevelde, "Active load control in islanded microgrids based on the grid voltage," *Smart Grid, IEEE Transactions on*, vol. 2, no. 1, pp. 139 –151, Mar. 2011.

[69] T. Vandoorn, J. D. M. De Kooning, B. Meersman, J. Guerrero, and L. Vandevelde, "Voltage-based control of a smart transformer in a microgrid," *Industrial Electronics, IEEE Transactions on*, vol. 60, no. 4, pp. 1291–1305, 2013.

[70] J. Guerrero, J. Vasquez, J. Matas, L. de Vicuna, and M. Castilla, "Hierarchical control of droop-controlled ac and dc microgrids; a general approach toward standardization," *Industrial Electronics, IEEE Transactions on*, vol. 58, no. 1, pp. 158 –172, jan. 2011.

[71] S. Darby, "The effectiveness of feedback on energy consumption," Environmental Change Institute, University of Oxford, Tech. Rep., Apr. 2006.

[72] D. Callaway and I. Hiskens, "Achieving controllability of electric loads," *Proceedings of the IEEE*, vol. 99, no. 1, pp. 184 –199, jan. 2011.

[73] P. Nyeng, "System Integration of Distributed Energy Resources: ICT, Ancillary Services, and Markets," Ph.D. dissertation, Technical University of Denmark, Jul. 2010.

[74] K. Åström and B. Wittenmark, *Computer-controlled systems : Theory and design*, 3rd ed. Prentice Hall, 1997, series: Prentice Hall information and system sciences series.

[75] D. Popović and V. Bhatkar, *Distributed Computer Control for Industrial Automation*, ser. Electrical Engineering and Electronics. M. Dekker, 1990.

[76] T. Mølbak, "Virtual Power Plants," presentation at IEEE Workshop Aalborg, Oct. 2010.

[77] D. Kullmann, O. Gehrke, and H. Bindner, "Asynchronous control of distributed energy resources using behaviour descriptions," in *Computing, Networking and Communications (ICNC), 2012 International Conference on*, 2012, pp. 216–220.

[78] "Sharing 700 MHz Public Safety Broadband Spectrum With Utilities: A Proposal," Utilities Telecom Council, Tech. Rep., Oct. 2012.

[79] S. Galli, A. Scaglione, and Z. Wang, "For the grid and through the grid: The role of power line communications in the smart grid," *Proceedings of the IEEE*, vol. 99, no. 6, pp. 998 –1027, june 2011.

[80] "The Zettabyte Era - Trends and Analysis," Cisco, Tech. Rep., 29 May 2013.

[81] N. Gershenfeld, R. Krikorian, and D. Cohen, "The internet of things," *Scientific American*, vol. 291, no. 4, pp. 76–81, October 2004.

[82] "Ieee standard communication delivery time performance requirements for electric power substation automation," *IEEE Std 1646-2004*, pp. 1 –24, 2005.

[83] Energy Information Administration, "Residential Energy Consumption Survey," U.S. Dept. Energy, Washington, DC, Tech. Rep., 2009.

[84] P. Bacher and H. Madsen, "Identifying suitable models for the heat dynamics of buildings," *Energy and Buildings*, vol. 43, no. 7, pp. 1511 – 1522, 2011. [Online]. Available: http://www.sciencedirect.com/science/article/pii/S0378778811000491

[85] S. Ihara and F. Schweppe, "Physically based modeling of cold load pickup," *Power Apparatus and Systems, IEEE Transactions on*, vol. PAS-100, no. 9, pp. 4142–4150, 1981.

[86] N. Lu, D. Chassin, and S. Widergren, "Modeling uncertainties in aggregated thermostatically controlled loads using a state queueing model," *Power Systems, IEEE Transactions on*, vol. 20, no. 2, pp. 725 – 733, may 2005.

[87] J. L. Mathieu, S. Koch, and D. S. Callaway, "State estimation and control of electric loads to manage real-time energy imbalance," *Power Systems, IEEE Transactions on*, vol. PP, no. 99, p. 1, 2012.

[88] C. K. Madsen and K. O. Thorthardottir, "Demard as Frequency Controlled Reserve: Advanced Modeling of Aggregating Frequency Responsive Loads in Power System Dynamic Simulation," B.Sc. Thesis, Jun. 2007.

[89] R. H. Shumway and D. S. Stoffer, *Time Series Analysis and Its Applications, 3rd Edition.* Springer, 2011.

[90] D. Angeli and P.-A. Kountouriotis, "A stochastic approach to "dynamic-demand" refrigerator control," *Control Systems Technology, IEEE Transactions on*, vol. 20, no. 3, pp. 581–592, 2012.

[91] J. Short, D. Infield, and L. Freris, "Stabilization of grid frequency through dynamic demand control," *Power Systems, IEEE Transactions on*, vol. 22, no. 3, pp. 1284 –1293, aug. 2007.

[92] Zhao Xu, J. Østergaard, and M. Togeby, "Demand as frequency controlled reserve," *Power Systems, IEEE Transactions on*, vol. 26, no. 3, pp. 1062 –1071, Aug. 2011.

[93] W. Zhang, J. Lian, C.-Y. Chang, and K. Kalsi, "Aggregated modeling and control of air conditioning loads for demand response," *Power Systems, IEEE Transactions on*, vol. PP, no. 99, pp. 1–10, 2013.

[94] N. A. Sinitsyn, S. Kundu, and S. Backhaus, "Safe protocols for generating power pulses with heterogeneous populations of thermostatically controlled loads," *Energy Conversion and Management*, vol. 67, no. 0, pp. 297 – 308, 2013.

[95] K. Schneider, J. Fuller, F. Tuffner, and R. Singh, "Evaluation of Conservation Voltage Reduction (CVR) on a National Level," Pacific Northwest National Laboratory, Tech. Rep., Jul. 2010.

[96] F. Schweppe, R. Tabors, J. Kirtley, H. Outhred, F. Pickel, and A. Cox, "Homeostatic utility control," *Power Apparatus and Systems, IEEE Transactions on*, vol. PAS-99, no. 3, pp. 1151 –1163, may 1980.

[97] K. Pandiaraj, P. Taylor, N. Jenkins, and C. Robb, "Distributed load control of autonomous renewable energy systems," *Energy Conversion, IEEE Transactions on*, vol. 16, no. 1, pp. 14–19, 2001.

[98] V. A. Smith and M. Kintner-Meyer, "Final Report for California Energy Commission: Smart Load and Grid-Friendly Appliances," California Energy Commission, Tech. Rep., Oct. 2003.

[99] D. J. Hammerstrom, "Pacific Northwest GridWise Testbed Demonstration Projects: Part II. Grid Friendly Appliance Project. PNNL-17079," Pacific Northwest National Laboratory, Tech. Rep., Oct. 2007.

[100] N. Lu and D. Hammerstrom, "Design considerations for frequency responsive grid friendly(tm) appliances," in *Transmission and Distribution Conference and Exhibition, 2005/2006 IEEE PES*, May 2006, pp. 647 –652.

[101] B. Biegel, L. H. Hansen, P. Andersen, and J. Stoustrup, "Primary Control by ON/OFF Demand-Side Devices," *IEEE Transactions on Smart Grid*, preprint.

[102] S. Chanana and A. Kumar, "Proposal for a real-time market based on the indian experience of frequency linked prices," in *Energy 2030 Conference, 2008. ENERGY 2008. IEEE*, 2008, pp. 1–5.

[103] ——, "Demand response by dynamic demand control using frequency linked real-time prices," *International Journal of Energy Sector Management*, Apr. 2010.

[104] J. Kondoh, N. Lu, and D. J. Hammerstrom, "An evaluation of the water heater load potential for providing regulation service," *Power Systems, IEEE Transactions on*, vol. 26, no. 3, pp. 1309 –1316, aug. 2011.

[105] J. Kondoh, "Autonomous frequency regulation by controllable loads to increase acceptable wind power generation," *Wind Energy*, vol. 13, no. 6, pp. 529–541, 2010. [Online]. Available: http://dx.doi.org/10.1002/we.375

[106] A. Molina-Garcia, F. Bouffard, and D. Kirschen, "Decentralized demand-side contribution to primary frequency control," *Power Systems, IEEE Transactions on*, vol. 26, no. 1, pp. 411 –419, feb. 2011.

[107] C. Li, J. Zhang, H. Shi, Y. Cao, L. Hi, B. Fang, and X. He, "Consumer Electrical Equipment Asynchronous and Coordinating Response for Frequency Regulation," in *Innovative smart grid technologies (ISGT europe), 4th IEEE PES International Conference and Exhibition on*, Oct. 2013.

[108] D. Trudnowski, M. Donnelly, and E. Lightner, "Power-system frequency and stability control using decentralized intelligent loads," in *Transmission and Distribution Conference and Exhibition, 2005/2006 IEEE PES*, may 2006, pp. 1453 –1459.

[109] M. Donnelly, D. Trudnowski, S. Mattix, and J. Dagle, "Autonomous Demand Response for Primary Frequency Regulation," Pacific Northwest National Laboratory, Tech. Rep., Jan. 2012.

[110] K. Samarakoon, J. Ekanayake, and N. Jenkins, "Investigation of domestic load control to provide primary frequency response using smart meters," *Smart Grid, IEEE Transactions on*, vol. 3, no. 1, pp. 282 –292, march 2012.

[111] M. Cheng, J. Wu, J. B. Ekanayake, and N. Jenkins, "Primary frequency response in the Great Britain power system from dynamically controlled refrigerators," *CIRED 22nd Annual Conference on Electricity Distribution*, Jun. 2013.

[112] C. Zhao, U. Topcu, and S. Low, "Frequency-based load control in power systems," in *American Control Conference (ACC), 2012*, 2012, pp. 4423–4430.

[113] ENTSO-E, "Draft Demand Connection Codes," 27 Jun. 2012.

[114] ——, "Network Code on Demand Connection - Frequently Asked Questions," ENTSO-E, Tech. Rep., 21 Dec. 2012.

[115] D. Hammerstrom, N. Zhou, and N. Lu, "Controller design of power quality-improving appliances," in *Power Electronics Specialists Conference, 2007. PESC 2007. IEEE*, 2007, pp. 1164–1169.

[116] F. Geth, N. Leemput, J. Van Roy, J. Buscher, R. Ponnette, and J. Driesen, "Voltage droop charging of electric vehicles in a residential distribution feeder," in *Innovative Smart Grid Technologies (ISGT Europe), 2012 3rd IEEE PES International Conference and Exhibition on*, 2012.

[117] S. Iacovella, K. Lemkens, F. Geth, P. Vingerhoets, G. Deconinck, R. D'Hulst, and K. Vanthournout, "Distributed Voltage Control Mechanism in Low-Voltage Distribution Grid Field Test," in *Innovative smart grid technologies (ISGT Europe), 4th IEEE PES International Conference and Exhibition on*, Oct. 2013.

[118] P. Richardson, D. Flynn, and A. Keane, "Local versus centralized charging strategies for electric vehicles in low voltage distribution systems," *Smart Grid, IEEE Transactions on*, vol. 3, no. 2, pp. 1020–1028, 2012.

[119] S. Y. Hui, C. K. Lee, and F. Wu, "Electric springs®;a new smart grid technology," *Smart Grid, IEEE Transactions on*, vol. 3, no. 3, pp. 1552 –1561, sept. 2012.

[120] C. K. Lee, N. Chaudhuri, B. Chaudhuri, and S. Hui, "Droop control of distributed electric springs for stabilizing future power grid," *Smart Grid, IEEE Transactions on*, vol. 4, no. 3, pp. 1558–1566, 2013.

[121] Ostkraft, EA Energianalyse, Vestfrost Solutions, Danfoss, and Technical University of Denmark, "Demand as Frequency-controlled Reserve: Implementation and practical demonstration programme," EUDP, Tech. Rep. 64009-0001, May 2013.

[122] I. M. Cecilio, A. M. Ersdal, D. Fabozzi, and N. F. Thornhill, "An Open-Source Educational Toolbox for Power System Frequency Control Tuning and Optimization," in *4th IEEE PES Innovative Smart Grid Technologies Europe (ISGT Europe)*, Oct. 2013.

[123] "Virtual weather station daily tabular data," Online, 2013, accessed November 25, 2013. [Online]. Available: http://www.bornholmervejr.dk/vws/daily.htm

[124] B. Gwisdorf, S. Stepanescu, and C. Rehtanz, "Effects of demand side management on the planning and operation of distribution grids," in *Innovative Smart Grid Technologies Conference Europe (ISGT Europe), 2010 IEEE PES*, 2010, pp. 1–5.

[125] S. Rajagopal, R. Roberts, and S.-K. Lim, "Ieee 802.15.7 visible light communication: modulation schemes and dimming support," *Communications Magazine, IEEE*, vol. 50, no. 3, pp. 72–82, 2012.

[126] G. Kaestle, "Voltage Level as Information Carrier in Emergency Grid Operation," in *6th European Conference of PV-Hybrids and Mini-Grids*, 2012.

Appendicies

Appendix A

"Demand as Frequency Controlled Reserve: Implementation and Practical Demonstration"

This paper was originally published in the proceedings of Innovative Smart Grid Technologies Europe Conference 2011, Manchester England.

Figure A.1: Close up of the Smartbox with cover removed.

Demand as Frequency Controlled Reserve: Implementation and practical demonstration

Philip J. Douglass *Student Member, IEEE*, Rodrigo Garcia-Valle *Member, IEEE*, Preben Nyeng *Member, IEEE*, Jacob Østergaard *Senior Member, IEEE*, and Mikael Togeby

***Abstract*—One of the challenges in electric power systems with a high penetration of renewable generation is the provision of ancillary services. Traditionally these services have been provided by conventional generation, but as power from renewable sources (wind and PV) displaces conventional generation, new providers of ancillary services are needed. Frequency regulation is critical because fluctuating energy sources increase the need for this service. At very high levels of renewable penetration, all available frequency regulation services will be called on, including demand-side resources. Electric loads that provide thermal energy services are attractive because their heat capacity allows electric power consumption to be moved in time without degrading the quality of service. This concept is being demonstrated in field tests on the island of Bornholm, Denmark.**

***Index Terms*—Demand side, frequency control, demonstration project.**

I. Introduction

NON-DIPATCHABLE renewable energy sources (RES) especially wind, photo-voltaic (PV), and run-of-river hydro have been successfully integrated into existing power systems with modest system balancing costs, but as RES come to dominate in some locations, fundamental changes to the electric power system may be needed.

In 2010 22% of Danish electricity production came from wind turbines [1] and on the windiest nights, all of domestic electricity demand has been satisfied by wind turbines. The national government road-map for the Danish energy system calls for a continued build-out of wind generation reaching 42% of electricity production by 2020 [2]. This level of RES production will lead to significant periods when the power delivered by wind turbines is large enough to satisfy all demand. The large thermal power plants that historically have been the backbone of the power system will not be needed to deliver energy into the electric system, but replacing the ancillary services these generators provide (e.g. short-circuit current, voltage regulation, frequency regulation) is an unresolved issue. The frequency controlled reserve in particular is interesting because the service from central power plants does not only need to be replaced, the total amount provisioned must be increased because the fluctuating output of wind and PV increases the need for this service.

Modern wind power plants have control functions for curtailing production which allows them to provide frequency regulating service [3]. However unlike thermal power plants which save on fuel costs when not producing at full capacity, wind energy is "spilled" during curtailment.

Domestic demands with small electricity consumption are an untapped resource for providing a frequency regulated reserve [4]. The recent availability of low cost micro electronics makes the idea feasible and has motivated much research in the field. The Pacific Northwest National Laboratory (PNNL) and others have suggested that individual household appliances suitable for temporary disconnection can provide fast reserve that can react within seconds, e.g. refrigerators and air conditioners [5]–[7].

Inspired by these relevant research activities, we have started our research on demand as frequency controlled reserve in Phase I of our research [8]–[11]. This paper is a continuation of that research effort with a practical demonstration under real-life conditions. Phase I focused on theoretical investigations and analysis. In Phase II, practical experiments will be done with the generic types of frequency control of demand that have been developed in Phase I [8].

The reserves that are provided by using frequency controlled demands have several advantages, e.g. fast responding speed and low cost. Most importantly, it can enhance the system stability for the future power system, where a high penetration of fluctuating renewable energy is foreseen [8], [12]. Compared to the under-frequency load shedding schemes commonly in use today which disconnect loads at the substation level during extreme contingencies, this concept is a fine grained response from loads which allows for both up and down regulation, and is invisible to the end user.

The next section describes in more detail the concept of using demand for frequency regulation. It is followed by a description of our implementation used for demonstrating the concept. Data from the demonstration are presented.

P. Douglass, R. Garcia-Valle, and J. Østergaard are with Centre for Electrical Technology, Technical University of Denmark, Elektrovej-Building 325, 2800 Kgs. Lyngby, Denmark {pjdo, rgv, joe}@elektro.dtu.dk.

Preben Nyeng is with Energinet.dk, Tonne Kjærsvej 65, 7000 Fredericia, Denmark pny@energinet.dk.

M.Togeby is with EA Energy Analyses, Frederiksholms Kanal 4, 3. th., 1220 Copenhagen K. mt@eaea.dk

II. Demand as a frequency controlled reserve (DFCR)[1]

The system frequency is a universally available parameter that signals the balance between power injection from generators and power withdrawal from loads within a synchronous area. When generation and consumption are not in balance, the frequency changes at the rate of

$$\Delta\omega = \frac{P_m - P_e}{M} \quad (1)$$

Where P_m is the mechanical torque provided by the prime movers, P_e is the electrical torque on the generators, M is the system's inertia, and $\Delta\omega$ is the change in angular velocity. Island power systems typically experience poor frequency quality because of low M values. The Nordic power system sees the largest frequency excursions during periods of low loading (nights and summer) when M is relatively low.

DFCR has been proposed as a means of providing frequency regulation services by utilizing the ability of certain loads to shift their power consumption in time without compromising the provision of energy services. Individual electrical appliances can measure the system frequency and react to deviations from nominal frequency by adjusting their consumption up or down. This is done without the expense of introducing external communication channels between the DER and a dispatcher.

Loads that provide services such as cooling (refrigerators, freezers, air conditioners) and heating (space heating, water heating) can use the heat capacity inherent in the devices to store energy typically for a period of hours. These loads can be interrupted for several minutes and still maintain temperature within the targeted range. This flexibility can be used to defer power consumption to avoid moments when demand exceeds supply as reflected by an actual system frequency below the nominal value. Similar functionality can be delivered by pumping systems with storage.

Even though each individual device operates in an on/off manner, with a large population of devices their frequency response in aggregate will be smooth.

III. The Bornholm Power System

The island of Bornholm is located in the Baltic Sea, and is the site of ongoing experiments testing concepts for new Smart Grid technologies. Bornholm has been chosen for these experiments because the electric energy system is a microcosm of Denmark, representing 1% of the nation's area, population, and electric load. In 2007 there were around 28,000 customers on the island, with a peak load of 56 MW, a minimum load of 13 MW. The topology of the MV and LV grid are typical for Denmark except that Bornholm maintains the ability to operate in planned island mode. At more than 30%, wind energy represents a larger portion of total energy supply than for Denmark as a whole [13]. Over half the electric energy consumed on Bornholm is imported, which contributes to the relatively poor continuity of service because the single connection to the Nordic transmission system via an undersea cable has been severed on several occasions. When Bornholm is disconnected from the Nordic transmission system, the wind turbines must be shut down to maintain acceptable quality of frequency. A previous experiment found that when running as an electrical island with less that 4% wind production, frequency quality was lower than the Nordic grid codes allow [14]. In [15], it was shown in planning future scenarios, the availability frequency regulation resources were a limiting factor to increased wind penetration in island operation.

[1]Other references have abbreviated this concept as DFR, but DFCR is used here to avoid confusion with digital fault recorders.

IV. Demonstration Setup

We have designed and produced approximately 200 DFCR devices which each can interface to one of 3 types of appliances: refrigerators, electric heaters and arbitrary loads via a relay. The DFCR hardware was custom made for the experiment using off the shelf components. A low-cost micro-controller is used as the main CPU, while secondary processors are used to make frequency measurements, and control a GSM/GPRS modem. Fig. 2 depicts a close up of the installed DFCR devices.

The block diagram of the device is illustrated in Fig. 3. The mains voltage is run through a measurement transformer and an analog filter before being fed into a 16-bit A/D converter. The A/D converter samples the voltage and calculates the system frequency using a zero-crossing

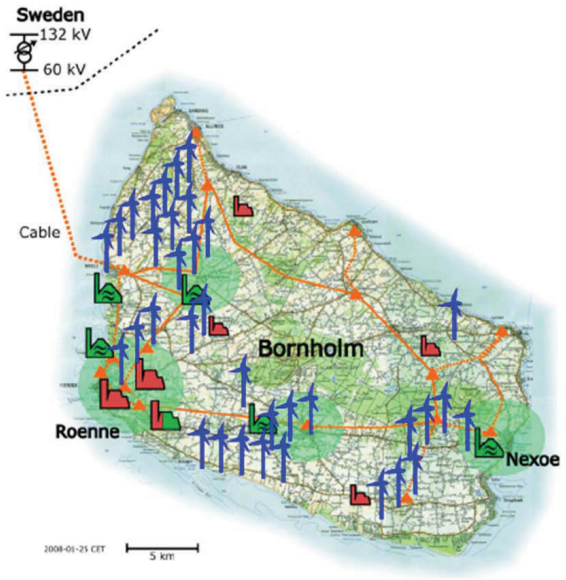

Figure 1. Map of the island of Bornholm showing 60kV transmission system (orange), wind turbines (blue), combined heat and power (red) [13].

Figure 2. Close up of the DFCR device with cover removed.

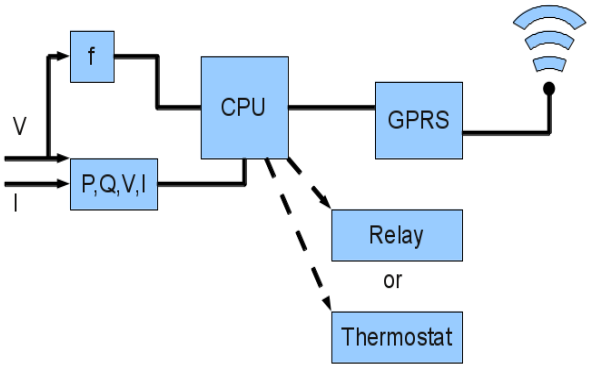

Figure 3. DFCR block diagram.

algorithm, averaging the measurements of 8 cycles. To document the operating characteristics of the device, an integrated circuit of a type often found in smart meters calculates the active and reactive power consumption at 2 second intervals. Measurements of frequency, power consumption, and device parameters (temperature, relay state) are recorded to an internal flash memory and uploaded to a server at regular intervals. Measurements are taken at a low resolution to build an image of the normal operation of the devices and when under/over-frequency events occur, the sampling frequency is increased to record high-resolution data. Both the low and high resolution sampling frequencies are configurable which was needed to throttle the quantity of data sent across the GPRS link.

HTTP is used to upload data, and download new configurations and firmware. Using a serial port connected to the GPRS modem, the CPU sends commands to the modem to establish HTTP connections [16], the TCP/IP stack is contained entirely within the modem firmware. Our server was written in the .NET framework and is hosted on a commercial web hotel. The server scripts interface to a database when adding and retrieving measurement data.

All measurements contain a time stamp. The clocks of the devices are synchronized to UTC by using the SNTP protocol [17].

The current measurement transformer was subject to significant parameter variations which required that each unit be individually calibrated.

A. Thermostatally Controlled Devices

In [11], a controller for a bottle cooler was developed and tested under labratory conditions. The ongoing experiment uses the same refrigerator model but increases the number of devices and tests them during normal usage conditions to reveal the aggregate behavior of a population of devices. Fifty bottle coolers like the one shown in Fig. 4 were installed restaurants, hotels and stores around Bornholm. The refrigerators contain a thermostat with two features necessary to interface with DFCR hardware: the ability to externally program temperature setpoint offsets, and an anti-short cycle feature which prevents damage to the compressor caused by restarting it before cooling liquid pressure has equalized [18]. There is no noticeable delay between changes in the setpoint offset and the thermostat's reaction.

Four parameters are given to control the response of the refrigerators:

- O_{max} Maximum temperature offset above user given value.
- O_{min} Minimum temperature offset below user given value.
- f_{max} Frequency where O_{min} is reached.
- f_{min} Frequency where O_{max} is reached.

The relationship between these parameters is shown in Fig. 5.

The experiment will test two types of frequency controlled reserve which roughly correspond to Nordel's specification of primary reserve (also called normal reserve), and secondary reserve (also called disturbance reserve) [19]. Both reserves specify a linear response to frequency deviations. Primary reserve mode is defined by $O_{min} = -O_{max}$, $f_{min} = 49.90Hz$ and $f_{max} = 50.10Hz$. Secondary reserve mode is defined by $O_{min} = 0$, $f_{min} = 49.50Hz$ and $f_{max} = 49.90Hz$.

Heater devices adjust the thermostat temperature down as frequency declines, so the definition of f_{max} and f_{min} are reversed.

B. Relay device

The on-off nature of the relay DFCR devices make them most appropriate for providing secondary reserve. To signal to users when the load was disconnected, a LED on the device turns on. The following parameters are specified:

- T_{maxd} Maximum duration of disconnection

T_{mind} Minimum duration of disconnection
T_{minc} Minimum connection duration after disconnection
T_{rdel} Reconnection delay
f_{off} Disconnect below frequency
f_{rec} Reconnect above frequency

Figure 4. DFCR device placed on the top of refrigerator, with serial communication wire visible.

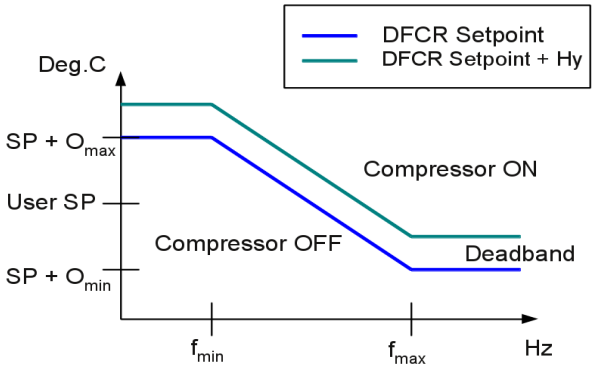

Figure 5. Relation between frequency and temperature setpoint offset for cooling application.

V. Preliminary results

In the start-up period, we focused on validating the data from the refrigerator devices to create a solid foundation for further experiments and analysis. To verify the frequency measurements and synchronization of time stamps, data was collected over one week. To verify the functioning of the thermostats, data from one day was analyzed.

A. Frequency Measurements and Time Stamp Synchronization

The system frequency is assumed to be the same throughout the synchronous area, so at a given point in time, the difference in frequency measurements from different devices can come from noise in measured signal, clock drift, and lack of precision in the time stamps. Lacking an independent source of frequency measurements we validated DFCR measurements by comparing frequency measurements taken on different devices at the same point in time. For each of the time stamps with 2 or more measurements, the average frequency was calculated and the standard deviation was found. The results from 397,000 measurements was $\sigma = 1.36585$ mHz. This level of error is well within the tolerances for our application. This analysis rounded timestamps to the nearest second, but the raw data has a resolution of milliseconds which indicates a potential to further narrow the level of error.

Figure 6 shows an example of high resolution frequency measurements taken over 40 seconds by 35 different devices.

B. Thermostats

To validate the functioning of the thermostats, the devices were configured to operate in normal reserve mode. The parameter values were

O_{max} = 2 °C
O_{min} = −2 °C
f_{max} = 49.90 Hz
f_{min} = 50.10 Hz

The expected result of this configuration was a positive correlation between refrigerator power consumption and system frequency, and a negative correlation between refrigerator air temperature and system frequency. To demonstrate this correlation, data samples were grouped by frequency in 25 mHz intervals in the range 49.9-50.1 Hz and two additional groups for samples above and below this range. For each group, the average power consumption measured by built-in metering circuit, and the average temperature as measured by the thermostat was found. The results plotted in Figures 7 and 8 show that the average power and average temperatures are with good agreement linearly dependent on the system frequency .

The only exception to the linear trend is the power consumption for the group $f < 49.90$ which is slightly

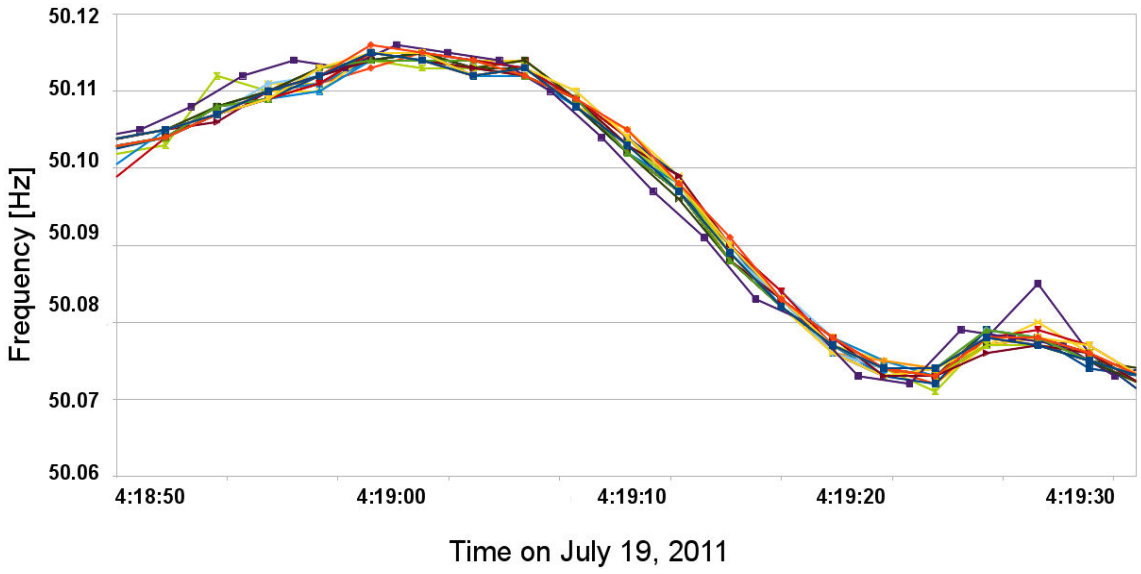

Figure 6. Typical high resolution measurement series during over-frequency with 2s sampling period over 40s. Measurements from 35 devices are superimposed.

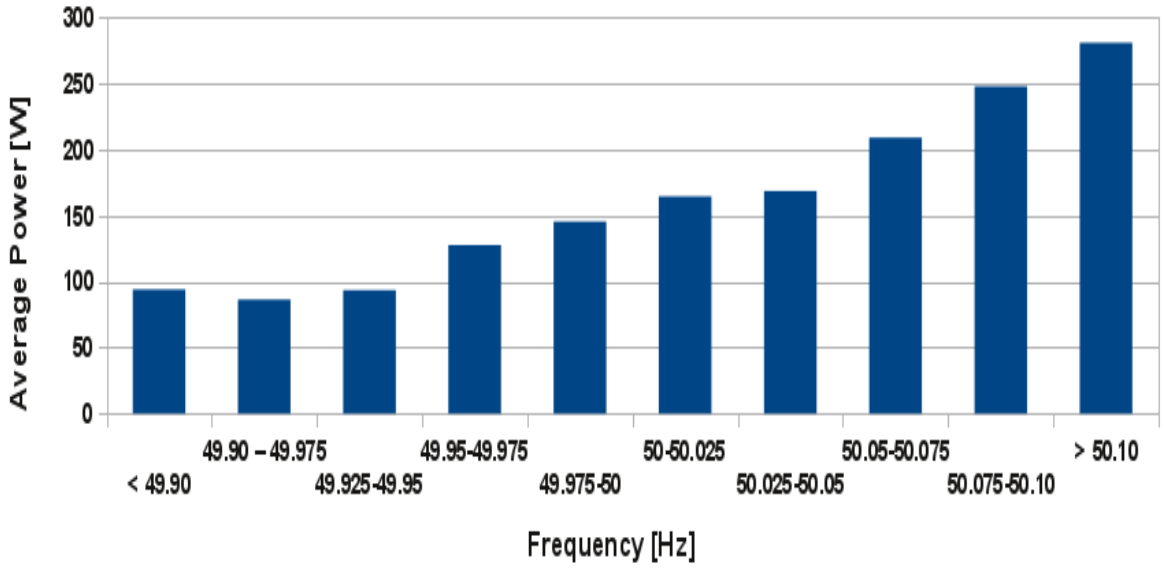

Figure 7. Relation between system frequency and power index.

higher that for $49.90 < f < 49.925$. Because the DFCR was configured to operate as a normal reserve, the thermostat setpoint was not changed at frequency values below 49.90. At the same time, the average temperature for the group $f < 49.90$ is above that for $49.90 < f < 49.925$. This indicates the presence of prolonged under frequency events, where the the increased power consumption of the low frequency group shows that the ability to shift power consumption in time has been exhausted.

VI. Discussion

In this demonstration project we have developed and tested devices which use electric loads to provide frequency controlled primary reserves. The results above verify the correct functioning of the developed DFCR devices with respect to their synchronization in time and thermostat response. While the DFCR increased the variation in air temperature of the refrigerators, earlier laboratory experiments have shown the variation in temperature of the goods stored inside is significantly less [11].

The devices we developed allowed existing products

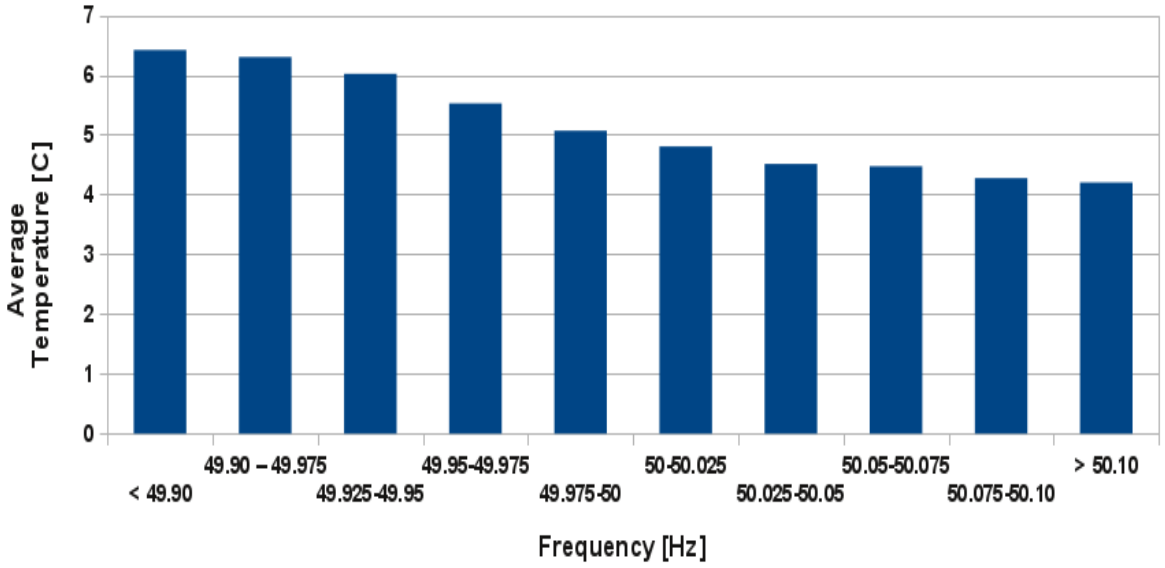

Figure 8. Relation between system frequency and average refrigerator air temperature.

to be retrofitted with DFCR functionality, but in a commercial roll out, the DFCR functionality would be built in to the appliance controller. Compared to conventional appliances, DFCR appliances would have the added expense of a circuit to measure the system frequency. This increase in the bill of materials could be subsidized by power system operators or financed by a market approach, e.g., participation in the Nordic ancillary services market.

The DFCR technology can be seen as an enhancement to the existing frequency dependent load, which is estimated rather than monitored. In a large scale roll out, monitoring many DFCR units can be achieved by estimation based on statistical sampling of a limited number of such appliances [20], [21]. Such a monitoring method may require the present reserve monitoring practice to be extend to specify the quality requirements including accuracy of the amount and availability.

For the DFCR to respond correctly during periods when the scheduled frequency deviates from the nominal frequency (i.e. during time correction), an external communication channel is required.

VII. Future Work

At the time of writing, the refrigerator DFCR devices had been deployed for only a couple weeks. The full experiment including refrigerators, floor heaters, and relay devices will run for the remainder of 2011, to provide a large data set for further statistical analysis. During this time, configuration parameters will be adjusted to allow the units to act as both primary reserve and secondary reserve. The highly accurate time stamps allows the units' transient response to large changes in system frequency to be studied.

A water treatment plant on Bornholm will participate in the experiment, allowing their large pumps to be controlled by DFCR.

In the future, the software on the devices will be extended to respond to an external control signal. This will be used in a follow-up experiment to demonstrate real-time pricing schemes.

During the development of the DFCR concept, the authors have also considered its coordination with other functions, such as DVCR for short-term voltage control [9], [10].

References

[1] Energinet.dk. [Online]. Available: http://www.energinet.dk/
[2] Energy Strategy 2050. The Danish Government, February 2011.
[3] G.C. Tarnowski, P.C. Kjær, S. Dalsgaard, A. Nyborg, Regulation and frequency response service capability of modern wind power plants, Power and Energy Society General Meeting, 2010 IEEE , vol., no., pp.1-8, 25-29 July 2010
[4] M. Kintner-Meyer, R. Guttromson, D. Oedingen, and S. Lang, Final Report for California Energy Commission: Smart Load and Grid-Friendly Appliances, Architecture Energy Corporation and Battelle Memorial Institute, 2003.
[5] B. J. Kirby, Spinning Reserve Provided From Responsive Loads. Oak Ridge, TN: Oak. Ridge Nat. Lab., 2003.
[6] PNNL, Grid Friendly Controller Helps Balance Energy Supply and Demand. [Online]. Available: http://www.gridwise.pnl.gov/docs/pnnlsa36565.pdf.
[7] J. A. Short, D. G. Infield, L. L. Freris, "Stabilization of Grid Frequency Through Dynamic Demand Control", *IEEE Transactions on Power Systems*, vol. 22, no. 3, august 2007
[8] Z. Xu, J. Østergaard, M. Togeby, Demand as Frequency Controlled Reserve, *IEEE Transactions on Power Systems*, vol.26, no.3, pp.1062-1071, Aug. 2011
[9] R. Garcia-Valle, da Silva L. C. P., Z. Xu and J. Østergaard. Smart demand for improving short-term voltage control on distribution networks, *GTD-IET Journal*, vol. 3, issue. 8, pp. 724-732, Aug. 2009.
[10] R. Garcia-Valle, da Silva L. C. P., Z. Xu and J. stergaard, Responsive Demand To Mitigate Slow Recovery Voltage Sags, European Transactions on Electrical Power, accepted for its publication, July 2011.

[11] P. Nyeng; J. Østergaard; M. Togeby; J. Hethey, Design and Implementation of Frequency-responsive Thermostat Control. International Universities Power Engineering Conference. Cardiff, Wales, 2010
[12] Z. Xu, M. Gordon, J. Østergaard, Towards a Danish power system with 50% wind - Smart grids activities in Denmark, IEEE PES General Meeting, 2009.
[13] J. Østergaard, J. E. Nielsen. The Bornholm Power System, An Overview. [Online] Available: http:www.powerlab.dk.
[14] Y. Chen, Z. Xu, J. Østergaard, Frequency analysis for planned islanding operation in the Danish distribution system - Bornholm In: Proceedings of the IEEE Universities Power Engineering Conference. Padova: Italy; 2008.
[15] J. R. Pillai, K. Heussen, P. A. Østergaard, Comparative analysis of hourly and dynamic power balancing models for validating future energy scenarios, *Energy*, Volume 36, Issue 5, May 2011, Pages 3233-3243, ISSN 0360-5442, DOI: 10.1016/j.energy.2011.03.014.
[16] Telit Wireless Solutions, Easy GPRS User Guide. 2010 [Online]. Available: http://telit.com/.
[17] D. Mills Network Time Protocol (Version 3): Specification, Implementation, and Analysis. [Online]. Available: http://rfc.net/rfc1305.html.
[18] Dixell, Installing and Operating Instructions XR30CX. [Online]. Available: http://www.dixell.com/.
[19] Nordel System Operation Agreement. 2006 [Online]. Available: http://www.nordel.org/.
[20] Elmodel Bolig. [Online]. Available: http://www.elmodelbolig.dk/.
[21] Priselastik Elforbrug hos de Større Elforbruger (Demand Response at Large Electricity Consumers), Dansk Energi Analyse and Norenergi, 2005.

Philip J. Douglass (Student Member '11) received his B.S. (Cum Laude) in Computer Science from the University of Maryland, College Park in 2001 and M.Sc. in Computer Systems Engineering from the Technical University of Denmark in 2003. Previously he worked as an embedded system developer in the telecommunications industry before starting a Ph.D. at the Centre for Electric Technology in 2010. His research interests include integration of telecommunications systems and energy systems, active distribution systems, and distributed energy resources.

Rodrigo Garcia-Valle (Student Member '99, M'08) received the electrical engineering degree from the National Polytechnic Institute of Mexico, in 2001, the M.Sc. degree from CINVESTAV-GDL, Mexico, in 2003 and obtained his Ph.D. degree from the University of Glasgow, UK, in 2007. In 2008, he was granted the Hans Christian Ørsted Award by DTU to carry out postdoctoral research activities. Since 2009 he holds the position as Assistant Professor. His research interests are dynamics, stability and control of electric power systems; synchrophasor measurement devices for smart transmission grids and renewable energy integration. He is an IEEE, IET and CIGRE member.

Preben Nyeng (M10) received the M.Sc. degree in industrial electrical engineering and the Ph.D. degree in power systems, from the Technical University of Denmark (DTU), Lyngby, in 2000 and 2011, respectively. He was with Logos Design A/S from 2000 to 2006, developing embedded hardware and software systems and related database and communications systems. From 2006 to 2011 he was with the Centre for Electric Technology at DTU, working in the field of smart grid, related information and communication technology and markets. In 2011 he assumed a position at Energinet.dk as Smart grid developer. Dr. Nyeng is a member of CIGRE, the International Council on Large Electric Systems.

Jacob Østergaard (M'95, SM'09) is a Professor and Head of Centre for Electric Technology, Department of Electrical Engineering, Technical University of Denmark, Lyngby. His research interests include integration of renewable energy, control architecture for future power system, and demand side. Professor Østergaard is serving in several professional organizations, including the EU SmartGrids advisory council.

Mikael Togeby received the M.Sc. and Ph.D. degrees from the Technical University of Denmark, Copenhagen, in 1983 and 1988, respectively. He is now Partner of Ea Energy Analyses A/S, Denmark. He has a long record of consultation service in electric energy industries. His interests include demand response, energy efficiency, and electricity market. Dr. Togeby is a member of several professional organizations, including the International Association for Energy Economics and the European Council for an Energy Efficient Economy.

Appendix B

Demand as Frequency Controlled Reserve: Experimental Results

B.1 "Smart Demand for Frequency Regulation: Experimental Results"

This paper appears in *IEEE Transactions on Smart Grid*, vol. 4, no. 3, pp. 1713-1720, Sept. 2013.

Smart Demand for Frequency Regulation: Experimental Results

Philip J. Douglass *Student Member, IEEE*, Rodrigo Garcia-Valle *Senior Member, IEEE*, Preben Nyeng *Member, IEEE*, Jacob Østergaard *Senior Member, IEEE*, and Mikael Togeby

***Abstract*—As renewable energy sources increase their penetration, the traditional providers of frequency regulation service, i.e. fossil fueled thermal power plants, will be displaced, motivating the search for novel providers such as demand-side resources. This paper presents the results of field experiments using demand as a frequency controlled reserve (DFCR) on appliances with programmable thermostats. The experiments conducted showed the response of a population of thermostatically controlled loads acting as normal reserves (up and down regulation) and disturbance reserves (up regulation only) as defined by the Nordic Grid Codes [1]. In addition, industrial pump loads and relay-controlled loads were tested as DFCR. The tests show that a population of refrigerators was able to deliver frequency reserves approximately equal to their average power consumption. Electric space heaters in the autumn season were able to provide frequency reserves of a magnitude 2.7 times their average power consumption.**

***Index Terms*—Demand side, frequency control, demonstration project.**

I. Introduction

TRADITIONALLY, electric generators are dispatched to follow passive loads. This mode of operation is infeasible with non-dispatchable stochastic energy sources such as wind and PV and one possible remedy is to dispatch loads to follow production. Today, many loads are equipped with microprocessors running firmware for controlling local processes. These loads could be programmed to actively monitor the state of the power system as a whole and schedule their own power use to help balance consumption with production.

Loads providing thermal energy services (e.g. refrigerators, heat pumps and resistive heaters) are well suited to following fluctuating generation because their inherent heat capacity acts as an energy storage device allowing electricity consumption to be shifted in time without compromising the quality of service. Thermostat controlled loads (TCLs) are a significant portion of total electric loads, representing around half of household electricity consumption in the USA [2].

P. Douglass, R. Garcia-Valle, and J. Østergaard are with Centre for Electric Power and Energy, Technical University of Denmark, Elektrovej-Building 325, 2800 Kgs. Lyngby, Denmark {pjdo, rgv, joe}@elektro.dtu.dk.

P. Nyeng is with Energinet.dk, Tonne Kjærsvej 65, 7000 Fredericia, Denmark pny@energinet.dk.

M. Togeby is with EA Energy Analyses, Frederiksholms Kanal 4, 3. th., 1220 Copenhagen K. mt@eaea.dk

Despite the declining cost of communications devices, providing a real-time digital communications interface from a system operator to small loads represents a significant cost barrier to widespread deployment. However, there is already a parameter which is universally available to indicate the instantaneous balance of electric energy production and consumption, namely the system frequency.

The relation between power generated, $P_{\mathrm{M}}(t)$, power consumed, $P_{\mathrm{L}}(t)$, and deviations in system frequency,$\Delta f(t)$, is given by the swing equation [3]

$$\Delta P_{\mathrm{M}}(t) - \Delta P_{\mathrm{L}}(t) = 2\mathrm{H}\frac{d\Delta f(t)}{dt} + \mathrm{D}\Delta f(t) \qquad (1)$$

where H is the inertia constant, and D is the load damping coefficient.

Loads may measure the system frequency and by adjusting their power consumption up or down as the system frequency rises or falls, they are able to provide reserves for frequency regulation. This concept is known as demand as a frequency controlled reserve (DFCR) [4], or alternatively Frequency Adaptive Power Energy Rescheduler (FAPER) [5], Dynamic Demand [6], Frequency-Sensitive Gridfriendly™Appliances [7], or Frequency Responsive Load Controller [8].

This paper presents the result of a field experiment where, for the first time, DFCR loads have been installed in an uncontrolled working environment and their performance as a group has been monitored.

The load damping coefficient captures the behavior of motors, which constitute a large portion of total load. Similar to motors, DFCR loads' power use in aggregate is proportional to system frequency, but there are several aspects that cause DFCR loads to be poorly modeled by their contribution to the load damping coefficient. These aspects are:

1) **Time Dependency**: DFCR loads imply an energy storage buffer, and this buffer's "state of charge" (SOC) depends on the historical progression of the system's frequency. The appliance's frequency response depends on the SOC the energy storage buffer.
2) **Discrete nature of loads**: many types of loads are either ON/OFF, it is only in aggregate that they can provide a gradual, linear frequency response.

3) **Parameter Design**: The damping coefficient of traditional loads is a natural property, rather than a design decision. With DFCR loads, the system planner has the freedom to specify the frequency response, rather than be constrained by the inherent properties of passive loads. The frequency response can be specified over at limited range of frequencies and be flat outside that band.

While the DFCR loads are physically located in the low voltage distribution system, it is the transmission system operator who needs to account for their behavior when specifying the requirements for frequency regulation reserves.

This paper is structured as follows: Section II describes the experimental setup including the design of the DFCR controller and loads, Section III describes the parameter configuration for operation in the Nordic power system. Section IV presents and discusses the results of the experiment. Finally, Section V concludes with a description of future work.

II. Experimental Setup

We have currently deployed approximately 70 DFCR appliances out of a planned 200 units, primarily on an island in the Baltic Sea, Bornholm, which is connected to the Nordic transmission grid by a 60 kV under-sea cable. Bornholm has a peak load of 55 MW and a high penetration of wind energy (over 30% of electric energy production annually), but when the island is disconnected from the Nordic grid, wind production must be curtailed to maintain acceptable frequency quality [9], [10].

Each DFCR system consists of two parts: a commercially available appliance which has been modified to expose a serial port to an external controller, and an external controller which we have produced for this experiment from off-the-shelf components [11]. The TCLs are composed of bottle coolers located in hotels, restaurants and convenience stores, and resistive electric heating systems placed in single family homes. Industrial loads were tested in a water treatment facility.

A. DFCR Controller Hardware

Fig. 1 shows a block diagram of the DFCR controller. The DFCR controller measures frequency using a zero-crossing algorithm and averaging over 8 cycles. Every 250 ms the CPU receives and processes frequency measurements. The controller timestamps all measurements with a real-time clock that is synchronized via the internet time protocol NTP. The accuracy of the timestamps and frequency measurements was evaluated by finding examples when multiple controllers took frequency measurements within the same second, and the resulting standard deviation of frequency measurements was 1.3 mHz [11].

An integrated circuit dedicated to power measurement measures voltage and current, and calculates active and reactive power consumption of the attached loads. Data on power consumption and system frequency, as well as parameters specific to the appliance under control are sampled once per minute, and stored into a large internal memory. In addition, when a large frequency excursion occurs, data is collected at a high resolution (as often as every 2 seconds). This data is periodically uploaded to a database using a GSM/GPRS wireless modem and the HTTP protocol.

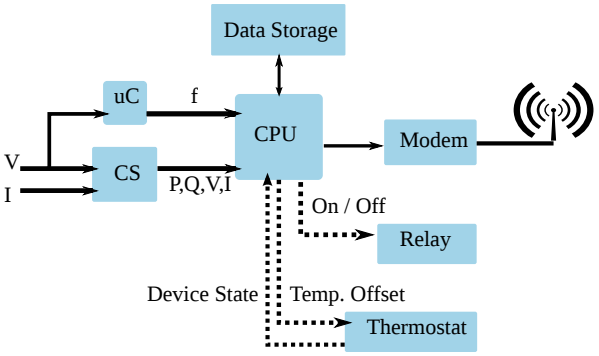

Figure 1. DFCR block diagram. The CPU is a low cost micro-controller with 8 kB of RAM. The system frequency is measured by a secondary micro-controller (uC). Power consumption (real and reactive) is calculated by a dedicated component (CS). The measurements are buffered to an SD card (Data Storage), and uploaded periodically to a database via GSM/GPRS (Modem). Some boxes have a relay built into the device, others communicate to programmable thermostats via a serial cable.

The DFCR controller parameters are configurable, and the firmware can be remotely upgraded. This facility was used to test different types of frequency reserves.

B. Loads

1) Bottle Cooling Refrigerators: The refrigerators used in the experiment are all identical bottle coolers with a glass door and internal light that remains on when the door is closed. They contained a programmable thermostat that, via a serial cable, delivered data to the controller about the internal state of the device and accepted configuration commands. The DFCR controller utilized a mode of the thermostat that added a temperature offset to the user-given setpoint. Only the operation of the compressor is affected by the external controller, the light and other internal processes which account for a residual power consumption are not affected by the DFCR function. Comparing power consumption before and while the compressor runs reveals that the compressor itself consumes on average 230 W. When the compressor is off but the light is on the refrigerator consumes 30 W and when the light is off it consumes 13 W. The daily load profile of the refrigerators reveals that the maximum consumption occurs at noon, when the power consumption is 20% higher than during the night.

The user configures the refrigerator thermostat with a temperature setpoint. The thermostat turns the compressor

on when the internal air temperature rises above the deadband of 2°C, and turns the compressor off when the air temperature reaches the setpoint. The thermostat includes an "anti-short cycle" feature, which ensures that at least 3 minutes elapse between stopping and restarting the compressor. This feature protects the motor from over loading at startup due to high pressures in the condenser. During normal operation, without introducing setpoint offsets, the ON/OFF cycle repeats every 15 minutes, where the compressor has a duty cycle of 32%.

The normal operation of the thermostat is periodically interrupted by the defrost cycle which turns the compressor off for approximately 30 minutes and allows the internal air temperature to rise well above the deadband. A refrigerator is in the defrost state 6% of the time. To analyze the effect of DFCR functionality, refrigerators in defrost state are excluded from the data set. The "anti-short cycle" feature also interferes with the ideal operation of the refrigerators, but unlike with the defrost state, there was no feedback from the thermostat to the DFCR controller as to when this feature was active, so its effect could not be explicitly accounted for.

In total, 40 refrigerators were deployed, and data was available from 35 of them for the time period chosen for analysis. The refrigerators that did not deliver data failed because of problems such as poor GSM connectivity, faulty thermostats or missing serial connection between the external controller and thermostat.

2) Electric Space Heaters: The electric heaters used in the experiment are resistive radiators in private residences with a rated power consumption between 0.5 kW and 2 kW. As with the refrigerators, the user gives a temperature setpoint, and the DFCR controller adds an offset to the setpoint depending on the system frequency. The operation of the thermostat is not as straightforward as the refrigerators because temperature measurements are filtered before being compared to the setpoint and deadband. This filtering is done to compensate for the heat generated by the microelectronics in the thermostat itself, and to optimize power consumption while accounting for the heat capacity of the home and the behavior of its occupants.

The heat load is highly influenced by ambient temperatures. The test period occurred from the beginning of October to the end of November where ambient temperatures on Bornholm averaged 8.0°C [12], and indoor temperatures of the test houses averaged 21.2°C.

3) General Purpose Relay-Controlled Loads: Data was collected from 10 controllers equipped with a relay that de-energized all attached loads. These units opened the relay when system frequency fell below a given configurable threshold, and reconnected when system frequency returned above a higher threshold, subject to time constraints on the minimum and maximum allowable disconnect time. Another time constraint ensured that after being disconnected, the load remained reconnected for a minimum time span. A more detailed presentation of this algorithm can be found in [4].

The loads connected to this controller were diverse including pumps for circulating water, resistive heaters, and small refrigerators. These loads were located in educational institutions, offices and homes.

4) Wastewater Treatment Plant: Treatment of wastewater is an energy intensive service with a large untapped potential for demand response. In Denmark wastewater treatment consumed 528 GWh of electric energy in 2009, accounting for 1.6% of all electricity consumption [13]. The central wastewater treatment plant serving Bornholm's largest city (pop. $\approx 14,000$) participated in the DFCR experiment by allowing some non-critical loads to be controlled to provide frequency controlled disturbance reserves. These loads were in the form of induction motors that pumped water, and moved cleaning brushes. The DFCR control box provided a binary input into an existing industrial control system which was responsible for actuating the loads. A signal from a DFCR controller indicated when the system frequency had fallen below a given threshold, and the industrial control system was reprogrammed to use this signal to interrupt processes that tolerated interruption, while giving first priority to ensuring that process constraints were not violated. The behavior of these loads are comparable to the relay-controlled loads, with the exception that the time constraints are handled by the industrial control system, not the DFCR controller.

DFCR units acting exclusively as power measurement devices were attached to each of the controlled loads. Data from 13 loads representing an aggregate average power consumption of 5.7 kW was analyzed.

5) Summary of Loads: A representative time series of the system frequency and aggregated power consumption of 3 types of DFCR loads is shown in fig. 2. During this time period the refrigerator loads are configured as a disturbance reserve (up regulation only), and show a weak response during the under-frequency excursion around minute 20. The water treatment plant, the largest load group, interrupts consumption for 15 minutes during the under-frequency excursion, and displays a short spike in consumption upon reconnection. Heater loads concentrate their consumption to time periods when frequency is above nominal, providing down regulation as well as up regulation.

III. Configurations of DFCR for the Nordic Power System

System operators seek to minimize the extent and duration of frequency deviations from the nominal value. The Nordic power system has been experiencing declining frequency quality for the past 10 years, in 2011 system frequency was outside the acceptable range of 50 Hz$\pm$100 mHz for more than 2% of the time [14]. During periods when frequency was below the acceptable range,

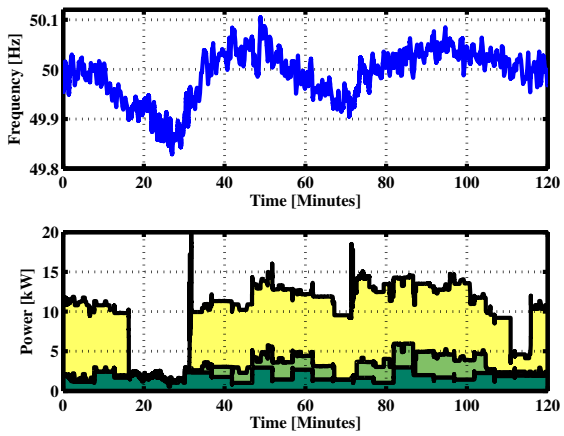

Figure 2. Time series of system frequency (top) and aggregate response of DFCR loads (bottom) over a representative two hour period. In the bottom sub-figure the consumption of different devices is stacked, with the refrigerators is dark green at the bottom, heaters in light green in the middle, and the water treatment plant in yellow at the top.

insufficient frequency controlled reserves were available to satisfy the n-1 reliability criteria.

The Nordic grid maintains frequency stability by purchasing frequency controlled reserves from central power plants in 4 hour blocks one day in advance. In the hour of operation, the system operator monitors system frequency for off-nominal excursions and tie lines for deviations from scheduled transfers, and manually activates the least cost up or down regulation resources to correct any imbalances. In the event of an imbalance between power supply and demand, the frequency controlled reserves act to stop the system frequency from changing, but they do not restore the frequency to the nominal value. At present, the Nordic system lacks an automatic frequency restoration reserve, and this results in long periods when the system frequency operates at off-nominal values.

The frequency controlled reserves are divided into two subcategories: Normal Reserve and Disturbance Reserve. The normal reserve is active in the range 49.90 Hz - 50.10 Hz, and requires a linear response from generators within 180 s. Generators which participate in this reserve are continuously adjusting their output to match the small fluctuations in system frequency, but their slow response, while favorable to operators of thermal power plants, has a negative effect on frequency quality. The disturbance reserve is active in the range 49.50 Hz - 49.90 Hz, providing an up regulation service. It is also a linear response, but it must act faster than the normal reserve, being 50% activated within 5 s, and fully activated within 30 s [1]. This type of reserve is intended to act on rare occasions, such as when a transmission line, or power plant trips. At present, because of the poor frequency quality mentioned previously, the disturbance reserve is overused, being activated about once an hour.

Table I
PARAMETERS FOR NORMAL RESERVE

Controller Type	Parameter Name	Value
TCL	Minimum Temperature Offset	-2°C
TCL	Maximum Temperature Offset	2°C
TCL	Lower Frequency Response Limit	49.90 Hz
TCL	Upper Frequency Response Limit	50.10 Hz

A. DFCR for Normal Reserve

The TCLs are well suited for continuous operation as a normal reserve, because the setpoint offsets can be effectively done in 0.1°C increments. When the devices were configured to operate as a normal reserve, the temperature setpoint given by the user corresponded to the thermostat setting at the nominal system frequency, 50.00 Hz. The thermostat temperature setpoint was offset from the user-given setpoint by a value linearly proportional to the deviation of the system frequency from nominal as described in [15].

The range of setpoint variations was chosen to exceed the size of the thermostat's deadband, so that a sudden change from 50.00 Hz to 49.90 Hz would turn all devices off, including those that had recently turned on. Values for the controller's parameters are given in table I. The relay-controlled loads, and the loads of the wastewater treatment plant are not suitable for operating continuously as a normal reserve.

B. DFCR for Disturbance Reserve

For the TCLs, operation as a disturbance reserve is similar to the normal reserve, with the differences being that the the thermostat is rarely offset, and when it is the offset is always towards the ambient temperature. The temperature offset range of the TCLs operating as disturbance reserve is -3°C at 49.70 Hz and 0°C at 49.90 Hz. This is a smaller range, but a larger deviation of temperature from the user-given setpoint than the normal reserve. A sustained setpoint deviation of -3°C could be unacceptable to users, but is allowable for a disturbance reserve because of the short time periods spent in this frequency range.

The relay-controlled loads, and the loads of the water treatment plant were all programmed to shed load at 49.90 Hz. Using a single cutoff threshold simplified the implementation and analysis of the devices, but from a system operator's perspective this is undesirable behavior. The risk caused by this implementation is exemplified by the large cohort of PV inverters in Germany which are all programmed to cut off production at 50.20 Hz [16]. In a large scale deployment, the threshold frequency would need to be spread over a range of values to avoid introducing disturbances caused by step changes in load.

The general purpose relay-controlled loads were given conservative time constraints to accommodate the diversity of load types, shown in table II. The time constraints on

Table II
PARAMETERS FOR DISTURBANCE RESERVE

Controller Type	Parameter Name	Value
TCL	Minimum Temperature Offset	-3°C
TCL	Maximum Temperature Offset	0°C
TCL	Lower Frequency Response Limit	49.70 Hz
TCL	Upper Frequency Response Limit	49.90 Hz
Relay	Minimum Disconnect Time	30 s
Relay	Maximum Disconnect Time	120 s
Relay	Minimum Reconnect Time	240 s
Relay/Water	Cutoff Frequency	49.90 Hz
Relay/Water	Reconnect Frequency	49.95 Hz

the signal sent to the wastewater treatment plant were set to very permissive values, and were rarely active.

IV. RESULTS AND DISCUSSION

This section presents the results of the experiment, grouped by configuration type and load type.

A. Normal Reserve

1) Refrigerators: Data was taken from 26 refrigerators over 16 weeks. Samples of frequency, power and temperature were taken by each control box every minute. The samples were sorted chronologically and the mean power consumption, and temperature values of the population were found for each minute. This method resulted in power consumption values scaled to the size of a single refrigerator, rather than the aggregate value of the population. The data from each minute was grouped by system frequency value and then the mean power consumption and temperature was found for each frequency group. The results for power consumption, shown in fig. 3, are well fit by a linear least squares approximation. The data set is less dense at frequency extremes because system frequency follows a Gaussian distribution around 50.00 Hz. At frequencies above 50.10 Hz and below 49.90 Hz, the linear trend breaks down because the thermostat's offset has reached the limit of it's deviation from the user-given setpoint.

The slope of the least squares linear regression is 0.431 kW/Hz. Given that the thermostat was changed with 20 °C/Hz, the relation of temperature offset to power consumption is 21.6 W/°C. The difference in average power consumption at 50.10 Hz and 49.90 Hz was 90.1 W. Compared to the compressor's power consumption of 230 W, we find that 39.2% of the compressor's power has been mobilized to participate in DFCR service. The average power consumption of the refrigerators (including light and residual consumption) was 89.4 W, slightly less than the power provided for the frequency response.

The distribution of values within each frequency group was analyzed by finding the quartiles, as shown in fig. 4. The difference between quartiles increases as frequency increases. For frequencies below 49.95 Hz, the first quartile is where all compressors in the population are off.

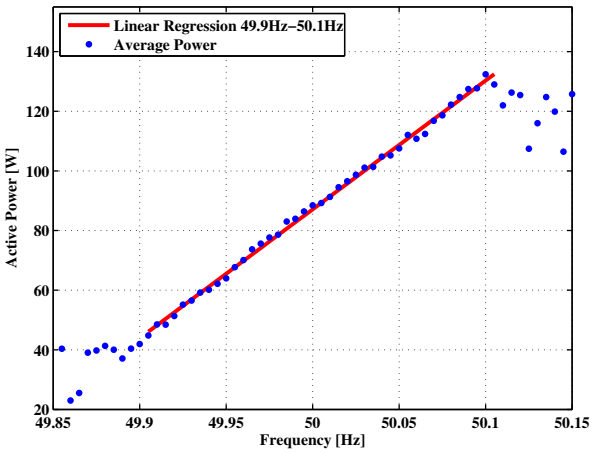

Figure 3. Average frequency response of a refrigerator with least squares linear regression. Temperature offset varied linearly with ±2°C in the range 49.90 Hz - 50.10 Hz, with 0°C offset at 50.00 Hz.

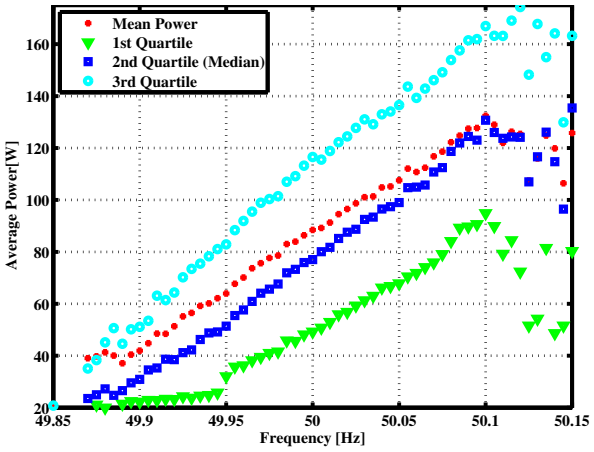

Figure 4. For each frequency group, mean power is shown together with the median, 1st and 3rd quartiles.

The power consumed by the refrigerators' compressor is used to cool the air inside, but the air temperature changes more slowly than power consumption, and is delayed by the heat capacity of the heat transfer circuit. Plotting average internal air temperature against average frequency for each minute, fig. 5 shows an inverse correlation of temperature to system frequency, as expected. The average temperature varies by approximately ±1.3°C from 49.90 Hz to 50.10 Hz, even though the thermostat setpoint has been offset by ±2°C.

Continuously changing the refrigerators setpoint offset increased the number of times that the compressor cycled ON and OFF by 10% compared to non-DFCR operation.

To reveal how the frequency response changed due to the frequency history, the data was divided into 3 groups based on the average historical frequency: low historical frequency ($\overline{f} < 49.975$ Hz), middle historical frequency (49.975 Hz $< \overline{f} <$ 50.025 Hz) and high historical frequency ($\overline{f} > 50.025$ Hz). The frequency

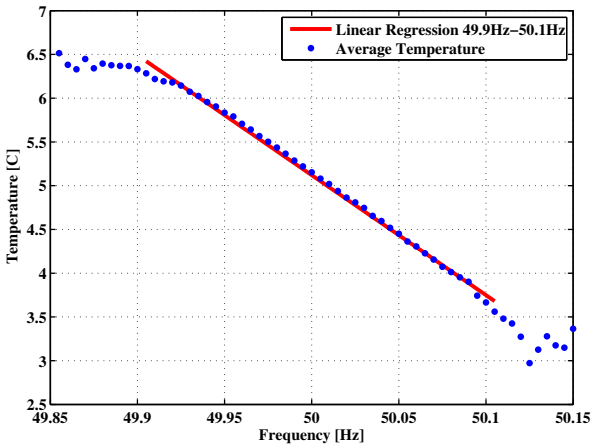

Figure 5. Average internal air temperature of refrigerators vs frequency with least squares linear regression.

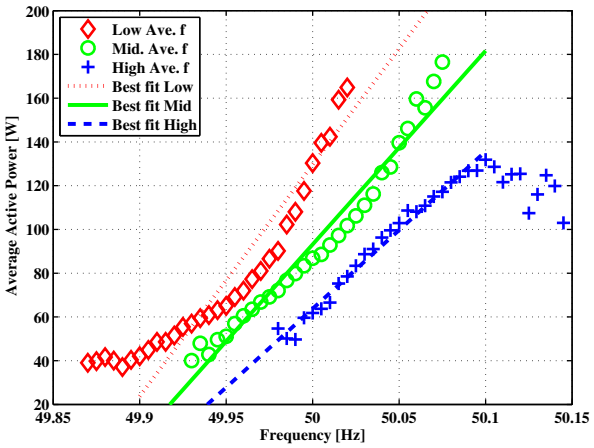

Figure 6. Frequency response at low, middle and high historical frequencies when calculating average frequency over 6 minutes, with best fit lines.

thresholds dividing groups were chosen to balance the number of samples falling into each group, with 50% of samples in the middle group. Comparing the frequency response of the 3 groups shows how it is influenced by the progression of frequency in the recent past. When the historical frequency has been high, the average power consumed at nominal frequency is lower than when the historical frequency has been in the middle or low range. The inverse happens when the historical frequency is lower than nominal. Fig. 6 shows the frequency response of the 3 groups when averaging the historical frequency over 6 minutes. The time period for averaging frequency values was varied from 2 to 20 minutes to reveal that time scale which has the most impact on the frequency response. The difference between the 3 groups is quantified by finding a linear best fit of each group, and then comparing the expected values at nominal frequency. The difference in expected values, shown in fig. 7, rises to a peak at 6 minutes before declining. This result indicates that frequency response is best predicted by combining the influence of the instantaneous frequency value and the average frequency of the preceding 6 minutes.

2) Electric Heaters: For a period of 8 weeks in autumn data was collected from 5 houses with electric heaters with a combined rating of 6 kW. The power consumption data was aggregated to reveal the total frequency response of the population, shown in fig. 8. The frequency response is asymmetric around the nominal frequency, with a steeper slope for up regulation (3.55 kW/Hz) than for down regulation (0.834 kW/Hz). Capacity of down regulation is exhausted around 49.93 Hz when the thermostat had been offset by 1.4°C. An asymmetric frequency response similar to the one shown in fig. 8 was observed in laboratory experiments with a refrigerator [15]. This behavior was attributed to a low duty cycle which gives a greater capacity for down regulation than for up regulation.

The frequency response between 49.90 Hz and 50.10

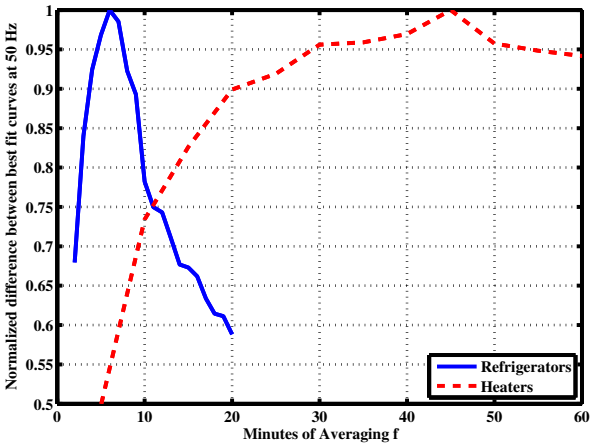

Figure 7. The difference between low, middle and high frequency best fit lines at nominal frequency for different sizes of time windows for calculating average frequency. The y-axis is normalized relative to the maximum difference observed for each device.

Hz was 435 W, 2.7 times the average power consumption of 160 W. The frequency response will depend greatly on the ambient temperature, and the time period under consideration contained periods when no heat demand was present. A subset of data from 2 houses over 11 days of favorable weather conditions showed a frequency response equivalent to 92% of the rated power of the heaters.

Fig. 7 shows that the time dependence of the frequency response is greatest when averaging historical frequency values over 45 minutes.

B. Disturbance Reserve

1) Refrigerators: The refrigerators were reconfigured to operate as a disturbance reserve for an 8 week period. Analyzing the frequency response results shown in fig. 9 shows that, despite the noise caused by a relatively small data set at extreme values, a frequency response is apparent at frequency values below 49.90 Hz and frequencies

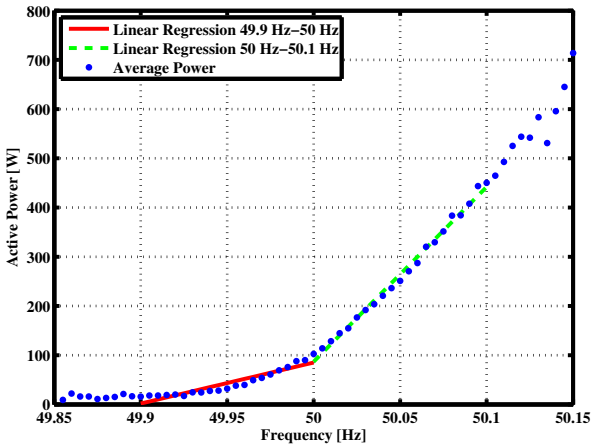

Figure 8. Frequency response of electric heaters with piecewise linear regression. The average power consumption approached 0W before the thermostat's offset limit at 49.90 Hz was reached.

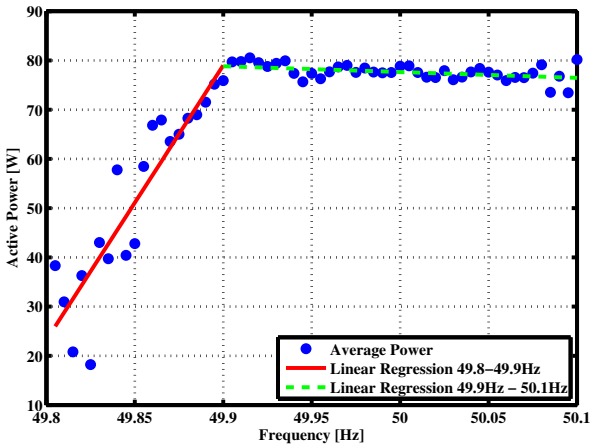

Figure 9. Frequency response of refrigerators acting as a disturbance reserve, shown with piecewise least squares linear regression in regions above and below 49.90 Hz.

above this value gave no response. The slope of the best fit line in the range 49.80 Hz - 49.90 Hz is 558 W/Hz, or 37 W/°C. Despite the fact that the slope of the temperature offset as a disturbance reserve (15°C/Hz) is lower than in the normal reserve (20°C/Hz), the frequency response per degree of temperature offset is almost twice as much. An explanation of this behavior can be found by considering that when a disturbance occurs the internal temperatures of the refrigerators are most likely in the nominal state, giving large room for deferring power consumption for the short duration of extreme under-frequency events. In the normal reserve case, system frequency is seen to dwell at off-nominal values for extended periods of time, weakening the average response.

The size of the data set at extreme frequencies is too small to conclude the total amount of frequency response provided by the refrigerators. For measurements takes below 49.85 Hz, the average power consumption was 42

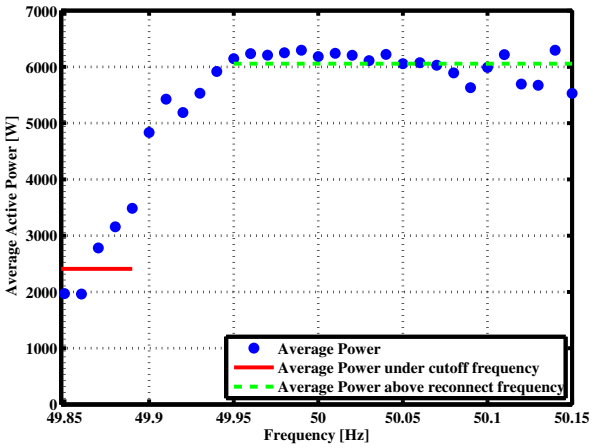

Figure 10. Frequency response of water treatment plant configured with disconnect frequency 49.90 Hz and reconnect frequency 49.95 Hz. Solid line shows average power consumption below cutoff frequency, dashed line shows average power consumption about reconnect frequency.

W, indicating that at this frequency the response was 36 W, equivalent to 46% of the average power and 16% of the compressor's power.

2) Water Treatment Plant: The water treatment plant displayed two modes of operation: normal and curtailed. In normal operation, load was measured to lie between 3 kW and 9 kW most of the time. When load was curtailed, the residual power consumption was around 0.25 kW. The relative frequency of operation in each of these two states determined the average active power consumption. The aggregate frequency response of all the loads in the water treatment plant measured over a 9 week period is shown in fig. 10. As expected, a step change in power consumption is observable at the cutoff frequency (49.90 Hz). Below the cutoff frequency, the average power consumption shows a linearly increasing trend because of time constraints on the DFCR signal, and because the plant controller occasionally overrides the DFCR signal to prevent violations of process constraints. The linearly increasing trend of average power consumption between the cutoff frequency and the reconnect frequency (49.95 Hz) was the result of hysteresis in the DFCR signal, as well as time constraints and process controller overrides.

The average power consumption above the reconnect frequency was 6.05 kW, compared to an average below the cutoff frequency of 2.41 kW, a reduction of 60%.

3) Relay-Controlled Loads: During the experimental period, the frequency response of the relay-controlled was the opposite of what we intended: lower frequencies corresponded to higher power consumption. This is explained by the dominating influence of time constraints on the state of the relays. When the system frequency was below the cutoff value, 60% of the time the loads were energized because of the constraint on the maximum disconnect time and minimum reconnect time. When frequency was above the cutoff value, 1% of the time the relays had de-

energized loads because of the minimum disconnection time constraint. The peak in power consumption occurs at the reconnect frequency, 49.95 Hz, and this is because of an inrush current and rebound effect as the loads restore their desired state after being interrupted. But the maximum disconnect time constraint meant that the loads could be energized at other low frequency values, and this resulted in power consumption at all low frequencies values being higher that when operating at nominal frequency.

The controller algorithm itself is not invalidated by these results, it is the parameter values need to be revised. The implementation behaved as specified, the problem was that the time constraints were not tuned to the actual frequency conditions of the Nordic power system. Raising the reconnect frequency would help mitigate the problem associated with the minimum reconnect time, and to work around the maximum disconnect time constraint the cutoff frequency could be lowered, so the reserve is active less often and for shorter time periods.

V. Conclusion and Future Work

This paper presents work on DFCR appliances that builds on previous laboratory experiments by scaling up the number of frequency controlled devices, increasing the diversity of loads under control, and testing them during daily use.

In absolute terms, the amount of power under DFCR control in this experiment was rather modest, on the order of 10 kW. However, relative to the power demand of each of the loads, the frequency response was significant. For demand-side resources in the residential sector to become economically viable, the fixed costs of providing this functionality must be small to match the small power demand of each individual unit. The DFCR controllers used in this experiment were not themselves cost effective, but the use of low-cost components for the core functions of measuring frequency and executing the DFCR algorithm support cost assumptions made in previous cost benefit analyses such as [4] and [17].

An analysis of the frequency and power consumption data of the TCLs found that while operating as a frequency reserve in the range 49.90 Hz - 50.10 Hz, the frequency response was larger than the average power consumption. The loads under control in the wastewater treatment plant reduced power consumption by an average of 60% during under-frequency events. The response of general purpose relay-controlled loads were sensitive to the time constraints, frequency threshold values and the distribution of frequency values for synchronous system where they are connected. The slope of response measured as W/Hz was larger when the refrigerators operated as a disturbance reserve, though the magnitude of response was smaller.

Because the DFCR controllers allow all control algorithms to be remotely upgraded, the experimental platform is generally useful for other demand response studies. When the DFCR study in concluded, the controllers will be reprogrammed to respond to an external price signal, rather than system frequency [18].

Acknowledgements

This work was supported by Danish Energy Agency's "Energy Technology Development and Demonstration Program" (EUDP). Special thanks to Christian Brandt Rasmussen, Rune Brus, Nina Marie Holmboe and Janos Hethey for their contributions.

References

[1] Pacific Northwest National Laboratory, "Grid friendly controller helps balance energy supply and demand." Online http://www.gridwise.pnl.gov/docs/pnnlsa36565.pdf, 13 Jun. 2006, accessed April 18, 2012. [Online]. Available: http://www.gridwise.pnl.gov/docs/pnnlsa36565.pdf

[2] Energy Information Administration, "Residential Energy Consumption Survey," U.S. Dept. Energy, Washington, DC, Tech. Rep., 2009.

[3] Hassan Bevrani, *Robust Power System Frequency Control*. Springer, 2009.

[4] Zhao Xu, J. Østergaard, and M. Togeby, "Demand as frequency controlled reserve," *Power Systems, IEEE Transactions on*, vol. 26, no. 3, pp. 1062 –1071, aug. 2011.

[5] F. Schweppe, R. Tabors, J. Kirtley, H. Outhred, F. Pickel, and A. Cox, "Homeostatic utility control," *Power Apparatus and Systems, IEEE Transactions on*, vol. PAS-99, no. 3, pp. 1151 –1163, may 1980.

[6] J. Short, D. Infield, and L. Freris, "Stabilization of grid frequency through dynamic demand control," *Power Systems, IEEE Transactions on*, vol. 22, no. 3, pp. 1284 –1293, aug. 2007.

[7] N. Lu and D. Hammerstrom, "Design considerations for frequency responsive grid friendly(tm) appliances," in *Transmission and Distribution Conference and Exhibition, 2005/2006 IEEE PES*, May 2006, pp. 647 –652.

[8] A. Molina-Garcia, F. Bouffard, and D. Kirschen, "Decentralized demand-side contribution to primary frequency control," *Power Systems, IEEE Transactions on*, vol. 26, no. 1, pp. 411 –419, feb. 2011.

[9] Y. Chen, Z. Xu, and J. Ostergaard, "Frequency analysis for planned islanding operation in the danish distribution system - bornholm," in *Universities Power Engineering Conference, 2008. UPEC 2008. 43rd International*, sept. 2008, pp. 1 –5.

[10] G. Tarnowski, P. Kjær, J. Østergaard, and P. Sørensen, "Frequency control in power systems with high wind power penetration," in *9th International Workshop on Large-Scale Integration of Wind Power into Power Systems*, 2010.

[11] P. Douglass, R. Garcia-Valle, P. Nyeng, J. Østergaard, and M. Togeby, "Demand as Frequency Controlled Reserve: Implementation and practical demonstration," *Innovative Smart Grid Technologies Europe*, 2011.

[12] Danish Meteorological Institute, "Weather Archive," Online, 2012, accessed December 12, 2012. [Online]. Available: http://www.dmi.dk

[13] Danish Energy Association, "Dansk Elforsyning Statistik," 2009.

[14] E-Bridge, "Analysis & Review of Requirements for Automatic Reserves in the Nordic Synchronous System," Tech. Rep., 21 May 2011.

[15] P. Nyeng, J. Østergaard, M. Togeby, and J. Hethey, "Design and implementation of frequency-responsive thermostat control," in *Universities Power Engineering Conference (UPEC), 2010 45th International*, 31 2010-sept. 3 2010, pp. 1 –6.

[16] K. Burges, P. Zolotarev, and J. Lehner, "Impact of Large-scale Distributed Generation on Network Stability During Over-Frequency Events & Development of Mitigation Measures," Sep. 2011. [Online]. Available: http://www.vde.com/en/fnn/pages/50-2-hz-study.aspx

[17] ENTSO-E, "Draft Demand Connection Codes," 27 Jun. 2012.

[18] C. Bang, F. Fock, and M. Togeby, "Design of a real time market for regulating power," EA Energy Analyses, Tech. Rep., Dec. 2011. [Online]. Available: http://www.flexpower.dk

B.2 "Demand as Frequency Controlled Reserve: Water Treatment, Relay-Controlled Loads, Micro-grid"

This paper is part of the final report for the "Demand as Frequency-controlled Reserve" project, not a peer-reviewed publication.

Demand as Frequency Controlled Reserve: Water Treatment, Relay-Controlled Loads, Micro-grid

Philip J. Douglass *Student Member, IEEE*

Abstract

This report is part of the "Demand as Frequency Controlled Reserve" project funded by the Danish EUDP. This report presents the results from 3 tests of frequency sensitive loads acting as primary frequency reserves: a water treatment plant with an industrial control system, diverse loads controlled by means of a relay, and refrigerators with programmable thermostats which were connected to a micro-grid.

I. Introduction

FREQUENCY regulation is an essential service for AC power systems. Providing this service using power generators is costly in financial and environmental terms because it requires part-loaded units. Using loads to provide frequency regulation service has been previously described in [1]–[5]. This report provides results from Demand as Frequency Controlled Reserve (DFCR) field experiments conducted with Bornholm's Forsyning's water treatment plant, general purpose relay-actuated loads, and refrigerators connected to a micro-grid on the small island of Christiansø.

II. Bornholm Forsyning's Wastewater Treatment Plant

Treatment of wastewater is an energy intensive service with a large untapped potential for demand response. In Denmark wastewater treatment consumed 528 GWh of electric energy in 2009, accounting for 1.6% of all electricity consumption [6]. The central wastewater treatment plant serving Bornholm participated in the DFCR experiment by allowing some non-critical loads to be controlled to provide frequency controlled disturbance reserves. These loads were in the form of induction motors that pumped water and induction motors that moved cleaning brushes. All motors were interfaced with power electronics that limited inrush current (soft-starters) and were actuated by an existing industrial control system (here referred to by the term "Supervisory Control and Data Acquisition" (SCADA)). A DFCR control Smartbox measured the AC system frequency and provided a binary input signal into the SCADA which indicated when the system frequency had fallen below a given threshold, shown in fig. 1. The SCADA used this signal to interrupt processes that tolerated interruption, while giving first priority to ensuring that process constraints were not violated, shown in fig. 2. The behavior of the control Smartbox is identical to the relay-controlled loads (discussed later) except that the time constraints were relaxed, as these were handled by the SCADA, not the Smartbox.

Measurement Smartboxes, with firmware identical in the control Smartbox but without an output signal, were installed at each load to gather data. The complete system is shown in fig. 2. Data was collected over a period of 9 weeks from 11 loads and 1 control Smartbox.

A. Results

The water treatment plant displayed two modes of operation: normal and curtailed. In normal operation, load averaged 5.8 kW. When load was curtailed, the residual power consumption averaged

P. Douglassis with Centre for Electrical Technology, Technical University of Denmark, Elektrovej-Building 325, 2800 Kgs. Lyngby, Denmark pjdo@elektro.dtu.dk.

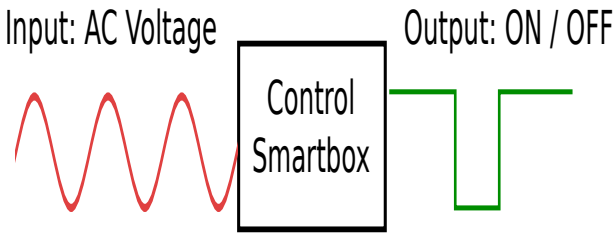

Figure 1. Diagram of control Smartbox. It takes an AC power supply as input, and produces a binary ON/OFF signal for which is then used an input to the SCADA.

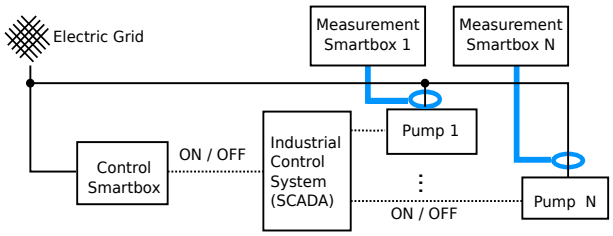

Figure 2. Diagram of Bornholm Forsyning's system. The grid AC power supply is given to a control Smartbox which generates an ON/OFF signal to the SCADA. The SCADA then controls the pumps based on the Smartbox signal and internal process constraints. A Measurement Smartbox is attached to each load to gather data on power consumption.

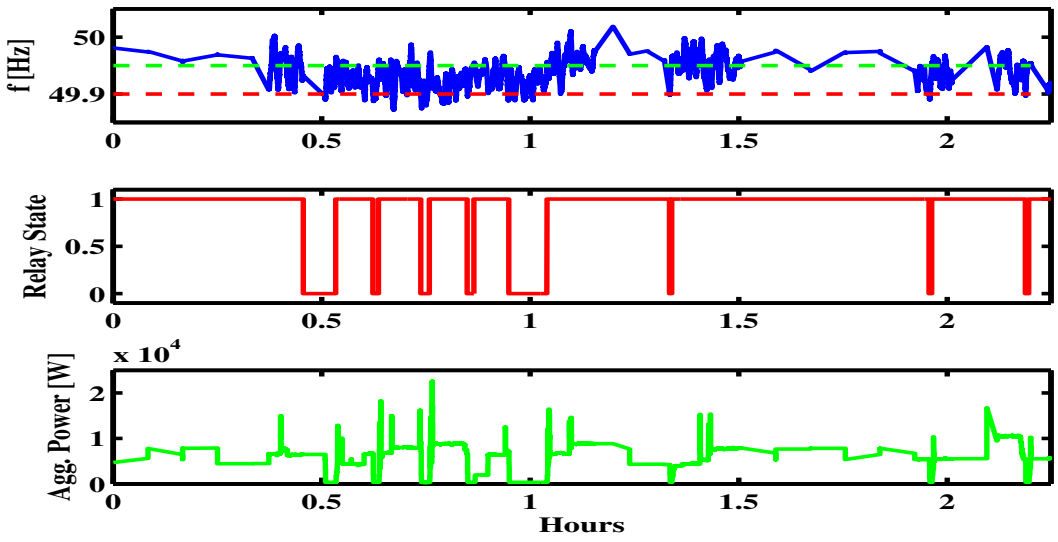

Figure 3. Typical time series from water treatment plant. Sampling frequency is 5 minutes and increases to 2 s for 5 minutes after each under-frequency event. In the top plot, frequency is shown with the cutoff frequency (dashed red) and reconnect frequency (dashed green). Every time the relay changes to the off state, power is curtailed. When the relay state changes to the ON state, a spike in power consumption is observed as motors accelerate.

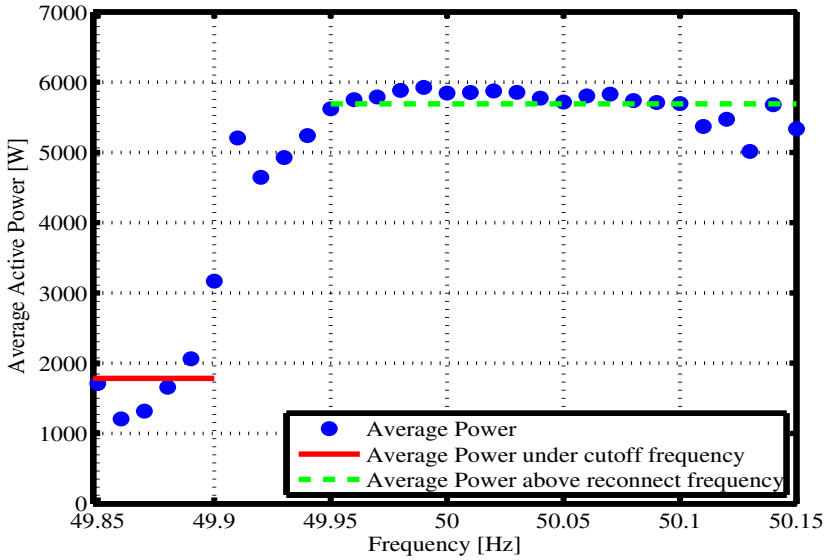

Figure 4. Frequency response of water treatment plant configured with disconnect frequency 49.90 Hz and reconnect frequency 49.95 Hz. Solid line (red) shows average power consumption below cutoff frequency, dashed line (green) shows average power consumption about reconnect frequency.

0.34 kW. A time series showing the typical operation pattern of the plant is shown in fig. 3. The relative frequency of operation in each of these two states determined the average active power consumption. The aggregate frequency response of all the loads in the water treatment plant measured over a 9 week period is shown in fig. 4. As expected, a step change in power consumption is observable at the cutoff frequency (49.90 Hz). Below the cutoff frequency, the average power consumption shows a linearly increasing trend because of time constraints on the DFCR signal, and because the plant controller occasionally overrides the DFCR signal to prevent violations of process constraints. The linearly increasing trend of average power consumption between the cutoff frequency and the reconnect frequency (49.95 Hz) was the result of hysteresis in the DFCR signal, as well as time constraints and process controller overrides.

The average power consumption above the reconnect frequency was 5.69 kW, compared to an average below the cutoff frequency of 1.78 kW, a reduction of 69%. The average power consumption, and hence, potential for frequency regulation, as a function of time of day did not display significant diurnal variation.

The speed of the load curtailment, and the effect of the SCADA on delay was analyzed by extracting time series of high-resolution data each time the control Smartbox change the state of the control signal. Data from 763 events was extracted. The timestamps of the time series' were normalized to the moment the control signal changed, and the power consumption was normalized to the level before load curtailment. Average power consumption, and quartiles describing the lowest 25% and highest 25% of samples was found at two second intervals (the sampling frequency), shown fig. 5. The results show that the load has a weak response in the first 2 s period after the curtailment signal is given, and is almost fully curtailed after 6 s. To see the effect of the SCADA, the state of the unused relay within the measurement Smartboxes was found. The measurement Smartboxes ran the same firmware as the control Smartbox, so differences between the relay state of the measurement Smartbox and the actual power consumption can be attributed to delays introduced by the SCADA. Fig. 6 shows the response of measurement Smartboxes. The respone in fig. 6 appears similar to fig. 5 at all time points, except at 4 s after the start of the event, where the measurement Smartboxes

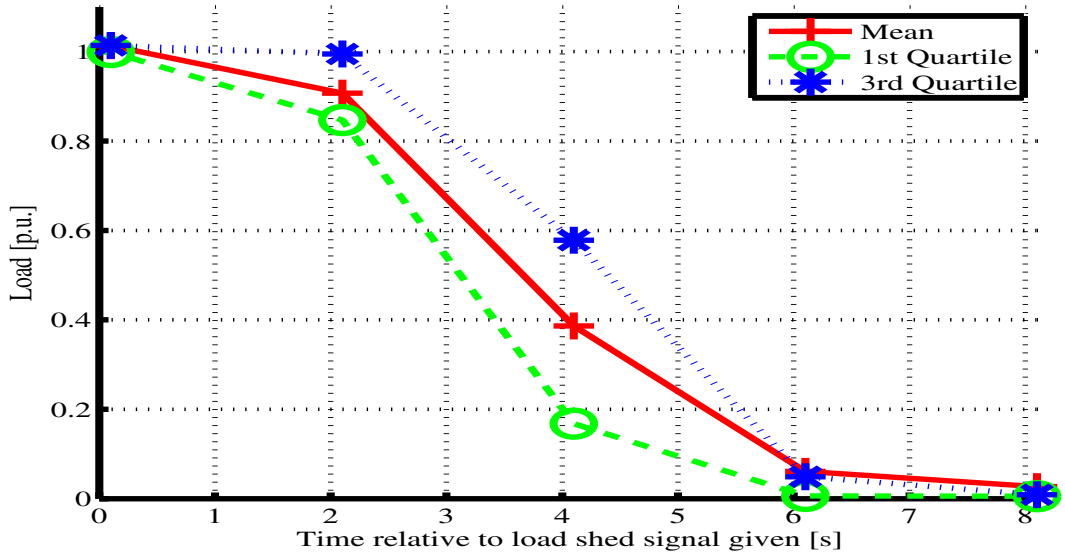

Figure 5. The response of water treatment plant to load curtailment signal. Average, and quartiles of power consumption of 763 events. Normalized in time relative to the time when the control Smartbox gave the load shed signal, normalized in power relative to the pre-curtailment load.

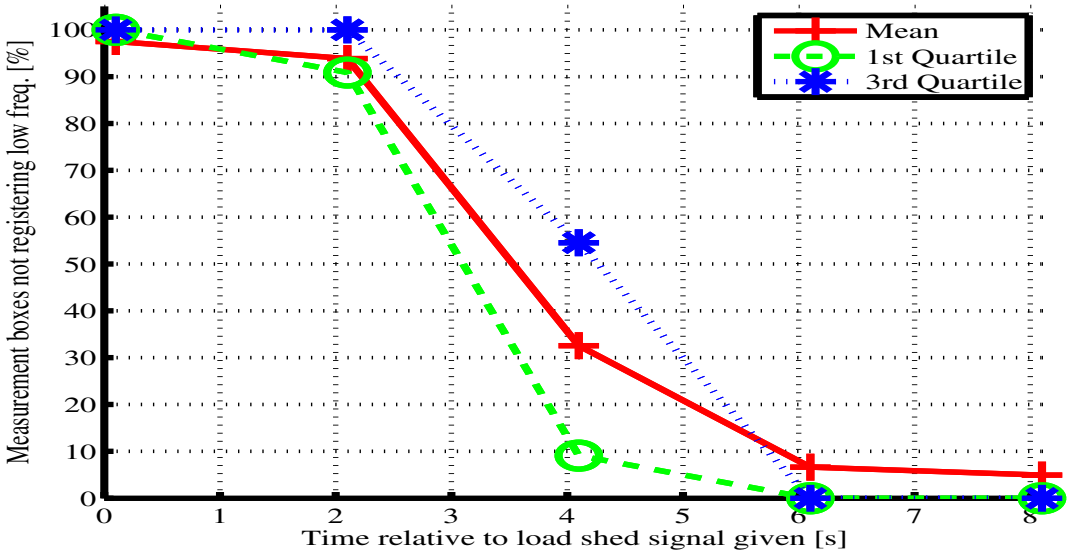

Figure 6. The response of the 11 measurement Smartboxes

are on average 70% curtailed, while the actual power measurements are only 60% curtailed.

Finally, the load profile upon restoring power was analyzed, shown in fig. 7. When the control Smartbox gave the restore signal, load returned to it's pre-curtailment level, though the 3rd quartile of events showed a short (5 s) transient increase of power consumption peaking at 140% the pre-curtailment power. The reason the spikes in power consumption apparent in fig. 3 are not more apparent in fig. 7 is that the spikes in power consumption that occurred each time load was restored were short (2 s), and spread out over a 30 s period, so that the average power consumption at each point in time was barely effected by the outliers.

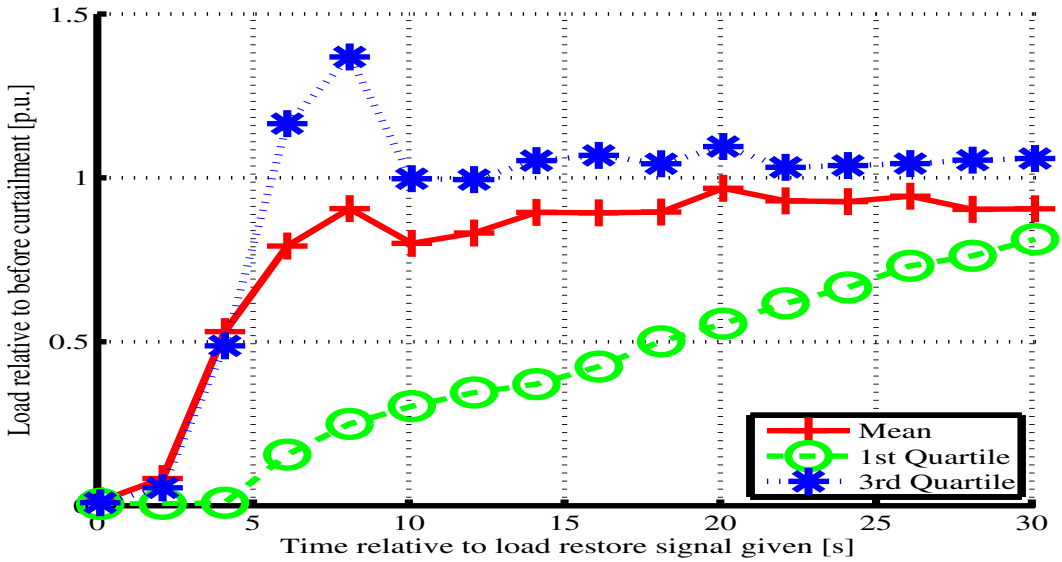

Figure 7. The response of water treatment plant to load restoration signal. Average, and quartiles of power consumption of 763 events. Normalized in time relative to the time when the control Smartbox gave the load restoration signal, normalized in power relative to the pre-curtailment load.

III. General Purpose Relay-Controlled Loads

A variety of loads were tested for frequency regulation service by connecting them to a relay which was controlled by a Smartbox. These units opened the relay when system frequency fell below a given configurable threshold, and reconnected when system frequency returned above a higher threshold, subject to time constraints on the minimum and maximum allowable disconnect time. Another time constraint ensured that after being disconnected, the load remained reconnected for a minimum time span. Fig. 8 shows the time constraints graphically, a more detailed presentation of this algorithm can be found in [3].

The loads connected to this controller were diverse including pumps for circulating water, resistive heaters, and small refrigerators. These loads were located in educational institutions, offices and homes. A single configuration was used on this diverse population of loads, and as a results the time constraints were chosen conservatively. The configuration of the parameters was as follows:

Parameter	Value
f_{off}	49.90 Hz
$f_{restore}$	49.95 Hz
t_{min_off}	30 s
t_{max_off}	120 s
t_{min_on}	240 s

Data was collected from 9 controllers over a period of 12 weeks.

A. Results

During the experimental period, the frequency response of the relay-controlled showed a weak frequency response because of the strong influence of time constraints. A typical time series, where the maximum disconnect time and minimum reconnect time determine relay state, is shown in fig. 9. When the system frequency was below the cutoff value, more than 60% of the time the loads were energized because of the constraint on the maximum disconnect time and minimum reconnect

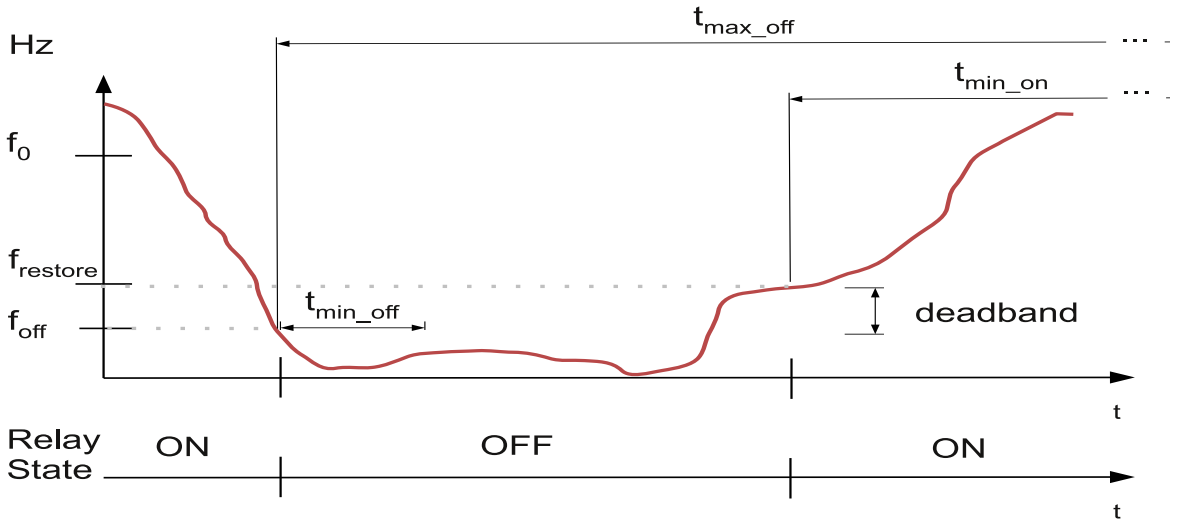

Figure 8. State of relay depends on system frequency and time constraints. Ideally, the relay is OFF when system frequency is below f_{off} and ON when system frequency is above $f_{restore}$. Time constraints take precedence over the ideal frequency response.

time, shown in fig. 10. A spike in power consumption occurs when the loads are reconnected because of an inrush current and rebound effect as the loads restore their desired state of operation. During normal operation, the average individual power consumption was 37.4 W. When the devices disconnected load, the average individual power consumption was 0.5 W. When the devices were in the Restore state, and the t_{min_on} constraint was active, the average individual power consumption was 43.5 W. The aggregate frequency response, shown in fig. 11, shows that power was curtailed on average from 310 W to 270 W, a reduction of 13 %.

These results show that the frequency response is highly sensitive to the parameter values, and in this case the parameter values were not optimized for the Nordic power system. Raising the reconnect frequency would help mitigate the problem associated with the minimum reconnect time, and to work around the maximum disconnect time constraint the cutoff frequency could be lowered, so the reserve is active less often and for shorter time periods. Recent work by Beigel, et.al. [7] has addressed the problem of designing frequency threshold values by means of analyzing historical frequency data of a synchronous area, a method which could be applied to these devices.

IV. Christiansø

Christiansø is a decommissioned naval base that is a popular tourist destination. Around 100 people live permanently on the 0.22 km^2 island [8]. Their electric power system is composed of 4 diesel powered generators, two with a rating of 180kW, one 130kW and one 60kW. At the moment, there is no renewable electricity generation, though the wind and solar resources are available.

Two bottle cooling refrigerators with DFCR functionality have been installed. The refrigerators were configured to provide disturbance reserves, as defined by the Nordic Power system grid codes. Measurements are taken at high and low resolutions, meaning 2 second and 5 minute intervals. Data was collected in the summer of 2011 with DFCR disabled to establish a base-case, and in the autumn/winter of 2012 with DFCR enabled.

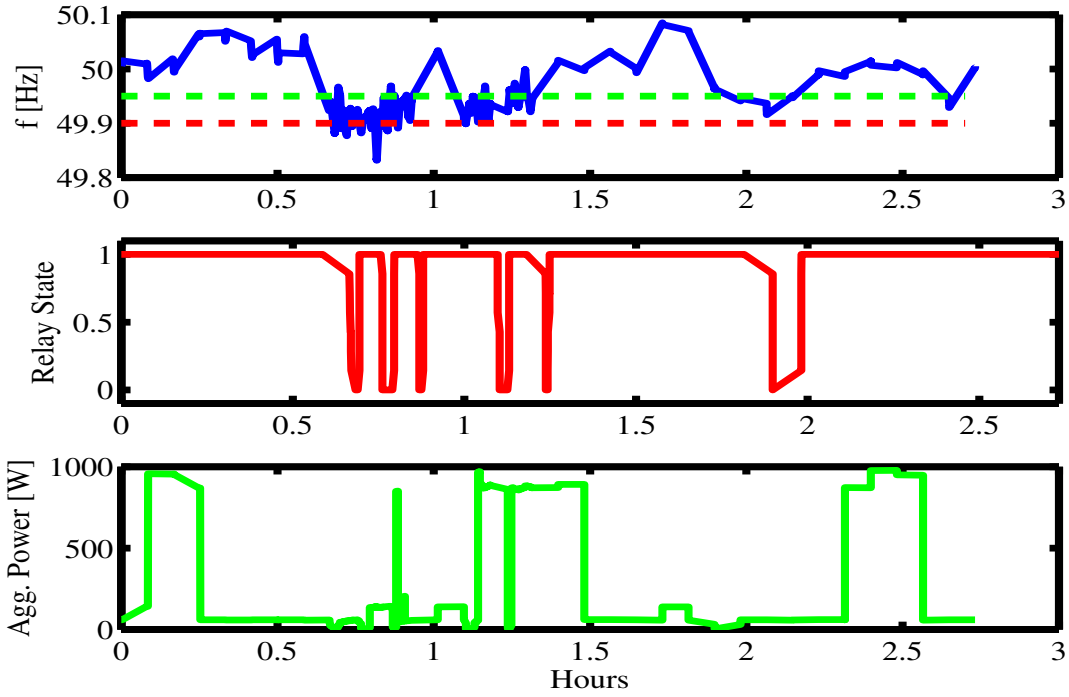

Figure 9. Typical time series of relay controlled loads with poorly configured time constraints. Frequency is shown at the top, aggregate power of all relay controlled loads in middle, and relay state at the bottom. When frequency declines, the loads are disconnected, but after the maximum disconnect time they are reconnected, with a spike in power consumption. When the loads are reconnected, the system frequency has declined to be lower than the initial cutoff frequency.

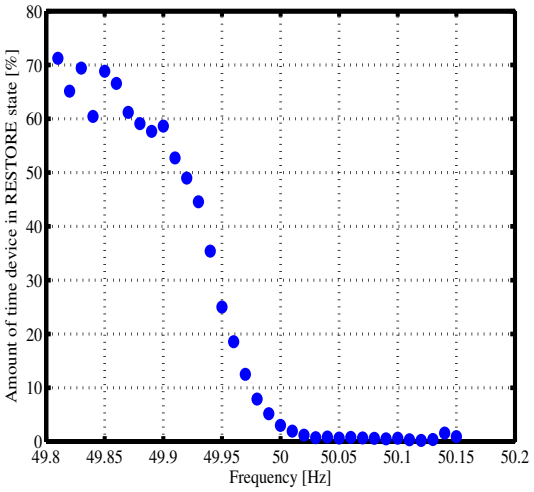

Figure 10. Amount of time where t_{min_on} constraint was active (”Restore“ state) as a function of frequency. In this poorly configured example, time constraints dominate the frequency response, and the devices uses power when the system operates below the cutoff frequency.

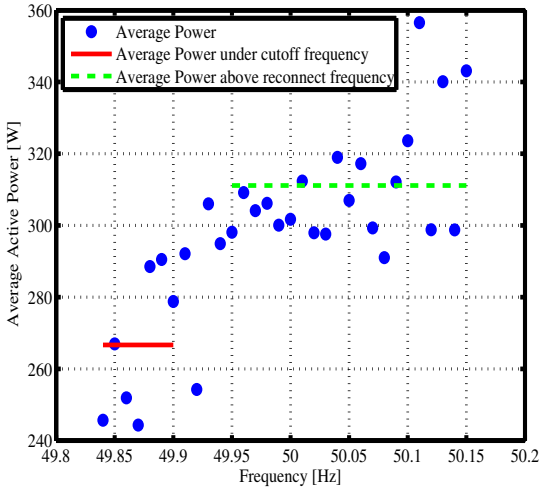

Figure 11. Average aggregate power consumption as a function of frequency. The frequency response is relatively small because of the predominance of time constraits.

A. Results

Compared to a large interconnected synchronous system, the frequency on the island has a mean value far from nominal, and frequency fluctuations are larger. The system operated in two distinct frequency regimes, corresponding to the operation of different generators in their fleet, visible in fig. 12. Data was grouped accordingly: group one from June 30 to July 26 2011, and group two from October 1 to January 31 2013. Within each group, the frequency measurements fit well into a normal distribution, with the average value of 50.00Hz for group one and 50.12Hz for group two. The standard deviation for group 1 was 43.4 mHz, for group 2 was 62.1 mHz. For comparison, when Bornholm's power system is operated as an island, the average frequency is 50.00 Hz, and the standard deviation is 40 mHz.

Because the configuration of the refrigerators did not account for the operation at off-nominal frequencies, the refrigerators configured as a disturbance reserve did not offset their thermostats for long periods of time. The frequency response, shown in fig. 13, reveals a wide variation in power consumption at frequencies far from the mean because of the sparsity of the data set. In the 4 month data collection period, the system frequency was below 49.90 Hz, the frequency where the demand response began, for 0.2 % of the time, less than 6 hours. A least squares linear best fit of the frequency response region (49.80 Hz - 49.90 Hz) shows a slope of 144 W/Hz, with large residuals. Compared to identical refrigerators connected to the Nordic power grid [9], the response on Christiansø appears to be much weaker (558 W/Hz vs 144 W/Hz).

The statistical, rather than direct, relation between system frequency and fridge power consumption means the relatively small data set from Christiansø leaves a large margin for error as to what the true slope of the response is. While the size of the data set did not allow strong conclusions to be drawn about the frequency response, this is a realistic scenario in the sense that a disturbance reserve is allocated to respond to rare conditions (i.e. large faults). Today utility operators are reluctant to rely on autonomous or indirectly controlled demand response because of the difficulty of verifying the response, and our results confirm that verification of statistical responses of a few units to rare events is difficult.

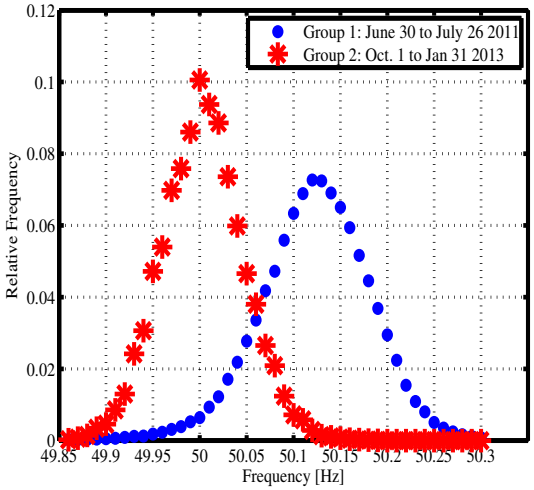

Figure 12. Frequency distribution on Christiansø in time periods June 20, 2011 to July 26, 2011 and October 1st, 2012 to January 31st, 2013.

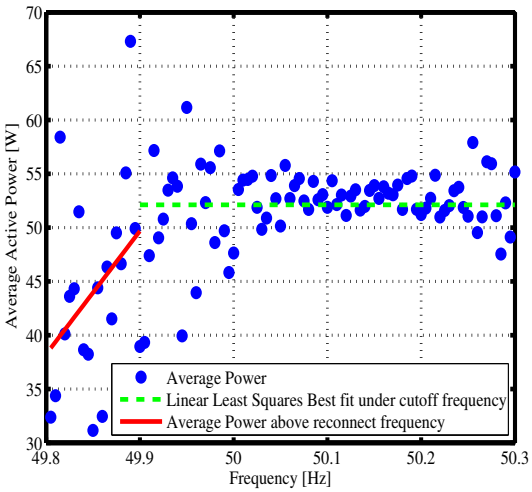

Figure 13. Frequency response of refrigerators on Christiansø configured according to Nordel's definition of disturbance reserve. The frequency response was rarely activated, and the variation of average power values at the low and high frequency extremes is explained by the relative sparsity of the data set.

V. Conclusion

This report has presented the behavior of frequency sensitive loads in three different contexts: a water treatment plant, general-purpose loads connected to a large power system, and refrigerators connected to a micro-grid.

The water treatment plant was a reliable source of frequency response, and the SCADA control layer introduced a delay smaller that the data sampling frequency of 2 s. The response of the general-purpose loads and refrigerators in the micro-grid was weak because the device parameters were not well aligned to the synchronous areas' respective frequency distributions.

REFERENCES

[1] J. Short, D. Infield, and L. Freris, "Stabilization of grid frequency through dynamic demand control," *Power Systems, IEEE Transactions on*, vol. 22, no. 3, pp. 1284 –1293, aug. 2007.

[2] P. Nyeng, J. Østergaard, M. Togeby, and J. Hethey, "Design and implementation of frequency-responsive thermostat control," in *Universities Power Engineering Conference (UPEC), 2010 45th International*, 31 2010-sept. 3 2010, pp. 1 –6.

[3] Zhao Xu, J. Østergaard, and M. Togeby, "Demand as frequency controlled reserve," *Power Systems, IEEE Transactions on*, vol. 26, no. 3, pp. 1062 –1071, Aug. 2011.

[4] D. P. Chassin, M. K. Donnelly, and J. E. Dagle, "Electrical power distribution control methods, electrical energy demand monitoring methods, and power management devices," US Patent US 8 073 573, 12 06, 2011. [Online]. Available: http://availabletechnologies.pnnl.gov/media/61_126201224640.pdf

[5] D. Trudnowski, M. Donnelly, and E. Lightner, "Power-system frequency and stability control using decentralized intelligent loads," in *Transmission and Distribution Conference and Exhibition, 2005/2006 IEEE PES*, may 2006, pp. 1453 –1459.

[6] Danish Energy Association, "Dansk Elforsyning Statistik," 2009.

[7] B. Biegel, L. H. Hansen, P. Andersen, and J. Stoustrup, "Primary Control by ON/OFF Demand-Side Devices," *IEEE Transactions on Smart Grid*, preprint.

[8] "Welcome to Christiansø," Online, accessed February 3, 2012. [Online]. Available: http://www.christiansoe.dk/

[9] P. J. Douglass, R. Garcia-Valle, P. Nyeng, J. Østergaard, and M. Togeby, "Smart demand for frequency regulation: Experimental results," *Smart Grid, IEEE Transactions on*, vol. 4, no. 3, pp. 1713–1720, 2013.

Appendix C

"Voltage Sensitive Load Controllers for Voltage Regulation and Increased Load Factor in Distribution Systems"

This paper appears in *IEEE Transactions on Smart Grid*, vol. 5, no. 5, pp. 2394-2401, Sept. 2014.

Voltage Sensitive Load Controllers for Voltage Regulation and Increased Load Factor in Distribution Systems

Philip J. Douglass, *Student Member, IEEE*, Rodrigo Garcia-Valle, *Senior Member, IEEE*
Jacob Østergaard *Senior Member, IEEE*, and Octavian Constantin Tudora

***Abstract*—This paper presents a novel controller design for controlling appliances based on local measurements of voltage. The controller finds the normalized voltage deviation accounting for the sensitivity of voltage measurements to appliance state. The controller produces a signal indicating desired power consumption which can be mapped to temperature setpoint offsets of thermostat controlled loads. In networks where lower voltage level corresponds to high system load (and vice versa), this controller acts to regulate voltage and increase the load factor. Simulations are conducted on low and medium voltage distribution systems with residential loads including voltage sensitive water heaters. In low voltage systems, the results of the simulations show the controller to be effective at reducing the extremes of voltage and increasing the load factor while respecting end-use temperature constraints. In medium voltage systems, the simulation results show the controller to be effective at reducing voltage fluctuations that occur at the 10-minute time scale.**

***Index Terms*—Demand Side; Voltage Regulation; Distributed Energy Resources; Autonomous Demand Response.**

I. Introduction

DISTRIBUTED generation (DG) connected to power distribution networks is becoming more common as a means to harvest diffuse renewable energy sources (RES). At the same time, in response to the need to reduce emissions and increase supply security, a growing share of the energy system is becoming electrified, increasing the load on the same distribution networks. DG and load growth are expanding the range of operating conditions of distribution systems, and unless large investments are made to upgrade the capacity of the networks, coordinated control of DG and loads will be needed to avoid overloading the systems.

In regions where photo-voltaic (PV) systems have seen rapid growth, widespread overvoltage problems have already been observed [1]. Existing methods to maximize feasible DG penetration levels in the presence of voltage constraints focus on controlling the active and reactive power output of DGs [2]–[4], but the potential of using controllable loads to mitigate voltage constraints is only beginning to be studied [5].

Autonomous loads without digital communication interfaces have been shown to be capable of providing primary frequency reserves [6] by controlling the loads based on local measurements of system frequency. Using locally measured RMS voltage values as a control input can be considered a continuation of the autonomous load control paradigm [7]. Controlling loads without digital communication interfaces circumvents the disadvantages introduced by digital communication, namely: cost, reliability, and speed.

The concept of using loads to influence voltage is similar to Under-Voltage Load Shedding (UVLS) that is used as a remedial measure to prevent blackouts [8] in situations when the system's demand for reactive power exceeds supply. Fine grained UVLS can target those appliances with the most effect on the voltage profiles (large load, low power factor) and least cost (tolerant of interruptions). The algorithm described in this paper uses load curtailment to raise voltage levels, but it addresses distribution level voltage constraints rather than transmission level constraints.

Sansawatt, *et al.* [9] showed more DG capacity can be integrated into distribution networks in the presence of overvoltages by first reducing DG power factor, and if the overvoltage persists after the capacity of DG to absorb reactive power is exhausted, by curtailing active power. Regulating the flow of active power may be necessary to stabilize voltage at high levels of DG penetration, but curtailing RES production is a high-cost method [10]. The algorithm proposed in this paper controls active power flows by modulating loads, achieving the same effect without the opportunity cost of spilled power.

Electric springs [11] are a demand side technology to adjust the power factor of loads to stabilize voltage, comparable to the $Q(U)$ method of controlling of DG interfaced with power electronics [4]. Followup work in [12] modified the original controller to automatically adapt the magnitude of the voltage reference to the local conditions observed at different locations in a feeder. The algorithm proposed in this paper also adapts to local voltage conditions, but it differs in adapting to differences in both the voltage magnitude and voltage variance. The electric spring assumes that loads can operate on a wide range of input voltages and powers. The algorithm proposed in this paper is more immediately applicable to implementation in existing ON/OFF appliances.

Controlling loads to affect local voltage profiles is a recent idea, but the converse of controlling feeder voltage to affect loads is well known under the name volt-var optimization (VVO) or Conservation Voltage Reduction. VVO utilizes the utility's voltage regulation resources to minimize the voltage delivered to customers without violating constraints. Many

The authors are with Center for Electric Power and Energy, Technical University of Denmark, Elektrovej-Building 325, 2800 Kgs. Lyngby Denmark. They can be reached at email addresses: pjdo@elektro.dtu.dk, rodrigo.garcia@ieee.org, joe@elektro.dtu.dk, tudorao@yahoo.com

loads, such as resistive headers, use less power at lower voltage levels, and the aggregate effect on energy consumption can be significant (3 - 6%) [13]. The dependence of power consumption on voltage is an intrinsic property of constant impedance loads; the algorithm described in this paper increases the response of loads to changes in voltage by means of the controller logic.

Vandoorn *et al.* [14] describes methods to use RMS voltage as a signal to control both the generation and load to optimize the utilization of fluctuating RES. Two load control algorithms are presented: one suitable for relay controlled loads where cutoff and reconnect voltage values are set to create a hysteresis region, and a second voltage droop algorithm that gradually modulates power consumption in linear proportion to RMS voltage levels. In [15] and [16] autonomous voltage droop load control algorithms were compared to centrally controlled optimal dispatch, and they found that the autonomous algorithms approached the optimal result. A fairness issue arises with voltage droop controllers because the controllers located close to an energy source give a very different response from those farthest away. This asymmetry breaks with the long-standing practice of providing customers with equivalent service irrespective of their location on a feeder. Configuring each load with customized sensitivity parameters could avoid this problem [15], but it becomes impractical for large systems.

The algorithm for an autonomous voltage-sensitive load controller (VSL) proposed in this paper is similar to [14]–[17] in the goals and methods, but differs in two significant ways: in using normalized RMS voltage levels rather than absolute voltage measurements, and in compensating for the effect of the loads' own consumption on measured voltage levels. Controlling loads based on a normalized voltage measurement shares the available distribution capacity fairly among customers in a feeder by spreading the response across all VSL controllers. The voltage levels are normalized by subtracting the expected voltage level and dividing by the estimated standard deviation. The need to compensate for the effect of loads' own power consumption voltage levels was revealed in lab tests [18]. Early prototypes oscillated rapidly between ON and OFF states as the voltage drop induced by activating the device was large enough to trigger the controller to deactivate the device again. The controller compensates for the influence of device state on voltage levels by using different values for the expected voltage level for each state.

This paper is structured as follows: Section II formulates the voltage control problem in distribution systems from the perspective of loads. Section III describes the control algorithm in detail. Section IV presents the simulation scenarios and results, and finally Section V concludes the paper.

II. Problem Formulation

Distribution system operators are required by law to meet power quality standards, avoiding overvoltage and undervoltage conditions. European standards for electric power delivery from public networks [19] specify that under normal conditions the 10 minute average RMS voltage level must be $230V \pm 10\%$. In the USA, voltage standards in [20] specify the optimal utilization voltage to be within -10% and $+4.3\%$ of nominal. As current flows through a transmission line, the magnitude of the voltage drop is given by:

$$\Delta V = IRcos(\Theta) + IXsin(\Theta) \tag{1}$$

where Θ is the power angle and R, X are the resistance and reactance of the transmission line. When $V \cong 1$ p.u., eq. (1) can be linearized giving the approximation:

$$\Delta V \cong PR + QX \tag{2}$$

where P, Q are the active and reactive power consumption. Fig. 1 illustrates a typical voltage profile along the length of a radial distribution system. Low Voltage (LV) distribution system conductors are predominately resistive $(R > X)$, and this analysis will not differentiate between the effect of active power and reactive power on the voltage drop. This analysis focuses on the active power because it has the largest magnitude, and because existing appliances do not allow reactive power to be controlled separately from active power.

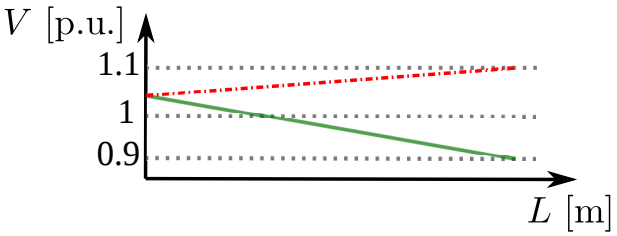

Figure 1. Idealized voltage profile along the length of a feeder. Two cases are shown: The low voltage case when load is high and DG production low (solid line). The high voltage case with reverse power flow, when production from DG located at the end of the feeder is high and load low (dashed line).

The P term in eq. (2) is the net load including DG production P_{DG}, uncontrolled residual loads $P_{\text{L,u}}$, and controllable VSLs $P_{\text{L,vs}}$:

$$P = P_{\text{DG}} - P_{\text{L,u}} - P_{\text{L,vs}}. \tag{3}$$

A simple distribution system with VSL is shown in Fig. 2. VSLs may also be co-located with DG to increase the self-consumption of the site. The appliances are assumed to have two discrete states (ON/OFF).

The purpose of the control algorithm analyzed in this paper is to modify $P_{\text{L,vs}}$ to counter the fluctuations in P_{DG} and $P_{\text{L,u}}$ to reduce the variation of P and V. This is done by controlling VSLs to use less power when they measure relatively low voltage and vice versa. The expected result will be to lower peak loads, raise minimum voltage levels, and reduce voltage fluctuations over short time scales (1-10 minutes). The loads will still respect their internal process constraints, so the final response of the VSL will not perfectly track the desired power consumption, but statistics gathered over time will show a reduced correlation between VSL and residual load.

In operating power systems, it is common practice for substations connecting the bulk transmission system to medium voltage (MV) distribution systems to regulate voltage within tight tolerances by the dispatch of reactive power and on-load

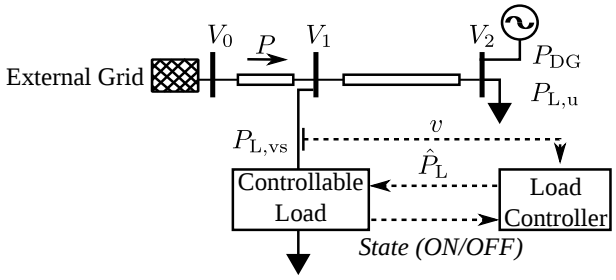

Figure 2. Oneline system diagram showing controllable load and DG in a radial feeder. Dashed lines represent control signal paths. The total power drawn from the grid is P. The VSL acts to regulate voltage V_1.

tap changing (OLTC) transformers. OLTCs are also finding new application in MV/LV transformers [1], [10]. VSLs can co-exist with OLTC only if the regulators are operated to hold voltage within a fixed deadband at their output terminals. Alternatively, if voltage regulation devices are operated to perform line drop compensation, they regulate voltage at a nominal supply point which could be at the end of the line. This results in the terminal voltage being raised under high load [1]. In this case, nodes between the OLTC and the nominal supply point will see the power vs. voltage relationship inverted, and the approximation in eq. (2) can not be applied. The proposed VSL controller can not be used at those nodes because of the danger of positive feedback: increasing load causes the OLTC to increase voltage, which in turn increases load again. Note that this caveat also applies to the other load control algorithms previously discussed [9], [11], [14]–[16].

OLTCs can be vulnerable to mechanical wear if fluctuating RES output triggers tap changes, and VSLs can be applied to reduce the short-term fluctuation of load and voltage by shifting some mechanical wear to load actuators.

In LV networks, measures to mitigate voltage fluctuations in real-time are not generally economically feasible, and compliance with voltage constraints is ensured during the network design and planning stages. Network planners dimension networks based on the expected peak load and peak DG production. The VSL controller has the effect of increasing the ratio of average load to peak load (load factor) of LV networks by pushing VSL duty cycle to be in anti-phase with other cyclic loads.

III. Control Algorithm

The control algorithm that this work evaluates is shown with a block diagram in Fig. 3, and can be summarized as follows:

1) Take RMS voltage samples, i.e. at sampling frequency of 1 second, denoted as $v[t]$ for the voltage measurement at time t.
2) Calculate the moving average of RMS voltage over a short interval $\hat{v}[t]$ to remove noise. An exponentially weighted moving average with smoothing constant α is used because this type of filter minimizes data storage requirements:

$$\hat{v}[t] = (1-\alpha)\hat{v}[t-1] + \alpha v[t].$$

3) Find the expected voltage level $\bar{v}[t]$. The expected voltage level is different depending on whether the appliance is ON or OFF, therefore find the moving averages of voltage over a long time interval separately for each state.
$\forall v[t], \mathrm{State}[t] = \mathrm{ON}$:

$$\begin{aligned} \bar{v}_{\mathrm{on}}[t] &= (1-\beta)\bar{v}_{\mathrm{on}}[t-1] + \beta v[t] \\ \bar{v}_{\mathrm{off}}[t] &= \bar{v}_{\mathrm{off}}[t-1] \end{aligned}$$

$\forall v[t], \mathrm{State}[t] = \mathrm{OFF}$:

$$\begin{aligned} \bar{v}_{\mathrm{on}}[t] &= \bar{v}_{\mathrm{on}}[t-1] \\ \bar{v}_{\mathrm{off}}[t] &= (1-\beta)\bar{v}_{\mathrm{off}}[t-1] + \beta v[t] \end{aligned}$$

$$\bar{v}[t] = \begin{cases} \bar{v}_{\mathrm{on}}[t], & \text{if State}[t] = \mathrm{ON} \\ \bar{v}_{\mathrm{off}}[t], & \text{if State}[t] = \mathrm{OFF}. \end{cases}$$

The smoothing constant β determines the half-life of the moving average, with $0 \leq \beta \ll \alpha < 1$.
4) Calculate gain G. This is done by finding the long-term moving variance of $\Delta V[t] = (\hat{v}[t] - \bar{v}[t])$:

$$\hat{\sigma}^2[t] = (1-\beta)\hat{\sigma}^2[t-1] + \beta(\Delta V[t])^2 \tag{4}$$

then the square root of the variance is found, giving the standard deviation $\hat{\sigma}$. This standard deviation is inverted to give the gain $\mathrm{G}[t]$:

$$\mathrm{G}[t] = \frac{1}{\hat{\sigma}[t]}. \tag{5}$$

5) The normalized voltage level is the product of $\mathrm{G}[t]$ and $\Delta V[t]$. The load control signal is the normalized voltage level scaled with proportionally constant K:

$$\hat{P}_{\mathrm{L}}[t] = \mathrm{K}G[t]\Delta V[t] \tag{6}$$

where $\hat{P}_{\mathrm{L}}[t]$ is the desired change in power consumption from loads at time t. Finally, $\hat{P}_{\mathrm{L}}[t]$ is constrained to lie in the range $[-1, 1]$, limiting the minimum and maximum values.

The desired power consumption will be given to a local load controller that will attempt to comply with the request within the constraints imposed by the final energy conversion process. Among possible controllable loads, this paper will examine the use of thermostat controlled loads (TCLs) for demand response because they represent a large load with inherent energy storage capacity. A desired change to power consumption is linearly mapped into an offset to the user-given thermostat temperature setpoint, as shown in Fig. 4, similar to the control for frequency-sensitive loads described in [21]. The thermostat setpoint T_{s} depends on the user preference T_0, the output of the VSL controller $\hat{P}_{\mathrm{L}}$, and the thermostat offset limit T_{ol}:

$$T_{\mathrm{s}} = T_0 + \hat{P}_{\mathrm{L}} T_{\mathrm{ol}}. \tag{7}$$

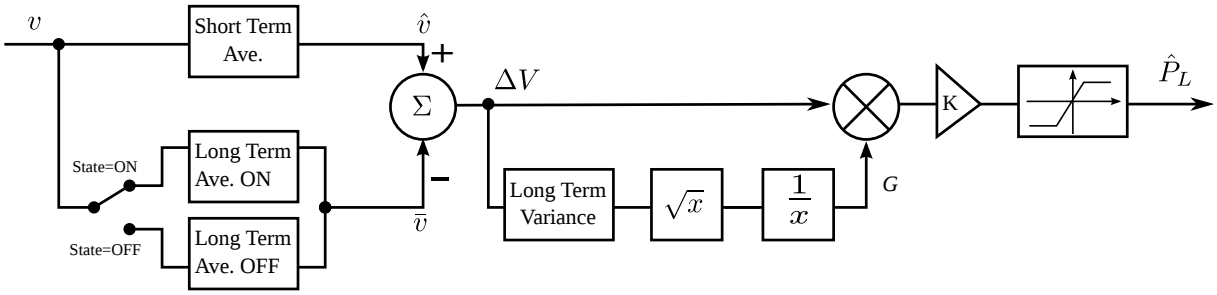

Figure 3. Block diagram of VSL controller. Moving averages of the voltage measurements are taken over short and long time scales. The difference between the two moving averages ΔV is multiplied by the gain G to give the normalized voltage deviation. The gain G is found by finding the moving standard deviation, then inverting. The output is scaled by a user-given constant K, and limited to be between [-1,1].

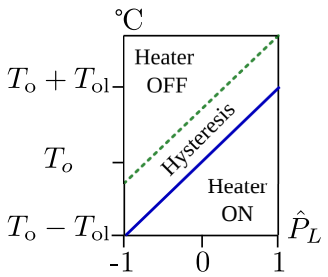

Figure 4. Dependance of thermostat setpoint on $\hat{P}_{\mathrm{L}}$ in heating application. Y-axis is process temperature, i.e. of water in hot water tank. The heater turns ON when the temperature falls below the solid line, and turns OFF when the temperature rises above the dashed line. The user given setpoint (T_o) is used when $\hat{P}_{\mathrm{L}} = 0$

Table I
VOLTAGE SENSITIVE WATER HEATER PARAMETER VALUES

Parameter	Min.	Max.
Heating element power	3 kW	5 kW
Tank capacity*	144 L	266 L
Users' thermostat setpoint (T_0)	48.9 °C	57.8 °C
Thermostat deadband (T_{db})	2.3 °C	4.6 °C
Tank jacket thermal conductance (U_{a})	2	4

* Note: Tank capacity is positively correlated with floor area of each residence.

IV. SIMULATION SCENARIOS & RESULTS

The feasibility of the proposed load control algorithm was shown by implementing it in a resource-constrained embedded system and testing it with mains power in the laboratory [18]. However, testing a single device did not reveal the system-wide effects of the device. Therefore in this work, the proposed load controller algorithm is evaluated with numerical simulations in GridLAB-D [22] using three network topologies of increasing complexity. The simulations use a quasi-steady-state simulation model, where the full non-linear 3-phase unbalanced load flow is solved at each time step for load conditions that evolve according to the internal states of individual devices. Voltage at the external grid connection, V_0, is fixed to 1 p.u. in all scenarios. Power consumption is measured at the external grid interface, and the aggregate power of the VSL and DG plants are measured.

A. Appliance Model for Voltage-Sensitive Load

The VSL was modeled as a hot water heater with constant water draw of 57 l/hr. The water heater model was chosen to approximate a generic energy storage device where the timing of electric energy demand is de-coupled from end-use demand. The controller algorithm was implemented in the simulation environment by modifying the software implementing the thermostat. Model parameters were subject to a uniform random distribution of the values shown in Table I, representing typical values of a heterogeneous population of appliances found in residences in the USA.

Inlet water temperature was fixed to $T_{\mathrm{in}} = 15.5$ °C. The single phase resistive heating element was modeled as a constant impedance load. Water temperature in the tank was modeled by a first order discrete difference equation:

$$T_{\mathrm{w}}[t+1] = \frac{1}{C}[\ (T_{\mathrm{o}}[t] - T_{\mathrm{w}}[t])U_{\mathrm{a}} + w[t]Q + q[t](T_{\mathrm{in}}[t] - T_{\mathrm{w}}[t])\ ] \tag{8}$$

where the water temperature T_{w} at time t depends on the ambient temperature T_{o}, the water temperature at the previous timestep, the thermal conductance of the tank jacket U_{a}, the control signal w, the gain of the heating element Q, the water demand q, inlet water temperature, and the heat capacitance of the full tank C. The ambient temperature depends on the state of the residence's HVAC system. The temperature of the hot water was modeled as a single body, neglecting the thermocline that arises in real tanks. The control signal $w[t]$ takes a value of 0 or 1 based on the rule:

$$w[t] = \begin{cases} 1, & \text{if } T_{\mathrm{w}}[t] < T_{\mathrm{s}}[t] \\ 0, & \text{if } T_{\mathrm{w}}[t] > (T_{\mathrm{s}}[t] + T_{\mathrm{db}}) \\ w[t-1], & \text{otherwise} \end{cases} \tag{9}$$

where T_{s} is given by eq. (7) and T_{db} is the thermostat deadband.

The VSL controllers are configured to offset the hot water heaters' setpoint by a maximum of $T_{\mathrm{ol}} = 3$ °C from the user preference.

In the small-scale simulations (2-bus, LV), the simulated controllers sample voltage values every second. In the large-scale simulation (MV), the minimum timestep was increased to 10 s to speed up simulation execution with a negligible loss of fidelity. The gain constant K is set to 0.4. The system was simulated with startup period that allowed the long-term

average values in the controller to converge to steady-state values, and then data was collected at one minute intervals for 10 days.

B. 2-Bus Proof of Concept

In this scenario the VSL is connected to a common bus (V_1) with conventional loads, shown in Fig. 5. The conventional loads are modeled as a small amount of residential plug and lighting loads that follow a typical diurnal load profile, and a second (conventional) hot water heater with a larger water demand than VSL water heater. The different water demand ensured that the duty cycles and cycle times of the two water heaters were different. The VSL used a short-term averaging smoothing constant equal to the time step ($\alpha = 0$) to allow immediate response to voltage changes. The long-term smoothing constant is set to $\beta = 1/10800$. The VSL tank had water storage capacity equal to 6.5 hours of consumption.

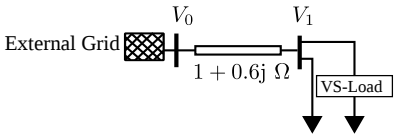

Figure 5. Oneline system diagram showing a 2-bus test system with voltage-sensitive and conventional loads in a radial feeder.

A base case scenario is simulated with an identical setup except that the VSL controller is disabled. A typical time series comparing power consumption in the base case and with the VSL scenario is shown in Fig. 6. The relation of the VSL to the total load is shown in Fig. 7.

The load duration curve in Fig. 8 shows distinct steps where the heating loads are active. In the base case, both heating loads are active about 10% of the time, and none are active about 45% of the time. With the VSL controller, there is no time when both heaters are active, while the time that no heaters are active is reduced to about 35%. This shows how the VSL controller moves load from high-load times to low-load times.

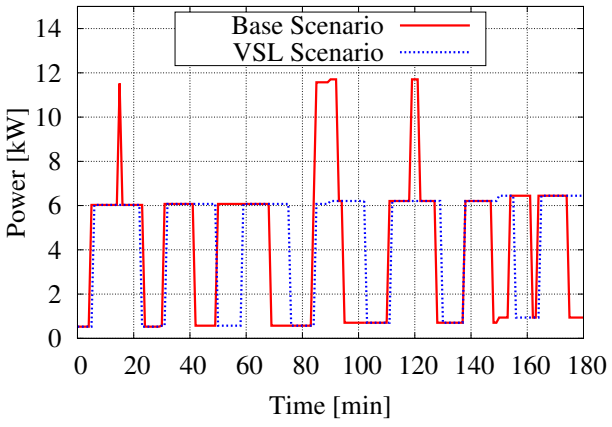

Figure 6. Time series of power consumption in 2-bus test system for base case and VSL.

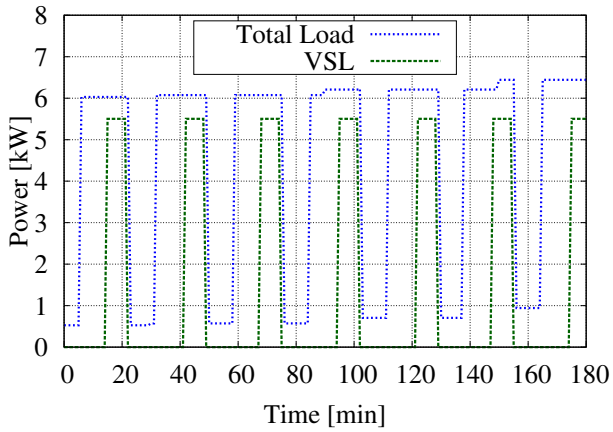

Figure 7. Time series of power consumption in 2-bus test system in the VSL scenario showing VSL power and the total system load.

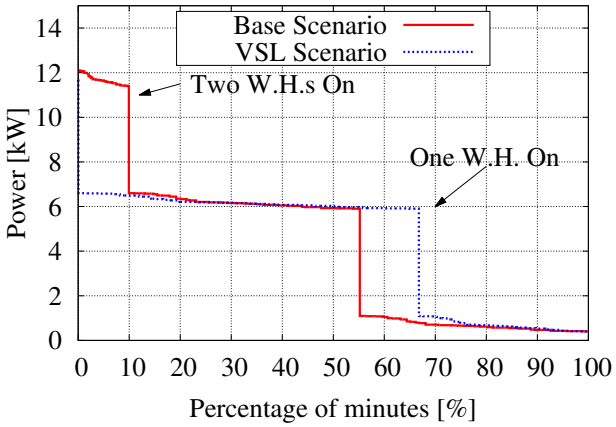

Figure 8. Load duration curve for base case and VSL in 2-bus test system.

C. LV Network

The performance of a group of VSL and conventional loads connected to a radial network was analyzed in the network shown in Fig. 9. As in the 2-bus scenario, V_0 is held constant, but unlike the 2-bus scenario, the impedance of the secondary radials, as shown in Table II, causes each VSL to measure a different voltage. The conventional loads are mainly composed of air conditioning appliances, together with residential plug and lighting loads. The cooling demand is synthesized from weather data distributed with GridLAB-D for the Pacific Northwest of the USA in August. Six VSL water heaters are simulated in a network with 10 houses. The VSL used a short-term averaging smoothing constant of $\alpha = 1/60$

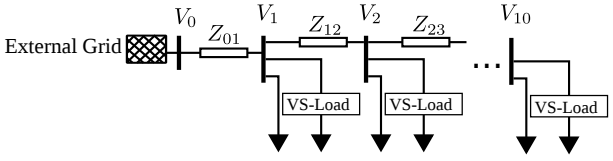

Figure 9. Oneline system diagram showing a low voltage radial network. Nodes number 1,2,3,4,8, and 10 contained VSL.

Table II
LINE IMPEDANCE VALUES FOR LV FEEDER

Name	R [Ω]	X [j Ω]
Z_{01}	0.096	0.008
Z_{12}	0.084	0.007
Z_{23}	0.012	0.010
Z_{34}	0.048	0.004
Z_{45}	0.096	0.008
Z_{56}	0.114	0.012
Z_{67}	0.096	0.008
Z_{78}	0.085	0.007
Z_{89}	0.076	0.006
Z_{910}	0.024	0.002

and a long-term smoothing constant of $\beta = 1/43200$. The energy demand from the VSL water heaters is 13% of the total energy demand of the system. Model parameters such as house size and air conditioning thermostat setpoint were subject to a uniform random distribution representing typical values found in northwestern USA.

The system was simulated in a base case and with VSL controllers. A representative time series comparing the base case to VSL is shown in Fig. 10. A representative time series showing the VSL as a portion of total loads is shown in Fig. 11.

The voltage regulation performance of the controller was characterized by finding the minimum voltage measurement and the average number of voltage measurements below 0.9 p.u. per house (corresponding to the System Temporary Average RMS Frequency Index$_{90}$ from [23]). Voltage fluctuations are quantified with a modified version of the voltage fluctuation index (VFI) from [24]:

$$\mathrm{VFI}_t = \sum_{k=1}^{N}\sum_{i=1}^{T} \frac{|U_{k,i} - U_{k,i-t}|}{NT} \times 100\%$$

where N is the number of measurement busses, T is the number of time steps, and t is the time period of fluctuations taken to be either 1 or 10 minutes. Performance of the controller with respect to capacity planning criteria was evaluated by finding the peak power demand, load factor, and the correlation coefficient between VSL and residual load ($\rho_{\mathrm{VSL,Load}}$). The performance is summarized in Table III.

Table III
PERFORMANCE OF VSL IN LV NETWORK

Parameter	Base	VSL
Peak Load	58.1 kW	49.6 kW
Load Factor	0.39	0.45
Corr. Coef. $\rho_{\mathrm{VSL,Load}}$	-0.02	-0.57
Ave. nr. V samples $<$ 0.90 p.u.	974	557
Voltage Fluctuation Index (t=1 min.)	8.46 %	8.01 %
Voltage Fluctuation Index (t=10 min.)	23.5 %	12.4 %
Min. Voltage	0.79 p.u.	0.81 p.u.

Compared to the base case, the peak power demand is reduced by 15% and the minimum observed voltage is increased by 2%, a significant improvement considering the total voltage variation tolerance of ±10% [19]. Adding VSL significantly increased the negative correlation between VSL and the uncontrolled load. The load duration curve, shown in Fig. 12, illustrates how the presence of VSL flattened

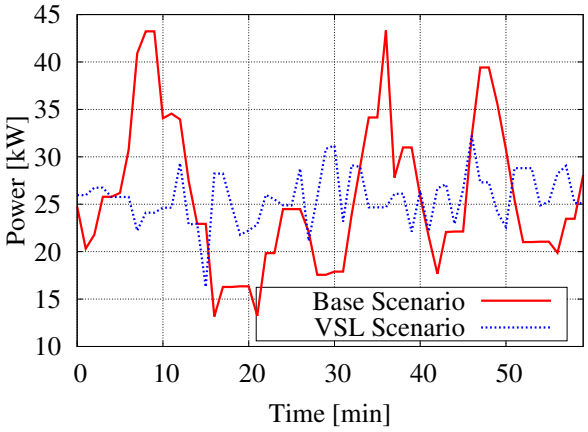

Figure 10. Time series of total load in LV radial network for base scenario and VSL scenario.

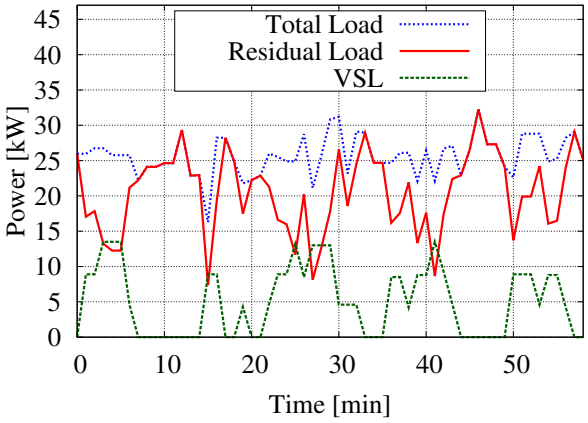

Figure 11. Time series of load in LV radial network in the VSL scenario showing the total system load decomposed into VSL and residual load fractions.

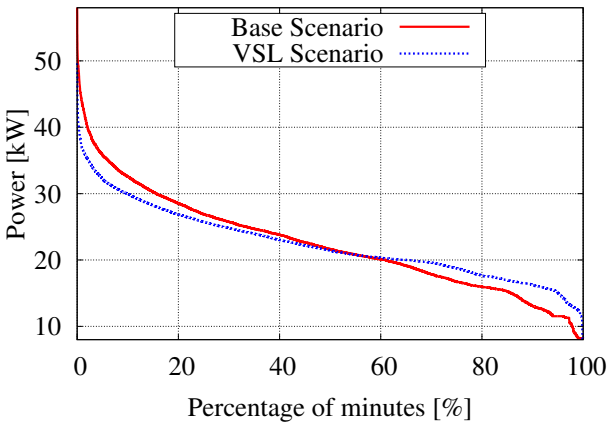

Figure 12. Load duration curves for base case and VSL simulated in LV radial network.

demand, shifting load from high demand periods to low demand periods. The distribution of voltage measurements in both scenarios is shown in Fig. 13. The VSL controller reduced the number of voltage measurements below 0.9 p.u. by more than 40 %. The VSL scenario reduced the voltage fluctuation index at the 1 minute time scale by 5 %, while fluctuations at the 10 minute time scale were almost halved.

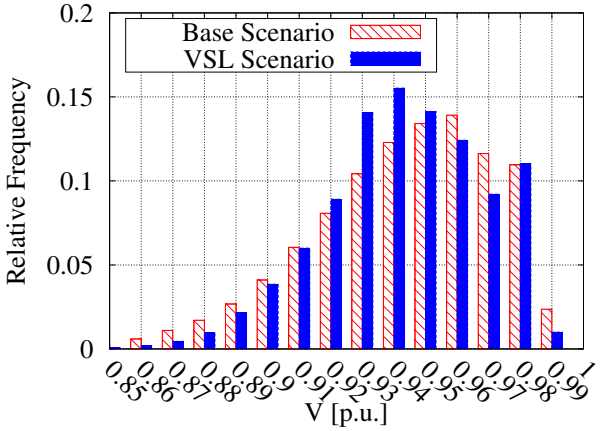

Figure 13. Distribution of voltage measurements in base case and VSL scenario.

Examining the fairness of the algorithm was done by recording the voltage and temperature offset for each VSL and finding distribution of those values, shown in Fig. 14 and Fig. 15. The results show that despite large differences in measured voltage values and variations, the devices have similar temperature offset distributions.

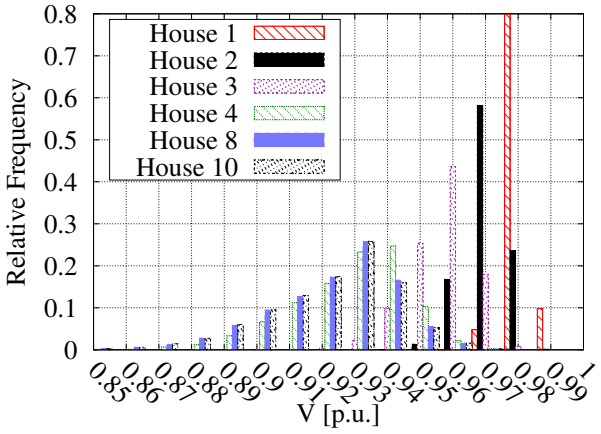

Figure 14. Distribution of voltage measurements at houses with VSL in the VSL scenario. House 1, located closest to the grid connection, sees the highest voltage and lowest variance.

D. MV Network with PV

A large scale model of a typical North American distribution system ("R-1-12.47-1" from [25]) was modified by doubling the line and cable resistances to represent a more stressed network. This network contained light industrial loads and

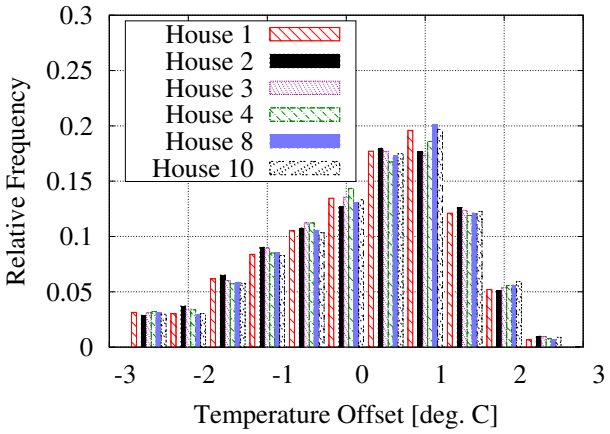

Figure 15. Distribution of temperature setpoint offsets. The devices show a similar distribution irrespective of their location.

1176 houses, each with a voltage sensitive water heater. Residential PV plants injecting power at unity power factor were included in each house, causing reverse power flows during sunny periods, and together the PV produced approximately the same amount of energy as was consumed by the VSL. High resolution PV production data from an operating 7 kW plant in our lab in Denmark was scaled to the size of each simulated residential PV plant. The spacial diversity of the feeder was simulated by randomly distributing PV plants into 6 groups, with production profiles delayed by 10 s between each group. Parameters describing the households such as floor area, thermal conductance, and thermostat setpoint preferences, were randomly distributed to represent typical values found in North American suburban residential districts. Water heaters accounted for 24% of total energy demand. The smoothing constants were identical to the LV scenario, $\alpha = 1/60$ and $\beta = 1/43200$

The load profile followed a diurnal variation, and HVAC demand was synthesized from weather data from the Pacific Northwest of the USA in January. Performance metrics comparing the base case to the VSL scenario are summarized in Table IV. The PV production, VSL consumption, residual load, and the net load over 4 days are shown in Fig. 16, with a single hour of sharp PV production transients enlarged in Fig. 17. Fig. 18 shows the total aggregate power in same hour for the base case and VSL.

Examining Fig. 17 reveals that the VSL is able to follow fluctuations in PV output in all except the shortest transients. Compared to the base case in Fig. 18, the VSL is able to reduce the net load variation, improving the short-term balance between PV production and load.

The size of the water heater energy buffer only allowed relatively short-term load shifting, and the size of the distribution system meant that short-term load diversity was high, thus there was little scope for improvement. The load peak was approached gradually, which exceeded the time scale of VSL load shifting, therefore only a 2% improvement is seen in this metric, and there are no significant differences in the voltage extremes. The peak reverse power flow (minimum net

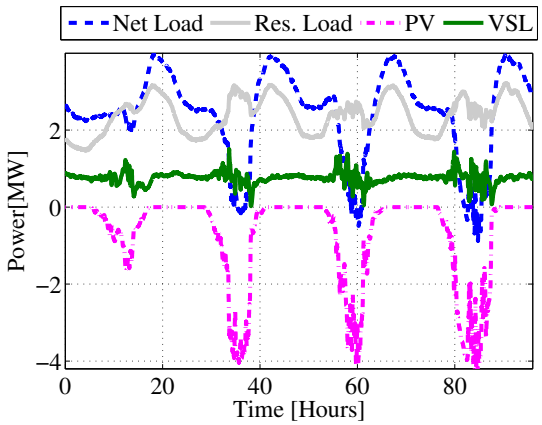

Figure 16. Time series showing 4 days of the simulation with VSL controller. The PV production shows the first day is overcast, the 2nd day clear, the 3rd and 4th days are partly cloudy with sharp cloud transients.

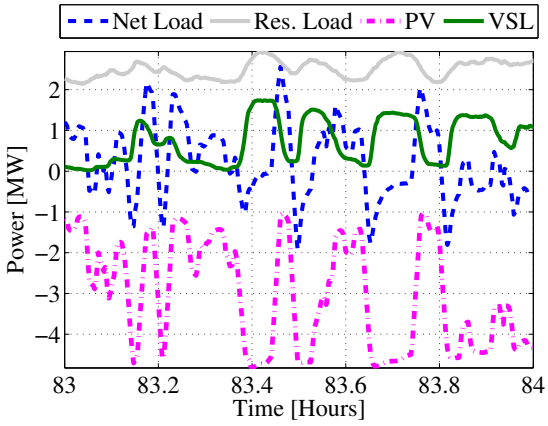

Figure 17. Enlarged time series from an hour with sharp cloud transients and net load fluctuating around 0 kW. The VSL varies consumption as the inverse of PV production.

load) was larger in the VSL case, as shown in Fig. 18 at time 83.5. This event is an extreme transient, where the delay in the VSL response allowed load to exceed the base case for 2 time steps.

For the whole simulation period, the water heaters' power consumption went from being positively correlated with the residual load in the base case, to being negatively correlated with residual load when the VSL controller was enabled. The inverse is observed with the correlation between water heater consumption and PV production, which went from a negative to positive correlation when the VSL controller was enabled. The presence of VSL lowered average system losses, indicating that PV power was consumed closer to where it was produced.

The VSL controllers reduced voltage variation by 26% at the 1 minute time scale and 64% at the 10 minute time scale. The average number a samples below the threshold 0.97 p.u. was reduced by 42%, the average number of samples above 1.02 p.u. was reduced by 55%.

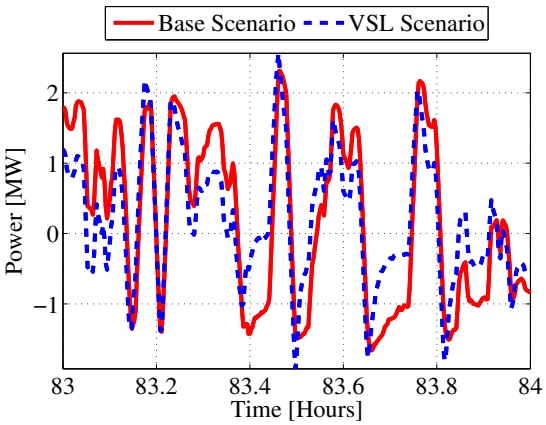

Figure 18. Enlarged time series of net load from an hour with sharp transients in PV production for base case and VSL scenario. The introduction of VSL reduces the variation in the net load.

Table IV
PERFORMANCE OF VSL IN MV NETWORK WITH PV

Parameter	Base	VSL
Max. Net Load	4130 kW	4050 kW
Min. Net Load	-1660 kW	-1920 kW
Corr. Coef. $\rho_{\mathrm{VSL,Load}}$	0.01	-0.03
Corr. Coef. $\rho_{\mathrm{VSL,PV}}$	-0.30	0.03
Ave. nr. V samples $<$ 0.97 p.u.	570	331
Ave. nr. V samples $>$ 1.02 p.u.	38.6	17.5
Voltage Fluctuation Index (t=1 min.)	0.63 %	0.47 %
Voltage Fluctuation Index (t=10 min.)	2.50 %	0.90 %
Min. Voltage	0.967 p.u.	0.968 p.u.
Max. Voltage	1.025 p.u.	1.025 p.u.
Ave. Line Losses	99.1 kW	97.7 kW

V. CONCLUSION

This paper has presented a design and numerical simulations of an autonomous load controller that contributes to stabilizing voltage levels and, in LV distribution systems, increases the load factor. This controller uses locally available measurements of RMS voltage and the state of the controlled appliance as inputs, and it produces a signal indicating desired power consumption suitable for control of thermostat controlled loads. The voltage response is spread evenly across all controlled devices in the network. Simulations have shown that when applied to domestic water heater loads with temperature constraints, this controller reduces the amount of voltage variation in distribution networks with the largest effects at the 10-minute time scale. Correlation between VSL and residual load was reduced compared to the base case, and correlation between VSL and DG production increased. In MV networks, using VSL to reduce short-term voltage fluctuations can relieve mechanical wear on voltage regulators. In LV networks, using VSL to increase load factor can allow network planners to approve higher DG penetration and higher loads than would otherwise be feasible.

This algorithm is simple enough to be implemented in the software of resource constrained microcontrollers found in white-goods appliances today, with the primary cost of implementation an increased frequency of appliance power cycling.

The controller benefits from coordination with other voltage regulation devices (such as OLTCs) to ensure that lower voltage corresponds to higher load and vice versa. Deploying the autonomous controller in distribution systems can mitigate the negative effects of high DG penetration and improve utilization of power distribution assets.

ACKNOWLEDGEMENTS

The authors would like to thank D. Chassin, J. Fuller, M. Hauer, and A. Fisher from the Pacific Northwest National Lab for their help with GridLAB-D.

REFERENCES

[1] M. Kaspirek, D. Mezera, and J. Jiricka, "Problems of Voltage Stabilization in MV and LV Distribution Grids Due to the Operation of Renewable Energy Sources," in *CIRED 22nd International Conference on Electricity Distribution*, Jun. 2013.

[2] Q. Zhou and J. Bialek, "Generation curtailment to manage voltage constraints in distribution networks," *Generation, Transmission Distribution, IET*, vol. 1, no. 3, pp. 492 –498, may 2007.

[3] C. Su, "Comparative analysis of voltage control strategies in distribution networks with distributed generation," in *Power Energy Society General Meeting, 2009. PES '09. IEEE*, july 2009, pp. 1 –7.

[4] E. Demirok, P. Casado Gonzalez, K. Frederiksen, D. Sera, P. Rodriguez, and R. Teodorescu, "Local reactive power control methods for overvoltage prevention of distributed solar inverters in low-voltage grids," *Photovoltaics, IEEE Journal of*, vol. 1, no. 2, pp. 174 –182, oct. 2011.

[5] F. Marra, G. Yang, C. Traeholt, E. Larsen, J. Ostergaard, B. Blazic, and W. Deprez, "Ev charging facilities and their application in lv feeders with photovoltaics," *Smart Grid, IEEE Transactions on*, vol. 4, no. 3, pp. 1533–1540, 2013.

[6] P. J. Douglass, R. Garcia-Valle, P. Nyeng, J. Østergaard, and M. Togeby, "Smart demand for frequency regulation: Experimental results," *Smart Grid, IEEE Transactions on*, vol. 4, no. 3, pp. 1713–1720, 2013.

[7] R. Garcia-Valle, L. P. Da Silva, Z. Xu, and J. Østergaard, "Smart demand for improving short-term voltage control on distribution networks," *I E T Generation, Transmission and Distribution*, vol. 3, no. 8, pp. 724–732, 2009.

[8] C. Taylor, "Concepts of undervoltage load shedding for voltage stability," *Power Delivery, IEEE Transactions on*, vol. 7, no. 2, pp. 480–488, Apr. 1992.

[9] T. Sansawatt, L. Ochoa, and G. Harrison, "Smart decentralized control of dg for voltage and thermal constraint management," *Power Systems, IEEE Transactions on*, vol. 27, no. 3, pp. 1637–1645, 2012.

[10] T. Stetz, F. Marten, and M. Braun, "Improved low voltage grid-integration of photovoltaic systems in germany," *Sustainable Energy, IEEE Transactions on*, vol. 4, no. 2, pp. 534–542, Apr. 2013.

[11] S. Y. Hui, C. K. Lee, and F. Wu, "Electric springs®;a new smart grid technology," *Smart Grid, IEEE Transactions on*, vol. 3, no. 3, pp. 1552 –1561, sept. 2012.

[12] C. K. Lee, N. Chaudhuri, B. Chaudhuri, and S. Hui, "Droop control of distributed electric springs for stabilizing future power grid," *Smart Grid, IEEE Transactions on*, vol. 4, no. 3, pp. 1558–1566, 2013.

[13] K. Schneider, J. Fuller, F. Tuffner, and R. Singh, "Evaluation of Conservation Voltage Reduction (CVR) on a National Level," Pacific Northwest National Laboratory, Tech. Rep., Jul. 2010.

[14] T. Vandoorn, B. Renders, L. Degroote, B. Meersman, and L. Vandevelde, "Active load control in islanded microgrids based on the grid voltage," *Smart Grid, IEEE Transactions on*, vol. 2, no. 1, pp. 139 –151, Mar. 2011.

[15] P. Richardson, D. Flynn, and A. Keane, "Local versus centralized charging strategies for electric vehicles in low voltage distribution systems," *Smart Grid, IEEE Transactions on*, vol. 3, no. 2, pp. 1020–1028, 2012.

[16] S. Iacovella, K. Lemkens, F. Geth, P. Vingerhoets, G. Deconinck, R. D'Hulst, and K. Vanthournout, "Distributed Voltage Control Mechanism in Low-Voltage Distribution Grid Field Test," in *Innovative smart grid technologies (ISGT Europe), 4th IEEE PES International Conference and Exhibition on*, Oct. 2013.

[17] F. Geth, N. Leemput, J. Van Roy, J. Buscher, R. Ponnette, and J. Driesen, "Voltage droop charging of electric vehicles in a residential distribution feeder," in *Innovative Smart Grid Technologies (ISGT Europe), 2012 3rd IEEE PES International Conference and Exhibition on*, 2012.

[18] O. C. Tudora, "Smart Demand for Voltage Control in Power Networks," Master's thesis, Technical University of Denmark, Nov. 2012.

[19] CENELEC, "EN 50160: Voltage characteristics of electricity supplied by public electricity networks," 2010.

[20] ANSI, "C84.1-2006 American National Standard for Electric Power Systems and Equipment - Voltage Ratings," 2006.

[21] Zhao Xu, J. Østergaard, and M. Togeby, "Demand as frequency controlled reserve," *Power Systems, IEEE Transactions on*, vol. 26, no. 3, pp. 1062 –1071, Aug. 2011.

[22] D. Chassin, K. Schneider, and C. Gerkensmeyer, "Gridlab-d: An open-source power systems modeling and simulation environment," in *Transmission and distribution conference and exposition, 2008. ieee/pes*, Apr. 2008, pp. 1 –5.

[23] D. Brooks, R. Dugan, M. Waclawiak, and A. Sundaram, "Indices for assessing utility distribution system rms variation performance," *Power Delivery, IEEE Transactions on*, vol. 13, no. 1, pp. 254–259, 1998.

[24] F. Viawan and D. Karlsson, "Combined local and remote voltage and reactive power control in the presence of induction machine distributed generation," *Power Systems, IEEE Transactions on*, vol. 22, no. 4, pp. 2003–2012, 2007.

[25] K. Schneider, Y. Chen, D. Engle, and D. Chassin, "A Taxonomy of North American Radial Distribution Feeders," in *Power energy society general meeting, 2009. PES '09. IEEE*, 2009.

Appendix D

"Design and Evaluation of Autonomous Hybrid Frequency-Voltage Sensitive Load Controller"

This paper was originally published in the proceedings of Innovative Smart Grid Technologies Europe Conference 2013, Copenhagen Denmark.

Corrigendum Dec. 2013– After publication, an error was discovered in Fig. 8: The value of $\hat{P}^{\mathrm{f}}$ was scaled to be half of the correct value. In the corrected figure, Fig. D.1, it is clear that $\hat{P}^{\mathrm{L}}$ is the arithmetic mean of $\hat{P}^{\mathrm{f}}$ and $\hat{P}^{\mathrm{V}}$. It should be emphasized that the error only affected the visualization of the simulated timeseries, not the validity of the simulation itself.

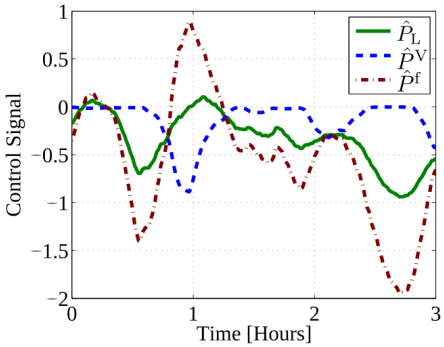

Figure D.1: Corrected Fig. 8: Representative time series of hybrid control $\hat{P}_{\mathrm{L}}$ signal and the voltage $\hat{P}^{\mathrm{V}}$ and frequency $\hat{P}^{\mathrm{f}}$ components.

Design and Evaluation of Autonomous Hybrid Frequency-Voltage Sensitive Load Controller

Philip J. Douglass, Rodrigo Garcia-Valle, Fabrizio Sossan, Jacob Østergaard
Technical University of Denmark,
Elektrovej-Building 325,
2800 Kgs. Lyngby, Denmark
Email: {pjdo, rgv, faso, joe}@elektro.dtu.dk

Preben Nyeng
Energinet.dk,
Tonne Kjærsvej 65,
7000 Fredericia, Denmark
Email: pny@energinet.dk

***Abstract*—The paper introduces an algorithm for control of autonomous loads without digital communication interfaces to provide both frequency regulation and voltage regulation services. This hybrid controller can be used to enhance frequency sensitive loads to mitigate line overload arising from reduced load diversity. Numerical simulations of the hybrid controller in a representative distribution system show the peak system load was reduced by 12% compared to a purely frequency sensitive load controller.**

I. Introduction

Time-sensitive and geographically distributed control of today's power system is achieved by the use of local control loops that measure system parameters and act upon them autonomously. Examples include speed droop governors, voltage regulators in synchronous generators, and on-load tap changing transformers.

Generators have primary responsibility for maintaining system frequency and voltage within specified limits with $P-f$ and $Q-V$ droop control. In large power systems with inductive transmission lines, these two control objectives are decoupled, but in the general case (including micro-grids with resistive lines) the two objectives are interrelated [1].

Local control loops are also being applied to distributed generation (DG) to allow small generation units to coordinate their actions and contribute the stabilizing system frequency and voltage without the overhead of a reliable data communications network. For example, photo-voltaic (PV) inverters connected to low voltage distribution systems in Germany are required to implement $P-f$ droop control to curtail active power when system frequency rises above 50.2 Hz [2], and research indicates that curtailing active power in response to voltage rises can increase feasible DG penetration [3].

Using loads to regulate system parameters through Under-Frequency Load Shedding (UFLS) and Under-Voltage Load Shedding (UVLS) is well established, but only as a last resort defense. Loads with inherent flexibility, such as thermostat controlled loads (TCLs), can be designed so power consumption is shifted in time without compromising the quality of energy service provided. These loads have the potential to modulate their active power consumption and contribute to stabilizing system frequency and voltage as a part of normal operation [4]. Continuing advances in micro-electronics allow sufficiently accurate measurement of system frequency and voltage by the low-cost microcontrollers typically found in white goods appliances. These measurements can provide input to load controllers that allow loads to participate in frequency and voltage regulation autonomously without reliance on real-time digital communications. Autonomous load controllers can be deployed in a "fit and forget" fashion or they may be built with digital communications interfaces to allow remote changes to configuration parameter values.

While autonomous frequency sensitive loads (FSL) have matured to be candidates for mass-deployment [5], the local consequences of reduced FSL load diversity that unavoidably results from providing frequency regulation service has not been addressed. Specifically, synchronizing loads in response to frequency variations threatens to cause line overload in congested distribution systems. To the extent that these constraints are reflected in RMS voltage deviations, autonomous loads can use RMS voltage as an input to a hybrid controller that dampens the frequency response if and only if line overload occurs.

This paper describes a novel autonomous load control algorithm that contributes to stabilizing system frequency and RMS voltage. The performance of this controller is analyzed by simulating its behavior when controlling TCLs in a representative distribution system.

This paper is organized as follows. Section II describes autonomous load control algorithms including the proposed hybrid frequency-voltage sensitive load controller. Section III describes the setup of the simulation environment and Section IV presents the results of the simulations. Finally, section V concludes the paper.

II. Autonomous Load Control

A. General Autonomous TCL Model

The autonomous load controller, which is a generalized version of the frequency sensitive load controller in [7], operates in the system shown in Fig. 1. The load controller samples the energy-carrying voltage waveform v, and the

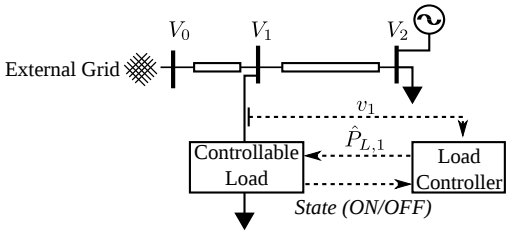

Figure 1. Oneline system diagram showing controllable load and DG in a radial feeder [6]. Dashed lines represent control signal paths.

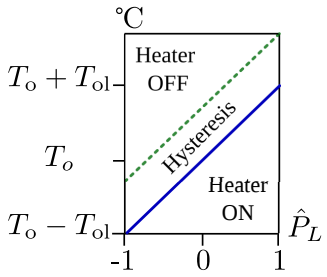

Figure 2. Dependance of thermostat setpoint on $\hat{P}_L$ in heating application [6]. Y-axis is process temperature i.e. of water in hot water tank. The heater turns ON when the temperature falls below the solid line, and turns OFF when the temperature rises above the dashed line.

state of the load (ON/OFF). The controller output $\hat{P}_{\mathrm{L}}$ is the desired load power consumption, normalized to lie between $[-1, 1]$ where -1 represents no power consumption, and 1 represents full power. The desired power consumption $\hat{P}_{\mathrm{L}}$ is given to a controllable load that will attempt to comply with the request, within the constraints imposed by the final energy conversion process.

This paper will examine the use of TCLs for demand response because they represent a large, and potentially controllable, load in residential areas. The thermostat setpoint T_{s} is the result of linearly mapping $\hat{P}_{\mathrm{L}}$ to an offset to the user-given thermostat temperature setpoint T_{o}, up (down) to the offset limit T_{ol}:

$$T_{\mathrm{s}} = T_{\mathrm{o}} + T_{\mathrm{ol}}\hat{P}_{\mathrm{L}}. \tag{1}$$

The thermostat state as a function of process temperature and thermostat offset is shown in Fig. 2.

B. Frequency Sensitive Loads

Claims that frequency sensitive loads (FSLs) are a large, feasible and low cost resource for primary frequency regulation are supported by analysis [7] and experiments [8].

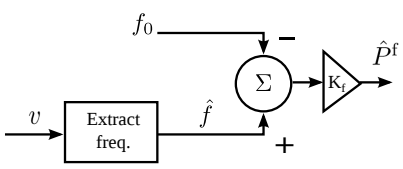

Figure 3. Frequency Response subsystem.

This has motivated recent efforts by European transmission system operators to consider mandating integration of frequency response into TCLs [5].

Fig. 3 shows a block diagram of the FSL controller that produces an output $\hat{P}^{\mathrm{f}}$ proportional to the measured AC frequency $\hat{f}$, where the sensitivity is given by the gain constant $\mathrm{K_f}$. The reader is referred to existing literature [9], [10] for a full discussion of the properties of FSLs, the salient issue for this work is the reduction in FSL diversity caused by the frequency response. The present practice of distribution system planners is to assume a random distribution of the internal state of loads and apply a coincidence factor to de-rate the installed capacity of a load class to the maximum expected aggregate load. Field tests of FSL for space heating show that in certain weather conditions the aggregate load approaches installed capacity [8] during high frequency events.

In [11] the authors propose a protocol for quickly restoring FSL diversity after a responding to an event, but the protocol does not alleviate the local transmission bottle-necks the arise during the event response itself. A blanket reduction of the capacity of FSLs is suboptimal because congested conditions may happen only in a few locations for a short time.

C. Voltage Sensitive Loads

The purpose of the voltage sensitive loads (VSL) controller is to regulate system voltage by modulating the power consumption of flexible loads. In networks where system load and RMS voltage are inversely correlated, a VSL that reduces power consumption when voltage is low is acting to increase total load diversity. Fig. 4 shows a block diagram of the voltage-sensitive load (VSL) controller, full details of this algorithm can be found in [6], a brief description is given here.

The controller is given a RMS voltage measurement and calculates a short-term moving average $\hat{v}$ over a time frame of seconds (the exact value is a configurable parameter), a function that filters out measurement noise and transient faults. This short-term average is then subtracted from the long-term average voltage value $\bar{v}$ giving the relative voltage difference ΔV. This difference is then scaled by a gain factor G to determine the desired power consumption of the load $\hat{P}^{\mathrm{V}}$.

The long-term average voltage value $\bar{v}$ is found by again using a moving average over a time period of hours to days (exact value is configurable, but it must be much greater than short-term value). Two long-term average voltage values are found: one long-term average of voltage measurements taken when the device is ON, and one when the device is OFF. Switching between the two values based on the state of the device compensates for the changes in voltage caused by the device itself.

The controller "auto-tunes" G, thus normalizing the voltage response relative to magnitude of observed voltage variations. The long-term moving variance of ΔV is found

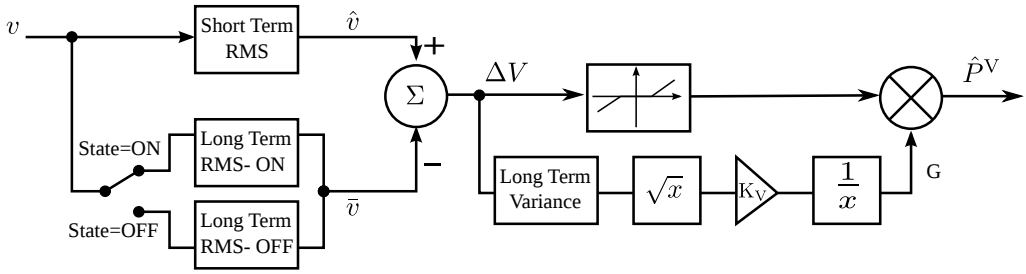

Figure 4. Voltage Response subsystem [6].

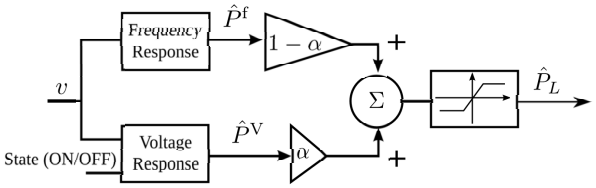

Figure 5. Block diagram of hybrid frequency and voltage sensitive load controller. Weighting factor α is limited to be between [0,1].

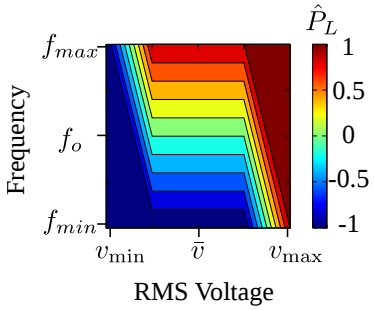

Figure 6. Dependance of $\hat{P}_L$ on voltage and frequency. The voltage response has a deadband around the expected value $\bar{v}$, while the frequency response has a continuously linear response.

over a time span equal to that used for calculating $\bar{v}$. The standard deviation σ is found as the square root of the variance, then multiplied by a fixed value K_V and inverted to give G.

One extension is made to the algorithm introduced in [6], the addition of a deadband which holds the controller output at zero for values of ΔV below a given threshold.

D. Hybrid Frequency-Voltage Sensitive Loads

The load control algorithm introduced in this work is shown with a high-level block diagram in Fig. 5. The output is the weighted sum, with weighting factor α, of a frequency response $\hat{P}^{f}$ and a voltage response $\hat{P}^{V}$, each of which has been described earlier in this section:

$$\hat{P}_L = (1-\alpha)\hat{P}^{f} + \alpha\hat{P}^{V}. \quad (2)$$

The output $\hat{P}_L$ is limited to be between [-1,1]. The optimal value of α will depend on the relative importance of frequency and voltage regulation in a specific power system.

The controller output value is shown graphically as a function of the outputs of two subsystems in Fig. 6, where the parameters of the voltage response are chosen such that there is a deadband around the long-term average voltage value $\bar{v}$.

III. Simulation Configuration

The performance of the proposed load controller algorithm is evaluated with numerical simulations using GridLAB-D [12] on a feeder representing a typical North American distribution system. GridLAB-D is a discrete event simulation platform that contains detailed models of electrical distribution system components and loads, together with weather data, and a framework for collecting statistics about the state of the network and loads. Unbalanced voltage values are found with high precision because the simulator calculates the full 3x3 mutual impedance matrix for each component as given in [13]. As an open-source project, it is amenable to modification, and the controller described in section II-D was implemented in C++ and compiled into the software.

Simulations were run over 10 days, with a minimum time step of 10 s for three scenarios: purely FSL, Hybrid and a base case where TCL setpoints were held constant.

A. Distribution Network Model

The network model is taken from [14] where typical North American network topologies were created from a survey of operating networks. The network contains a mix overhead lines, underground cables, unbalanced laterals, 1175 residences, 750 transformers, and a total of 1900 busses. The uncontrolled conventional loads in the system are represented as HVAC loads with a heat load synthesized from typical weather conditions of the Pacific Northwest in January, and ZIP loads (constant impedance, constant current, and constant power) that follow a preset schedule derived from the daily demand patterns observed in the USA. House parameters such as size, indoor temperature preference, and insulation were subject to a uniform distribution, for full details see [15].

Distributed generation in the form of PV was added to each house in the distribution system. The size of the PV systems were chosen so they produced in aggregate approximately the same amount of energy as the water heaters consumed over the test period. PV production time

series were derived from data taken in April from a 7 kW PV system in our lab in Denmark and scaled to the size of each residential system in the simulation, with spacial diversity created by randomly assigning each residence to 6 groups and skewing production profiles by 10 s between each group.

System frequency was generated from measurements taken in the Nordic power system as part of a field experiment [8]. Using a pre-recorded frequency time series simplified the simulation by preventing the changes in load from effecting frequency values.

B. Thermostat Controlled Load Model

In the simulations the controlled load is modeled as a hot water heater. Model parameters such as water heater power, capacity, thermostat setpoint, thermostat deadband and insulation were subject to a random distribution representing typical values found in the USA. The water demand of each household was constant at $q[t] = 57$ l/hr representing mean household water consumption, a constant demand assumes a decoupling of the energy demand to heat water and the time of water use. The single phase resistive heating element was modeled as a constant impedance load and the inlet water temperature was fixed to $T_{\text{in}}[t] = 15.5$ °C. Water temperature in the tank was modeled by a first order discrete equation

$$T_{\text{w}}[t+1] = \frac{1}{C}[\ (T_{\text{o}}[t] - T_{\text{w}}[t])U_{\text{a}} + w[t]Q + q[t](T_{\text{in}}[t] - T_{\text{w}}[t])\ ] \quad (3)$$

where the water temperature T_{w} at time t depends on the ambient temperature T_{o}, the water temperature at the previous timestep, the thermal conductance of the tank jacket U_{a}, the ON/OFF signal from the thermostat w, the gain of the heating element Q, the water demand q, and the heat capacitance of the full tank C. The temperature of the hot water was modeled as a single body, neglecting the thermocline that arises in real tanks.

C. Controller Configuration

Simulations were run for a base case with static thermostat settings ($T_{\text{ol}} = 0$), scenarios with purely FSLs ($\alpha = 0$), and a balanced hybrid configuration ($\alpha = 0.5$). In the FSL and hybrid scenarios, the load controllers are configured with a maximum temperature offset of $T_{\text{ol}} = 3$ °C. The gain of the purely FSL controller was $K_{\text{f}} = -30$ °C/Hz. In the hybrid controller, the frequency gain was increased to $K_{\text{f}} = -73$ °C/Hz. The voltage-sensitive controller had a short-term average smoothing constant of 1/60 and a long-term average smoothing constant of 1/43200. The deadband was set to one standard deviation σ, and the voltage gain K_{V} chosen so the controller saturated when $\Delta V = 2.5\sigma$.

Table I
PERFORMANCE OF BASE CASE, FSL AND HYBRID CONTROLLER

Parameter	Base	FSL	Hybrid
Ave. W.H. Power	757 kW	781 kW	781 kW
Ave. $\hat{P}_{\text{L}}$	n.a.	-0.001	-0.008
Ave. Daily Max. Load	3925 kW	7086 kW	6251 kW
W.H. power at Max.	838 kW	4090 kW	3409 kW
Mean Losses	99 kW	107 kW	105 kW
Ave. Daily Min. V	0.989 p.u.	0.975 p.u.	0.979 p.u.

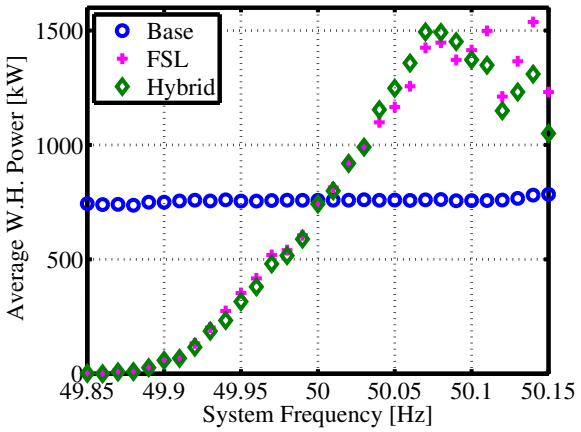

Figure 7. Average water heater power as a function of system frequency.

IV. SIMULATION RESULTS

First, the frequency response of the water heaters is evaluated by grouping each sample of aggregate power consumption by system frequency. The average water heater power as a function of frequency is shown in Fig. 7. The frequency response of the FSL controller matched closely the frequency response of the hybrid controller up until around 50.1 Hz when both controllers saturate.

Table I summarizes key performance statistics of the system. In both the FSL case and hybrid case, the power consumption of the TCLs increased by 3% compared to the base case, even though the thermostat offset had a slight negative bias. This is because the power consumption of the TCLs is asymmetrical with respect to thermostat offset.

The large amount of FSL greatly worsens the average of the daily peak power consumption measured at the external grid connection from under 4 MW in the base case to over 7 MW. Substituting the FSL with the hybrid controller reduces the peak power to 6.25 MW, an improvement of 12% over the purely frequency sensitive controller, but still significantly worse than the base case. Looking at the power consumption of the water heaters at the daily peak load, the hybrid controller reduced the power of the water heaters at the peak load by 16% compared to the FSL. The average of daily minimum voltages is lowest with the FSL, improved with the hybrid controller, but best in the base case.

A typical time series showing the frequency response,

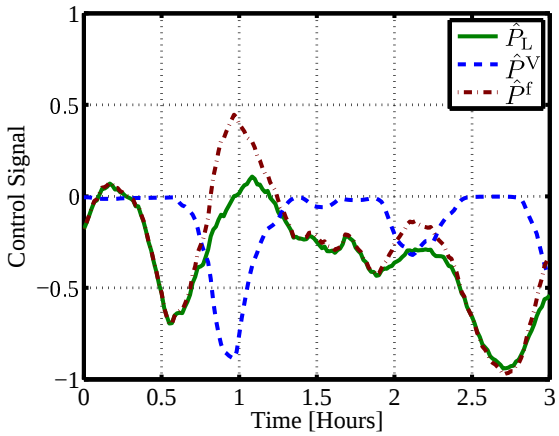

Figure 8. Representative time series of hybrid control $\hat{P}_L$ signal and the voltage $\hat{P}^V$ and frequency $\hat{P}^f$ components.

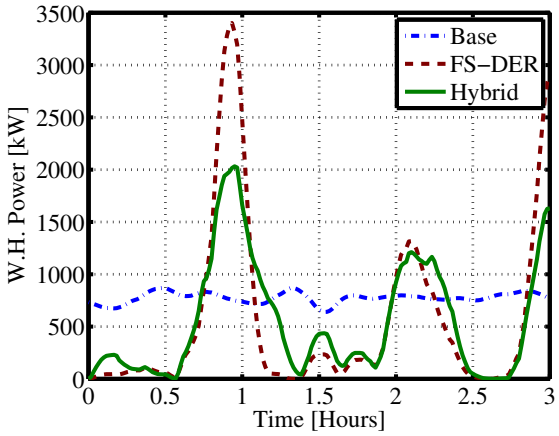

Figure 9. Time series of aggregate water heater power consumption for base case, FSL and hybrid controller.

voltage response, and the combined hybrid response is shown in Fig. 8. It shows in the first half-hour the voltage response lies in the deadband. Around the one hour mark the voltage response moves in the opposite direction as the frequency response, dampening the frequency response. In the beginning of the second hour, the voltage response has the same sign as the frequency response reenforcing the response. The aggregate power consumption of the water heaters shown for the base case, FSL and hybrid controller for the same time period in Fig. 9. The hybrid controller has a similar load shape as the FSL but the hybrid controller has clipped the sharp spike in demand at the end of the first hour. The base case shows very little variation in the aggregate water heater power consumption, so it is apparent that any frequency response would worsen the TCL load diversity.

V. Conclusion

An autonomous hybrid frequency-voltage sensitive load controller was introduced and analyzed in this paper. The hybrid controller is a linear combination of two subsystems: a frequency response that modulates load power in proportion to system frequency, and a voltage response that modulates load power in proportion in relative deviations in voltage. The hybrid controller allows frequency sensitive loads providing frequency regulation to be integrated into congested distribution systems by moderating the frequency response when voltage deviations indicate congestion in the distribution system.

Simulations in GridLAB-D show that the introduction of frequency sensitive loads (FSL) significantly increases the system's peak load compared to a base case. A hybrid controller with a comparable frequency response reduced the system's peak load by 12% compared to the FSLs. The minimum voltage levels observed in the feeder were similarly better for the hybrid controller relative to the FSL, though both voltage and peak power levels were not restored to the level of the base case.

References

[1] K. De Brabandere, B. Bolsens, J. Van den Keybus, A. Woyte, J. Driesen, and R. Belmans, "A voltage and frequency droop control method for parallel inverters," *Power Electronics, IEEE Transactions on*, vol. 22, no. 4, pp. 1107–1115, 2007.

[2] VDE, "VDE-AR-N 4105:2011-08 Power generation systems connected to the low-voltage distribution network - Technical minimum requirements for the connection to and parallel operation with low-voltage distribution networks," 1 Aug. 2010. [Online]. Available: http://www.vde.com/en/fnn/pages/n4105.aspx

[3] T. Sansawatt, L. Ochoa, and G. Harrison, "Integrating distributed generation using decentralised voltage regulation," in *Power and Energy Society General Meeting, 2010 IEEE*, july 2010, pp. 1 –6.

[4] F. Marra, "Electric Vehicles Integration in the Electric Power System with High Wind Penetration - the Charge/Discharge infrastructure," Ph.D. dissertation, Technical University of Denmark, Mar. 2013.

[5] ENTSO-E, "Draft Demand Connection Codes," 27 Jun. 2012.

[6] P. J. Douglass, R. Garcia-Valle, O. C. Tudora, and J. Østergaard, "Voltage Sensitive Load Controllers for Voltage Regulation and Increased Load Factor in Distribution Systems," *submitted to Smart Grid, IEEE Trans. on*, 2013.

[7] Zhao Xu, J. Østergaard, and M. Togeby, "Demand as frequency controlled reserve," *Power Systems, IEEE Transactions on*, vol. 26, no. 3, pp. 1062 –1071, Aug. 2011.

[8] P. J. Douglass, R. Garcia-Valle, P. Nyeng, J. Østergaard, and M. Togeby, "Smart demand for frequency regulation: Experimental results," *Smart Grid, IEEE Transactions on*, vol. 4, no. 3, pp. 1713–1720, 2013.

[9] J. Short, D. Infield, and L. Freris, "Stabilization of grid frequency through dynamic demand control," *Power Systems, IEEE Transactions on*, vol. 22, no. 3, pp. 1284 –1293, aug. 2007.

[10] M. Donnelly, S. Mattix, D. Trudnowski, and J. Dagle, "Autonomous demand response for primary frequency regulation," Pacific Northwest National Laboratory, Tech. Rep., Jan. 2012.

[11] N. A. Sinitsyn, S. Kundu, and S. Backhaus, "Safe protocols for generating power pulses with heterogeneous populations of thermostatically controlled loads," *Energy Conversion and Management*, vol. 67, no. 0, pp. 297 – 308, 2013.

[12] D. Chassin, K. Schneider, and C. Gerkensmeyer, "Gridlab-d: An open-source power systems modeling and simulation environment," in *Transmission and distribution conference and exposition, 2008. ieee/pes*, Apr. 2008, pp. 1 –5.

[13] W. Kersting, *Distribution System Modeling and Analysis*, ser. The electric power engineering series. Taylor & Francis, 2012.

[14] K. Schneider, Y. Chen, D. Engle, and D. Chassin, "A Taxonomy of North American Radial Distribution Feeders," in *Power energy society general meeting, 2009. PES '09. IEEE*, 2009.

[15] "GridLAB-D Residential Module User's Guide," 2013. [Online]. Available: http://sourceforge.net/apps/mediawiki/gridlab-d/

Appendix E

"Direct Load Control by AC Frequency Modulation"

This paper was originally published in the proceedings of the 6th European Conference on PV-Hybrid Mini-Grids, Chambéry France, April 2012.

Direct Load Control by AC Frequency Modulation

Philip J. Douglass and Shi You

Centre for Electrical Technology, Technical University of Denmark

Elektrovej-Building 325, 2800 Kgs. Lyngby, Denmark

{pjdo,sy}@elektro.dtu.dk

Abstract

Fine-grained under frequency load shedding called “demand as a frequency controlled reserve“ (DFCR) has been shown to be a promising method of providing frequency regulation service from distributed loads [1]. Micro-grids with a large portion of intermittent renewable generation will benefit greatly from this technology because their low inertia.

The paper proposes a operating procedure for utilizing DFCR loads for energy balancing, expanding DFCR’s well known role as a power balancing resource. The system operator can use DFCR for energy balancing by adjusting the frequency controller of generators to schedule off-nominal system frequency values.

The feasibility of the proposed system is evaluated on an existing small island power system.

I Introduction

As photovoltaic (PV) module prices continue to fall and diesel prices rise, the penetration of PV generation is expected to increase in diesel fueled isolated power systems. The amount of PV generation in an isolated system is limited by the minimum forecast daytime load in the absence of battery storage systems or curtailment. To provide reliable electric power during periods of low renewable energy sources (RES) production, a dispatchable generator must have sufficient capacity to serve the peak load. If the

system contained dispatchable loads, they could be activated during periods of high RES production adding to the minimum load, and they could be deactivated during periods of low RES production, lowering the capacity requirements of the dispatchable generator.

When frequency responsive DFCR loads were field tested in a small island power system, problems arose because the devices assumed the system's mean value for frequency was always the nominal frequency, but on the island, the system frequency was observed at off-nominal values for extended periods of time. It was clear from the sampled frequency data that the system was operated in two distinct frequency regimes and this observation lead us to investigate whether these frequency regime changes could be detected and utilized.

Loads suitable for DFCR operation will typically have constraints on the energy demanded over a given time period, but some loads may have additional time constraints on their operation. These time constraints have precedence over the frequency response, and have the potential to lead to undesirable system behavior.

Modulating AC system frequency has been used to curtail production in microgrid systems [2], and frequency responsive loads have been described in [1,3,4], but the authors are unaware of previous work describing the modulation of frequency for controlling loads with time constraints.

This paper is organized as follows. Section II describes the behavior of DFCR in micro-grids. The proposed system operation concept is described in detail in Section III, followed in Section IV by a case study of the island of Christiansø in the Baltic Sea. Finally, Section V is a discussion and Section VI concludes the paper.

II DFCR loads in Micro-grids

A micro-grid is modeled with 4 lumped entities: dispatchable generators with droop frequency controllers, stochastic RES generators (PV modules), DFCR load and finally residual (high priority) load, see Figure 1.

Typical automatically controlled loads (such as thermostat controlled loads) operate in two states, OFF and ON, with the duty cycle controlled to keep the energy level within desired bounds. A DFCR controller will alter the phase of the duty cycle to defer energy consumption away from time periods when the grid is overloaded. The only way to create

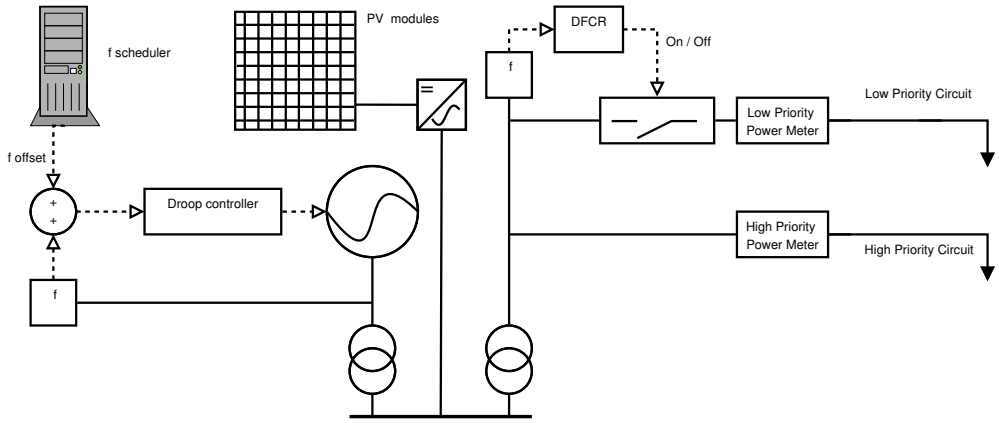

Figure 1: Oneline diagram showing relation between generator governor and DFCR. Solid lines represent electric conductors, dotted lines represent data transfer paths.

a smooth and reliable frequency response with OFF/ON loads is to have a population of devices with a diversifying parameter such as differing frequency thresholds. A small synchronous system will have a small population of DFCR loads, where each one may be a significant portion of the total load. Therefore, the diversity of a large population can not be counted on.

Energy constraints for loads are represented by the maximum time the device is allowed to be disconnected from the electric energy supply (t_{max_off}), and the minimum time it must remain reconnected after being disconnected (t_{min_on}). Processes with startup costs and shutdown costs, such as an induction motor's inrush current, will have additional constraints besides a minimum demand for electric energy over a given time period. The startup and shutdown costs are represented by the minimum ON time (t_{min_on}) and the minimum OFF time (t_{min_off}).

DFCR with time constraints is suitable to act as disturbance reserve, reducing load during large and infrequent drops in frequency, but is unsuitable to act as a continuous regulation resource within the normal frequency operating range. The problem with DFCR as a continuous regulation resources is acute both when RES production is high and the load low, and when RES production is low and the load is high.

When the RES production is more than the residual load, the droop controlled dispatchable generator cannot further reduce production, and the DFCR load is critical to absorbing the RES energy over-production. If the DFCR load is constrained by t_{min_off},

frequency will rise uncontrollably in the absence of alternative frequency regulation resources (i.e. dump load).

When RES production is low, the t_{min_on} constraint of DFCR can compromise the security of the system. In a scenario where the dispatchable generators do not have the capacity to supply the DFCR and the residual load simultaneously, DFCR load constrained by t_{min_on} can cause the system frequency to decline uncontrollably (until axillary frequency regulation resources such as shedding of high priority loads are activated), see Figure 2.

III Dispatch of DFCR loads

The control of distributed energy resources is typically classified as either direct or indirect [5]. Direct control corresponds to the architecture of existing utility SCADA systems where commands are issued from a centralized controller and remote terminals respond to the commands in a deterministic manner. Frequency controlled reserves are not usually considered as directly controlled because the control signal (system frequency) is not actively generated, but rather results from the intrinsic behavior of the power system. Dispatchable generators participating in frequency regulation are able to alter the system frequency by altering the parameters of their frequency controller, see Figure 4. When frequency measurements are averaged over long time periods to filter out the intrinsic volatility of the system power balance, changes in the generators' frequency regulation parameters can be detected by DFCR loads.

A droop controller will produce power proportional to the system frequency, with lower frequencies resulting in higher power output. Thus, at steady-state conditions, the frequency will indicate the amount of load on the droop controlled generator. In the presence of limited generation resources and a significant amount of frequency dependent demand, lowering the system frequency can be used as a proactive measure to balance load and generation by selective load shedding. Changing the system frequency target on some frequency regulation resources, but not others reallocates the energy production between the two groups of resources (ie. supply-side and demand-side).

The DFCR algorithm for relay-based devices described in [1] has a frequency threshold (f_{off}) below which the load is disconnected. Loads are reconnected when

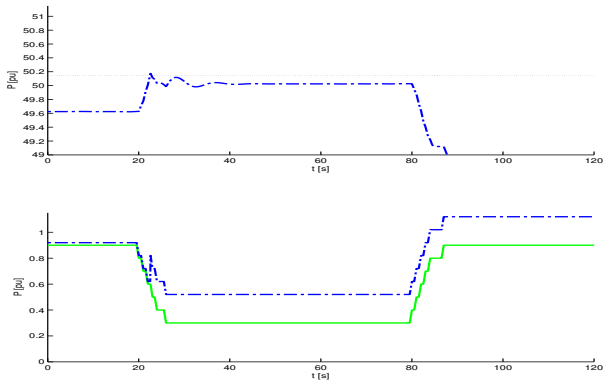

Figure 2: DFCR with t_{min_on} constraints during a transient spike in RES output. Top graph shows frequency with the black horizontal line $f_{restore}$. The bottom graphs show loads (minus RES production). The solid green line represents the residual load, the blue dashed line shows the addition of DFCR loads.

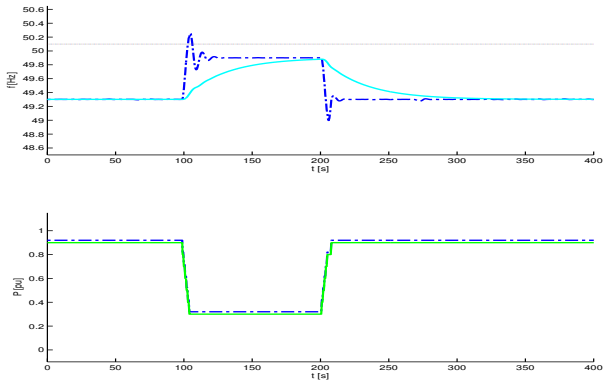

Figure 3: The top graph shows the system frequency (dark blue) and the frequency subjected to a low pass filter (light blue). $f_{restore}$ for the filtered frequency is the solid black line. The system frequency does not stay above the threshold long enough for the filtered value to cross the reconnect value, so the DFCR remains off.

system frequency is above a second, higher threshold frequency ($f_{restore}$), creating a simple deadband. A wide enough deadband would avoid spurious changes to DFCR state, but this has the disadvantage that when the system resides inside the deadband the DFCR state is uncertain because it depends on historical frequency deviations rather than the current frequency.

To narrow the deadband while avoid spurious switching DFCR state, the DFCR can pass the frequency samples through a low pass filter before comparing the value to preset thresholds. A moving average or exponentially-weighted moving average filter could be utilized.

A similar algorithm was described in [6], where different cutoff frequencies existed for short-term frequency deviations (i.e. 1s) and longer-term deviations (i.e. 5 min.). This algorithm is well suited for the proposed scheme because a small but consistent deviation from nominal frequency on a long time scale will force devices into either the ON or OFF state. Changes to the long-term average frequency are feasible to provoke, even when the frequency varies widely in the short-term.

Figure 3 shows how DFCR with a low pass filter will not change state when subject to steep ramps of RES generation.

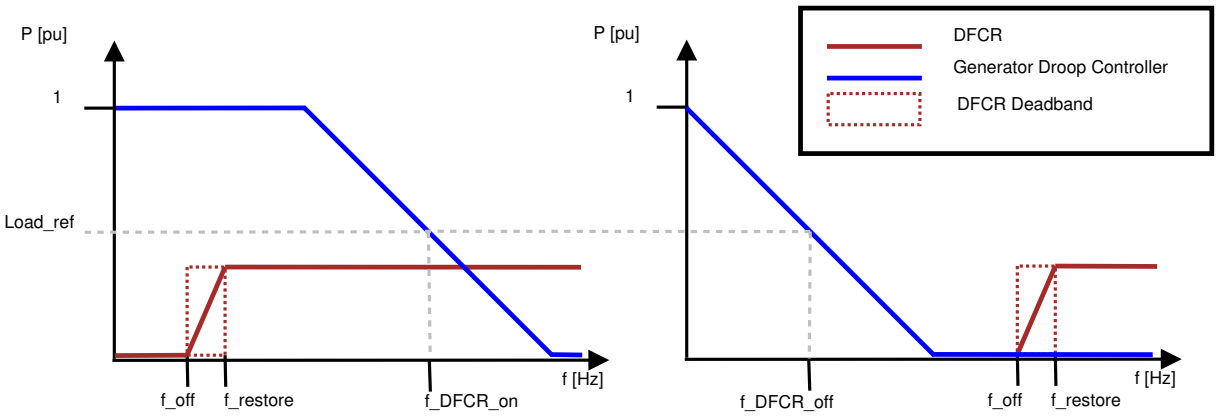

Figure 4: Left: DFCR devices dispatched in ON state by allocating droop controlled reserves to well above f_{off}. Right: DFCR devices dispatched in OFF state by operating droop controlled reserves well below $f_{restore}$.

IV Case Study: Christiansø

Christiansø is a decommissioned naval base which is a popular tourist destination. Around 100 people live permanently on the 0.22km^2 island. Their electric power system is composed of 4 diesel powered generators, two with a rating of 180kW, one 130kW and one 60kW. At the moment, there is no renewable electricity generation, though the wind and solar resources are available.

Two bottle cooling refrigerators with DFCR functionality have been installed as part of an ongoing experiment [7]. Frequency measurements were collected when the DFCR functionality was disabled to characterize the system.

Two modes of operation were observed, and within each mode, the frequency measurements fit well into a normal distribution, with the average value of 50.00Hz for group one and 50.11Hz for group two. The standard deviation for group one was 43.4mHz, for group two 137.3mHz. The moving average of high resolution frequency measurements from group two was found and the standard deviation of these filtered values was 48mHz.

The normal distribution of frequency samples implies that 99.9999% of the time the value will be within $\pm 5\sigma$ of the mean. Conversely, the system frequency will be farther than $\pm 5\sigma$ from the mean approximately 50 milliseconds per day. If the generators were set to produce at $f_{DFCR\_on} = f_{restore} + \sigma = f_{off} + 5\sigma$, then the filtered frequency would be above $f_{restore}$ 84% of the time, and below f_{off} 25ms per day.

With a deadband $4\sigma = 200mHz$, then the average frequency to dispatch DFCR in the ON state with high confidence would be $f_{DFCR\_on} = 50.150Hz$. To be highly certain that the DFCR devices are OFF, the average frequency would have to be $f_{DFCR\_off} = 49.850Hz$. This range of frequency offsets is slightly larger that that already observed during normal operation on Christiansø, but considered feasible without significantly effecting the functioning of conventional loads. Alternatively, if $f_{DFCR\_on} = f_o$, the $f_{DFCR\_off} = f_o - 6\sigma = 49.700Hz$.

The EN 50160 standard [8] used in Europe requires that island power system maintain their frequency at $50Hz \pm \%2$ ($49Hz$ to $51Hz$) for 95% of a week and $50Hz \pm 15\%$ ($42.5Hz$ to $57.5Hz$) for 100% of the time. A mean value of 49.700Hz gives a margin to the statutory minimum frequency of $700mHz$, which is acceptable during unfaulted operation.

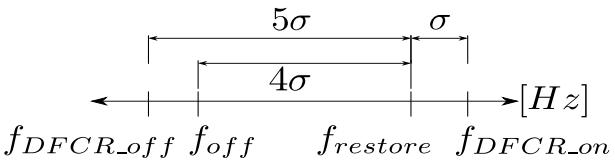

Figure 5: Relative placement of DFCR frequency thresholds and generator setpoints.

Parameter	Relative Value	Value
f_o		50Hz
σ		50mHz
f_{off}	$f_o - 2\sigma$	49.9Hz
$f_{restore}$	$f_o + 2\sigma$	50.1Hz
f_{DFCR_on}	$f_{restore} + \sigma$	50.150Hz
f_{DFCR_off}	$f_{off} - \sigma$	49.850Hz

Figure 6: Suggested parameter values for DFCR operation on Christiansø with thresholds symmetric to f_o

V Discussion

The difference between target frequency values would have to be larger than the typical variation of frequency (i.e. $> 5\sigma$) but if disturbances pushed the system frequency into a neighboring frequency band, the autonomous action of the DFCR would act to restore the frequency to the targeted value. The utility's load control performance would depend on how closely the autonomous action of the DFCR conformed to pre-established schedules. By designing the DFCR threshold levels and target frequencies, arbitrary levels of load control performance can be achieved. Metrics for measuring frequency quality would be redefined as deviations from the target frequency, not deviations from nominal.

VI Conclusion

The paper has proposed a new operating concept which utilizes DFCR, a highly distributed under frequency load shedding method, as part of direct load control scheme. Frequency sensitive loads are dispatched by adjusting the generators' frequency controller to target off-nominal frequencies. The feasibility of this concept was demonstrated by simulations, and by analyzing data collected from an operating small island power system. The analysis shows that DFCR loads can be dispatched with high reliability without endangering the system's ability to remain within the range of acceptable frequencies.

References

[1] Zhao Xu, J. Østergaard, and M. Togeby. Demand as frequency controlled reserve. *Power Systems, IEEE Transactions on*, 26(3):1062 –1071, aug. 2011.

[2] Steca Elektronik GmbH. Steca RCC-02 Operating Instructions. Online `http://www.stecasolar.com/index.php?Steca_Xtender_Zubehoer_en`. Accessed February 9, 2012.

[3] J.A. Short, D.G. Infield, and L.L. Freris. Stabilization of grid frequency through dynamic demand control. *Power Systems, IEEE Transactions on*, 22(3):1284 –1293, aug. 2007.

[4] David P. Chassin, Matthew K. Donnelly, and Jeffery E. Dagle. Electrical power distribution control methods, electrical energy demand monitoring methods, and power management devices, 2011. Patent US 8073573.

[5] D.S. Callaway and I.A. Hiskens. Achieving controllability of electric loads. *Proceedings of the IEEE*, 99(1):184 –199, jan. 2011.

[6] A. Molina-Garcianda, F. Bouffard, and D.S. Kirschen. Decentralized demand-side contribution to primary frequency control. *Power Systems, IEEE Transactions on*, 26(1):411 –419, feb. 2011.

[7] P. Douglass, R. Garcia-Valle, P. Nyeng, J. Østergaard, and M. Togeby. Demand as Frequency Controlled Reserve: Implementation and practical demonstration. *Innovative Smart Grid Technologies Europe*, 2011.

[8] Standard. EN 50160: Voltage characteristics of electricity supplied by public electricity networks, 2010.

Appendix F

"System Frequency as Information Carrier in AC Power Systems"

This paper appears in *IEEE Transactions on Power Delivery*, vol. 30, no. 2, pp. 773-782, April 2015.

System Frequency as Information Carrier in AC Power Systems

Philip J. Douglass *Member, IEEE*, Kai Heussen *Member, IEEE*, Shi You *Member, IEEE*, Oliver Gehrke, Jacob Østergaard *Senior Member, IEEE*

***Abstract*—Power generators contain control systems able to regulate system frequency, but the frequency setpoint values are only rarely modified from nominal values. This paper describes design considerations for a communication system from generators to frequency sensitive distributed energy resources (FS-DER) using changes to frequency setpoint values of generators. Signaling discrete system states by generating off-nominal system frequency values can be used as a novel narrowband unidirectional broadcast communications channel. This paper describes two protocols for utilizing off-nominal frequencies to carry information: First, a protocol for dispatching blocks of FS-DER that is suitable for systems restricted to relatively slow rates of change of frequency (ROCOF). Second, for systems that allow higher ROCOF values, the feasibility of using power generation resources as a power line communication transmitter is shown. Data from an operating islanded power system with diesel generators is analyzed to demonstrate the feasibility of the proposed communication system in systems fed by rotating machines. The feasibility of the proposed communication system in systems fed by power electronics is shown with laboratory tests of a 20 kVA inverter. The inverter was found to have a maximum ROCOF of 2.2 Hz/s, sufficient to enable its use as a power line communication transmitter.**

***Index Terms*—Power Frequency Communication; Ultra Narrow Band; Energy Management; Load Management; Voltage Source Inverters; Distributed Energy Resources; ROCOF.**

I. Introduction

TRANSITIONING electric energy systems to renewable energy sources (RES) will increase the sustainability as well as the complexity of the power system. The low power density of RES favors distributed generation (DG), and as a result, the number of entities actively participating in maintaining system stability will increase greatly. The fluctuating production profile of RES and scarcity of large-scale electric energy storage motivates the creation of energy management systems that include loads.

While the availability of low-cost microcontrollers allows software control of even the smallest loads, creating a communications network that reaches out to many separate units is a costly endeavor. Real-time constraints on the control of power systems impose additional costs on communication systems. And where such a communication system has been established, maintaining the N-1 protection criteria requires that failure of the communication system does not compromise system security. Therefore a robust fallback state must be defined.

The authors are with Center for Electric Power and Energy, Technical University of Denmark, Elektrovej-Building 325, 2800 Kgs. Lyngby, Denmark {pjdo, kh, sy, olge, joe}@elektro.dtu.dk.

The physical characteristics of the voltage waveform (AC frequency and RMS voltage) can be measured at the point of energy consumption, and can reveal valuable information about the state of the power system. Utilizing local measurements for autonomous control of distributed energy resources (DER) was first proposed in [1]. The physical characteristics of the voltage waveform are subject to disturbances, but to the extent that system operators can maintain the parameters within known intervals, the parameters can be used for communication.

Power line communication has been in use since the pioneering days of public electric energy systems. Using the AC system frequency (50 Hz or 60 Hz) as a carrier for frequency modulation, called power frequency communication (PFC), was first introduced with the TWACS communication system [2]. The TWACS transmitters described in [2], [3] are intended for modifying frequency of a single radial feeder in a large synchronous area. This paper investigates a general framework for using AC system frequency for transmitting information which differs from TWACS in the following ways: the information reaches an entire synchronous area; it can utilize more of the available bandwidth; it can operate with or without time-dependent decoding; and it utilizes energy sources as transmitters. The motivation for this framework is to create energy management systems with lower costs and higher reliability relative to existing alternatives by reducing the number of system components.

An overview of the communication system model, adapted from the authors' previous work in [4], is shown in Fig. 1. Frequency sensitive distributed energy resources (FS-DER) and conventional passive loads are connected to a controllable generator through a power grid. A series of symbols $(S_k, S_{k+1}, ...)$ are mapped to frequency set point changes that are given to the generator. The generator changes the system frequency, and these changes are measured by FS-DER, which is able to reconstruct the original series of symbols.

This paper describes two protocols for encoding information with system frequency. The first protocol dispatches FS-DER by transmitting the value of a single discrete parameter and is suitable for large power systems with slow frequency dynamics. The second protocol creates a general purpose PFC channel in systems with fast frequency dynamics.

The remainder of the paper is structured as follows: Section II gives background in frequency control of power systems. Section III describes existing PFC systems. Section IV describes the general methods for deriving constraints for the communication system that are applied in Sections V & VI to

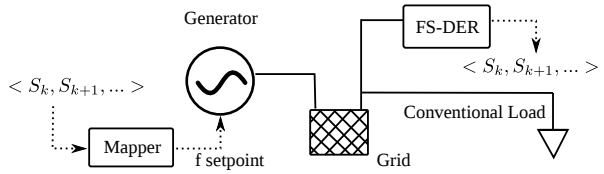

Figure 1. Communication system model with solid lines representing electrical energy transmission paths and dashed lines representing logical signaling paths. Symbols ($S_k, S_{k+1}, ...$) are encoded into system frequency values which are detected by FS-DER.

FS-DER dispatch and PFC transmission respectively. Section VII shows the feasibility of the proposed communication schemes with case studies of two types of islanded power systems: a diesel dominated system, and an inverter dominated system. Section IX is a discussion, and Section X concludes the paper.

II. Power System Frequency Control

Power systems must keep system frequency within a narrow range, and frequency stability can be a limiting factor for increasing penetrations of fluctuating RES [5].

A. Standards

The EN 50160 standard [6] used in Europe specifies the physical characteristics of electric energy delivered to customers. A large interconnected power system is required to deliver power with a frequency specified as:

50 Hz ± 1 % for 99.5 % of the year
50 Hz $+4$ %, -6 % for 100 % of the time.

Small island power systems have a wider tolerance and must be designed for frequency constraints:

50 Hz ± 2 % for 95 % of a week
50 Hz ± 15 % for 100 % of the time.

Proposed grid codes from ENTSO-E [7] relax the constraints on system frequency for large systems, allowing unlimited operation in the range 50 Hz ± 2 %. The proposed grid codes require generators to remain online at all times when the rate of change of frequency (ROCOF) is less than 2 Hz/s.

B. Synchronous Machine Dominated Systems

In a system with synchronous generators, system frequency is a noisy signal. Disturbances to system frequency are caused by imbalance between mechanical power provided to rotating generators ΔP_{g} [p.u.] and electric power withdrawn by loads ΔP_{l} [p.u.]. In a single-machine system the ROCOF is given by the swing equation [8]:

$$ROCOF = \Delta \dot{f} = \frac{f_{\mathrm{o}}}{2H}(\Delta P_{\mathrm{g}} - \Delta P_{\mathrm{l}}) \qquad (1)$$

where f [Hz] is the system frequency, f_{o} [Hz] is the nominal frequency and H [s] is the system inertia. When loads are uncontrollable, controlling generator power is the only way to maintain power balance.

For systems with multiple generators, Eq. (1) can be used to estimate the average system frequency by creating a lumped model of the system inertia:

$$H = \sum_{i \in N} H_i$$

where H_i is the inertia contribution of each of i generators in the set N. Power production (ΔP_{g}) can be similarly aggregated.

In a multi-machine system, the frequencies observed at various busses are not uniform on very short time scales (from 10s of cycles to seconds) [9], a phenomena the lumped model can not describe. The effect of this short-term frequency variation is negligible in the proposed communication system because of a low-pass filter of frequency measurements in the FS-DER.

The response of the system to transient imbalances is determined by the magnitude of the power imbalance, the system's inertia and time constants on ramping up (or down) the primary and secondary frequency controlled reserves. During large imbalances, load shedding, or other special protection schemes are triggered and modify the system response. In the event of a disturbance, primary frequency regulation acts to stabilize the frequency on short time scales (seconds to minutes) by reestablishing the balance between generation and load. Primary frequency regulation is done by a $(P-f)$ droop response which makes generator power inversely proportional to system frequency. The droop response results in a steady state frequency deviation. To restore system frequency to the setpoint frequency, a slower secondary control loop responds to the integral of the frequency deviation.

Large synchronous generators are characterized by relatively slow response times to operating point changes. The spinning mass of the rotor contributes inertia to the system (H in eq. (1)), limiting the ROCOF during imbalances. Motors also contribute to system inertia, but relative to the rated power they contribute less than half the inertia of generators [10].

In the off-line planning stage, system planners perform simulation studies to determine the adequacy of primary and secondary frequency regulation resources [11]. These studies are deterministic in nature, so to account for uncertainty about the actual state of the real system, a number of credible scenarios are studied to cover the range of expected operating conditions. These studies determine the minimum frequency (nadir) after the largest expected contingency and the distribution of frequency values during normal operation. Frequency regulation resources are provisioned to ensure that performance constraints are met at all busses in the worst case scenario.

In addition to limits on system frequency, ROCOF must also be kept within well defined constraints. Events that provoke high ROCOF values place stress on synchronous machines, and ROCOF sensitive relays are part of generator protection schemes. Grid-connected DG will often have ROCOF relays to prevent unintended island operation [12]. Today, interventions are not generally needed to prevent the ROCOF from exceeding this requirement, but in synchronous areas with a growing penetration of non-synchronous generation, inertia

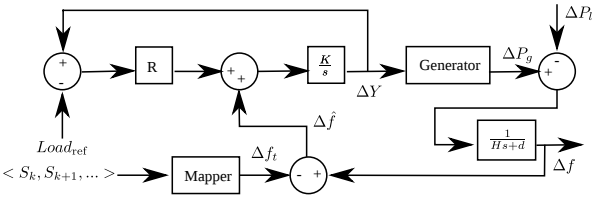

Figure 2. Simplified block diagram of a droop controlled generator used as a transmitter of information, adapted from [8]. A series of symbols $< S_k, S_{k+1}, ... >$ is encoded to frequency setpoint values Δf_t by a simple 1-to-1 mapping and then given to the standard droop controller. The system's inertia H and load damping factor d determine how quickly a power imbalance ($\Delta P_g - \Delta P_l$) changes system frequency Δf.

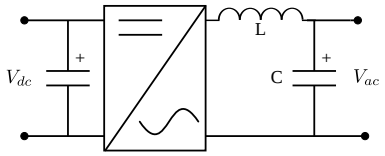

Figure 3. Inverter with LC output filter functions to convert DC primary energy source into AC.

will decline, and ROCOF will increase, to a level where mitigation efforts are needed [13].

When modeling the use of synchronous machines as transmitters of information, a generic generator is considered which covers all generation resources. Fig. 2 shows a block diagram of a conventional droop controlled generator whose speed governor is modulated with a stream of input symbols. The symbols are mapped to frequency setpoints using a look-up table. Decomposing the generator block in Fig. 2 of a rotating machine would reveal a transfer function from fuel delivery to turbine torque to electric power and the time delays involved in all sub-processes. Secondary frequency control is accomplished by changing $Load_{\text{ref}}$ [MW] values.

In large interconnected systems generator frequency setpoints are occasionally set to off-nominal values to correct deviations between electrical time and UTC. In the continental European power system, frequency setpoints are adjusted to 50.01 Hz or 49.99 Hz for up to 24 hours [14].

C. Inverter Dominated Systems

Inverters take a DC power source and apply power electronics to produce an AC sine wave with low distortion. The architecture of a generic inverter is shown in Fig. 3. They are classified as either voltage source inverters (VSI) or current source inverters (CSI). A system without rotating generators needs at least one VSI to produce a reference frequency to which CSI can synchronize [15]. Synchronous areas dominated by VSI can be found in any island where the primary power sources or transmission links are based on DC technology.

When energy sources are connected to an AC power system through VSIs, the system frequency is controlled by embedded real-time software, without physical constraints tied to the swing equation, eq. (1). In [16], a synchronous system was dubbed an "empty network" if all power sources and loads lacked inertia. In practical power systems fed only by inverters, physical inertia will be provided only by motors. If all rotating machines in a synchronous area are motors, or generators with constant power output, there will be no disturbances to the system frequency generated by the VSI, and frequency will be seen as constant on all busses.

In the context of using system frequency to carry information by changing frequency setpoint values, a low amount of physical inertia is an advantage because it allows rapid changes in system frequency (high ROCOF). For a VSI, the parameters of the generator block in Fig. 2 will have time delays on the order of the input sampling rate, well under 20 ms.

D. FS-DER for Primary Frequency Regulation

Previous work on FS-DER has focused on using flexible loads to supplement large generators performing primary frequency regulation [17]–[19]. The availability of low-cost microelectronics to accurately measure system frequency has made it feasible for loads as small as household appliances to act as FS-DER for primary frequency regulation. Ongoing efforts to draft transnational grid codes in Europe cite the value of primary frequency regulation services from FS-DER to justify mandating their deployment on thermostat controlled loads [20].

A frequency sensitive load controller programmed for primary frequency regulation will shift the phase of the load duty cycle to defer energy consumption away from periods when the grid is overloaded, as indicated by a low system frequency.

The FS-DER algorithm for discrete relay-based devices described in [21] has a frequency threshold $f_{\text{off+}}$ [Hz] below which the load is disconnected. Loads are reconnected when system frequency is above a higher threshold frequency $f_{\text{on-}}$ [Hz], creating a simple hysteresis. A block diagram of the FS-DER controller is shown in Fig. 4. Frequency measurements $f[k]$ [Hz] are sent through a low pass filter to produce $\hat{f}[k]$ [Hz] before comparing the value to preset thresholds. This filtering reduces the effects of noise in the frequency signal, and reduces the deviation between the measured frequency and the system average frequency.

The algorithm in [21] can be generalized to more complex DER that have more than two states of operation or to aggregated blocks of DER. The controller will transition to state S at time k when the measured and filtered system frequency $\hat{f}[k]$ enters the decision region given by:

$$f_{S-} \leq \hat{f}[k] \leq f_{S+}. \tag{2}$$

Filtered system frequency $\hat{f}[k]$ must be between the lower frequency threshold f_{S-} [Hz] and the upper frequency threshold f_{S+} [Hz] to trigger a state change.

Some processes, like refrigerator compressors, have timing constraints on how quickly they can start-up and shutdown. When these devices are used as FS-DER and system frequency fluctuates between the switching thresholds, the timing constraints take precedence over the frequency response. Therefore a reliable response from these FS-DER is only realized when they infrequently change state. To address this, section V describes how to design FS-DER thresholds and frequency

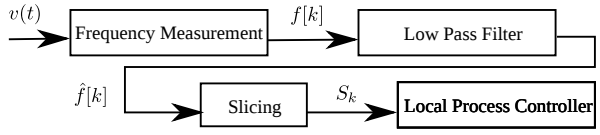

Figure 4. Block diagram of FS-DER controller. In time period k, the frequency $f[k]$ of the incoming voltage waveform $v(t)$ is filtered and then compared to pre-set threshold values (slicing), resulting in state S_k which is given as input to the controller of the local energy conversion process.

setpoints to achieve a pre-determined probability of changing state.

III. Power Frequency Communication (PFC)

Standard frequency band allocation of the power line media gives utilities access to the lowest frequencies [22], and low bandwidth communication systems operating below the standard frequency range operate at speeds as low as 0.001 bps [23]. Conventional power line communication superimposes high frequency components onto the fundamental energy carrying voltage waveform, but higher frequencies have greater signal attenuation per unit distance. In contrast, power frequency communication (PFC), which uses the energy carrying voltage waveform itself as a carrier for frequency modulation, is able to distribute signals without limitations on distance.

A. Two Way Automatic Communication System (TWACS)

TWACS is the an implementation of PFC currently utilized for remote meter reading, distribution automation, and outage management [24]. TWACS can modulate system frequency on a single radial feeder by injecting current to distort the downstream voltage waveform, thus modifying timing of the voltage zero-crossing. Because the AC voltage signal must be continuous phase, frequency shift keying is used to encode symbols. TWACS encodes up to two data bits with 1 AC cycle, giving a data rate of 100 bps [2].

A drawback of the original TWACS frequency modulation technique [3] is that the transmitting device introduces reactive power losses. The advent of synchronous areas dominated by inverter connected generation introduces the possibility of modulating system frequency at the power source at minimal marginal cost.

A TWACS receiver calculates system frequency by measuring the time elapsed between the zero-crossings, the same frequency measurement method as a FS-DER controller [25].

B. Frequency Modulation in Inverter Dominated Micro-Grids

In isolated micro-grids, VSIs available today can dispatch DG by changing the system frequency to off-nominal values. This feature relies on DG compliance with grid codes for large synchronous areas [26] that require CSIs to implement a $(P-f)$ droop when system frequency is above a critical value (i.e. 50.2 Hz), thus providing emergency down regulation reserves. Modulating AC system frequency is used by VSI battery controllers to indicate battery charge status and to curtail production in islanded microgrid systems in the event that production exceeds load and energy storage devices are full [15], [27], [28].

These products demonstrate that VSIs can reliably produce off-nominal AC frequencies to communicate to DG, and they show that the normal operation of loads are not adversely effected by off-nominal frequencies. The protocol described in Section V modulates frequency, but unlike existing VSIs, does so in discrete domains. The resulting signal is used by all FS-DER, including both DG and loads.

IV. Constraints on Frequency Modulation

This section describes methods for determining the constraints on system frequency setpoints. First, the limits to the range of frequency setpoint values (the bandwidth) are found. Second, limits to the rate of change of symbols (the baud rate) are found.

A. Range of Frequency Setpoints

To maintain system integrity, the minimum frequency after a large disturbance must be above the trip thresholds of under-frequency protection relays. If the maximum frequency deviation after a disturbance in the negative/positive direction is given as $\Delta f_{\text{max-}}/\Delta f_{\text{max+}}$ [Hz], and the technical minimum/maximum frequencies are $f_{\text{limit-}}/f_{\text{limit+}}$ [Hz], the system operator can choose frequency setpoints f_{s} [Hz] within the interval $F_{\text{s,dist}}$ given by:

$$F_{\text{s,dist}} = [f_{\text{limit-}} + \Delta f_{\text{max-}} \ , \ f_{\text{limit+}} - \Delta f_{\text{max+}}]. \tag{3}$$

The standards referenced in Section II-A require the system frequency to reside within a given interval $\text{F}_{\text{ok}} = [f_{\text{min}}, f_{\text{max}}]$ with a given likelihood P_{ok}. This can be formulated as a constraint on the probability P of a frequency f being observed within F_{ok} during operation with frequency setpoint f_{s}:

$$\text{P}(f \in \text{F}_{ok}; f_{\text{s}}) \geq \text{P}_{\text{ok}}. \tag{4}$$

Consider the known probability density function $p(f; f_{\text{o}})$ for a system operating with given frequency setpoint f_{o}. We shall assume that small frequency offsets δ to f_{o} do not to change the shape of the probability density function (PDF):

$$\text{P}(f \in [a,b]; f_{\text{o}}) = \text{P}(f \in [a+\delta, b+\delta]; (f_{\text{o}}+\delta)). \tag{5}$$

The set of permissible frequency setpoints $F_{\text{s,ok}}$ which satisfy eq. (4) is found by finding a frequency range where the probability of residing in F' during operation with frequency setpoint f_{o} is exactly P_{ok}:

$$\text{P}(f \in F'; f_{\text{o}}) = \text{P}_{\text{ok}}. \tag{6}$$

The set F' is defined in the following expression:

$$F' = [f_{\text{o}} \ - \ \Delta \ f'_{\text{min}} \ , \ f_{\text{o}} \ + \ \Delta \ f'_{\text{max}}] \subset \text{F}_{\text{ok}}. \tag{7}$$

The parameters $\Delta \ f'_{\text{min}}, \Delta \ f'_{\text{max}}$ in eq. (7) can be derived by integrating across selected regions of the system frequency PDF, see Section IV-C. The parameters become the margins

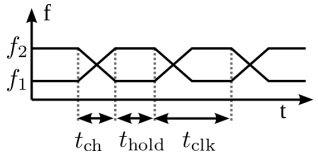

Figure 5. Timing diagram of PFC protocols. The time to change between symbols is t_{ch}. The hold time t_{hold} can be small.

that the operator must maintain between $f_{\min}, f_{\max}$ and f_s. As a result, the interval of $F_{\text{s,ok}}$ is given by:

$$F_{\text{s,ok}} = [f_{\text{min}} + \Delta f'_{\text{min}} \ , \ f_{\text{max}} - \Delta f'_{\text{max}}]. \tag{8}$$

The intersection of sets $F_{\text{s,dist}}$ and $F_{\text{s,ok}}$ gives the complete range of valid frequency setpoints F_{s}, resulting in an available bandwidth, f_{w} [Hz]:

$$F_{\text{s}} = F_{\text{s,dist}} \cap F_{\text{s,ok}} \tag{9}$$

$$f_{\text{w}} = \max(F_{\text{s}}) - \min(F_{\text{s}}). \tag{10}$$

B. Transmission Rate and ROCOF Constraints

A system operator who chooses to vary system frequency setpoints will have to maintain ROCOF constraints during the transition from one frequency setpoint to another. A ROCOF budget will subtract the maximum ROCOF seen during a contingency $ROCOF_{\text{max}}$ [Hz/s] from the technical limits $ROCOF_{\text{limit}}$ [Hz/s], and the resulting difference will give the budget for additional $ROCOF_{\text{pfc}}$ [Hz/s] introduced when changing between frequency setpoints:

$$ROCOF_{\text{pfc}} = ROCOF_{\text{limit}} - ROCOF_{\text{max}}. \tag{11}$$

In systems with rotating machines $ROCOF_{\text{pfc}}$ may also be limited by the power available from frequency regulation resources P_{reg} [p.u.] relative to the system inertia, given by substituting P_{reg} for the power imbalance in eq. (1). VSIs may have software limits on the maximum ROCOF.

A timing diagram showing the transition between frequency setpoints is shown in Fig. 5. The hold time t_{hold} [s] depends on the length of low pass filtering on the receiver, desired error rate, the size of the decision region and, where applicable, the accuracy of clock synchronization between sender and receiver.

The time taken for the system frequency to rise/fall t_{ch} [s] is a function of the spacing between frequency setpoint f_S and its neighbor $f_{(S-1)}$, $\Delta f_{\text{sp}} = f_S - f_{(S-1)}$, and the $ROCOF_{\text{pfc}}$:

$$t_{\text{ch}} \geq \frac{\Delta f_{\text{sp}}}{ROCOF_{\text{pfc}}}. \tag{12}$$

The sum of the rise/fall time and hold time give the total time to transmit one symbol t_{clk} [s]:

$$t_{\text{clk}} = t_{\text{ch}} + t_{\text{hold}}. \tag{13}$$

C. System Frequency Probability Density Function

The methods described in this paper assume the PDF of system frequency is known. The PDF can be determined empirically, as in [29], or by analysis. Analytically, the system frequency is a stochastic process with two regimes. During normal operation the values are close to f_s and the PDF conforms well to a Gaussian distribution. This regime is characterized by the random (de-)activation of loads and efforts of the primary and secondary frequency controllers on generators to restore the frequency to the setpoint value. However, extreme frequency excursions as a result of faults occur more often than a Gaussian distribution predicts, resulting in a "fat tail" distribution. The system frequency requirements from Section II-A are specified in two parts to reflect these two regimes.

Analysis of data collected from one location in the Nordic power system [30] shows frequency deviations are *less* likely than predicted by a Gaussian distribution up to $f_o - 3\sigma$, where σ is the standard deviation of frequency measurements. The Gaussian regime ends before frequency values of $f_o - 6\sigma$, which are expected to occur once every 2000 years in a Gaussian distribution, but were observed 6 times in one year.

Within the Gaussian regime of frequency measurements, the Gauss error function (erf) gives a closed form solution to eq. (6) and eq. (7) when the frequency standard deviation σ is known. The normal distribution is symmetric around the mean value, so we can define:

$$\Delta f' = \Delta f'_{\text{min}} = \Delta f'_{\text{max}}. \tag{14}$$

Eq. (6) and eq. (7) can then be combined and solved for $\Delta f'$:

$$\text{erf}\left(\frac{\Delta f'}{\sigma\sqrt{2}}\right) = P_{\text{ok}}. \tag{15}$$

A narrow system frequency PDF is desirable when using system frequency as an information carrier. Without increasing the power and speed of frequency regulation resources, the frequency PDF seen by FS-DER can be narrowed by lengthening the low pass filter shown in Fig. 4. The cost of a longer low pass filter is an increased t_{hold} to allow the filtered frequency values ($\hat{f}$) to converge to the system average frequency.

V. Dispatch of FS-DER

By relaxing the operational constraint that the frequency setpoint must always be the nominal frequency ($f_{\text{s}} \neq f_{\text{o}}$) during normal operation, system frequency can be modulated to communicate the value of a single discrete variable to FS-DER. In systems with low $ROCOF_{\text{pfc}}$, the time to transition between setpoints t_{ch} will be large, therefore it is only feasible to encode one symbol per time period, and decoding must be time-invariant. A further restriction with this protocol is that state changes only occur between adjacent states, as shown in Fig. 6. Finally, the design assumes the hold time t_{hold} is long enough to give a high probability of the sampled and filtered frequency $\hat{f}$ falling within the decision region of the intended state.

Both the transmitter and receiver need to agree *a priori* on frequency setpoint and threshold values. Frequency thresholds

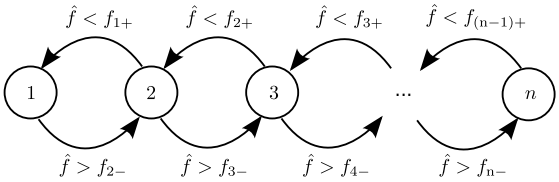

Figure 6. When dispatching FS-DER by modulating system frequency, state transitions only occur between neighboring states.

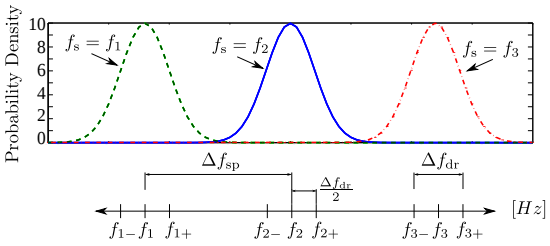

Figure 7. Top: Probability density of frequency samples for three system frequency setpoints: f_1, f_2, f_3. Below: The placement of set-points and the threshold values for dispatch of discrete blocks of FS-DER.

must be chosen so that they are separated by enough distance to avoid spurious unintended state changes during t_{hold}. A wide Δf_{sp} avoids spurious changes to FS-DER state, but a wide Δf_{sp} simultaneously reduces the number of symbols feasible within in a given bandwidth and increases t_{ch}.

Assume the size of the decision region Δf_{dr} [Hz] to be the same for all symbols and defined as:

$$\Delta f_{\text{dr}} = f_{S+} - f_{S-}. \tag{16}$$

To find appropriate frequency thresholds for encoding system states, the designer needs to be given a goal for the desired probability of a FS-DER residing in an unintended state (P_{e}), and the PDF of system frequency measurements. The minimum distance between a frequency setpoint f_S, and the neighboring setpoints $f_{(S-1)}, f_{(S+1)}$ is found by first finding a frequency interval $[f'_{\text{sp-}}, f'_{\text{sp+}}]$ such that:

$$\text{P}(f \in [f'_{\text{sp-}}, f'_{\text{sp+}}]; f_{\text{o}}) = 1 - P_{\text{e}}. \tag{17}$$

Then Δf_{sp} is given by:

$$\Delta f_{\text{sp}} = \frac{1}{2}(f'_{\text{sp+}} - f'_{\text{sp-}} + \Delta f_{\text{dr}}). \tag{18}$$

Fig. 7 shows the placement of set-points and state change thresholds for a system with 3 symbols, and a Gaussian PDF for frequency measurements. In this case, value of $\Delta f_{\text{sp+}}$ and $\Delta f_{\text{sp-}}$ can be found using the Gauss error function as in eq. (15):

$$f'_{\text{sp}} = f'_{\text{sp-}} = f'_{\text{sp+}} \tag{19}$$

$$\text{erf}\left(\frac{f'_{\text{sp}}}{\sigma\sqrt{2}}\right) = 1 - P_{\text{e}}. \tag{20}$$

For a given frequency bandwidth f_{w}, the number of discrete symbols N encoded in that bandwidth is one more than the

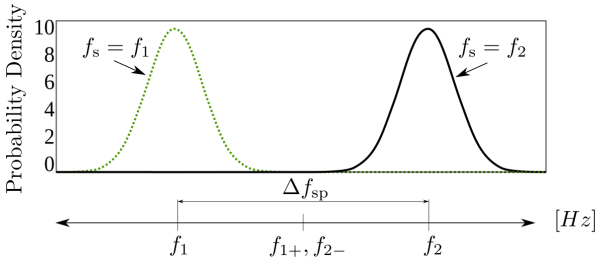

Figure 8. Top: Probability density of frequency samples for two system frequency setpoints: f_1, f_2. Below: The placement of set-points and the threshold values for PFC where $f_{1+} = f_{2-}$.

number of whole frequency spacings that fit in the bandwidth:

$$N = 1 + \left\lfloor \frac{f_{\text{w}}}{\Delta f_{\text{sp}}} \right\rfloor. \tag{21}$$

VI. Generator Speed Governors as Transmitters for Power Frequency Communication

In synchronous areas that allow a high $ROCOF_{\text{pfc}}$, system frequency can be modulated fast enough to allow arbitrary digital information to be transmitted to FS-DER. In contrast to the protocol described in section V which transmitted the value of a single variable, this protocol can transmit the values of many variables allowing the operator to distribute more information about the system state.

The transmitter (generator) and receiver (FS-DER) must be synchronized, so a data clock is recovered and data packages delimited. Synchronization of clocks and package delimiters is done with a preamble, as in TWACS [2], and not elaborated upon. The decoding of frequency measurements is time independent relative to the start of the data package.

The placement of frequency setpoints for PFC uses the eq. (17) where the decision region is chosen to be $\Delta f_{\text{dr}} = \Delta f_{\text{sp}}$, so there is no hysteresis region between adjacent symbols, as shown in Fig. 8. This wider decision region maps each frequency sample to the nearest setpoint value. The frequency samples taken during t_{ch} will be ignored, and only frequency samples taken during t_{hold} are decoded.

When the frequency of the data clock is below twice the AC system frequency ($t_{\text{clk}}^{-1} \leq 2f_{\text{o}}$), dedicating cycles to rise/fall transition between frequencies is unnecessary ($t_{\text{ch}} = 0$). The transmitter is able to independently regulate the time between zero-crossings of each half-cycle and thus achieves the highest possible data transmission rate of PFC.

Higher level protocols can build upon the physical layer provided by PFC, but the relatively low bandwidth of PFC will force application designers to consider the tradeoff between the length of data transmitted and the time taken for transmission.

VII. Case Studies on Islanded Power Systems

Using system frequency to encode information is most relevant for small synchronous systems because they already have a relatively wide range for their system frequency, and their generally smaller capacity margins motivate the use of energy management systems.

The small synchronous system studied is a microgrid located on the island of Christiansø in Denmark, a decommissioned naval base which is a popular tourist destination. Around 100 people live permanently on the 0.22 km^2 island and their electric power generation fleet is composed of 4 diesel fueled generators. The analysis that follows assumes that the operator will live up to the frequency quality requirements of small islands presented in Section II-A.

A. Christiansø: Diesel Powered Micro-Grid

Two bottle cooling refrigerators with FS-DER functionality have been installed as part of a field experiment [25]. Frequency measurements were collected over a period of 4 months [31].

The timeseries of frequency measurements had a standard deviation of $\sigma = 62$ mHz. Passing the frequency measurements through a 5-minute moving average filter reduced the standard deviation to $\sigma = 50$ mHz.

The frequency distribution of Christiansø was centered around 50.12 Hz, so taking this as f_o, the PDF is:

$$\mathrm{P}(f \in [f_\mathrm{o} - \ 130 \text{ mHz}, f_\mathrm{o} + \ 110 \text{ mHz}]; f_\mathrm{o}) = 1 - 0.05. \quad (22)$$

Assuming that f_o is a setpoint value that can be arbitrarily changed, and assuming that the lower absolute frequency limit $f_{\text{limit-}}$ and upper absolute frequency limit $f_{\text{limit+}}$ are not breached during credible contingencies, the range of valid setpoints given by eq. (9) is [49.13 Hz , 50.89 Hz].

Turning to the spacing between frequency setpoints Δf_sp, we take the desired error rate to be $P_\mathrm{e} = 10^{-4}$. The decoder operates with a 5-minute moving average low pass filter. The detection region is given as $\Delta f_\mathrm{dr} = 100$ mHz. Using eq. (17), analysis of the filtered data reveals $f'_{\text{sp-}} = 49.83$ Hz and $f'_{\text{sp+}} = 50.28$ Hz, giving $\Delta f_\mathrm{sp} = 275$ mHz by eq. (18). By eq. (21), the number of distinct symbols feasible in this system is 7. The allocation of frequency setpoints is shown in table I with f_o re-calibrated to the standard 50 Hz.

The length of the low pass filter (5 min.) gives a minimum $t_\mathrm{hold} = 300$ s. Even if we generously assume $t_\mathrm{ch} = 0$, the best case baud rate is 12 symbols per hour.

The frequency setpoints for PFC must be separated by $\Delta f_\mathrm{sp} = 450$ mHz. The feasible data rate of PFC is also 12 bits per hour because increased spacing between frequency setpoints does not significantly influence t_ch.

B. Laboratory Test: Inverter Dominated Micro-Grid

The increasing cost of diesel fuel, emissions constraints, and decreasing costs of RES have motivated the operator on Christiansø to investigate replacing their current generation fleet with RES which may be inverter connected. To simulate the energy source in such an system, a VSI in our laboratory was tested to characterize the speed of response to changes in frequency setpoints. The inverter, produced by IE Power, had a rated DC input of 136 V, and rated 3-phase AC output of 400 V, a power rating of 20 kVA, and a frequency range of 47.5 Hz to 52.5 Hz. The DC side of the inverter was fed by a vanadium flow battery whose performance was characterized in [32]. Frequency setpoints are communicated to the inverter by means of a current loop, an inherently analog control signal. Instead of directly measuring this current, the voltage across the input terminals of the inverter was measured, as the measured voltage is proportional to the current flowing in the circuit. The input voltage indicating the frequency setpoint and the output voltage of one phase of the inverter with no-load was measured by a Yokogawa WT500 power analyzer and a Yokogawa DL750 oscilloscope. The power analyzer measured voltage at a relatively high resolution (1 mV), but a relatively low temporal resolution (100 ms). The oscilloscope had a high temporal resolution (100 μs), but lower voltage resolution (33 mV). Separate test runs of the same frequency setpoint sequence were recorded using the power analyzer and oscilloscope.

Table I
SUGGESTED PARAMETER VALUES FOR FREQUENCY SET-POINTS ON CHRISTIANSØ WITH 7 SYMBOLS, SYMMETRIC AROUND f_o.

Parameter	Relative Value	Value
f_o		50 Hz
Δf_sp		275 mHz
Δf_dr	2σ	100 mHz
f_1	$f_2 - \Delta f_\mathrm{sp}$	49.175 Hz
f_2	$f_3 - \Delta f_\mathrm{sp}$	49.450 Hz
f_3	$f_\mathrm{o} - \Delta f_\mathrm{sp}$	49.725 Hz
f_4	f_o	50.000 Hz
f_5	$f_\mathrm{o} + \Delta f_\mathrm{sp}$	50.275 Hz
f_6	$f_5 + \Delta f_\mathrm{sp}$	50.550 Hz
f_7	$f_6 + \Delta f_\mathrm{sp}$	50.825 Hz

The power analyzer calculated AC frequency at each time step using an undisclosed internal algorithm. AC frequency was extracted from the oscilloscope data using a zero-crossing algorithm with linear interpolation, a method validated in a previous experiment with FS-DER [25]. Measurement noise found in the 100 μs data series was mitigated by applying at 4-sample sliding-window moving average, and the cycle-by-cycle frequency calculations were again averaged over two periods to reduce variance. Assuming that an analog-to-digital converter similar to the oscilloscope is feasible to implement in an embedded system, the frequency measurements derived from analysis of oscilloscope data closely matches what would be seen by a low-cost FS-DER.

Steady-state frequency measurements taken by the power analyzer showed a standard deviation of 3.5 mHz and

$$\mathrm{P}(f \in [f_\mathrm{o} - \ 14 \text{ mHz}, f_\mathrm{o} + \ 14 \text{ mHz}]; f_\mathrm{o}) = 1 - 10^{-4} \quad (23)$$

and

$$\mathrm{P}(f \in [f_\mathrm{o} - \ 8 \text{ mHz}, f_\mathrm{o} + \ 8 \text{ mHz}]; f_\mathrm{o}) = 1 - 0.05. \quad (24)$$

A sequence of frequency setpoints was programmed using a high level software API, and these software commands were converted into current levels by a digital-to-analog converter. Measuring the frequency setpoint at the terminals of the inverter removed any delays introduced by the high-level software, and only the timing of the inverter is tested. Changes to frequency setpoints are tested at 3 orders of magnitude: ± 1 Hz, ± 100 mHz, and ± 10 mHz, shown in Fig. 9.

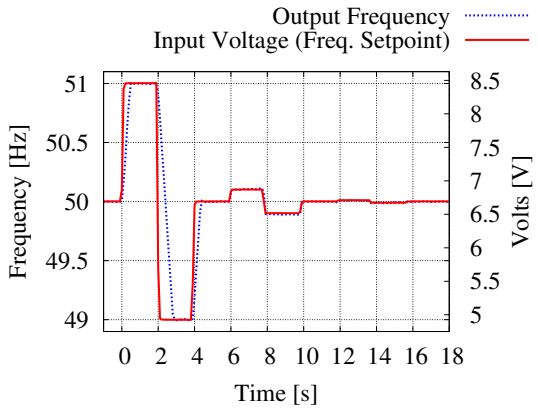

Figure 9. Test sequence of frequency setpoints given to inverter, and the output frequency as measured by the power analyzer. At time 0 s the setpoint changes from 50 Hz to 51 Hz. After 2 seconds, the setpoint is changed to 49 Hz, and at time 4 s the setpoint returns to 50 Hz. At time 6 s the setpoint is changed to 50.10 Hz, at time 8 s it is changed to 49.90 Hz. Finally, barely visible at this scale, at time 12 s the setpoint is changed to 50.01 Hz, then 49.99 Hz at time 14.

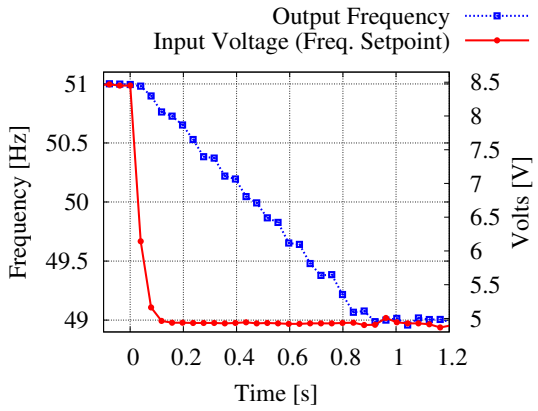

Figure 10. Step change of frequency setpoint of -2 Hz. Voltage and frequency measurements derived from the oscilloscope data points are shown at 40 ms (2-cycle) intervals.

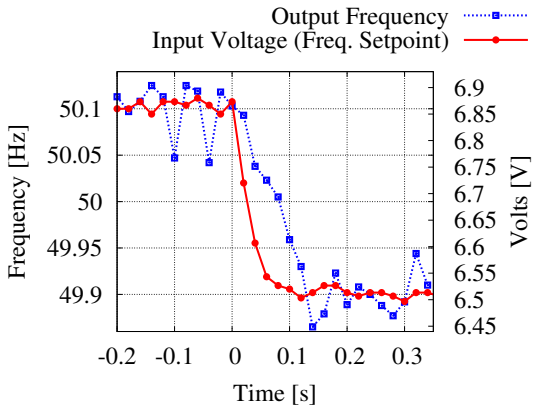

Figure 11. Step change of frequency setpoint of -200 mHz. Voltage and frequency measurements derived from the oscilloscope data points are shown at 20 ms (1-cycle) intervals.

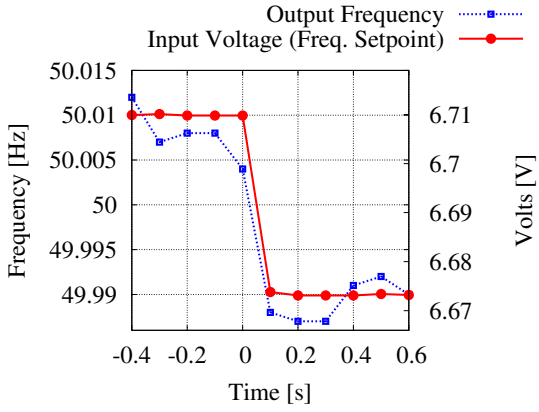

Figure 12. Step change of frequency setpoint of -20 mHz. Voltage and frequency measurements derived from the power analyzer with data points shown at 100 ms (5-cycle) intervals.

Fig. 10 shows a close up as the inverter changes frequency setpoint from 51.00 Hz to 49.00 Hz, using data from the oscilloscope. At time 0, the voltage across the inverter input terminals falls from 8.5 V to 5 V. The output frequency immediately begins to decline, and stabilizes 900 ms after the input began to change. A change of 2 Hz in 0.9 s gives a ROCOF of 2.2 Hz/s.

Fig. 11 shows the response to -200 mHz change in frequency setpoint starting at 50.10 Hz, again using data from the oscilloscope. At time 0 the input signal begins to change, and 140 ms later, output frequency has dropped below the intended setpoint of 49.90 Hz, giving a ROCOF of 1.4 Hz/s.

Finally, the response of the inverter to a -20 mHz frequency setpoint change is shown in Fig. 12. This figure is based on data from the power analyzer because the change in input voltage was too small to measure with the oscilloscope. The output frequency falls below the setpoint value one time step (100 ms) after the input begins to change. The time resolution of the power analyzer frequency measurements was insufficient to determine if the output frequency changed faster than the observed 0.2 Hz/s.

To find the range of feasible frequency setpoint values we use eq. (14) and eq. (24), to specify the value of $\Delta f' = 8$ mHz. This results in an available bandwidth of $f_{\text{w}} = 1.98$ Hz.

To find the spacing between frequency setpoints Δf_{sp}, we take the desired error rate to be $P_{\text{e}} = 10^{-4}$, the same as in Section VII-A. The decision region is given as $\Delta f_{\text{dr}} = 2\sigma = 7$ mHz. Using the definition of f'_{sp} from eq. (19) and the value of $f'_{\text{sp}} = 14$ mHz from eq. (23), eq. (18) gives $\Delta f_{\text{sp}} = 17.5$ mHz.

From eq. (21) we see that the bandwidth can accommodate up to 114 discrete symbols.

Recall for PFC $\Delta f_{\text{dr}} = \Delta f_{\text{sp}}$, and $f'_{\text{sp}} = 14$ mHz, so eq. (18) gives $\Delta f_{\text{sp}} = 28$ mHz. If the $ROCOF_{pfc}$ value of 1.4 Hz/s can also be achieved for this smaller change in frequency setpoint, $t_{\text{ch}} = 20$ ms, or exactly one AC cycle at 50 Hz. The time t_{hold} is determined by the length of a low-pass filter in the receiver. The zero-crossing algorithm used in this analysis required a low-pass filter of 2-cycles to reduce variance, so if $t_{\text{hold}} = 40$ ms, $t_{\text{clk}} = 60$ ms giving a maximum bit rate of 16.6 bps.

VIII. Discussion

Compared to other power line communication protocols, the proposed protocols should be inexpensive to implement because they use existing generator speed governors to encode data and allow decoding devices to be implemented with commodity low-cost microcontrollers. The use of carrier frequencies below the system frequency allows the signal to propagate for an effectively unlimited distance.

Parameter values for the proposed AC frequency modulation system will vary greatly between synchronous systems. Large synchronous systems will have very low $ROCOF_{\text{plc}}$ values because of high inertia. This makes it infeasible to use generator speed governors for PFC, but this does not exclude using the limited available bandwidth for dispatching FS-DER. Inverter dominated synchronous areas have high $ROCOF_{\text{plc}}$ values that enable PFC to be implemented. In the VSI tested in Section VII-B the ROCOF was a nonlinear function of the size of the frequency step, so for this device the denominator in eq. (13) will be a function of Δf_{sp}. The maximum ROCOF of the VSI was limited by a parameter in its embedded software, it is possible that the power electronics hardware could support higher ROCOF values.

Detailed discussion of applications of the proposed protocols is outside the scope of this paper, but to illustrate the difference between the two protocols, their application to price dissemination is considered. Using the FS-DER dispatch protocol allows the current electricity price to be reflected by the system frequency, allowing marginal consumers to judge if the utility of their consumption exceeds the current price. With PFC and a bit rate high enough to send the price values for the current and future operation periods, consumers would have the information needed to optimize their consumption across a longer time horizon.

The probability of communication errors, P_{e}, is a design parameter. In practical systems it will not be low enough to entirely eliminate the possibility of disturbances causing errors in communication. The applications that utilize this communication system will need to be robust in the presence of such errors. For example, when using PFC, checksums in the protocol can be employed to validate the integrity of messages. When using system frequency to dispatch FS-DER by synchronous generators, the linkage between low frequency and excess load requires that lower frequencies lead to lower system load and/or greater DG production.

Many loads are indifferent to variations in system frequency, but off-nominal frequency may lead to higher losses in machines optimized for a particular frequency, such as generators and legacy industrial processes [33]. This concept could have a negative effect on machine efficiency; however, there will be systems where the the benefit of distributing information for demand response outweighs these costs.

IX. Conclusion

The paper has shown how existing frequency regulation resources can be applied to transmitting discrete information. Explicitly signaling discrete system states by generating off-nominal system frequency values can be used as a novel narrowband unidirectional broadcast communications channel between system operators and FS-DER. Systems that are restricted to slow changes in system frequency can communicate the value of a single discrete variable to FS-DER, while systems that allow fast changes to system frequency can implement general purpose unidirectional broadcast power frequency communication (PFC). Using generators as PFC transmitters does not require any additional power electronics and eliminates the energy losses associated with previous PFC transmitters.

Data collected from an diesel fueled islanded power system shows that it is feasible to encode 7 discrete symbols for FS-DER dispatch. Laboratory tests of at 20 kW VSI showed that it was able to respond to frequency setpoint changes with a ROCOF of between 2.2 and 0.2 Hz/s depending on the size of the setpoint change. In a VSI dominated micro-grid, analysis of the experimental data shows that a PFC bit rate of 16.6 bps is feasible.

References

[1] F. Schweppe, R. Tabors, J. Kirtley, H. Outhred, F. Pickel, and A. Cox, "Homeostatic utility control," *Power Apparatus and Systems, IEEE Transactions on*, vol. PAS-99, no. 3, pp. 1151 –1163, may 1980.

[2] S. Mak and D. Reed, "TWACS, A new viable two-way automatic communication system for distribution networks. Part I: Outbound communication," *Power Apparatus and Systems, IEEE Transactions on*, vol. PAS-101, no. 8, pp. 2941 –2949, aug. 1982.

[3] S. T. Mak, "A new method of generating TWACS type outbound signals for communication on power distribution networks," *Power Apparatus and Systems, IEEE Transactions on*, vol. PAS-103, no. 8, pp. 2134 – 2140, aug. 1984.

[4] P. J. Douglass, S. You, and K. Heussen, "Broadcast communication by system frequency modulation," in *Smart Grid Communications (SmartGridComm), 2012 IEEE Third International Conference on*, 2012, pp. 199–204.

[5] J. R. Pillai, K. Heussen, and P. A. Østergaard, "Comparative analysis of hourly and dynamic power balancing models for validating future energy scenarios," *Energy*, vol. 36, no. 5, pp. 3233 – 3243, 2011.

[6] CENELEC, "EN 50160: Voltage characteristics of electricity supplied by public electricity networks," 2010.

[7] ENTSO-E, "Draft Network Code for Requirements for Grid Connection applicable to all Generators," 24 Jan. 2012.

[8] P. Kundur, N. Balu, and M. Lauby, *Power system stability and control*. McGraw-Hill New York, 1994.

[9] V. Terzija, "Adaptive underfrequency load shedding based on the magnitude of the disturbance estimation," *Power Systems, IEEE Transactions on*, vol. 21, no. 3, pp. 1260 –1266, aug. 2006.

[10] IEEE Task Force, "Standard load models for power flow and dynamic performance simulation," *Power Systems, IEEE Transactions on*, vol. 10, no. 3, pp. 1302 –1313, aug 1995.

[11] I. Egido, F. Fernandez-Bernal, P. Centeno, and L. Rouco, "Maximum frequency deviation calculation in small isolated power systems," *Power Systems, IEEE Transactions on*, vol. 24, no. 4, pp. 1731 –1738, nov. 2009.

[12] J. Vieira, W. Freitas, W. Xu, and A. Morelato, "Efficient coordination of rocof and frequency relays for distributed generation protection by using the application region," *Power Delivery, IEEE Transactions on*, vol. 21, no. 4, pp. 1878 –1884, oct. 2006.

[13] "Rate of Change of Frequency (ROCOF) DS3 Advisory Council Discussion Paper," Online, EirGrid, SONI, Tech. Rep., 2 Feb. 2012, accessed September 19, 2012. [Online]. Available: http://www.eirgrid.com/operations/ds3

[14] UCTE, "Operations Handbook Appendix 1: Load Frequency Control," 16 Jun. 2004.

[15] L. A. C. Lopes, F. Katiraei, K. Mauch, M. Vandenbergh, and L. Arribas, "PV Hybrid Mini-Grids: Applicable Control Methods for Various Situations," International Energy Agency, Tech. Rep., Apr. 2012.

[16] M. Reza, A. Dominguez, P. Schavemaker, A. Asmara, F. Viawan, and W. Kling, "Controlling the power balance in an 'empty network'," *Int. J. of Energy Technology and Policy*, vol. 5, no. 5, pp. 584 – 603, 2007.

[17] J. Short, D. Infield, and L. Freris, "Stabilization of grid frequency through dynamic demand control," *Power Systems, IEEE Transactions on*, vol. 22, no. 3, pp. 1284 –1293, aug. 2007.

[18] P. J. Douglass, R. Garcia-Valle, P. Nyeng, J. Østergaard, and M. Togeby, "Smart demand for frequency regulation: Experimental results," *Smart Grid, IEEE Transactions on*, vol. 4, no. 3, pp. 1713–1720, 2013.

[19] M. Donnelly, D. Trudnowski, S. Mattix, and J. Dagle, "Autonomous Demand Response for Primary Frequency Regulation," Pacific Northwest National Laboratory, Tech. Rep., Jan. 2012.

[20] ENTSO-E, "Draft Demand Connection Codes," 27 Jun. 2012.

[21] Zhao Xu, J. Østergaard, and M. Togeby, "Demand as frequency controlled reserve," *Power Systems, IEEE Transactions on*, vol. 26, no. 3, pp. 1062 –1071, Aug. 2011.

[22] CENELEC, "EN 50065-1: Signalling on low-voltage electrical installations in the frequency range 3 kHz to 148,5 kHz - Part 1: General requirements, frequency bands and electromagnetic disturbances," 2011.

[23] S. Galli, A. Scaglione, and Z. Wang, "For the grid and through the grid: The role of power line communications in the smart grid," *Proceedings of the IEEE*, vol. 99, no. 6, pp. 998 –1027, june 2011.

[24] "Aclaratech," Online, 2012, accessed September 27, 2012. [Online]. Available: http://www.aclaratech.com/

[25] P. Douglass, R. Garcia-Valle, P. Nyeng, J. Østergaard, and M. Togeby, "Demand as Frequency Controlled Reserve: Implementation and practical demonstration," in *Innovative Smart Grid Technologies (ISGT Europe), 2011 2nd IEEE PES International Conference and Exhibition on*, 2011, pp. 1–7.

[26] VDE, "VDE-AR-N 4105:2011-08 Power generation systems connected to the low-voltage distribution network - Technical minimum requirements for the connection to and parallel operation with low-voltage distribution networks," 1 Aug. 2010. [Online]. Available: http://www.vde.com/en/fnn/pages/n4105.aspx

[27] SMA Technogie AG, "Sunny Island 5048u Installation and Instruction Manual, Version 1.0," 2007.

[28] P.-O. Moix, "A Minigrid of Individual Solar Home Systems," in *6th European Conference of PV-Hybrids and Mini-Grids*, 2012.

[29] B. Biegel, L. H. Hansen, P. Andersen, and J. Stoustrup, "Primary Control by ON/OFF Demand-Side Devices," *IEEE Transactions on Smart Grid*, preprint.

[30] Z. Xu, J. Ostergaard, M. Togeby, and F. Isleifsson, "Evaluating frequency quality of nordic system using pmu data," in *Power and Energy Society General Meeting - Conversion and Delivery of Electrical Energy in the 21st Century, 2008 IEEE*, 2008, pp. 1–5.

[31] P. J. Douglass, "Integrating Autonomous Load Controllers in Power Systems," Ph.D. dissertation, Technical University of Denmark, Dec. 2013.

[32] H. Bindner, C. Krog Ekman, O. Gehrke, and F. Isleifsson, *Characterization of Vanadium Flow Battery*, ser. Denmark. Forskningscenter Risoe. Risoe-R. Danmarks Tekniske Universitet, Risø Nationallaboratoriet for Bæredygtig Energi, 2010.

[33] ENTSO-E, "Supporting Paper for the Load-Frequency and Reserves Network Code - Working Draft," 23 Jan. 2013.

www.elektro.dtu.dk
Department of Electrical Engineering
Center for Electric Power and Energy
Technical University of Denmark
Ørsteds Plads
Building 348
DK-2800 Kgs. Lyngby
Denmark
Tel: (+45) 45 25 38 00
Fax: (+45) 45 93 16 34
Email: info@elektro.dtu.dk